UNIVERSITY OF CALIFORNIA,
IRVINE

Taming Giants:
Studies on the Growth, Regulation, and Evolution of Dusty, Star-Forming Galaxies in the Early Universe

DISSERTATION

submitted in partial satisfaction of the requirements
for the degree of

DOCTOR OF PHILOSOPHY

in Physics

by

Arianna S. Long

Dissertation Committee:
Professor Asantha Cooray, Chair
Professor James Bullock
Professor Caitlin Casey

2022

DEDICATION

To little Arianna, who had no idea that the future could hold so many beautiful and wondrous adventures. And to my life partner, Patrick: I could spend eternity as a rock on a cliff with you and be perfectly content...but I'm glad we're here now doing the things we've always dreamed of together.

TABLE OF CONTENTS

Page

LIST OF FIGURES **v**

LIST OF TABLES **vi**

ACKNOWLEDGMENTS **vii**

VITA **ix**

ABSTRACT OF THE DISSERTATION **xiv**

1 Introduction **1**
- 1.1 Preface . . . 1
- 1.2 Why Dust Matters . . . 2
- 1.3 Dusty, Star-Forming Galaxies: What's in a Name? . . . 3
- 1.4 Black Holes and Galaxies: A Gravitational Love Story . . . 5
- 1.5 Galaxy Clusters: From Fireworks to Fossils . . . 8

2 A Case Study at $z = 4$ - Long et al. 2020 **12**
- 2.1 Introduction . . . 12
- 2.2 Observations . . . 14
  - 2.2.1 HST WFC3 . . . 14
  - 2.2.2 Gemini FLAMINGOS-2 . . . 16
  - 2.2.3 Spitzer IRAC . . . 16
  - 2.2.4 Herschel SPIRE . . . 16
  - 2.2.5 ALMA . . . 17
- 2.3 Photometry and Counterpart Selection . . . 18
  - 2.3.1 Near-Infrared Photometry . . . 18
  - 2.3.2 Identifying HST and Gemini Counterparts . . . 19
  - 2.3.3 Generating Respective Herschel Flux Densities . . . 20
  - 2.3.4 Deblending IRAC Counterparts . . . 23
- 2.4 SED Modeling . . . 26
- 2.5 DRC Compared to Field Galaxies . . . 29
  - 2.5.1 Main Sequence Evolution . . . 30
  - 2.5.2 Gas Properties . . . 32
- 2.6 Cluster Halo Mass at $z = 4$ . . . 39

2.7 Summary and Conclusions . . . 44

3 Growing Black Holes Do Not Quench DSFGs - Brown et al. 2019 46
3.1 Introduction . . . 46
3.2 Multi-wavelength Data . . . 51
3.2.1 X-ray Data . . . 52
3.2.2 Infrared Data . . . 54
3.2.3 Redshifts . . . 55
3.3 AGN Sample Selection . . . 56
3.4 Results and Discussion . . . 60
3.4.1 Average L_{IR}^{SF} vs. Average L_{AGN} . . . 60
3.4.2 Average L_X vs. Average L_{IR}^{SF} . . . 63
3.4.3 Dust Covering Factors . . . 67
3.4.4 AGN Contribution in the Infrared . . . 72
3.5 Summary and Conclusions . . . 75

4 Missing Massive Galaxies - Long et al. 2022 77
4.1 Introduction . . . 77
4.2 Model Ingredients . . . 82
4.2.1 The Infrared Luminosity Function . . . 84
4.2.2 AGN Contributions to Total Infrared Luminosity . . . 86
4.2.3 The Star-Forming Main Sequence . . . 88
4.2.4 Stellar Mass Number Density . . . 93
4.3 Model Results | The Dust-Obscured Stellar Mass Function . . . 96
4.4 Discussion . . . 101
4.4.1 The Descendant Quiescent Stellar Mass Function . . . 102
4.4.2 Massive, Dust-Obscured Galaxies and Their Descendants . . . 103

5 Summary and Conclusion 109
5.1 A Case Study at $z = 4$ - Long et al. 2020 . . . 109
5.2 Growing Black Holes Do Not Quench DSFGs - Brown et al. 2019 . . . 110
5.3 Missing Massive Galaxies - Long et al. 2022 . . . 112
5.4 Future . . . 113

Bibliography 114

Appendix A Appendix Title 162

LIST OF FIGURES

Page

2.1 Multiwavelength Imaging of the Distant Red Core 15
2.2 Deblending IRAC Example 24
2.3 Best Fit Spectral Energy Distributions 25
2.4 The Star-Forming Main-Sequence at $z \sim 4$ 30
2.5 Molecular Gas Mass Fractions Versus Stellar Mass 35
2.6 Halo Mass Estimates for the Distant Red Core 38
2.7 Halo Mass Evolution of Protoclusters 42

3.1 Parent Survey Maps 49
3.2 X-Ray and Redshift Sample Distribution 50
3.3 Our Sample Versus Lanzuisi et al. 2017 51
3.4 Example SEDs 55
3.5 AGN in Infrared Color Space 57
3.6 AGN Bolometric Luminosity versus Star Formation Luminosity 60
3.7 A model of AGN Bolometric Luminosity versus Star Formation Luminosity 61
3.8 AGN Dust Covering Factors 65
3.9 Covering Factors and Hardness Ratios 66
3.10 Comparing Infrared and X-Ray AGN Luminosity, and Fractional AGN Contributions to Total Infrared Luminosity 68
3.11 AGN Fractions as a Function of X-Ray Luminosity 69
3.12 AGN Fraction as a Function of Host Galaxy Luminosity 71

4.1 A Cartoon of the Model Presented 81
4.2 Main-Sequence and Starburst Gaussian Mixtures 91
4.3 Corner Plot Showing Posterior Parameter Distributions for SMF Parameters 94
4.4 Redshift Evolution of Derived SMF Parameters 95
4.5 The Dust Obscured Stellar Mass Function 100
4.6 Number Density of Massive $M > 10^{10.5}\,M_{\odot}$ Galaxies 105

LIST OF TABLES

Page

2.1 Measured Flux Densities for Cluster Members 21
2.2 Measured Flux Densities for Cluster Members Continued 21
2.3 Galaxy Properties Derived from SED Fitting 29

3.1 Population counts and field coverage of the multi-wavelength flux catalogs used to generate 703 individual SEDs. 52

4.1 Physical relationships and respective parameter spaces used in this model. See Section 4.2 for details on these values and their motivation. 83
4.2 Parameters for the resulting broken power law fits. 99
4.3 Number Densities and Stellar Mass Densities 102

ACKNOWLEDGMENTS

First and foremost, I would like to thank my husband: thank you for over a decade of support, and seven years of endless cheerleading and championing; thank you for pushing me to pursue my dreams, despite how ridiculous I thought they were; thank you for holding me down when I'd spiral out from stress; thank you for feeding me, cleaning the house, walking the dog, and serving as a buffer (my protector); thank you for make me smile and bringing deep belly laughs to our daily routine; thank you for coaching me. Thank you. Thank you. Thank you. I cannot say it enough. This dissertation is partially yours and is why I'm so glad to finally call you "Mister Doctor".

Thank you to my sweet fur-baby, Charlie 'Turkey' Bean. You're the reason I made sure to get a little sunlight and fresh air every day. You bring us endless joy, and I owe so much of my health and happiness to your sweet little face.

Thank you to my scientific / academic mentors, who walked the path before me so that I could walk it a little easier. Thank you so much to my advisor, Asantha Cooray. You held out your hand to me when I was a fledgling astronomer at CSULA, and then offered me support in every opportunity that crossed our paths since. Sometimes it was scary, or hard, but you always had faith that I could do it (whatever 'it' was). Thank you. Thank you to Franklin Dollar for seeing infinite multitudes within me and refusing to entertain any of my words of self-doubt. Thank you to Mike Cooper for listening, guiding, and supporting me with what always felt like your full attention; you helped me become the scientist, and person, I am today. Thank you to Caitlin Casey for your deep and unwavering faith in me, and in my science; your support over these last couple of years has quite literally changed my life and I cannot thank you enough for seeing in me what can't always see in myself. I'm so excited for these next few years together. Thank you to the community of scientists who continually show up and show out in support of my continued success: Vivian U, Julie Wardlow, James Bullock, Jingzhe Ma, Catherine Espaillat, Susan Terebey, Allison Kirkpatrick, Steph Sallum, Coral Wheeler, Seyda Ipek, Nicole Cabrera Salazar, Jedidah Isler, and so many more. Thank you to my friends and peers who constantly challenge me to be a better, more complete person, and who supported me through it all: Erini Lambrides, Catherine Bliss, Katy Rodriguez Wimberly, Laura Gollub, Manuel Paul, Francisco Mercado, Tae Baxter, Jackie Champagne, Olivia Cooper, Chelsea Reid, Andrea Nelson, Julian Sadur, Jonathan Barnes, Derek Watson, Michael Capotosto, Michael Harrison, Anicca Harriot, Geraldine Ezeka, Keila Miles, Diana Powell, Brittany Miles, and so many more. I would not be here without this community of support. Thank you. Thank you. Thank you all.

Thank you to the broader, more "official" communities of support including LUMA, Vanguard-STEM, the UCI SRP program, UCI's Competitive Edge, and the Black in Astro / STEM community. It was in these spaces that I learned to acknowledge and love all parts of myself, and learned to see my uniqueness as a strength. It was in these spaces that I became whole.s

Finally, thank you to my family – all of you. We are a large and *very* non-traditional group and, despite it all, I always felt nothing but love and support from each and every one of you. Thank you for believing in me, thank you for celebrating me, and thank you for listening to my scientific rants when I know you weren't always interested. I love you all.

I would like to acknowledge the use of materials in this work in Chapter 2 and 3 is a reprint of the material as it appears in The Astrophysical Journal. The co-author Asantha Cooray directed and supervised research which forms the basis for the thesis/dissertation. I also acknowledge support from NASA Program GO 15464, the Ford Foundation Dissertation Fellowship, and the Eugene Cota Robles Fellowship.

Co-authors of this research were supported in part by NASA grants NNX15AQ06A and NNX16AF38G, research from *Hubble* Space Telescope programs HST-GO-14083.002-A and HST-GO-13718.002-A, NSF grants AST-131331, AST-1714528 and AST-1814034, an STFC Ernest Rutherford Fellowship (ST/P004784/2), the University of Texas at Austin College of Natural Sciences, the Research Corporation for Science Advancement for a 2019 Cottrell Scholar Award sponsored by IF/THEN, an initiative of Lyda Hill Philanthropies, the Spanish Ministry of Science, Innovation and Universities (MICIU) under the 2014 Ramn y Cajal program RYC-2014-15686 and AYA2017-84061-P, the later one co-financed by FEDER (European Regional Development Funds).

This research is based on observations made with the NASA/ESA *Hubble Space Telescope* obtained from the Space Telescope Science Institute, which is operated by the Association of Universities for Research in Astronomy, Inc., under NASA contract NAS 526555 (Program GO 15464). This work is based [in part] on observations made with the *Spitzer Space Telescope*, which was operated by the Jet Propulsion Laboratory, California Institute of Technology under a contract with NASA. This work makes use of the following ALMA data: 2013.1.00449.S, 2013.A.00014.S, and 2013.1.00449.S. ALMA is a partnership of ESO (representing its member states), NSF (USA) and NINS (Japan), together with NRC (Canada), MOST and ASIAA (Taiwan), and KASI (Republic of Korea), in cooperation with the Republic of Chile. The Joint ALMA Observatory is operated by ESO, AUI/NRAO and NAOJ. The National Radio Astronomy Observatory is a facility of the National Science Foundation operated under cooperative agreement by Associated Universities, Inc. This research has also made use of data from HerMES project. HerMES is a *Herschel* Key Programme utilizing Guaranteed Time from the SPIRE instrument team, ESAC scientists and a mission scientist. The HerMES data was accessed through the *Herschel* Database in Marseille (HeDaM - http://hedam.lam.fr) operated by CeSAM and hosted by the Laboratoire d'Astrophysique de Marseille. HerMES DR3 was made possible through support of the *Herschel* Extragalactic Legacy Project, HELP (http://herschel.sussex.ac.uk). This research made use of Astropy,[1] a community-developed core Python package for Astronomy [12, 11].

[1]http://www.astropy.org

VITA

Arianna S. Long

RESEARCH INTERESTS

Massive galaxy evolution, submillimeter galaxies, galaxy (proto)cluster formation, galaxy and black hole co-evolution, building inclusive STEM spaces

EDUCATION

Doctor of Philosophy in Physics 2022
University of California, Irvine
Advisor: Dr. A. Cooray

Masters of Science in Physics & Astronomy 2017
California State University, Los Angeles
Advisors: Dr. S. Terebey & Dr. A. Cooray

Bachelor of Science in Applied Mathematics, Minor in Computer Science 2014
Towson University

PUBLICATIONS

Long, Arianna S., et al. 2022. *Missing Giants: Dusty, Star Forming Galaxies as Drivers of Massive Galaxy Formation*. ApJ, in prep.

Casey, C. M., et al. incl. **Long, Arianna S.**, (2021). *Mapping Obscuration to Reionization with ALMA (MORA): 2 mm Efficiently Selects the Highest-Redshift Obscured Galaxies*, ApJ, accepted, arXiv:2110.06930

Lambrides, E, et al. incl. **Long, Arianna S.**, 2020. *Merger or Not: Quantifying Human Biases in Identifying Galactic Merger Signatures*. ApJ, 919, 43

Chan, A., **Long, Arianna S.**, and Cooray, A. 2021, *Characteristics of an Extreme Dusty Star-forming Galaxy at* $z = 4.5$, RNAAS, 5, 5

Champagne, J., et al. incl. **Long, Arianna S.** 2021. *Comprehensive Gas Characterization of a* $z = 2.5$ *Protocluster: A Cluster Core Caught in the Beginning of Virialization?* ApJ, 913, 110

Zavala, J, et al. incl. **Long, Arianna S.** 2021, *The Evolution of the IR Luminosity Function and Dust-obscured Star Formation in the Past 13 Billion Years*. ApJ, 909, 165

Long, Arianna S., et al. 2020, *Emergence of an Ultra-Red, Ultra-Massive Galaxy Cluster Core at* $z = 4$. ApJ, 898, 133L

Ma, J., Cooray, A., Nayyeri, H., **Brown, Arianna S.**, et al. 2019, *Spitzer Catalog of Herschel-Selected Ultrared Dusty, Star-Forming Galaxies*. ApJS, 244, 30

Brown, Arianna S., et al. 2019, *Infrared Contributions of X-Ray Selected Active Galactic Nuclei in Dusty Star-Forming Galaxies*. ApJ, 871, 87

Ma, J., **Brown, Arianna S.**, et al. 2018, *SOFIA/HAWC+ Detection Of A Gravitationally Lensed Starburst Galaxy at* $z = 1.03$. ApJ, 864, 60

AWARDS, GRANTS, & FELLOWSHIPS

NASA Hubble Fellowship Program: Hubble Fellow	2022
NSF Astronomy & Astrophysics Postdoctoral Fellowship (declined)	2022
Ford Foundation Dissertation Fellowship	2021-2022
AAS National Osterbrock Leadership Program Grant, $48k	2020
UCI School of Physical Sciences: Women in Natural Sciences Award	2020
Nomination: UCI's Most Promising Future Faculty Award	2020
UCI Physics & Astronomy: Outstanding Contributions to the Department	2019
UCI Tom Angell Fellowship for Excellence in Mentorship	2019
Honorable Mention: Ford Foundation Predoctoral Fellowship	2019
UCI Eugene Cota-Robles Graduate Fellowship	2017-2022
Honorary Fellow: UCI-NSF Machine Learning & Physical Sciences Program	2017-2019
UCI Doctoral Diversity Fellowship	2017
Travel Grant: Women in Astronomy IV	*June* 2017
Cal State L.A. Emeriti Association Fellowship	2016-2017
NASA DIRECT-STEM Scholarship Program & Research Internship	2015-2017
Computing, Sciences, And Mathematics in College Scholars Scholarship	2012-2014

OBSERVING EXPERIENCE

W.M. Keck Observatory: MOSFIRE, 5 nights	2022*A*
W.M. Keck Observatory: LRIS, 2 nights	2022*A*
JWST: 200h, Cycle 1 ID 1727 (Co-I)	2021
ALMA Observatory: 25h, Cycle 7 2019.1.01257.S (Co-I)	2019
W.M. Keck Observatory: NIRC2 LGS/AO, 2 nights	2019*B*
***Hubble Space Telescope*: 8 orbits, Cycle 25 GO-15464, $64.3k (PI)**	2018

W.M. Keck Observatory: NIRC2 LGS/AO, 1 night 2017*A*

PROFESSIONAL TALKS

∗ = invited, all talks unless otherwise noted

∗University of Kansas Astronomy & Space Physics Seminar	*Apr* 2022
∗Kavli Institute for Cosmological Physics at U. Chicago Seminar	*Oct* 2021
∗Cosmic Dawn Center (DAWN), Copenhagen	*Sept* 2021
∗JHU & Space Telescope Galaxies and AGN Seminar	*Sept* 2021
∗UW Madison Astronomy Seminar	*May* 2021
∗UC Davis Astronomy Seminar	*May* 2021
∗Harvard CfA Galaxy Cluster Seminar	*Apr* 2021
National Society of Black Physicists	*Nov* 2020
∗UC Berkeley Astronomy Lunch Seminar	*Oct* 2020
∗Protoclusters: Galaxies in Confinement Workshop	*Sept* 2020
NOAO Dusting the Universe Conference (poster)	*Mar* 2019
UCI Reines Lecturer Student Seminar	*Mar* 2019
UCI-NSF Machine Learning and Physical Sciences Annual Conference	*June* 2018
NASA DIRECT-STEM Annual Conference	*May* 2018
UCI Summer Research Symposium (talk)	*Aug* 2017
∗MIRO Principal Investigator Meeting (poster)	*May* 2017
CSU Statewide Student Research Competition	*Apr* 2017
CSULA Annual Student Research Symposium (1st place)	*Feb* 2017
229th AAS Meeting (poster)	*Jan* 2017
Satellites & Education Conference XXIX	*Aug* 2016
228th AAS Meeting (poster)	*June* 2016
CSU Statewide Student Research Competition	*Apr* 2016
CSULA Annual Student Research Symposium (1st place)	*Feb* 2016

ADVISING & LEADERSHIP

Advising:

Amy Ralston (UCI grad, 2020-2021)

LeAnn Liu (UCI undergrad, 2020-2021)

Alyssa Chan (UCI undergrad, 2020-2021)

Hunter Connors (UCI undergrad, 2019-2020)

Program Development & Leadership:

Chief Program Officer - VanguardSTEM *Jan* 2022-*current*

Guerilla Mentoring Director - VanguardSTEM *June* 2021-*Jan* 2022
An online mentoring program for women of color in STEM.

Program Coordinator - League of Underrepresented Minorities *Jan* 2021-*current*
An online peer mentoring and professional development program for women of color academics in astronomy. Website: sites.bu.edu/luma/

Co-Founder - UCI Physics & Astronomy Community Excellence 2018-∞
A multifaceted peer mentoring program for undergrads, grads, and postdocs.
We're funded now! Website: uci-pace.github.io //

DIVERSITY, EQUITY, & INCLUSION WORKSHOPS & SEMINARS

: ∗ = invited

∗Speaker - AGEP-Graduate Research Supplement (GRS) Conference *Aug* 2021

∗Speaker - KU Multicultural Scholars Program - Inspiring Scholars *Apr* 2021

∗Workshop - APS National Mentoring Community Conference *Feb* 2021
Workshop Title: *Building a Mentor Network for Intersectional Identities*

∗Writer - #VanguardSTEM National Mentoring Month *Jan* 2021

∗Workshop - UCI LEADS Undergraduate Program *Oct* 2020
Workshop Title: *Methods for Mitigating Imposter Syndrome*

∗Workshop - UCI Competitive Edge Graduate Student Program *Aug* 2020
Workshop Title: *Building A Mentor Network*

UCI Inclusive Excellence Inaugural Cohort Certificate Program *Aug* 2020

∗Workshop - APS National Mentoring Community Conference *Feb* 2020
Workshop Title: *Departmental Inclusivity Resources*

Lead & Panelist - APS/UCI Conference for Undergraduate Women in Physics *Jan* 2020

Poster Presentation - Inclusive Astronomy 2 Conference *Oct* 2019

Graduate Student Rep - UCI P&A Inclusive Excellence Committee 2018-2020

Graduate Student Rep - UCI P&A Graduate Admissions Task Force 2018-2020

PROFESSIONAL SERVICE

LOC Member - APS/UCI Conference for Undergraduate Women in Physics *Jan* 2020
Graduate Student Representative - UCI Inclusive Excellence Committee 2017-2020
Professional Development Chair & Facilitator - UCI Physics Grad Caucus 2017-2019
Co-I & Community Discussion Lead - UCSC Osterbrock Sierra Conference 2017-2018

TEACHING & OUTREACH

Scientific American - Featured Print Article *Jan* 2021
Title: Ancient Galaxy Clusters Offer Clues about the Early Universe
University of Kansas: Intro to Astronomy - Guest Speaker *Nov* 2020
Parsing Science Podcast Guest *Nov* 2020
UCI Physics 7LD / Electricity & Magnetism Teaching Assistant *Summer* 2020
ISEE PDP Pedagogy Program (*canceled due to COVID-19) 2020
Contributing Writer - *MERCURY* by the Astronomical Society of the Pacific 2019
Invited Judge & Speaker - CSULA Annual Student Research Symposium *Feb* 2018
Graduate Panelist - CalBRIDGE Workshop *Feb* 2018
Co-Organizer & Co-Host - UCI Eclipse Party *Aug* 2017
Invited Keynote - Satellites & Education Conference XXX *July* 2017
Virtual Speaker - DreamWakers 2017-∞
Physics II Curriculum Developer - Journal of Visualized Experiments 2016-2017
Volunteer & Technical Instructor - Black Girls Code, Los Angeles 2016-2018

ABSTRACT OF THE DISSERTATION

Taming Giants:
Studies on the Growth, Regulation, and Evolution of Dusty, Star-Forming Galaxies in the Early Universe

By

Arianna S. Long

Doctor of Philosophy in Physics

University of California, Irvine, 2022

Professor Asantha Cooray, Chair

Half of all cosmic starlight is obscured by dust and re-radiated at cooler, infrared wavelengths. The majority of stellar mass is built in these dust-obscured regions at $z > 0.5$ – with the most extreme manifestation taking place in a rare population of galaxies: dusty, star-forming galaxies (DSFGs). DSFGs form stars at extreme rates ($\sim 10^{2-3}\,M_\odot\,yr^{-1}$), becoming extremely massive ($M_* \geq 10^{10}$) in just a few hundred million years. Prodigious star formation generates abundances of dust that obscures starlight, making some DSFGs nearly invisible to even the deepest rest-frame ultraviolet and optical surveys. Though rare in the local Universe, DSFGs are a thousand times more populous at $z \sim 1-3$. What is their evolutionary fate and what might their descendants look like today? In my doctoral research, I led detailed case studies, large statistical analyses, and I developed an empirically-based numerical model to uncover critical insights into the answers of these questions. I focus on constraining the stellar growth and evolution of DSFGs discovered with the *Herschel Space Observatory*, complemented by data from the *Chandra X-ray Observatory*, *Hubble Space Telescope* (HST), *Spitzer Space Telescope*, and other ground-based telescopes.

First, I present a detailed case study on a protocluster of DSFGs found at $z = 4$, the Distant Red Core (DRC). In this work, I presented the first measurement of both the stellar *and* cold gas content in a massive, $z > 3$ protocluster, and determined that this protocluster occupies an exceptionally massive

dark matter halo ($\gtrsim 10^{14}\,M_{\odot}$), potentially in tension with a simple ΛCDM cosmological model. I forward evolved the protocluster members to show that these galaxies will likely become the massive quiescent ellipticals dominating cluster cores by $z \approx 2-3$. Then, I present my first lead-author work where I showed that there was no statistically significant evidence of star formation suppression in dusty galaxies with actively growing black holes when compared to those without. This implies that feedback and heating from actively growing supermassive black holes may not be the primary mechanism that shuts down of star formation in massive galaxies at $z > 1$. I also derived the first statistically significant quantification of black hole versus star-forming emission as a function of wavelength, which can be used to argue for/against certain photometric filters as "pure" star-formation indicators in distant, dusty galaxies. Finally, I present my latest in-progress work where I use empirical data on dusty star-forming galaxies to create a novel, numerical model that re-shapes the primary function describing stellar mass assembly in the Universe: the stellar mass function. Using the infrared luminosity function as a nearly-complete census of dust-obscured galaxies, I built a Markov Chain Monte Carlo model that infers the stellar masses of mock populations of dusty galaxies throughout cosmic time. Current results show that the massive end ($M \geq 10^{11}\,M_{\odot}$) of the most robust galaxy stellar mass functions in the literature are deficient by up to an order of magnitude; this is of major concern for galaxy evolution models, which often invoke extreme feedback prescriptions (e.g. AGN) to prevent galaxies from growing much beyond this pivotal mass. Using simple assumptions to forward evolve these mock DSFGs, I demonstrate that massive DSFGs at early times can evolve to match the observed population densities of massive quiescent galaxies at later times, and are therefore the likely dominant ancestral population. Many of the results and predictions presented in this thesis are immediately testable with with uniformly-selected galaxy samples from Cycle 1 *JWST* GTO / ERS programs.

Chapter 1

Introduction

1.1 Preface

During the course of my graduate career, I've been incredibly fortunate to receive training and opportunities to explore various paths in science communication. Out of all of the podcasts, public speaking events, and other sci-comm opportunities, writing in particular stood out as a passion of mine. Since the start of my PhD, I've written several articles for science enthusiasts, primarily published in the Astronomical Society of the Pacific's *Mercury Magazine* and even once for the hard-copy version of *Scientific American*. Thus, I dedicate this introduction to these works, and to those who are interested in astronomy without the technical background.[1] For scientists seeking a more in depth introduction to my works, you may find them in Chapters 2-4.

[1] I was not the first to do this, and I thank Katy RW for the idea.

1.2 Why Dust Matters

"We're made of star-stuff."

In 1980, Carl Sagan made this statement on public television in his show Cosmos. This quote rippled through generations, inspiring future scientists and backyard observers for years to come. In fact, upon meeting new people, many recite this Sagan quote to me, and occasionally some folks begin rolling up their sleeves to show me a corresponding tattoo. But the particular star-stuff Sagan referred to is actually less than one measly percent of a galaxy's composition. So, what is this super important star-stuff and why does it matter if there is so little of it in the Universe?

Sagan is actually referring to dust. No, not the dust that you so desperately need to wipe away from behind your computer screen (although that comes from human skin, and we humans are made of star-stuff . . . but that's beside the point). I'm talking about cosmic dust; the dust that lives in space, existing in every corner; the dust that helps create all of our stars, planets, and moons, and rains down on our planet every single second of the day. This dust is actually a lot more like soot, in both size and molecular makeup; it is structurally complex and has an organic (carbon-based) chemical composition. And, like the dust in the corners of your home, it used to be viewed as a major nuisance.

Dust grains are the perfect size to block incoming starlight. For centuries, astronomers would observe stars and galaxies using telescopes built to view the optical universe. At the optical wavelengths, which are wavelengths similar to what our human eyes can see, you will mostly see adult stars. If there is any dust in the way, even just a very small amount, that dust will absorb the visible light coming from the stars and leave you essentially blind to stars behind it. Even worse: new stars form in extremely dense, cold clouds of molecular gas where the gas can freeze onto dust particles throughout the cloud. So, if you wanted to study how stars form inside a stellar nursery using an optical telescope, you would essentially be observing the outsides of a big, dark, and opaque cloud floating in space. It wasn't until the late 1960s that astronomers began pondering

ways to see through that dust, exploring the idea that dust heated by visible starlight might re-emit that light at lower energies – i.e. infrared light.

Adapted from my 2019 Article in the ASP's Mercury Magazine "The Curious Case of Dusty, Star Forming Galaxies".

1.3 Dusty, Star-Forming Galaxies: What's in a Name?

In the 1990s, the Cosmic Background Explorer (COBE) was launched to explore the extragalactic background light at infrared and submillimeter wavelengths. Extragalactic background light is the accumulation of all of the radiation from stars and galaxies since the birth of the Universe. COBE's measurement was groundbreaking. It revealed that infrared extragalactic background light is nearly as strong as the visible background light. Naturally, astronomers wanted to link this infrared background light to galaxies. However, upon doing so, astronomers discovered that only half of the infrared background light could be explained by all of the galaxies in the known Universe at that time (remember: the majority of those galaxies were discovered only by means of visible telescopes). Combined with similar observations made previously by the IRAS telescope in the 1980s, astronomers took these results as proof that there has to exist a significant number of galaxies that are too dusty to be detected at optical wavelengths. Several years later, infrared telescope technology advanced enough to birth the Submillimeter Common-User Bolometer Array, the Spitzer Space Telescope, and the Herschel Space Observatory, among many other instruments, and the dusty veil hiding the existence of millions of galaxies in our Universe was finally lifted.

These infrared bright galaxies have many names in astronomy. Depending on how they are detected, how near or far they are, and many other characteristics, you may hear them referred to as submillimeter galaxies (SMGs), (ultra)luminous infrared galaxies (LIRGs or ULIRGs), or dusty, star-forming galaxies (DSFGs). Here, we will refer to them as DSFGs as I believe this class of

galaxy has really earned this name.

By tracing warm dust content through infrared light, we can also trace star formation activity. As new stars form deeply embedded within cold clouds of dust and gas, their bright UV and optical light warms the surrounding dusty envelope, which in turn re-radiates at infrared wavelengths. The Milky Way is forming stars at a rate of about 3 times the mass of the Sun per year. DSFGs, however, are forming stars at a rate of 100-1000 times the mass of the Sun per year, sometimes even more – hence the 'SF' part of the acronym. On average, DSFGs are 10-100 times more massive than the Milky Way but can occupy a physical volume up to 99% smaller than that of our galaxy. So, DSFGs are extremely compact, extremely massive, and extremely dusty. Why are they so extreme?

The extreme existence of DSFGs is still exotic to many astronomers. Most cosmological simulations that seek to model the formation of our Universe cannot reconcile the sheer number of DSFGs we observe today, let alone explain how they form in the first place. What we do know thus far is that DSFGs are most populous in the early and intermediate Universe, and that they tend to contain large amounts of cold gas. This is important because the early Universe was primarily neutral (i.e. cold) Hydrogen and Helium, which meant that the first galaxies to form were likely giant, gravitationally bound spheres rich with gas ready to form new stars at a rapid pace. Where you find massive, gas rich stars forming at a rapid pace, you will also find powerful (and frequent) supernovae which enrich their surroundings with heavier elements and, you guessed it, dust!

However, this fast-paced lifestyle comes at a price. Researchers calculate that these rates of star formation are unsustainable in the long term. DSFGs are projected to deplete their cold gas reservoirs so rapidly that some might not ever reach the 'spiral disk' phase of galaxy evolution, and instead turn into what we astronomers affectionately refer to as massive 'red-and-dead' elliptical galaxies, galaxies that have little to no gas and are no longer forming any new stars. Some astronomers believe DSFGs undergo several major mergers with each other early on, and that's how some DSFGs seem to have such massive amounts of gas and dust and non-disk-like shapes. However, the evolution of DSFG morphology is still a topic of heated debate, likely containing

some complex combination of several theories, so I leave this part to the whims of your imagination.

While we have observed many DSFGs at far-infrared and cooler wavelengths, we still need observations in other parts of the spectrum to fully understand their properties. Additionally, there are many observational hurdles to overcome. For example, many DSFGs are seen as they were in the earlier Universe, when galaxies were more populous and galaxy mergers more frequent. Depending on the sensitivity of a given telescope, two galaxies merging while flinging around cold gas and dust may look like one big blob-like galaxy, two distinct galaxies, or maybe even just one of the galaxies is bright at that given wavelength but the other one isn't due to different evolutionary stages or chemical compositions. These observational effects can greatly limit our understanding of DSFG populations. Thus, many astronomers, including myself, are exploring ways to use multi-wavelength observations to overcome these hurdles so we can better understand the strange existence and evolution of DSFGs.

Adapted from my 2019 Article in the ASP's Mercury Magazine "The Curious Case of Dusty, Star Forming Galaxies".

1.4 Black Holes and Galaxies: A Gravitational Love Story

Black holes are possibly the most unique objects in the universe, partly because they are only influenced by gravity, not radiation. In fact, that's what makes them 'black' — their incredible mass has such a strong gravitational pull that even the light whizzing by it from nearby stars gets sucked in. This mass is believed to be one of the main 'cogs' in the wheel of our galaxy, helping to keep it all together. But the real consequences of living a supermassive black hole life can only be understood on time scales that our human lives can't grasp.

If you think of the age of the universe as a calendar year with the Big Bang occurring on Jan. 1 at 12 a.m. and our current present day being 11:59 p.m. on Dec. 31, galaxies and black holes

started forming somewhere around Jan. 22. Unfortunately, there is still a heated debate as to how the first black holes formed: some believe they have to be the remnants of the first stars after they ran out of fuel and went supernova, whereas others believe some black holes could form almost instantaneously if there was enough gas in a confined space to collapse in on itself. It's likely a combination of both and, as the field of gravitational wave astronomy blossoms, we hope to have a better, more specific idea in the near future.

Either way, one thing is for sure in our current day picture, where you find a supermassive black hole, you will also find a galaxy. We take this as surefire evidence that supermassive black hole and galaxy evolution are intimately tangled together. Like any symbiotic relationship, one must wonder: what does each party get out of this? We know supermassive black holes are part of the glue that keeps a galaxy together, but what does the galaxy give to the black hole? The answer: mass.

When a supermassive black hole is growing by actively consuming nearby matter, be it dust, gas, or unfortunate nearby stars, we refer to it as an active galactic nucleus, or AGN. Now, occasionally, a cloud of gas flies into Sgr A*, but otherwise the stars around our own supermassive black hole are in a generally stable orbit, much like the planets orbiting the Sun in our solar system. So, Sgr A* is not, by definition, an AGN. At least not right now.

It takes a lot to be classified as an AGN; specifically, it takes a lot of radiation. In fact, typical AGN emit more radiation across the entire electromagnetic spectrum than all of the stars in its host galaxy combined. This makes AGN individually the most powerful objects in the universe. All that power beaming out from such an incredibly tiny region within a galaxy means that when we go to observe that galaxy at any wavelength, the image is often dominated by a very bright, tiny dot at the center (hence the term 'nucleus'). And hiding in that nucleus is a supermassive black hole surrounded by hot gas and dust rushing towards an imminent fate.

But how did the gas and dust get there in the first place? Gravity.

The first black holes and galaxies in the universe were likely smaller than our Milky Way today. They grew over time as they merged together, driven by their mutual gravitational attraction. Simulations of these merging scenarios detail beautiful tangos where galaxies swing past one another, barely touching the first few times, but eventually slamming into each other forming one single larger galaxy that comes complete with a single larger black hole. The new supermassive black hole has a larger appetite due to its larger mass. As the dust literally settles within the new galaxy, it's dragged toward the nucleus where a looming beast awaits its feast.

The gas and dust get closer to the black hole, orbiting faster and faster, getting squeezed into the shape of a disk by angular and gravitational forces. This disk is the metaphorical feedbag of the black hole, providing all the matter it needs to consume and grow. The disk is also incredibly hot, creating lots of ultraviolet and X-ray emission, and its ultra-fast circular motion blasts hot winds of radiation across the entire galaxy.

All this dust-dragging and radiation-blasting is great for the supermassive black hole, but it comes at a price. The matter that was dragged into the nucleus could have instead helped form brand new stars for the galaxy. The winds blasting off the disk may disturb or sweep away potential stellar nurseries (a.k.a. clouds of cold gas and dust), again depriving the galaxy of any new star formation. In fewer cases, AGN produce two very powerful opposing jets that shoot material out of the entire galaxy and into the void.

Simulations show that over time these effects may slow or completely prevent new stars from forming within the galaxy. If new stars don't form, then gas and dust production slow from the lack of supernovas. If gas and dust production slow, then the supermassive black hole has nothing to feed on. Theoretically, this cycle continues until either another gas-rich galaxy comes along and merges with the dying one, or until new stars stop forming altogether and the black hole is forced to live hungry and in dark isolation.

Observing the relationship between AGN and star formation is difficult. As humans, we are simply

not alive long enough to watch this interplay happen. To make matters worse, observing AGN and star formation processes is quite complex. Baby stars are hidden in clouds of warm gas and dust, and so are AGN. Thus, researchers often quantify how much star formation is going on by looking for warm dust; but, one can also judge how powerful an AGN is using similar observations. So, it's increasingly important that we learn how to best detangle the two processes when observing a galaxy far away. This allows us to get us a step closer in understanding how soon after an AGN ignites are the effects most powerful on the galaxy, and at which "point of no return" can a galaxy be officially diagnosed as dying.

Adapted from my 2019 Article in the ASP's Mercury Magazine "Black Holes and Galaxies: A Gravitational Love Story".

1.5 Galaxy Clusters: From Fireworks to Fossils

All around us in nearby space — within, say, 300 million to 600 million light-years — astronomers see dead or dying elliptical galaxies gathered in great ensembles called galaxy clusters. These clusters hold the fossilized remains of the most massive galaxies ever formed — hundreds to thousands of them slowly dancing around one another, gravitationally bound forever in their permanent graves.

But galaxy clusters present a problem for astronomers. Most clusters seem to have been established by the time the universe was only half of its current age. That means the galaxies within those clusters must have birthed most of the stars they contain early in cosmic history. It appears that these galaxies grew to the size of the Milky Way or larger but up to 10 billion years more quickly. How did they get so big, so fast, and then die so young?

To get to the bottom of this, astronomers have created simulations to understand the possible births and lives of cluster galaxies based on data from hundreds of real senior galaxy clusters nearby. This

is essentially the equivalent of taking thousands of photos of senior citizens and using physics to model what these citizens might have looked like when they were babies. As you can imagine, a lot of assumptions and theories go into these models, so we need pictures of middle-aged, teenage, and baby clusters to really test our theories. Thankfully, in the last decade, we've started filling in our evolutionary photo album with more middle-aged and teenage pictures ... but we're seriously lacking baby photos.

Galaxy cluster "babies," also known as protoclusters, can be difficult to identify because they don't have the same qualities as their descendants. Until recently, most of our methods for spotting clusters were developed to preferentially select dying elliptical galaxies or the hot gas that pervades the space between them. Elliptical galaxies and hot intracluster gas appear at the later stages of galaxy cluster evolution, so we need new methods to find their bluer, more star-forming infant counterparts. To make things more difficult, protoclusters are often spread far apart on the sky because the galaxies have yet to fully coalesce into the dense structures we see today. When our most famous and precise telescopes have cameras that span only the width of a pencil (the Hubble Space Telescope, for instance), it is not surprising that we cannot piece together protocluster puzzle pieces that are spread across the sky at distances more than 100 times greater than our telescope's field of view.

All of this means that until recently, the tools to find and study protoclusters usually missed a key population of galaxies. From the late 1990s through the early 2010s the Submillimeter Common-User Bolometer Array, the *Herschel Space Observatory*, the South Pole Telescope, and the *Spitzer Space Telescope* revolutionized our understanding of the dust-obscured universe by unveiling millions of galaxies that were previously invisible. Starting about 15 years ago, astronomers began studying the clustering properties of dusty star-forming galaxies, and they found that these powerhouses live preferentially near other large and actively star-forming galaxies. But the state of technology was still behind our ambitions; the resolution of infrared and millimeter telescopes was still so low that multiple galaxies would get blended into one large object, even if those galaxies

were far apart but lay along the same line of sight. The age of the infrared universe was here, but we needed sharper and more sensitive instruments to fully comprehend what we were seeing.

Finally, in 2013, the Atacama Large Millimeter/submillimeter Array (ALMA) arrived. High in the Chilean desert, this collection of nearly 70 radio dishes works together as a single telescope, reaching resolutions up to 600 times sharper than that of the *Herschel* telescope. The observatory is excellent at detecting dusty, gaseous stellar nurseries throughout star-forming galaxies. With it, astronomers have begun discovering early protocluster systems that are both shocking and exciting.

These corners of space are violent. They are overabundant with rare, extreme galaxies like DSFGs and AGN, with visibly disturbed shapes from violently merging with their neighboring galaxies. Galaxy merging is believed to trigger extreme bursts of star formation as huge reservoirs of gas collide. According to detailed simulations, these processes are also believed to accelerate galaxy evolution, bringing the senior lifestyle to the cluster galaxies at a much more rapid pace than their isolated peers.

The protoclusters are also already shockingly massive. When weighing all of the components (stars, gas, and dark matter), we find that some of these protoclusters are so massive that they nearly violate the laws of the most massive allowable object in the Universe. (Dark matter is the most abundant form of matter in any given galaxy and in the universe as a whole. All galaxies and clusters are thought to be surrounded by blobs, or halos, of this mysterious stuff. And although it is invisible and poorly understood, dark matter leaves a clear gravitational signal. There are a variety of ways to infer the amount of dark matter in a given astronomical object, and to cover those methods would require several additional theses.) Although there are healthy margins of error on these calculations, the discrepancies look even worse when we consider the fact that some of these observations are capturing only a small percentage of the likely galaxy cluster members; there are probably more galaxies in these protoclusters that were simply out of the narrow field of view of our telescopes and thus not included in the calculations. These mismatches will most likely grow as we continue surveying and studying these protoclusters.

Our investigations on extreme and early protoclusters force us to reconsider our understanding of galaxy cluster formation. Because the galaxies in clusters are likely to be some of the first galaxies ever, we must determine how such massive objects can form so quickly. Doing so is not just an issue of constraining the physical mechanics and chemistry of star formation inside the first galaxies. It is also a matter of investigating the timing of the conditions that lead dark matter to gravitationally collapse into halos, seeding galaxies. Is it possible that galaxies and structure began forming earlier in the universe than we thought? What does that mean for our understanding of the formation of the first elements? Could these galaxies have forged the right ingredients to build stars with habitable planets around them — and perhaps hosted some of the first forms of life in the universe?

Some of these questions probably will not be answered during my lifetime, but I and other astrophysicists are working hard and fast to address the others. Already we are carrying out more observations of these known protoclusters across the electromagnetic spectrum. We are also developing new methods for identifying large samples of dusty protocluster candidates. With more examples, we may be able to determine whether DSFG-rich protoclusters represent examples of a common, yet previously invisible, phase of galaxy evolution that all clusters go through or just rarities. Observers and theorists are forming new collaborations to learn how early in the history of the Universe conditions were right for protoclusters akin to those we have discovered — pockets of space overdense with tremendous rates of star formation and outsized masses.

The best way to test our physical models is to look at extremes. In the next few years these colossal congregations of exceptional galaxies will be putting humanity's grasp on the cosmos to the test.

Adapted from my 2021 Article in the Scientific American "Ancient Galaxy Clusters Offer Clues about the Early Universe" and my 2019 article in the ASP's Mercury Magazine "Why Do Galaxies in Large Clusters Age Prematurely?".

Chapter 2

A Case Study at $z = 4$ - Long et al. 2020

2.1 Introduction

Environmental impacts on galaxy evolution are best understood at $z < 2$. In observational studies on the local Universe all the way out to $z = 1.5$, galaxy clusters are known to host excess populations of red and massive galaxies when compared to coeval field counterparts [229, 402, 298, 393, 337, 224]. In order to form these massive, quiescent populations, studies suggest that clusters must form the majority of their mass ($\sim 50\%$) and initiate rapid quenching by $z = 2$ [e.g. 70, 297, 313], which means clusters at $z \gtrsim 3$ should host many actively star-forming galaxies [67, 63]. Unfortunately, observational selection biases bear inconclusive results on whether there exists an excess of star-formation activity in early cluster environments at $z > 2$ [e.g. 363, 205, 68]. This is likely due to the fact that the methods originally developed to find clusters were inherently built to detect near-virialized clusters at $z \lesssim 2$ with strong red sequences already in place [e.g. 141, 319, 112, 329, 61] and/or evidence of a hot X-ray emitting intracluster medium [e.g. 319, 271, 415, 31].

Full characterization of $z > 3$ early cluster, aka protocluster [294], environments is vital to our efforts in understanding several cosmological processes, including the collapse of filamentary

structures [e.g. 387], the formation and assembly of massive halos in ΛCDM [e.g. 369, 162], and the births of the most massive galaxies in the Universe: brightest cluster galaxies [e.g. 88, 310, 69**?**]. Currently, most protoclusters cataloged at $z > 3$ are discovered and characterised based on their rest-frame optical/UV emission owing to their selection techniques (e.g. systematic narrow-band/spectroscopic searches for overdensities of Lyα emitters, Hα emitters, and/or LBGs [e.g. 396, 78, 44, 205, 222, 173]). However, these techniques are blind to a rare but important phase of massive galaxy evolution that contributes immensely to cosmic star formation: dusty, star-forming galaxies (DSFGs, see Casey, Narayanan and Cooray 2014 [51] for a review; see also HAE229 in [99, 82], and [83]).

Recent far-IR and sub-millimeter observations have uncovered populations of dusty, star-forming galaxies residing in overdense environments at $z > 2$ [e.g. 136, 58, 82, 65, 48, 388, 184, 264, 143, 160, 209]. Their incredible bursts of star formation over short periods of time at high-z makes DSFGs ideal candidates for driving rapid stellar mass build up at $z > 3$ in protoclusters, before the widespread onset of a red sequence is in place. The strong presence of DSFGs in these overdensities is not a coincidence, but likely a key part of protocluster evolution [47].

Detailed multiwavelength characterization has been carried out at the individual galaxy level for many $z \lesssim 3$ nearly-virialized protoclusters with DSFGs [e.g. 357, 48, 388, 83], but most newly discovered $z \gtrsim 3$ protoclusters with DSFGs either (a) have only a handful (1-3) of these rare starbursts [78, 44, 403, 300], (b) are DSFG-rich but with resolved observations limited to only their far-IR and sub-mm properties [264, 174], or (c) are not yet spectroscopically confirmed members of the protocluster [57, 160]. In order to fully assess the role and evolution of DSFGs in overdense environments (e.g. are they the primary progenitors of BCGs or other massive spheroidals seen in modern day clusters?), we must seek and then explore the properties of these rare and extreme environments across the energy spectrum.

The work presented here is the first to link resolved stellar emission with cold dust and gas from star-forming regions in a spectroscopically confirmed $z = 4$ protocluster rich with DSFGs. We

combine high-resolution *Hubble Space Telescope* (*HST*) data, deep Gemini FLAMINGOS-2 data, and deep *Spitzer* IRAC observations to probe the rest-frame UV of an extremely dense protocluster core spectroscopically confirmed at $z = 4.002$ with the *Atacama Large Millimeter/sub-millimeter Array* (ALMA): the Distant Red Core (DRC). The DRC was identified by Ivison et al. 2016 [191] as the single reddest source in a systematic search for high-z, extreme star-forming systems in the $\approx 600\,\mathrm{deg}^2$ *Herschel* Astrophysical Terahertz Large Area Survey [*H*-ATLAS, 110] based on "red" *Herschel* SPIRE flux densities ($S_{500} > S_{350} > S_{250}$, [191, 9]). Follow up APEX LABOCA 870 μm imaging across a 10′ field confirmed a significant ($2.15^{+0.8}_{-0.5}$) overdensity of DSFGs [228], and subsequent ALMA 2-3 mm spectroscopic scans on the two brightest 870 μm emitters resolved an astounding 10 DSFGs at $z_{spec} = 4.002$ within a $260\,\mathrm{kpc} \times 310\,\mathrm{kpc} \times 87\,\mathrm{Mpc}$ region [293, see also [131]], making the DRC core one of the rarest and most dense concentrations of DSFGs known at high-z (see [264] for a similar structure at $z = 4.3$).

In Section 2.2, we present multiwavelength data and counterpart identification; in Section 2.4, we describe the spectral energy distribution (SED) fitting process; in Section 2.5 we present our results comparing individual protocluster members to field galaxies, and in Section 2.6 we discuss the DRC in context of global galaxy cluster evolution; we summarize our conclusions in Section 2.7. Throughout this paper, we adopt a cosmology of $\mathrm{H}_0 = 70\,\mathrm{km\,s^{-1}\,Mpc^{-1}}$, $\Omega_M = 0.3$, and $\Omega_\Lambda = 0.7$.

2.2 Observations

2.2.1 HST WFC3

In *HST* Cycle 25, we used the F125W filter to observe a subset of eight ultra-red *Herschel* objects with precise coordinates from ALMA observations and clear *Spitzer* IRAC counterparts (PID: 15464, PI: A. Brown). We used a four-point dither pattern with a 653 s exposure per frame, achieving a total on-source integration time of 43.5 minutes over the F125W band. We use

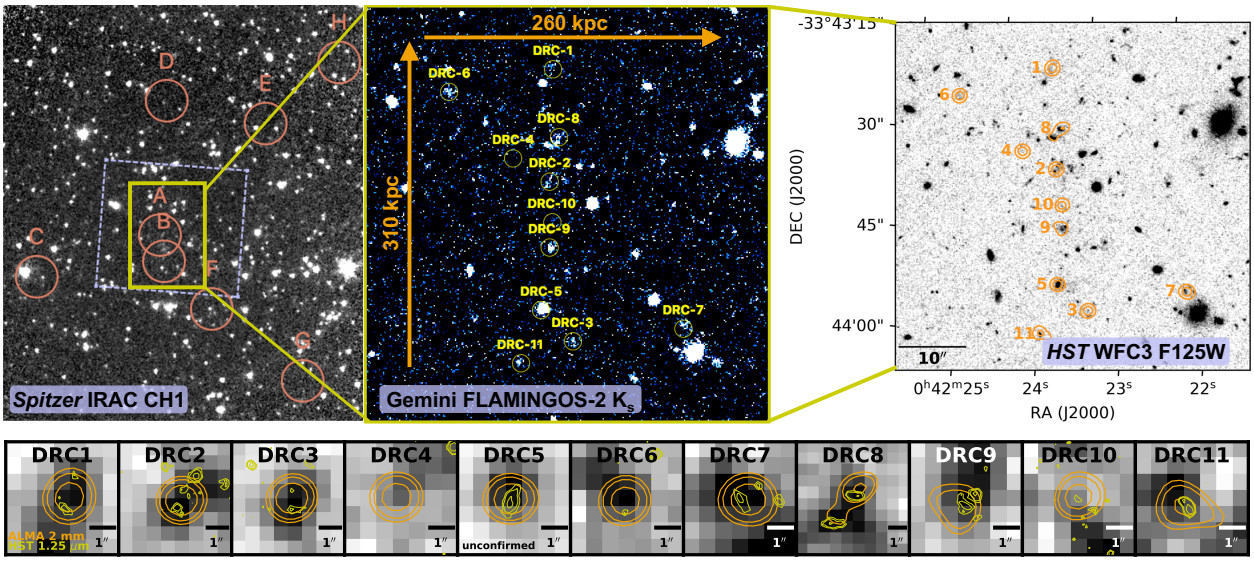

Figure 2.1: *Top*: On the left is a zoomed out *Spitzer* IRAC 3.6 μm image with the positions of other potential protocluster members outside of the DRC (objects C-H, as seen in 870 μm LABOCA imaging in [293]) circled in pink. The blue dashed box shows the *HST* 1.25 μm image footprint over the core of the protocluster (the DRC). The middle panel is a zoomed in Gemini FLAMINGOS-2 K_s-band image of the protocluster core, with ALMA positions for each DRC component encircled in green. Finally, on the right we present a zoomed in image of the DRC as seen by *HST* at 1.25 μm. Overlaid in orange are ALMA 2 mm contours at 2σ and 5σ. DRC-4 is attenuated in the Gemini and *HST* images, as is DRC-10. *Bottom*: Observed-frame *HST* 1.25 μm and ALMA 2 mm continuum contours overlaid on *Spitzer* IRAC 3.6 μm images for all DRC components (regardless of positive near-IR detection). ALMA contour levels (orange) are at 2, 3, and 5σ; *HST* contour levels (yellow) are at 2.5, 3.5, and 7σ. At $z = 4.002$, an arcsecond corresponds to a spatial scale of ~7.1 kpc. In this study, we consider objects within 1.14″ (~ 8 kpc) of the ALMA centroid to be the collective rest-frame optical/near-IR counterpart. For nearly all objects, this includes only the 1.25 μm bright objects within the shown ALMA contours, except for DRC-8 where we include the additional near-IR bright galaxy in the southwest region due to the overlapping shape of the ALMA contours. See section 2.3.2 for more details.

the final calibrated data from the Barbara A. Mikulski Archive for Space Telescopes (MAST), which is combined and corrected using the standard WFC3 reduction pipeline (`calwf3` v3.4.2 and `DrizzlePac` v2.1.21). At this wavelength (1.25 μm), we determine 3σ depths of $m_{AB} = 22.5$ on point-like sources and a PSF of 0.18″.

2.2.2 Gemini FLAMINGOS-2

In 2014, the FLAMINGOS-2 instrument on the Gemini-South telescope observed the DRC for a total of ∼4 hours in the K_s-band (PID: GS-2014A-Q-58, PI: L. Dunne). Here, we use the same reduced data presented in Oteo et al. 2018 [293] (Section 2.5, therein), which reaches a final 3σ depth of $m_{AB} = 25$ with an average seeing of 0.72″.

2.2.3 Spitzer IRAC

In Cycle 13, as part of a follow-up campaign to measure the rest-frame optical emission for 300 $z \gtrsim 4$ ultra-red DSFGs, the *Spitzer* Space Telescope Infrared Array Camera (IRAC) imaged the DRC at 3.6 μm and 4.5 μm (PID: 13042, PI: A. Cooray, see also Ma et al. 2019 [235]). Images in each band were taken over a 36-point dither pattern with a 30 s exposure per frame, achieving a total integration time of 18 minutes per band. We use the reduced post-basic calibrated data (pBCDs) from the *Spitzer* Science Center (vS19.2), achieving depths of $m_{AB} = 24$ and 26, and PST limits of 0.93″ and 1.13″, respectively.

2.2.4 Herschel SPIRE

Data Release 2 of the *H*-ATLAS survey [110, 391, 237] captured the DRC at rest-frame far-IR wavelengths. SPIRE observations were taken in parallel over the South Galactic Pole, with FWHMs

of 17.8″, 24.0″, and 35.2″ at 250, 350, and 500 μm, respectively. Ultra-red sources were selected with a 3.5 σ detection threshold at 500 μm flux densities (S_{500}) > 30 mJy, with $S_{500}/S_{250} \geq 1.5$ and $S_{500}/S_{350} \geq 0.85$ [191]. We refer the reader to [191], [391], and [237] for extensive details on observations and source extraction, and to Section 2.3.3 for details on deblending *Herschel* SPIRE data.

2.2.5 ALMA

As presented in Oteo et al. 2018 [293], successful spectroscopic confirmation of DRC members required several spectral scans using the *Atacama Large Millimeter Array* (ALMA) to unambiguously detect more than one emission line. We refer the reader to [293] for the full chronicle, and briefly summarize the data used in this work below.

The DRC core has a spectroscopic redshift of $z_{\rm spec} = 4.002$, determined via ALMA 2 mm spectral scans (PID: 2016.1.01287.S, PI: I. Oteo) carried out over two pointings, with an average synthesized beam size of 1.6″. All sources but DRC-5 were spectroscopically confirmed via detection of ^{12}CO(6–5) emission, and up to four additional emission lines detected for some of these objects (including [C I](1–0), $H_2O(2_{11} - 2_{02})$, ^{12}CO(4–3), and ^{12}CO(2–1); PID: 2013.1.00449.S, P.I. A. Conley; PID: 2013.A.00014.S, PI: R.J. Ivison; and PID: 2013.1.00449.S, PI: R.J. Ivison). At z = 4.002, the respective field of view for the 2 mm mosaic is roughly 675 kpc × 433 kpc with a physical synthesized beam size of 11.4 kpc; thus, these sources are unresolved at sub-mm wavelengths (with the exception of DRC-1 which was imaged with 0.12″ resolutions at 870 μm in PID: 2013.1.00001.S, PI: Ivison; this data is not included in this analysis).

2.3 Photometry and Counterpart Selection

Here we review the photometry and counterpart selections used in this analysis. In Section 2.3.2, we discuss how we carry out near-IR counterpart identification for each DRC component, and in Sections 2.3.4 and 2.3.3, we discuss the deblending techniques used to derive fluxes for each DRC component in the *Spitzer* IRAC data *Herschel* SPIRE data, respectively. The resulting photometry is tabulated in Table 2.1 and 2.2.

2.3.1 Near-Infrared Photometry

For all observed-frame near-IR data (*HST*, Gemini, and *Spitzer*), we use the SOURCE EXTRACTOR package [24] in single-image mode to identify objects, and assign total fluxes based on `FLUX_ISO` values, as many sources had disturbed morphologies not easily identified by elliptical projections. We compare our photometry for several stars also in the 2MASS catalogs [350] and find a $< 10\%$ difference in flux density estimates. In the following paragraph, we discuss the signal-to-noise limits employed throughout this work.

For *HST* data, we measure 9/11 DRC sources at S/N $\gtrsim$ 2. In this band, only 5/11 sources have S/N > 3; we choose to keep the additional four objects with $3 >$ S/N $\gtrsim 2$ as these objects are clear (S/N $= 4 - 5$) detections at in the K_s band (2.2 μm), and the positional offsets between the sources as seen in the F125W and K_s filters are $\leq 0.4''$ (which is ~1-2 pixels or less in the Gemini image). For the deeper FLAMINGOS-2 data, we detect 9/11 DRC objects at S/N > 3, with the remaining two objects, DRC-4 and 10, at S/N < 2 (which is consistent with HST). In the 3.6 μm and 4.5 μm *Spitzer* images, 8/10 and 9/10 DRC components are detected at S/N > 3, respectively. However, 6/10 of these objects are blended with neighboring sources. In Section 2.3.4, we describe the process for deblending the IRAC counterparts with their neighbors.

2.3.2 Identifying HST and Gemini Counterparts

Upon inspection, many DRC members break apart into several rest-frame UV ($\lambda = 2500$) counterparts within their respective ALMA contours, several of which exhibit clumpy and/or interacting morphologies (Figure 2.1). These morphologies are expected for the majority of galaxies at high-redshifts ($z > 1$), due to increased merger fractions and star formation activity during this epoch of the Universe [e.g. 72, 392, 117, 118, 1, 89, 35, 343, but see also [178]]. Moreover, studies suggest that the bright sub-mm flux from DSFGs hails not just from isolated starbursts, but also from merger-induced starbursts and/or pairs of galaxies (not necessarily individually bursting) undergoing a spiral infall [154, 85, 182, 145, 165, 164, 166, 354, 279, 60, 143, 71, 251] – and, in overdense regions like that of protocluster environments, there is an increased merger fraction compared to coeval field environments [146, 122, 231, 175].

Considering the aforementioned evidence, and the large ALMA beam sizes relative to the HST resolution, we decide to treat each ALMA object as it's own global physical star-forming system, capturing all observed-frame near-IR bright objects within a physically motivated radius on the order of galactic scales: ~ 8 kpc ($1.14''$ at $z = 4$, also seen in [413]). This chosen radius emits from the center of the ALMA 2 mm emission for each object, within which we deem all rest-frame UV bright objects as a cumulative counterpart. We note that, for many of the sources with multiple near-IR counterparts, the center of the ALMA emission does not align with a singular near-IR bright object. Instead, it is often centered between two or more objects, which is unsurprising considering that dust and stellar offsets are not uncommon in DSFGs [e.g. 60, 49]. The physical distance chosen ensures we capture only closely interacting pairs, individual galaxies dominated by patches of star-forming regions / giant molecular clouds, and/or systems with irregularly shaped dust and stellar offsets due to recent gravitational interactions or to strong dust extinction [seen in e.g. 413, 60, 49, 143, 71]. The only exception to this case is DRC-8 in which we choose to include the additional rest-frame UV object $\sim 2''$ to the southwest of the brightest part of the ALMA centroid as the ALMA observations appear to also detect this additional object.

For 5/11 sources (nos 1, 2, 7, 8, and 9), more than one *HST* counterpart is found within the 1.14″ (8 kpc) radius (see Figure 2.1). With the available data, we cannot definitively rule out the possibility of low-redshift interlopers in the optical/near-IR data. However, for DRC objects 1,2,7, and 8, which show multiple possibly interacting components, the FWHM of the CO(6 – 5) emission used to originally spectroscopically confirm cluster membership is extremely broad ($> 1000\,\mathrm{km\,s^{-1}}$, see Figure 2 in [293]). We interpret this as evidence that these four objects are likely ongoing merger events, and therefore the 2-3 mm continuum measurements represent star-formation triggered within the global system. Object 9 does not have the broad emission, but shows morphologies indicative of a disturbed system with possible dust offsets from the preceding interactions.

For the 5/11 sources with more than one *HST* counterpart,we sum the respective fluxes to form a total observed-frame 1.25 μm flux for each ALMA DRC component – still only including *HST* sources with S/N $\gtrsim$ 2. Uncertainties from multiple counterparts are added in quadrature. The Gemini observation, affected by seeing, is more blended than the *HST* image. So, where necessary, we repeat this exact method for multiple objects detected within the same radius in the K_s-band image, although this only applies to two sources: DRC-2 and DRC-7. As mentioned earlier in this section, DRC-8 also includes two objects in the *HST* and Gemini flux density measurements (both at S/N > 3), with the uncertainties added in quadrature.

We note that these assumptions could result in an overestimation of the stellar component in the SED fitting process, and thus we interpret the resulting properties as loose estimates and take care to include all uncertainties in our analyses and figures throughout this work.

2.3.3 Generating Respective Herschel Flux Densities

In each of the *Herschel* SPIRE images, the DRC is blended together as a single object. The protocluster was systematically selected as an "ultra-red" source based on it's rising SPIRE flux densities ($S_{500} > S_{350} > S_{250}$, [191]) believed to trace the Wien side of the far-infrared blackbody

ID	$S_{1.25\,\mu m}$ [μJy]	$S_{2.2\,\mu m}$ [μJy]	$S_{3.6\,\mu m}$ [μJy]	$S_{4.5\,\mu m}$ [μJy]	$S_{250\,\mu m}$ [mJy]
DRC-1	2.46 ± 1.03	4.16 ± 0.76	6.11 ± 1.28	5.73 ± 0.97	11.14 ± 5.54
DRC-2	8.56 ± 2.26	4.02 ± 0.86	11.21 ± 3.69	4.89 ± 1.46	16.22 ± 7.53
DRC-3	1.39 ± 0.77	5.14 ± 0.88	5.49 ± 1.64	6.60 ± 1.58	12.43 ± 5.94
DRC-4	< 1.0	< 0.40	< 2.10	< 1.29	< 7.18
DRC-5	12.98 ± 2.31	18.41 ± 0.73	19.12 ± 3.44	20.86 ± 3.54	< 3.23
DRC-6	1.64 ± 0.83	4.62 ± 1.16	4.62 ± 0.74	3.80 ± 0.53	< 6.59
DRC-7	7.32 ± 1.76	4.34 ± 0.58	6.67 ± 1.60	6.86 ± 1.37	< 3.63
DRC-8	16.89 ± 3.71	3.81 ± 0.70	5.09 ± 0.99	3.20 ± 1.06	< 4.34
DRC-9	11.67 ± 2.22	3.85 ± 0.58	4.27 ± 1.28	3.74 ± 0.93	< 5.22
DRC-10	< 1.16	< 0.59	2.78 ± 0.42	1.50 ± 0.30	< 5.98
DRC-11	3.47 ± 1.19	2.82 ± 0.56	3.73 ± 0.56	2.55 ± 0.36	< 2.98

Table 2.1: Measured flux densities for each cluster member. Measurements listed without uncertainties are used as upper limits. See Section 2.3.1 and 2.3.3 for more details. DRC-5 is not spectroscopically confirmed at $z = 4.002$ like the other 10 members. We still include this object in our analyses in Sections 2.5 and 2.6, and note any impacts on the global cluster properties if DRC-5 is indeed not a true member of this cluster core. For DRC-8, we list the total combined flux for the two galaxies lying within the ALMA contours seen in the *HST* image; at 2.2 μm, the two components were recognized as one singular object.

ID	$S_{350\,\mu m}$ [mJy]	$S_{500\,\mu m}$ [mJy]	$S_{2\,mm}$ [μJy]	$S_{3\,mm}$ [μJy]
DRC-1	34.34 ± 7.59	45.23 ± 9.24	2117 ± 58	406 ± 28
DRC-2	< 15.64	< 10.35	723 ± 11	154 ± 10
DRC-3	24.85 ± 6.42	18.38 ± 9.11	659 ± 10	218 ± 22
DRC-4	< 10.28	< 7.18	347 ± 99	75 ± 17
DRC-5	< 6.67	< 3.78	295 ± 94	110 ± 12
DRC-6	< 4.55	< 4.72	282 ± 65	102 ± 11
DRC-7	< 6.25	< 8.71	176 ± 82	–
DRC-8	< 6.79	< 7.74	55 ± 10	–
DRC-9	< 5.50	< 3.21	42 ± 11	–
DRC-10	< 5.09	< 3.20	40 ± 7	–
DRC-11	< 7.21	< 4.60	39 ± 9	–

Table 2.2: Measured flux densities for each cluster member *continued*.

for galaxies at $z \gtrsim 4$. Ivison et al. 2016 [191] measured a total flux for the DRC (aka SGP-354388) of 26.6 ± 8.0, 39.8 ± 8.9, and 53.5 ± 9.8 mJy at 250, 350, and 500 μm, respectively; additional follow-up SCUBA-2 and LABOCA 850-870 μm measurements also resolved the DRC (but this data is not used in this analysis). In the following, we describe how we determine individual object flux densities or upper limits.

Using ALMA positional priors for each DRC component, we deblend the far-IR emission with the probabilistic deblender XID+ [185].[1] XID+ is a tool designed specifically to deblend SPIRE maps using higher-resolution positional priors and a Bayesian inference to obtain the full posterior probability distribution function on flux estimates.

When all 11 sub-mm bright objects are considered in the fit, the results produce flux densities < 10 mJy with S/N ~ 1 for each source. These estimates are considerably close to (or below) the reliability thresholds defined in [185] (5 and 10 mJy for 250 and 350-500 μm, respectively) and might indicate that none of these galaxies would be detected individually in *Herschel* surveys if they were separated. However, XID+ is reliant on the high-res positional priors of known dusty objects, which we have with ALMA data, and we also know that all objects (except DRC-5) sit at the same redshift; this means that objects that are brightest in the 2 mm observations are likely more massive/dust-rich than their fainter co-cluster members. Thus, we performed another deblending fit using only the six objects brightest at 2 mm - this produced similar results as the 11-object fit. Finally, when iterating XID+ on the *four* brightest 2 mm objects only (nos. 1-4), we recover the majority of the SPIRE flux with estimates above the reliability threshold and at S/N $\gtrsim 2$ significance for members 1, 2, and 3. We interpret this ensemble of fits to mean that objects 1-3 are likely the main contributors to the *Herschel* SPIRE fluxes, and that contributions from the other sources are negligible/undetectable at the shallow depths of this survey. This is also found to be true in the Smith et al. 2019 [**?**] ALMA detected cluster, where the majority of the *Herschel* and SCUBA-2 sub-mm flux was be attributed to the three (out of ten) brightest ALMA sources.

[1] http://herschel.sussex.ac.uk/XID_plus

We adopt the fluxes as detections in the SED fitting process for objects 1-3, and use the results from the first pass (that included all 11 sources) as generous upper limits in the SED-fitting process for the remaining individual galaxies. In the Appendix, we show the best-fit SEDs and discuss the galaxy properties for objects 1-3 that result from a fit using the (smaller) upper limits derived in the first XID+ pass (which used all 11 sources instead of four). In general, when using the upper limits for all sources, we find no major differences on the implications discussed in this analysis for these galaxies or for the cluster as a whole.

We note that without these SPIRE upper limits / flux density estimates, our SED models generate a much larger far-IR component for each member (with flux densities on the order of $5-10\times$ larger than what the deblended values predict). Furthermore, we find that SED fits using the deblended values produce galaxy-level properties that are within 1σ uncertainty of those found in Oteo et al. 2018 [293] (which were generated by fitting the 2 mm data to ALESS SED templates). Without them, the resulting stellar masses and dust luminosities are much greater (2-10× greater, which is unphysical in several cases). Thus, we find these upper limits and fluxes critical to our SED-fitting process.

2.3.4 Deblending IRAC Counterparts

For several objects (e.g. DRC-2, DRC-8, and DRC-9), the 3.6 μm and 4.5 μm flux is blended with nearby sources outside of the projected 1.14″ merging radius. To avoid overestimating stellar properties, we deblend the IRAC photometry using TPHOT [255, 254], a software package designed to extract and deblend photometry from low resolution images (IRAC) using high resolution priors (HST). We use SOURCE EXTRACTOR [24] to generate the relevant input catalogs and segmentation maps, then we apply SWARP [25] to both IRAC images to match the HST/F125W image pixel resolution (0.127″). Finally, we use PYPHER to generate a convolution kernel between the IRAC and *HST* PSFs. To achieve optimal performance, we ran TPHOT using FFT convolution and a

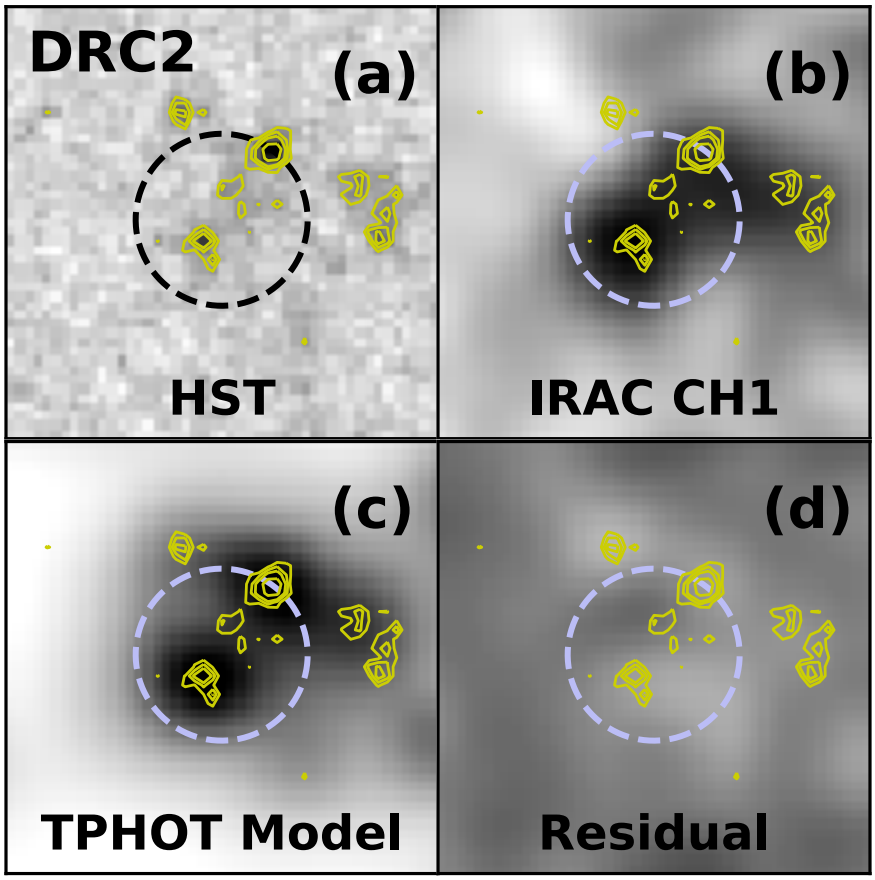

Figure 2.2: A progression example of the TPHOT modeling and deblending process for DRC-2. Contours match the *HST* contour stamps in Figure 2.1. The dashed circle represents a radius of 1.14″ in which all sources within are considered a cumulative near-IR counterpart to the ALMA centroid; this includes the source sitting on the circle for DRC-2. We use TPHOT to deblend IRAC fluxes for protocluster members that appear blended with nearby neighbors outside this radius (see Section 2.3.4 for more details). (a) is the *HST* image of the disturbed DRC-2; (b) is the corresponding *Spitzer* IRAC 3.6 μm image that's been SWARP-ed [25] to match the *HST* pixel resolution; (c) is the modeled IRAC image TPHOT creates using *HST* positional priors and a PSF convolution kernel, and (d) is the residual flux remaining after extraction of the modeled flux from the original IRAC map. We see no systemic issues in our residual maps and recover 85 – 100% of the original flux for sources with clear singular IRAC counterparts (e.g. members 5 and 7), and thus consider our deblended fluxes reliable. See Section 2.3.4 for more details.

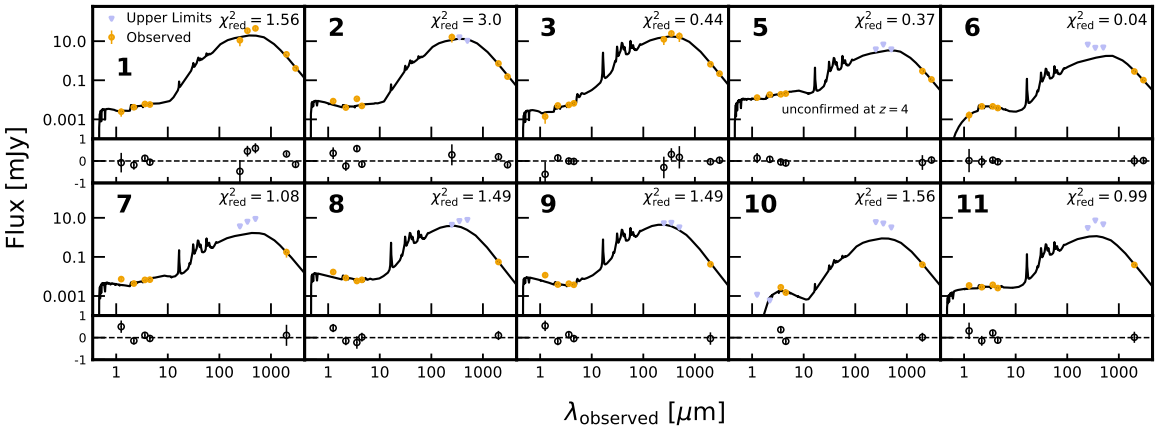

Figure 2.3: Best fit spectral energy distributions from CIGALE for each member considered in this paper. Observed fluxes (including those that are found via deblending) are plotted as orange dots, while upper limits are plotted as blue triangles. We use the combined flux densities for all *HST* and Gemini sources within 1.14″ of each of the DRC's ALMA centroids (see Section 2.3.2). In the top left is the ID for each member and in the top right is the reduced χ^2 value for each fit. Beneath each SED is the relative percent difference between the observed and model fluxes. For several sources, DRC-2 in particular, there is a visible offset between the modeled flux and the 3.6 μm measured flux; this emission is measured in a band wide enough to capture redshifted Hα flux, which is expected in excess in a highly disturbed, bursty system such as this. DRC-4 is not shown as only upper limits were measured in all bands. See Section 2.4 for SED fitting details.

cells-on-objects fitting configuration with the LU linear system solver.

Since not all objects detected in the *HST* map are also detected in the IRAC images, the exact fraction of IRAC flux recovered during the TPHOT fitting process is difficult to quantify. However, we recover 85 – 100% of the original IRAC flux (measured using SOURCE EXTRACTOR) for sources with clear singular IRAC counterparts (e.g. members 5 and 7). Additionally, visual inspection of the residual maps from our fitting procedure confirms no major systemic issues were generated during the convolution process (e.g. systemic offsets, shadows from inaccurate PSFs/kernels, black spots from spurious overestimated fluxes). Thus, we interpret our fits as successful and consider the resulting deblended fluxes as representative.

We also explored whether astrometric offsets between the *Spitzer* IRAC images and *HST* images could affect our counterpart matching and deblending process. We searched for all *HST* counterparts in a 1.6″ radius (corresponding to the IRAC Channel 1 FWHM) from the IRAC sources and found

an average offset of δRA = $0.06 \pm 0.34''$ and δDEC = $0.24 \pm 0.34''$ between matched counterparts, which is comparable to the *HST* FWHM but significantly smaller than the IRAC FWHM. These offsets were not systematic in any direction.

Since TPHOT-IRAC photometry is based on *HST* coordinates, the IRAC fluxes are summed in a similar fashion: S/N $<$ 2 sources are used only as upper limits in the SED fitting process (see Section 2.4), and the remaining fluxes are summed to form a single measurement that's used in the SED modeling process, with uncertainties added in quadrature.

2.4 SED Modeling

We use the CIGALE [Code Investigating GALaxy Emission, 41, 290, 33] SED modeling tool in `python` to generate SEDs for each of the 11 objects. CIGALE uses an energy balance principle based on conservation of energy between stellar emission, dust attenuation, and dust emission from UV to far-IR wavelengths, and estimates individual galaxy properties using a Bayesian approach (see [290] for full details). We select flux densities measured at signal-to-noise $\gtrsim$ 2 (listed in Table 2.1 and 2.2). Detections with S/N $<$ 2 are used as upper limits in the SED fitting process, which are treated in the SED fitting process as described in detail in [330] and [33]. We refer the reader to Section 2.3.2 and 2.3.4 for details on multiwavelength counterpart selection.

We use the following templates and modules to model each DRC member: a Chabrier IMF [56] with a delayed star formation history; the Bruzual et al. 2003 [40] stellar population synthesis models; the Calzetti et al. 2000 [43] starburst dust attenuation curve, and the Drain and Li 2007, 2014 [105, 104] two component dust emission models. We fit over a wide range of e-folding times ($5 - 200$ Myr, given the age of the Universe at this redshift), metallicities ($0.0001 - 0.05\,Z_\odot$), and UV slopes ($\beta = -1.75 - 2$, [52]). For the dust emission component, we allow the models to explore all PAH mass fractions available in the module, minimum diffuse dust radiation intensities, $U_{\rm min}$, of

0.1, 0.5, 1, 5, 10, or 50 (from adult stellar populations) combined with a fixed maximum radiation field intensity of 10^7 (from star-forming regions, [104]), a fixed mid-IR power-law slope of 2 [46], and possible percentages of dust emission linked to star-forming regions (as opposed to ambient heating by adult stars) of 50, 75 and 100%.

We present the best fit models in Figure 2.3 and corresponding galaxy properties in Table 2.3 for all components. We do not include a SED model for DRC-4 as only upper limits are measured at $\lambda_{\rm obs} < 2\,$mm; still, we list SED-estimated properties for DRC-4 and caution against further interpretation of these values without further photometry to constrain them. For the remaining objects: all of the best-fit model SEDs have reduced $\chi^2 < 2$, except for DRC-2 with $\chi^2_{\rm red} \approx 3$. For this object, the higher χ^2 is likely due to the excess emission measured at observed-frame $3.6\,\mu$m; DRC-2 is likely an ongoing major merger (see e.g. Figure 2.1), and the excess $3.6\,\mu$m emission may be driven by increased (and redshifted) Hα flux from a recent extreme star-formation event, captured in the wide-banded IRAC Channel 1 [352]. We also note that our resulting SFRs and infrared luminosities are similar to those found in Oteo et al., within 1σ uncertainty.

While the reduced χ^2 values are acceptable, we recognize that complex SED modeling techniques can be highly degenerate when there are more free parameters than data points to constrain them. This is particularly true for DSFGs as this population's stellar properties are not yet fully characterized. For example, while a stellar initial mass function (IMF) with more massive stars is favored for DSFGs [e.g. 17, 428, 42, see also [166]], employing different IMFs, each weighted towards more massive stars, can result in a $2-3\times$ difference in stellar mass estimates [e.g. 258, 157, 259]. Moreover, variations in star formation histories and stellar population synthesis models can further degenerate stellar mass estimates in DSFGs [e.g. 157, 261, 413].

For this work, we can check the SED-derived stellar masses by comparing them to estimates based on rest-frame $1.6\,\mu$m absolute magnitudes (observed-frame $\lambda = 8.0\,\mu$m), which is taken directly from respective best fit SEDs. This wavelength traces the stellar peak while also limiting the effects of dust extinction, as well as contributions from thermally pulsing asymptotic giant branch stars

and/or AGN [158, 58, 168]. We derive an average M_H of -26.06 ± 1.40, which is in agreement (within uncertainty) of the SMGs studied in Hainline et al. 2009 [158] and Simpson et al. 2014 [349]. We apply the mass-to-light ratio $L_H/M_* = 7.9$, which was derived from a sample of SMGs in [158] and used for protocluster DSFGs in Chapman et al. 2009 [58] and Casey 2016 [47], deriving stellar masses that are within a factor of two of the SED-derived estimates.

These similarities between stellar mass estimates could be driven by the unconstrained mid-IR portion of the SED that is red-ward of the observed frame 4.5 μm measurement. We do not have data to constrain the redder side of the rest-frame 1.6 μm ($\lambda_{obs} = 8\,\mu$m) bump, and emphasize that further analysis and follow up observations are necessary to fully characterize these objects. Still, many other $z > 2$ protoclusters in the literature that have optical/near-IR and far-IR measurements were analyzed using similar SED decomposition methods. Thus, we move forward using the SED-derived properties in this paper to put the DRC into context with outside literature.

The possible presence of active galactic nuclei (AGN) embedded within a galaxy could also introduce additional uncertainties in the SED fitting process [e.g. 111, 272, 114, 269, 64]. AGN-warmed dust is shown to have the strongest contributions (> 30%) between rest-frame $\lambda = 1.0 - 30\,\mu$m [e.g. 39], which could cause an overestimation of up to 60% in stellar mass for an individual galaxy. However, this is less of an issue for SED-derived stellar masses within the DSFG population [261]. If present, AGN contributions would likely have the most significant impact on DRC-6, the only galaxy for which Oteo et al. 2018 identifies radio emission in excess of the FIR-radio correlation and flat radio spectrum known for typical (i.e. non-active) DSFGs [188]. DRC-3 also exhibits an upturn in the mid-IR shown in the increasing 3.6 μm to 4.5 μm measured flux, which may also be indicative of a heated dust component from an obscured AGN.

ID	$\log(L_{IR})$ $[\times10^{12}L_\odot]$	SFR $[M_\odot/yr]$	$\log(M_*)$ $[\times10^{10}\,M_\odot]$	$\log(M_{H_2})$[a] $[\times10^{11}\,M_\odot]$	T_d[b] [K]
DRC-1	19 ± 5	1744 ± 1162	16 ± 7	8.62±2.15	35
DRC-2	10 ± 8	1132 ± 1013	8 ± 6	2.94±0.73	40
DRC-3	18 ± 8	1527 ± 1303	17 ± 12	2.68±0.67	42
DRC-4[c]	4	200	16	1.41±0.35	28
DRC-5[d]	4 ± 11	167 ± 375	15 ± 8	1.20±0.30	31
DRC-6	2 ± 2	190 ± 190	3 ± 2	1.14±0.29	21
DRC-7	2 ± 6	227 ± 303	5 ± 5	0.71±0.18	31
DRC-8	5 ± 4	394 ± 448	6 ± 2	0.22±0.06	56
DRC-9	2 ± 2	226 ± 281	3 ± 2	0.17±0.04	64
DRC-10	1 ± 1	60 ± 88	2 ± 1	0.16±0.04	40
DRC-11	1 ± 1	114 ± 142	2 ± 1	0.16±0.04	43
Avg[e]	6 ± 6	543 ± 586	9 ± 6	1.76±2.36	40± 12

Table 2.3: Galaxy properties derived from SED fitting. (a) Molecular gas masses are derived from converting 2 mm flux densities to rest-frame 850 μm luminosities. See Section 2.5.2 for more details. (b) Dust temperatures derived from SED fitting described in Section 2.4. (c) All properties for DRC-4 are general estimates, based only on using upper limit near-IR photometry in SED fitting. See Section 2.4 for more details. (d) Properties derived assuming DRC-5 is at $z = 4.002$ (not confirmed). (e) Averages do not include DRC-4.

2.5 DRC Compared to Field Galaxies

When dissecting the individual properties of cluster versus field galaxies out to $z \sim 2$, studies find weak evidence of distinguishable differences between the populations, often suggesting minor increases in the quiescent and/or quenched fraction and the massive galaxy population in overdense environments [e.g. 205, 425]. In the following sections, we discuss some differences we do (or don't) see in our protocluster core population of DSFGs when compared to $z \sim 4$ field galaxies, and stress that more stringent conclusions could be drawn with additional optical/near-IR data. DRC-4 is not included in this analysis, making our focus on only ten of the DRC components (one of which, DRC-5, is not yet spectroscopically confirmed at $z = 4.002$).

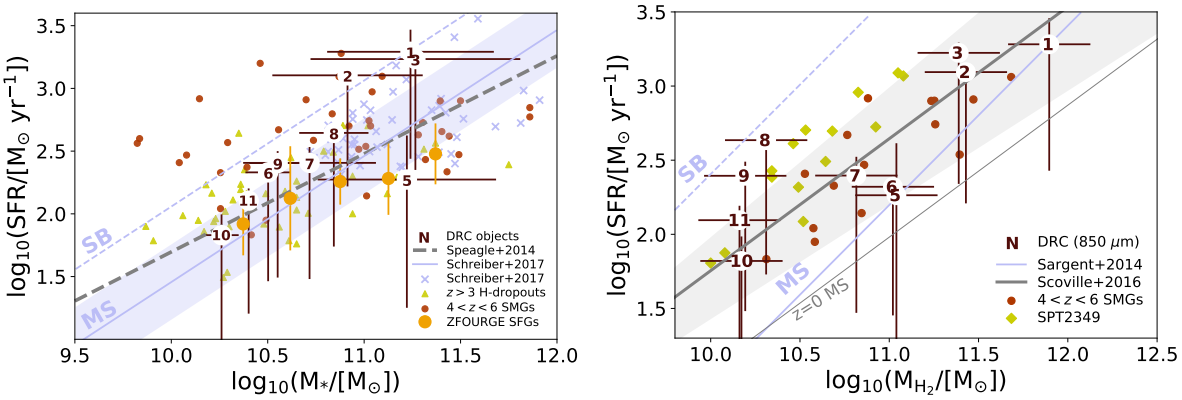

Figure 2.4: *Left*: The SFR–M_* relationship at $z \sim 4$. All DRC components (except DRC-4, see Section 2.4) are represented by their IDs. The orange points represent the average $3 < z < 4$ main-sequence found in [380]. Red points are $z \gtrsim 4$ SMGs taken from [132] and [339]. Green triangles represent the massive star-forming $z > 3$ H-band dropout population from [404]. Blue x's represent the ALMA Redshift 4 Survey of massive ($M_* > 5 \times 10^{10}\,M_\odot$) star-forming galaxies [335]. The blue and grey lines represent the $z = 4$ main-sequence derived in [335] and [356], respectively, with the blue shaded region corresponding to the 1σ uncertainty from the Schrieber et al. sample, and the dashed line corresponding to the starburst region 4× above the main-sequence. *Right*: Molecular gas mass versus star formation rate. Green triangles are from a $z = 4.3$ sub-mm protocluster [264], red points are from the [339] $< z >= 4.4$ ALMA continuum sample, and the gray line marks the star formation law at $z = 4$ generated by Equation (2) in [339]. Redshift independent main sequence (solid) and starburst (dashed) relationships from [328] are in blue.

2.5.1 Main Sequence Evolution

In Figure 2.4 left, we compare the SFRs and stellar masses for each DRC member to other known $z \sim 4$ populations. We include a sample of mass complete ($M_* \gtrsim 1.6 \times 10^{10}\,M_\odot$) $3 < z < 4$ main-sequence star-forming galaxies from the ZFOURGE survey [380], massive dusty $3 < z < 6$ star-forming galaxies [404], a SFR-limited ($\geq 100\,M_\odot\,yr^{-1}$) sample of $4 < z < 6$ ALMA observed SMGs with *HST* counterparts [132], and a population of magnification-corrected gravitationally lensed SMGs at similar redshifts from [339].

In general, all cluster core members are massive, averaging at $9 \pm 6 \times 10^{10}\,M_\odot$, and reside within 1σ of the $z \sim 4$ [335] and [380] star-forming main sequences. Nine out of ten of the protocluster members in discussion are likely larger than $\sim 3 \times 10^{10}$ solar masses, while only 64/654 (or $\sim 10\%$)

of $z > 3$ ZFOURGE galaxies achieve such high stellar mass [380, and the true $z = 4$ percentage is likely even less]. In the higher-redshift SMG samples, we find a much higher fraction of massive galaxies [$\sim 70\%$, 339, 132], which may be more representative of the DRC SMGs. While some $z = 2$ studies report high fractions of massive galaxies in overdense environments [e.g. 205], such a high fraction in the DRC may be driven by selection bias towards massive and bursty systems; further followup observations searching for nearby normal star-forming galaxies are required to substantiate this claim.

Stellar mass functions of far-IR bright star-forming galaxies at $z \sim 4$ estimate a number density of $n \sim 10^{-3.6}\,\mathrm{Mpc}^3$ for objects $> 3 \times 10^{10}\,\mathrm{M}_\odot$ [334]; in a $260\,\mathrm{kpc} \times 310\,\mathrm{kpc} \times 87\,\mathrm{Mpc} \approx 7\,\mathrm{Mpc}^3$ comoving volume like this protocluster, we expect to see 0.00049 galaxies as massive as each of the DRC members. This corresponds to a galaxy overdensity of $\delta_{\mathrm{gal}} = (8 - 0.00049)/0.00049 > 10,000\times$ the field density. While this value may decrease once more protocluster members are confirmed in a wider volume, it underpins the evolutionary concept outlined in Casey 2016 [47] where overdensities of rare and massive DSFGs are likely correlated, not serendipitous, with massive protocluster evolution.

Protocluster members closest to the starburst[2] region, components 1-3, morphologically exhibit possible interactions or ongoing mergers in the rest-frame UV, which some studies argue is a primary driver of a galaxy's presumed short-lived starburst phase [e.g. 324]. We also note that a part of the [335] sample occupies a similar high-mass near-bursty region of the SFR-M_* plane. This sample is a closer evolutionary proxy to the DRC, focusing strictly on massive ($> 5 \times 10^{11}\,\mathrm{M}_\odot$) *HST* H-band selected and ALMA observed star-forming galaxies at $3.5 < z < 4.7$. However, only two of these sources were identified as undergoing close ($< 1''$) interactions, with additional environmental information currently unavailable. Moreover, there exist several DRC components that are on or below main-sequence with disturbed or merging rest-frame UV morphologies. Thus, on the SFR-M_* plane, it is unclear whether merging activity in overdense regions creates starburst

[2]In this work, starbursts are defined as having SFRs that are 4× greater than the main sequence at a given stellar mass [315]

galaxies.

Unraveling any inherent differences in this protocluster core versus field populations, such as an increased fraction of massive galaxies and/or starburst activity, requires further observations. Additional observations in the rest-frame UV/optical could establish the presence of normal star-forming galaxies, galaxies with post-starburst signatures, as well as quiescent early-type galaxies (which we are now seeing out to $z \sim 3.5$ in the field, e.g. [128]) – all of which would pose significant implications on the galaxy growth and evolution in overdense environments. Precise spectroscopic redshift information on these additional populations would also constrain the impact of filamentary dynamics on galaxies in early protoclusters.

2.5.2 Gas Properties

Cluster environments as global systems are expected to have massive intracluster reservoirs of gas. Yet, at the individual galaxy level, some studies show that there is little to no change in gas mass fractions when considering galaxy environments out to $z \sim 2.5$ (e.g. Darvish et al. 2018 [84] and Zavala et al. 2019 [425], see also [375] and [287]). In Figures 2.4 (right) and 2.5, we explore whether this holds for DRC galaxies.

We derive molecular gas masses using the method outlined in Scoville et al. 2016 [339]. This method is built on the observed and theoretical link between the Rayleigh-Jeans tail that traces dust emission and the molecular gas within the ISM of SMGs; and, it is calibrated using the ratio between rest-frame 850 μm luminosity ($L_{850\,\mu m}$) and molecular gas mass (M_{H_2}). This ratio, aka $\alpha_{850\mu\mathrm{m}}$, absorbs inherent variations in dust temperature, opacities, and abundances, and was further calibrated using CO (1-0) measurements in DSFGs. We use the value given in Scoville et al. where $\alpha_{850\mu\mathrm{m}} = 6.7 \pm 1.7 \times 10^{19}\,\mathrm{erg\,s^{-1}\,Hz^{-1}\,M_{\odot}^{-1}}$. Considering possible variations in true galaxy dust temperature, gas mass uncertainties using this method are estimated at $\sim 25\%$. We refer the reader to Appendix A of [**?**] for further details on derivation and resulting uncertainties.

For each individual galaxy, we convert observed-frame 2 mm flux densities ($\lambda_{\rm rest} = 400\,\mu$m) to molecular gas masses using the following equation:

$$\begin{aligned} \mathrm{M_{H_2}} &= 1.78\,\mathrm{S}_{\nu_{\rm obs}}\,[\mathrm{mJy}]\,(1+z)^{-4.8} \\ &\times\left\{\frac{\nu_{850\mu\mathrm{m}}}{\nu_{obs}}\right\}^{3.8}(D_L\,[\mathrm{Gpc}])^2 \\ &\times\left\{\frac{6.9\times10^{19}}{\alpha_{850\mu\mathrm{m}}}\right\}\frac{\Gamma_{\rm RJ}}{\Gamma_{\mathrm{RJ},\,z=0}}\,10^{10}\,\mathrm{M}_\odot \end{aligned} \tag{2.1}$$

where $\mathrm{S}_{\nu_{\rm obs}}$ is the observed flux density at $\lambda_{\rm rest} > 250\,\mu$m (where the dust is considered optically thin), ν_{obs} is the frequency of the observed flux density (= 150 GHz), and D_L is the luminosity distance at $z = 4.002$. $\Gamma_{\rm RJ}$ is the Rayleigh-Jeans (RJ) correction factor for deviation from the rest-frame Planck function (i.e. $B_{\nu_{\rm rest}}/\mathrm{RJ}_{\nu_{\rm rest}}$), developed in **?**] and given by

$$\Gamma_{\rm RJ}(\nu, T_d, z) = \frac{h\nu_{obs}(1+z)/kT_d}{e^{h\nu_{obs}(1+z)/kT_d}-1} \tag{2.2}$$

where h is the Planck constant, k is the Boltzmann constant, and T_d is the galaxy's mass-weighted dust temperature (assumed to be 25 K to be consistent with other work). Using this approach, we estimate molecular gas masses at $0.16-8.6\times10^{11}\,\mathrm{M}_\odot$, with an average $\mathrm{M_{H_2}} = 1.76\pm2.36\times10^{11}\,\mathrm{M}_\odot$ (see Table 2.3). While a cooler dust temperature is possible for DSFGs [e.g. 15 K 186], it is unlikely the case for the DRC since the temperature of the CMB at this redshift is ~ 13.5 K. Using a hotter dust temperature, such as the individual temperatures determined in the SED fitting process (e.g. 40 K, see Table 2.3), results in only a marginal decrease in molecular gas mass estimates (by $\sim 10-20\%$, or $\sim 0.1-0.4$ dex).

For objects 1-4, the values derived using both $T_d = 25$ and the SED-derived dust temperatures

are within $\sim$ 1 dex of the gas masses derived using [C I](1-0) line emission in Oteo et al. Due to possible degeneracies in SED-derived dust temperatures and to remain consistent with outside literature, we move forward in this analysis using the gas masses estimated with a mass-weighted dust temperature of 25 K.

Objects 1-6 also have 3 mm observations, which is closer to the rest-frame 850 μm ($\lambda_{\rm obs} = 4.25\,\mu$m) emission used to derive the Scoville et al. relationship. Under the same assumptions listed above for the 2 mm data, we determine 3 mm gas estimates for DRC objects 3, 5, and 6 that are slightly larger (by 0.06, 0.14, and 0.31 dex, respectively); for objects 1, 2, and 4 the 3 mm gas estimates are smaller (by 0.17, 0.12, and 0.05 dex, respectively). With the exception of DRC-6, the differences between the 2 and 3 mm estimates are generally within the included 1σ uncertainties on the 2 mm estimates. Since 2 mm data is available for all sources, and the differences between the two mass estimates are marginal, we choose to use the 2 mm-derived gas masses (over the 3 mm) throughout this work.

With the above method, we avoid the major uncertainties that come with assumed gas mass estimates from CO SLED analysis at high-J transitions. High-J transitions, like the $J = 6 \rightarrow 5$ transition line detected in DRC objects, trace denser regions of gas than the lower J transitions, which trace cooler, diffuse gas reservoirs throughout the galaxy. Still, as a comparison to our luminosity-derived gas masses, we derive line-driven gas masses using the ^{12}CO(6-5) luminosities provided in Oteo et al.

Assuming that DRC objects have similar spectral line energy distributions (SLEDs) as other high-z SMGs, we can use the ^{12}CO(6-5) line luminosity to convert to the ground-state ^{12}CO(1-0) luminosity, as tabulated in [34]. We assume a CO-to-H_2 conversion factor of $\alpha_{\rm CO} = 1.0\,{\rm M}_\odot\,({\rm K\,km\,s^{-1}\,pc^2})^{-1}$, as used in Bothwell et al. and others for SMGs [e.g. 373], and determine gas masses of $\rm M_{H_2} = 0.1 - 6 \times 10^{10}\,M_\odot$, about an order of magnitude smaller than the masses derived using the dust continuum tracer.

In Figure 2.4, we show DRC members on the SFR-$\rm M_{H_2}$ plane using the molecular gas masses

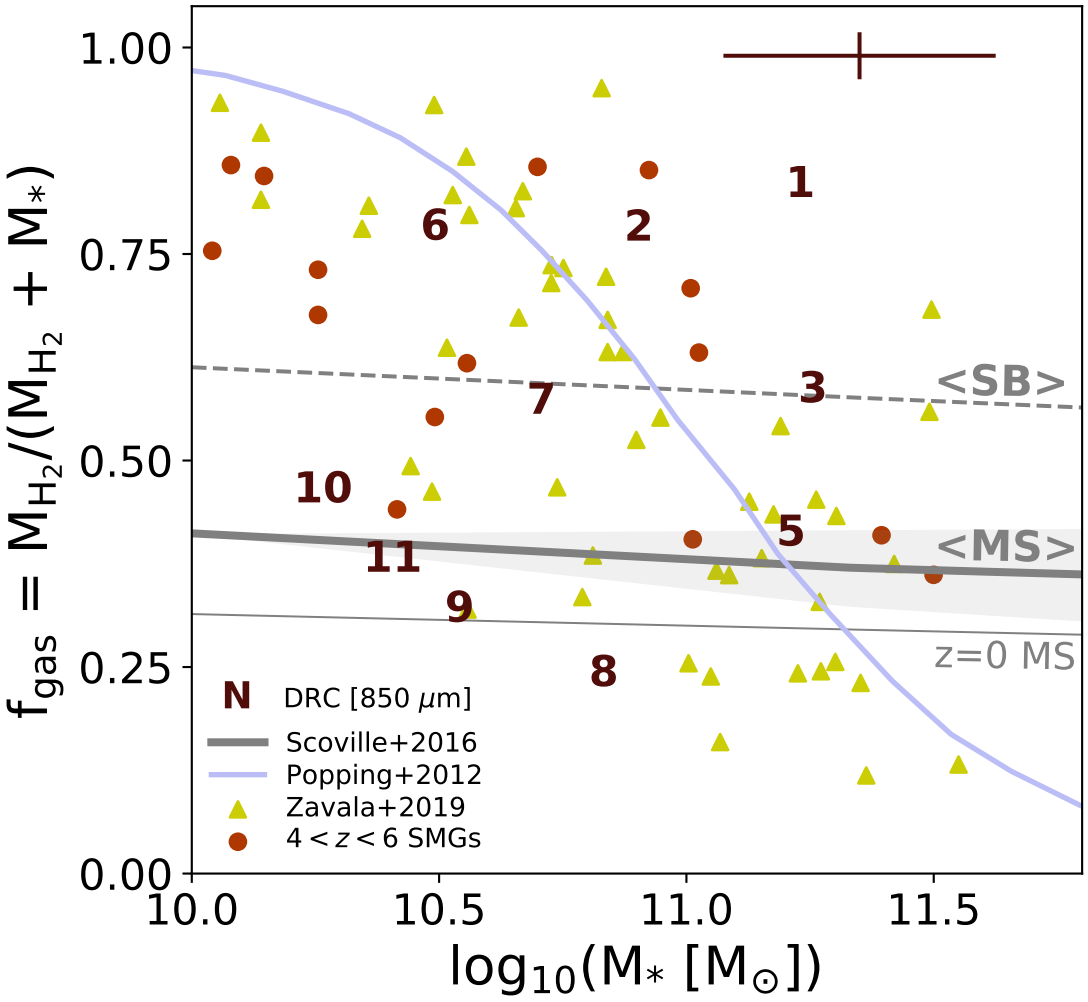

Figure 2.5: Molecular gas mass fraction as a function of stellar mass. Numbers mark the individual DRC components. The average 1σ uncertainty for DRC components is provided in the top right corner. The blue curve represents the $\langle z \rangle = 2$ relationship derived in [309], where high mass galaxies are expected to have lower gas mass fractions (due to both gas depletion and halo shock heating). Red points mark $z \sim 4$ field SMGs [339], and green triangles mark $z = 2 - 3$ ALMA-detected protocluster galaxies [218, 143, 375, 425]. Solid and dashed grey lines represent the average gas mass fraction from [339] for main-sequence and starburst galaxies at $z \sim 4$; we also show the average for main-sequence galaxies at $z = 0$ evolved from the [339] relationship.

derived with the 2 mm flux densities. Eight out of ten members lie within the main-sequence regime with total gas masses $> 10^{10}\,M_\odot$ – estimates that are similar in mass and spread to the [339] DSFG sample and the similarly compact and star-forming $z = 4.3$ SPT-2349 protocluster of DSFGs [264, 174]. About 50% of our sample have relatively large gas masses at $> 10^{11}\,M_\odot$, while the same is only true for none of the SPT protocluster (core) members and 6/15 of the $z \geq 4$ SMG sample. DRC-8 and 9 have elevated SFRs near the starburst regime (above the expected $z \sim 4$ main-sequence star-formation law at a given molecular gas mass [339]). These objects also lie within the M_*-SFR main-sequence which may suggest that their high star-forming efficiencies (=SFR/M_{H_2}) are driven by relatively small gas reservoirs rather than extreme rates of star-formation.

Assuming a closed box scenario with a constant star-formation rate and no major influx of cold gas, we can estimate individual gas depletion timescales, $\tau_{\rm depl} = M_{H_2}/{\rm SFR}$. Of course, in overdense regions like these, mergers and fresh gas inflows are expected, but we can still use the instantaneously measured gas depletion times to understand the efficiency at which these objects are turning gas into stars at this given moment (while also neglecting any impacts from feedback).

Despite their large gas reservoirs, DRC objects will deplete their gas in an average of $\sim 260 \pm 180$ Myr, which is similar to the mean $\tau_{\rm depl}$ for the SPT $z = 4.3$ protocluster [264] and the $z > 4$ field SMG sample [339], at 122 ± 53 and 300 ± 160 Myr, respectively. DRC gas depletion timescales are more consistent with general field SMG gas surveys at high-z [~ 100 Myr, e.g. 373, 8, 420] than those of local interacting infrared luminous galaxies [e.g. 323]. If we assume that no major gas is flowing in to support these SFRs, these timescales may indicate that these objects will deplete their gas reservoirs by $z \sim 3$.

Dividing stellar mass by the star-formation rate, we can estimate the stellar-mass build up timescale (assuming that these SFRs have been sustained in the past); we derive build up timescales ranging from 70-300 Myr with a median of $\sim$160 Myr – which is within the expected lifespan of the starbursting phase for submillimeter galaxies [e.g. 278]. Still, in deep potential wells like that of this overdensity, gas is expected to flow in at increased rates, which may actually sustain these

extreme bouts of star-formation for longer periods of time. Further deep observations for extended, cold gas surrounding the protocluster would be necessary to confirm this latter scenario.

An additional metric we can inspect is the gas mass fraction, $f_{gas} = M_{H_2}/(M_{H_2} + M_*)$, which is expected to decrease with increasing stellar mass [e.g. 309, 138]. In Figure 2.5, we see that this appears to be the case for the Scoville et al. $z \sim 4$ field SMGs [339] and other $z = 2 - 3$ protoclusters [425, 375, 143] – as well as for DRC members. DRC members span a wide range of gas fractions, from 25-80%, with an average $f_{gas} = 52 \pm 20\%$, across all galaxy stellar masses. Objects 8 and 9 have some of the smallest gas reservoirs ($< 3 \times 10^{10}\,M_\odot$), are within the SFR-$M_*$ main-sequence law, and also lie at the bottom edge of the f_{gas}-M_* expected relationship. With gas depletion timescales of ~ 50 Myr, it is possible that these objects are much closer to depleting their gas supplies than the other core members, and on their way to becoming some of massive quiescent galaxies that dominate in cluster cores by $z \sim 3.5$ [e.g. 88, 190].

Understanding the growth and quenching of gas reservoirs in overdense environments at $z > 3$ requires additional follow-up observations in the rest-frame far-IR/sub-mm. While we show that the population of SMGs in a protocluster spans a wide range of gas-richness, we cannot draw further conclusions on whether specific quenching (or enhancement) activity is driven by environment until there are additional observations of other protocluster members, both within the DRC and other $z > 3$ overdensities. With follow up dust continuum surveys of these overdensities, we can further constrain overarching questions in early cluster evolution, such as: How early does extreme stellar mass build up cease for brightest cluster galaxy progenitors? Do the majority of galaxies in overdense environments go through a starburst phase that's sustained with cold gas flows and, if so, at what point would virial shock heating disrupt these flows?

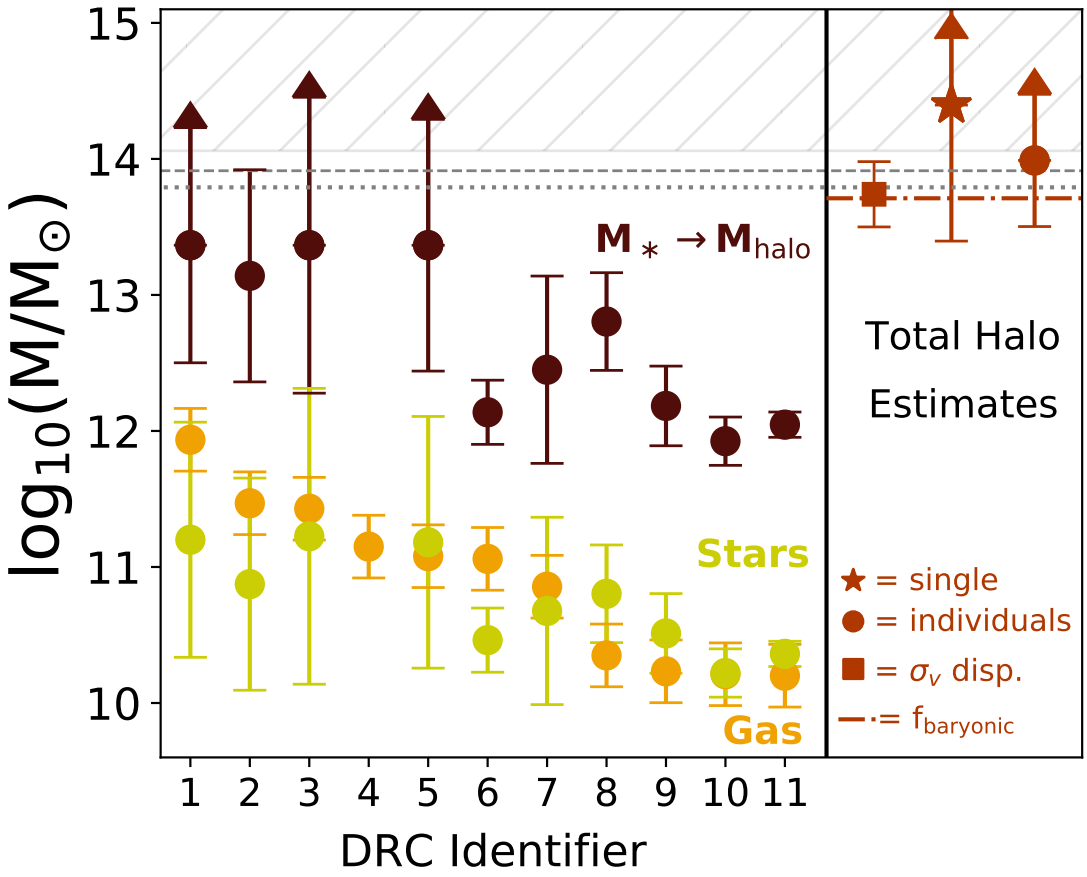

Figure 2.6: Halo mass estimates for the DRC. On the left, we show mass estimates for stars, gas, and total halos for each individual DRC component (gas only for DRC-4, see Section 2.4). The orange corresponds to the gas mass estimates using the rest-frame 850 μm technique as outlined in [339] and Section 2.5.2. The green corresponds to the stellar masses estimated using SED fitting, as outlined in Section 2.4. The dark red represents the individual total halo masses derived using stellar abundance matching at $z = 4$ from [22]. The dotted, dashed, and hatched regions represent the 1, 2, and 3σ exclusion curves for the most massive halos expected to be observable at $z = 4$ in the $\sim$ 600 deg^2 *H*-ATLAS survey [163]. On the right, we show total halo mass for the entire DRC, estimated using various methods. The square and corresponding error bars represents the range of halo masses found in [293] using velocity dispersion methods. The circle represents the sum of the halos from each individual DRC component as seen in dark red on the left. For the star: all DRC objects are treated as subhalos within one single overarching halo; their individual stellar masses are summed into a singular massive stellar component that's then used to reverse engineer halo mass estimates using stellar-to-halo mass ratios from [22]. Finally, the dark red dash-dotted line represents the halo mass assuming a baryonic-to-halo mass fraction of 5%.

2.6 Cluster Halo Mass at $z = 4$

Weighing a high-z protocluster requires a variety of assumptions. Typical methods used to derive galaxy cluster masses (e.g. measuring X-ray emission from the super-heated intracluster medium (ICM), or tracing Sunyaev-Zeldovich distortions on the CMB) are unavailable for objects like the DRC as most of these methods are fine-tuned for nearly or fully virialized $z \lesssim 1$ clusters with an ICM. Oteo et al. 2018 [293] attempt to overcome this by combining the velocity dispersion method [119] with ALMA ^{12}CO(6 − 5) line velocities to estimate a total DRC halo mass of $3 - 9 \times 10^{13}\,M_\odot$. This method requires an assumption that the DRC is already virialized. However, $z > 3$ protoclusters exhibit generally aspherical mass distributions with large effective radii that vary based on the chosen line of sight [e.g. 232, 63]; this is because eventual $z \sim 0$ cluster members are tens to hundreds of Mpc apart at $z > 3$. In the following, we weigh the DRC using three different methods, each of which comes with it's own assumptions and uncertainties. We present these estimates in Figure 2.6 and 2.7. As in the previous sections, we do not include DRC-4 in any calculations as we do not have reliable stellar mass estimates.

First, we derive a modest estimate of the total cluster halo mass by summing the halo masses of each individual galaxy. This estimate requires the assumption that individual galaxy halos are closer to virialization than the protocluster itself, and that each galaxy formed it's own halo prior to coalescing in this overdense region. We use the stellar-to-halo abundance matching relationship in [22], which is developed assuming that the bulk of baryonic mass in dark matter halos is tied up in adult stars, and that massive galaxies trace massive halos. We note that the [22] $z = 4$ relationship does not extend into the stellar mass range we observe for the DRC, and thus those objects with stellar masses greater than $> 10^{11}\,M_\odot$ are placed at the fixed maximum value of $M_{\rm halo} = 2 \times 10^{13}\,M_\odot$. This is applied to DRC objects 1, 3, and 5 - all three of which have stellar masses within uncertainty of the Behroozi et al. most massive halo bin.

We determine individual halo masses of $M_{\rm DM} = 1 - 12 \times 10^{12}\,M_\odot$, with an average halo mass

of $8 \pm 4 \times 10^{12}\,M_\odot$ (Figure 2.6, left), similar to other average DSFG halo masses seen overdense environments [e.g. 159]. Summing up the individual components translates to a total cluster halo mass of $5 \pm 2 \times 10^{13}\,M_\odot$ (Figure 2.6, right). Errors are determined from uncertainties in stellar mass. This estimate agrees with the those derived in [293]. We note that if we do not include DRC-5 in this estimate (as it is not a spectroscopically confirmed member), the total halo mass drops to $\sim 4 \times 10^{13}\,M_\odot$ – roughly $< 20\%$ less massive.

If we instead assume that these galaxies are (and maybe always have been) sitting and growing in the same halo, then the previous method would likely be an overestimate that "double counts" dark matter mass in overlapping halos. Assuming each of these galaxies is close enough to be occupying one single massive halo (which, according to velocity space, may be true for 8/10 objects), one might sum all stellar masses into a single total stellar mass for the halo and then interpolate that value over the relationship in [22]. Unfortunately, this total stellar mass goes well beyond the established $z = 4$ Behroozi et al. relationship. Thus, to conceptualize this estimate, we instead use the stellar to halo mass ratios in Behroozi et al. (Fig. 7) for the largest $z = 4$ halo mass value ($\sim 10^{13}\,M_\odot$), which is set to $M_*/M_{halo} = 0.003$. Combining this value with the total stellar mass for the DRC, we reverse estimate the cluster halo mass at $> 3 \times 10^{14}\,M_\odot$. This is ~ 0.5 dex larger than the previous estimates, and the most massive estimate in this study. The lower limit of this method assumes a smaller halo and a more efficient stellar to halo mass ratio of $M_*/M_{halo} = 0.02$ - which results in a cluster halo mass of $4 \times 10^{13}\,M_\odot$, a value similar to that of the most massive *individual* galaxy halos. If DRC-5 is not included in either estimate, the total halo mass drops by about 30%.

Finally, if we instead assumed a generous fixed baryonic-to-dark matter fraction of 5% [e.g. 20], summing all stellar and gaseous components, we estimate a halo mass of $5 \times 10^{13}\,M_\odot$ – similar to the individual halo mass estimate determined above, as well as the calculation from Oteo et al.

In Figure 2.6, we compare these estimates to the 1, 2, and 3σ exclusion curves for how likely a massive halo is to exist at $z = 4$ in ΛCDM cosmology, as derived in [163][3] – i.e. these exclusion

[3]We determine these curves / statistics using the publicly available code from [163] at:

curves mark the most massive clusters possible at 68, 95, and 99.7% likelihood within the *H*-ATLAS survey region of $\sim 600\,\mathrm{deg}^2$, with 1, 2, and 3σ corresponding to upper mass limits of 6, 8, and $12{\times}10^{13}\,\mathrm{M}_{\odot}$, respectively.

Within uncertainty, each of the total halo mass estimates for the DRC do not necessarily break the 3σ (99.7%) exclusion curve – i.e. our current data portrays a massive structure that is rare in the Universe, but not improbable. However, we argue for a variety of reasons that our understanding of the DRC's true weight is incomplete (and therefore likely underestimated). Firstly, at large scales, these methods do not account for other additional cluster members that have yet to be detected, such as normal star-forming galaxies, post-starburst, and/or quiescent galaxies. We emphasize the impact of this point: the majority of galaxies in DSFG-rich $z < 3$ protoclusters are normal star-forming systems [$\sim$ 85%, Table 1 in 54]; normal star-forming galaxies contain the majority of the cosmic stellar mass budget [17, 315, 327], and are found in large numbers in protoclusters out to $z \sim 6$ [e.g. 160]. Thus, the presence of up to 10× as many normal SFGs as DSFGs in this protocluster core would have significant impact on the mass estimates, and therefore rarity, of the DRC.

At smaller scales, the abundance matching method is developed on the basis that the most massive component in all halos is the stars; while the DRC presents gas-poor galaxies, it is still possible for gas-rich members to exist throughout the structure but outside of the ALMA field-of-view of this cluster core. Moreover, at high-z, it is possible for large gas reservoirs to become significant (or even the *main* baryonic) contributors to the overall mass budget [e.g. 54].

In Figure 2.7, we compare DRC total halo mass estimates to that of other known protoclusters over a wide range of redshifts. At it's lowest estimate, it is already equally as massive as $z = 2 - 3$ protoclusters [most of which have halo mass estimates using the same stellar-to-halo matching technique at the individual galaxy level, 47], and at its largest the DRC is nearly as massive as $z = 1$ virialized clusters [360, 427, 286, 243]. Again, we emphasize that additional, non-negligible

https://bitbucket.org/itrharrison/hh13-cluster-rareness/src/master/.

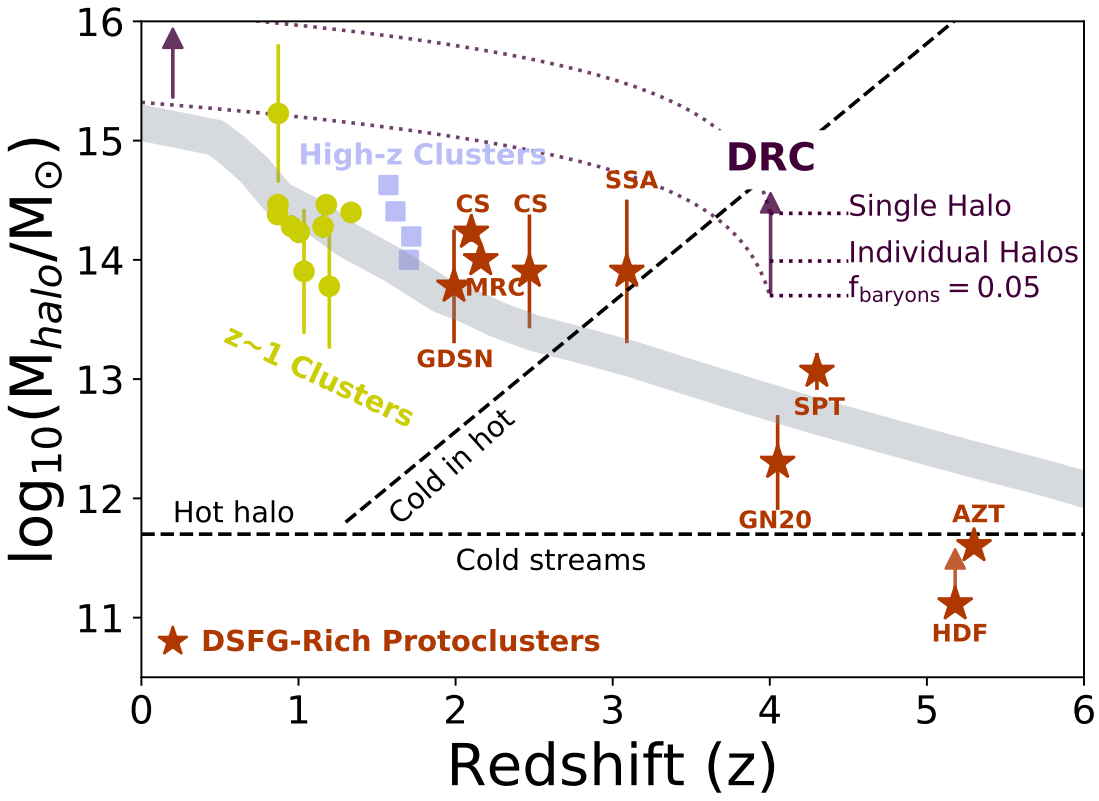

Figure 2.7: The halo mass evolution of protoclusters. For the DRC, we show the halo mass estimates from two methods in purple (presented in Section 2.6): (i) generating halo masses using stellar-to-halo abundance matching [22] at the individual galaxy level (second highest estimate), (ii) the total halo mass if we combine all DRC stellar mass into a single component and use a range of stellar-to-halo mass ratios (most massive estimate), and (iii) the halo mass estimate found using the baryonic-to-dark matter ratio of 5% (least massive estimate). The purple curves from $z = 4$ to $z = 0$ show the predicted evolution of halo growth for a *single* halo in the Millenium and Millenium-II simulations [252, 123]; we show the evolution for each of the DRC estimates. We consider these estimates as lower limits in this analysis as there are likely additional protocluster members not captured in the ALMA data. Green dots represent $z \sim 1$ galaxy clusters from the GCLASS survey [394]; blue squares represent $z = 1 - 2$ virialized clusters [286, 360, 427, 243]; red stars represent SMG-rich $\gtrsim 2$ protoclusters: the GOODS-N $z = 1.99$ protocluster rich with AGN and SMGs, the COSMOS $z = 2.10$ and 2.47 protoclusters, the MRC1138256 aka 'Spiderweb' protocluster at $z = 2.16$, the SSA22 $z = 3$ AGN and DSFG rich protocluster, the $z > 4$ GN20, AzTEC-3, and HDF 850.1 overdensities (with 1-3 DSFGs each), as well as SPT2349-56, the $z = 4.3$ protocluster of 14 SMGs [362, 208, 29, 58, 78, 376, 221, 44, 206, 403, 177, 422, 82, 48, 97, 62, 388, 47, 264, 174]. The grey line shows the expected halo mass evolution of a Coma-like cluster [61]. The black dashed lines mark the different regions of gas inflow and cooling mechanisms on massive halos; gas inflows onto halos above the critical shock heating halo mass at $\sim 10^{12}$ $M_\odot$ are shock heated and thus the galaxy within is strangulated [89]. Galaxies in the "cold in hot" regime may have penetrating cold gas flows that help sustain growth.

mass is likely missing from the DRC in the form of less star-forming galaxies or other far-IR bright sources not within the original ALMA field-of-view - as found to be true for the SMG-rich SPT2349-56 protocluster at $z = 4.3$ [264]. Follow up ALMA spectroscopic scans on far-IR bright regions surrounding the SPT protocluster has yielded an additional 15 (to the original 14) protocluster members, potentially doubling prior halo mass estimates [174]. This demonstrates that, until a thorough study on the larger scale of the structure is carried out, the true observed mass of the DRC (and other high-z protoclusters like it) will remain unknown.

Given the high mass that appears in place for the DRC already at $z = 4$, we consider next how the DRC may evolve compared to massive clusters seen locally today. Based on the evolutionary track for a Coma-like cluster derived in [61, grey line in Figure 2.7], we can generally estimate that the DRC will evolve to $\gtrsim 10^{15}\,M_\odot$ by $z = 0$. This is under the assumption that an overdensity such as the DRC (with $\delta_{gal} > 10,000\times$ the field density for massive galaxies, see Section 2.5.1) traces one of, if not the, most massive halos in the large scale structure of the protocluster. We also derive a $z = 0$ halo mass following [**?**] by using the mean halo growth rate as a function of redshift and observed halo mass from the Millennium and Millenium-II simulations [252, 123]. Using this method and the $z = 4$ two different stellar-to-halo mass estimates outlined above, we derive a $z = 0$ mass of $M_{z=0} \approx 2 - 8 \times 10^{15}\,M_\odot$. This halo mass is extremely large, rivaling that of fully evolved galaxy clusters seen locally today [e.g. 140, 134]. Both halo mass evolution functions require a variety of assumptions of which we cannot constrain; e.g. the method used in [223] was derived for a single halo, and the growth curves derived in [61] are highly dependent on the presumed volume of the observed galaxy overdensity. Considering these caveats, as well as a lack of additional constraints on the large scale structure of the DRC, and the uncertainties in stellar mass estimates, we state generally that the DRC is a massive cluster progenitor that will likely evolve $\gtrsim 10^{15}\,M_\odot$ by $z = 0$.

Overall, the list of factors that influence the future of this protocluster's growth is long, complex, and opaque (e.g. mergers, gas inflows, AGN, etc.). Still, with follow-up observations and simulation

deep dives, we may be able to begin untangling the halo assembly past and future for massive cluster progenitors at $z > 3$. Additional rest-frame UV/optical observations that map the extent of the DRC's large scale cluster would constrain the true mass distribution of the fated cluster. A deeper dive into simulations of massive cluster formation could shed light on halo mass configurations and distributions within protocluster galaxies, which can then be used to calibrate against standard abundance matching techniques for isolated halos. These efforts are left for future studies.

2.7 Summary and Conclusions

In this paper, we present a multiwavelength analysis on a $z = 4.002$ SMG-rich, ultra-massive protocluster: the Distant Red Core. We combine new *HST* and *Spitzer* data with existing Gemini, *Herschel*, and ALMA data to model spectral energy distributions for each respective ALMA object (Figure 2.3, except DRC-4), taking care to deblend low resolution *Spitzer* IRAC data where needed (Section 2.3.4). Stellar masses and SFRs are derived from SED-fitting with CIGALE (Section 2.4). Molecular gas mass estimates are derived using the observed-frame 2 mm ALMA data (probing the Rayleigh-Jeans region of the dust continuum) with the [339] methodology.

We confirm a population of massive ($M_* > 10^{10}\,M_\odot$) galaxies in place when the Universe was only 1.5 Gyr old. When comparing to field galaxies on SFR-M_* plane (Figure 2.4), our results confirm that – even at $z = 4$ – protocluster galaxies can be viewed as a high-mass (and possibly more bursty) extension of the star-forming main-sequence for coeval isolated field galaxies. Similarly, though several objects contain large gas reservoirs ($M_{H_2} \gtrsim 10^{11}\,M_\odot$), all lie within the SFR-M_{H_2} main-sequence plane. When compared to $z = 2 - 3$ protocluster and $z \sim 4$ field counterparts, the DRC objects have similar gas mass fractions that follow the expected inverse $f_{gas} - M_*$ relationship. These systems also have short gas depletion timescales ($\sim 260 \pm 180$ Myr) on par with field SMGs which, in a closed box scenario, means that these objects will exhaust their gas supplies in time to become massive quiescent galaxies that dominate at cluster cores by $z \sim 3$.

Using multiple methods, we derive a total $z = 4$ protocluster halo mass of $\sim 10^{14}\,M_{\odot}$, and show that this value teeters on the edge of the most massive halo allowable/observable in the $600\,\mathrm{deg}^2$ *H*-ATLAS survey volume (Figure 2.6). We estimate that the DRC will evolve to become an ultra-massive cluster with a total halo mass $> 10^{15}\,M_{\odot}$ (possibly even $> 10^{16}\,M_{\odot}$) at $z = 0$ (Figure 2.7). For both the $z = 4$ and $z = 0$ calculations, we argue that a more massive estimate may be appropriate based on the assumption that other significant galaxy populations within the protocluster's large scale structure are not included in this analysis. Still, even if additional protocluster members are confirmed, more multi-wavelength studies of $z > 3$ DSFG-rich protoclusters combined with studies on the evolution of mass distributions and the gas duty cycle in cluster formation simulations are necessary to fully appreciate and characterize complex systems such as the Distant Red Core.

Chapter 3

Growing Black Holes Do Not Quench DSFGs - Brown et al. 2019

3.1 Introduction

Nearly all massive galaxies are believed to host a super-massive black hole (SMBH) at their center [204, 239, 176]. Current research suggests that central black holes gain mass through a combination of both coalescence and bursts of mass accretion from the environment as the host galaxy evolves [197, 401, 355, 341, 399, and references therein]. The peak epoch of central black hole accretion, as the main source of active galactic nuclei (AGN), coincides with the peak epoch of star-formation in the universe at $z \approx 1-2$ [95, 234, 3, 366, 32, 5], and also major galaxy merger events [95, 180, 383, 115, 317]. Furthermore, in our local universe there exists a tight correlation between SMBH mass and host galaxy bulge mass and stellar velocity dispersions [125, 244, 153, 203, and references therein], whereas higher redshift SMBHs have been found in smaller host galaxies than expected [e.g. 344, and references therein]. These results signify that SMBH growth and galaxy growth are co-evolutionary processes and that these processes may regulate each other over time

to produce the galaxy and SMBH sizes we observe today.

Both central black hole growth and star formation rely on the abundance of cold molecular gas [75, 353, 90, 98, 32]. While cold dust and gas collapse to trigger star formation, the SMBH at the galaxy core gravitationally attracts cold gas and dust into a clumpy obscuring reservoir a few parsecs out from the SMBH, which fuels a thin, hot SMBH accretion disk with a radius typically $\lesssim 1$ parsec [6, 385, 386, 179, 87]. The AGN feeds off the reservoir (hereby referred to as a torus; although it is now accepted that the dust is distributed in a more clumpy manner as opposed to a smooth donut structure [281, 282, 346]) with a mass accretion process that emits X-ray, UV, and optical light [e.g. see 155]. The X-ray, UV and optical light is partially absorbed by the surrounding dusty toroidal structure, then re-emitted in the infrared, making most AGN bright in the mid-IR, but not all AGN are X-ray bright [e.g. 384, 365, 77, 101]. The current AGN unified model posits that AGN can be classified by the orientation of the dusty torus to the observer's line of sight [6, 389]: Type 1 AGN are usually observed face-on through a cavity in the torus and are typically bright in the X-ray, UV and optical spectrum; Type 2 AGN may be intrinsically less luminous or are observed at an angle through the torus, and are thereby obscured by high column densities of dust and gas ($N_H > 1.5 \times 10^{24}\,\mathrm{cm}^{-2}$) from the observer's line-of-sight, enough so that most or all of the X-ray emission is absorbed and undetected [e.g. 2, 214]. However, recent observations are challenging this scheme [e.g. see section 3.1 of 27] and suggesting that observational differences in obscuration between AGN are mostly driven by individual SMBH accretion rates [e.g. 233, 314] or host galaxy obscuration [e.g. 147, 284, 60, 5].

AGN accretion and outflow mechanisms are theorized to play a major role in galaxy evolution, via heating up, consuming and/or blasting away the host galaxy's remaining cold gas and dust necessary to create new stars, thereby triggering a star-formation quenching phase [95, 161, 181, 121, and references therein]. In observations, some AGN feedback processes are instantaneously strong enough to affect star formation in the host galaxy [e.g. 368, 312, 322, but also see [227]]; however, the exact contribution of the AGN phase to the physical properties of galaxies, compared to other

mechanisms from stellar processes, is still not well understood [e.g. 347, 135, 96, 133], particularly for the most powerful AGN [e.g. 361, 318]. To study the effect of powerful AGN on their host galaxies, it is necessary to have a large statistical sample of AGN with multi-band observations to individually derive and constrain their physical properties.

One of the main degeneracies in determining the evolutionary relationship between AGN and host galaxy star-formation lies in their mutual obscuration by warm dust [92, 370, 234]. The radiation originating from warm dust in stellar nebulae and from the obscuring torus around AGN are both bright in the mid to far-IR spectrum and thus necessary to disentangle prior to using IR radiation as an indicator for any host galaxy dust properties, including measurements of dust temperatures, host galaxy stellar mass, and star-formation rates; without this decomposition, there is a risk of measurement overestimation and, therefore, an increase in uncertainties. AGN accretion and outflow mechanisms release a large amount of energy detectable at nearly all wavelengths, in particular X-rays from the accretion disk [see 37, for a review of AGN viewed in the X-ray spectrum] and radio signatures from synchroton radiation [e.g. 263, 30, 194, 66]. These features are the most commonly utilized as identifiable signatures that could be used to distinguish AGN from their host galaxies [102, 91, 275, 37].

Observational studies and models of IR SEDs for local AGN reveal radiative flux densities that generally increase through the mid-IR then rapidly decline starting somewhere between $40\,\mu m < \lambda < 100\,\mu$m out to sub-millimeter wavelengths [269]. Prior to the *Herschel Space Observatory* [304], observations were limited out to $\lambda < 200\,\mu$m only for a small sample of very far-IR bright, mostly local objects [e.g. 292, 156]. *Herschel* has been instrumental in constraining the dust SEDs for large samples of local and high redshift AGN and star forming galaxies, revealing a universe that is optically obscured by dust and therefore undetected at shorter wavelengths [e.g. 268, 370, 51, and references therein].

In this paper, we use multi-wavelength infrared observations from the *Herschel* Space Observatory [150, 306] combined with the *Spitzer* Space Telescope [407], along with optical wide-area

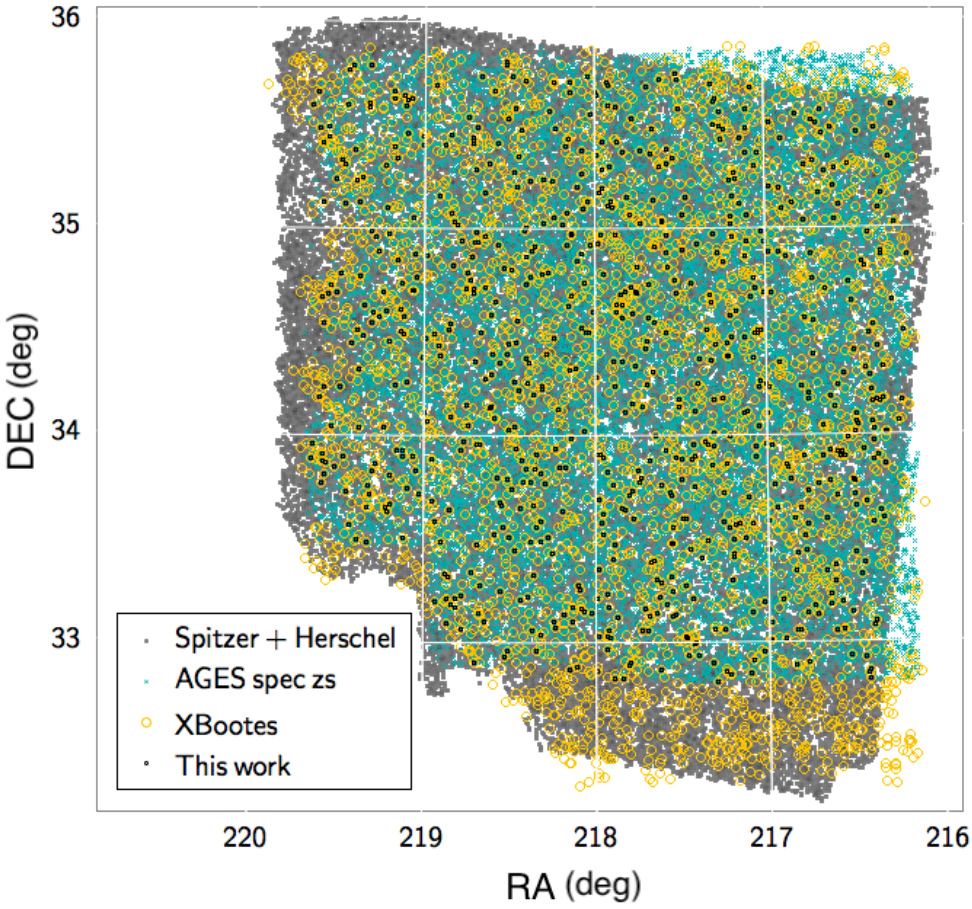

Figure 3.1: Survey map for the parent surveys from which our main sample is derived. Grey points mark all galaxies with a S/N > 3 in the MIPS 24μm band and at least one SPIRE band; blue points denote all galaxies in the AGES survey with spectroscopic redshifts; gold circles outline all of the X-ray sources in the XBoötes survey; black points mark our final sample of 703 AGN and host galaxies which spans $\sim 7\,\mathrm{deg}^2$. Respective survey coverage and depths are discussion in Section 3.2.

observations, and X-ray data from the *Chandra* X-ray Observatory [406] to construct the AGN and host galaxy SEDs and explore the warm dust properties in the context of AGN accretion activity. We focus on X-ray selected AGN in the wide 9.3 deg^2 Bo*ö*tes legacy field [192] with mid and far-IR counterparts detected by *Herschel* and *Spitzer* [291, 10]. The rich amount of data in the IR allows us to avoid the uncertainties that arise from single-band SED fitting. Furthermore, the multi-wavelength detections allow us to reliably use SED decomposition models to isolate AGN contribution in the infrared, reducing the likelihood of AGN contamination when estimating host galaxy properties.

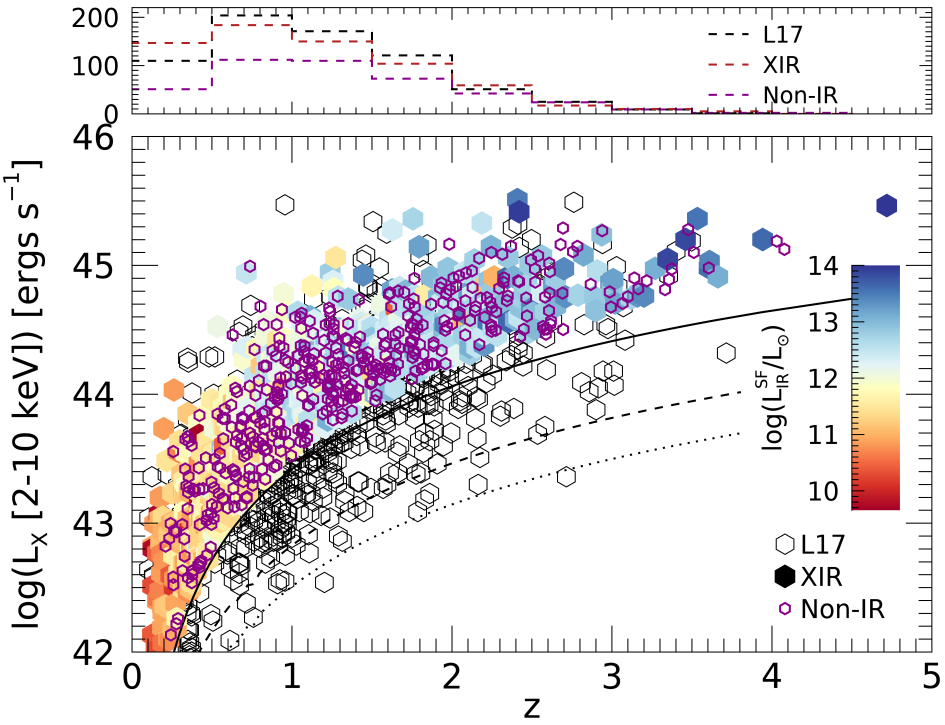

Figure 3.2: Distribution of rest-frame X-ray luminosities and spectroscopic redshifts for our AGN sample. The solid circles are the 703 X-ray AGN with *Spitzer* 24 μm and far-infrared *Herschel* detections. Colors represent rest-frame, infrared luminosities corrected for AGN contamination derived from individual respective SEDs (see Section 3.3). The purple circles are the 425 X-ray AGN without mid/far-IR detections. The black empty circles are the AGN used for analysis in L17. The black solid line represents the X-ray flux limit of the *Chandra* XBoötes survey [274]; for comparison, the dashed and dotted lines mark the sensitivity limits of the *XMM-Newton* [**?**] and *Chandra* [**?**] surveys in the COSMOS field, respectively. Shown in the top panel is the number of sources in our XIR sample (red), non-IR sample (purple), and in L17 (black) in redshift bins of size 0.5.

This paper is organized as follows. Section 3.2 describes the multi-wavelength survey data used in this analysis. Section 3.3 details the AGN sample selection procedure. In Section 3.4, we discuss the derivation of AGN and host galaxy properties and the results in the context of other published studies; section 3.5 provides a summary of this work. Throughout this study, we assume a cosmology with $H_0 = 70\,\mathrm{km\,s^{-1}}$, $\Omega_m = 0.3$, and $\Omega_\Lambda = 0.7$.

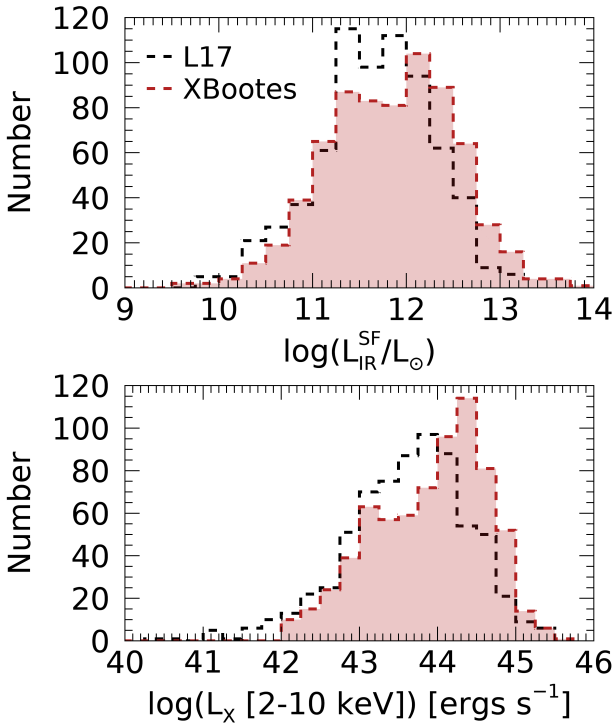

Figure 3.3: Distributions of AGN and host-galaxy properties comparing this sample (red) and [212, aka L17 in black] samples. *Top*: Histogram of rest-frame, AGN-corrected infrared luminosities in bins of 1 dex, with median infrared luminosities of 1.95×10^{45} ergs s^{-1} and 2.69×10^{45} ergs s^{-1} for L17 and our sample, respectively. *Bottom*: Histogram of rest-frame X-ray luminosities in bins of 1 dex; our sample has a slightly higher median X-ray luminosity of $L_X = 1.07 \times 10^{44}$ erg s^{-1} compared to the L17 median X-ray luminosity of $L_X = 4.79 \times 10^{43}$ erg s^{-1}.

3.2 Multi-wavelength Data

The survey observations used in this study are centered in the Boötes field at α = 14h 30m 05.71s, δ = +34° 16′ 47″.5 [192]. We use publicly available photometric catalogs ranging from optical to far-infrared wavelengths, complemented with X-ray data and spectroscopic redshifts, with known active galaxies [10] and clusters of AGN [36]. The multi-wavelength observations cover different areas across the Boötes field (see Figure 3.1). Table **??** summarizes the data used and respective approximate field coverage.

The wide-area XBoötes survey provides us with a unique opportunity to probe a large population of the most powerful AGN, half of which are also embedded in galaxy powerhouses with total

Name	Bands	Survey Size	N Detected
XBoötes [274]	0.5-7 keV	~ 9.3 deg^2	703
NDWFS [192]	B_w, R, I, and K	~ 9.3 deg^2	652
IR Boötes Imaging Survey [144]	H and J	~ 9.3 deg^2	~325
SDWFS [10]	3.6, 4.5, 5.8 and 8.0 μm	~ 10 deg^2	~330
HerMES MIPS [291]	24 μm	~ 10 deg^2	703
HerMES PACS [291]	110 and 170 μm	~ 3 deg^2	138 and 181
HerMES SPIRE [291]	250, 300 and 500 μm	~ 8.5 deg^2 shallow, ~ 3 deg^2 deep	489, 398, and 159

Table 3.1: Population counts and field coverage of the multi-wavelength flux catalogs used to generate 703 individual SEDs.

infrared luminosities (L_{IR}) greater than $10^{12} L_\odot$ (also known as ultra-luminous infrared galaxies or ULIRGs). Some weakly accreting AGN and AGN obscured by Compton thick hydrogen column densities ($N_H > 1.5 \times 10^{24}$ cm^{-2}) may be missed by X-ray surveys [e.g. 2, 214]. However, studies confirm no single waveband can be used to select a complete sample of AGN, and X-ray detections remain one of the most reliable identification methods [e.g. 15, 253, 116, 73, 14, 37, and references therein].

3.2.1 X-ray Data

Our AGN sample is selected from the *Chandra* XBoötes Survey, a 5-ks X-ray survey of the 9.3 deg^2 Boötes Field as defined in the NOAO Deep Wide-Field Survey [NDWFS; 274]. This survey covers the full area defined by NDWFS with 126 individual 5 ks contiguous pointings at uniform observational depths of $f_{0.5-7\,\mathrm{keV}} \sim 8 \times 10^{-15}$ erg s^{-1} cm^{-2}, yielding 3293 point sources with four or more counts. Rest-frame X-ray luminosities are determined by the following equation [4]:

$$L_X = 4\pi \times D_L^2 \times F \times (1+z)^{\Gamma-2} \tag{3.1}$$

where D_L is the luminosity distance, F is the hard band X-ray flux, z is the redshift and a photon index of $\Gamma = 1.9$, which is typical for an unabsorbed X-ray luminous AGN [e.g. 397, 277]. To remain consistent in comparison to other studies, we translate our full band $0.5 - 7$ keV luminosities to $2 - 10$ keV hard band luminosities with a conversion factor of 0.78, which is the ratio of respective intensities over each keV energy range for $\Gamma = 1.9$. Due to the shallow nature of the XBoötes Survey, spectral fitting to correct for X-ray absorption is difficult or unachievable at an individual level for ~90% of our sources [see **?** 274, for a more detailed discussion], so we leave the observed fluxes to be interpreted at face value. We select sources with X-ray luminosities $L_X > 10^{42}\,\mathrm{erg\,s^{-1}}$ as lower luminosity sources may contain contamination from host galaxy processes [e.g. supernovae, X-ray binaries and massive stellar outflows; 311, 265, 266**?**].

The X-ray survey depth of this study allows us to probe a larger population of the brighter end of the AGN luminosity function (see Figure 3.2). Figure 3.3 (bottom) displays the X-ray population distribution of this sample. The wider coverage of the XBoötes Survey allows us to study a large sample of powerful AGN with 50% of the 703 selected sources residing at or above $L_X = 1.07 \times 10^{44}\,\mathrm{ergs\,s^{-1}}$; similar studies using surveys that may be deeper but cover smaller areas in the sky yield populations of weaker AGN; for example, Lanzuisi et al. 2017 [212] (L17, hereafter) analyzed 692 X-ray selected AGN in the COSMOS field [338] with a median $L_X = 4.79 \times 10^{43}\,\mathrm{ergs\,s^{-1}}$.

3.2.2 Infrared Data

Mid-IR and far-IR fluxes are collected from Data Release 4 of the *Herschel* Multi-tiered Extragalactic Survey[1] [HerMES; 291]. Far-IR observations were taken by the *Herschel* Spectral and Photometric Imaging Receiver (SPIRE) at 250 μm, 350 μm, and 500 μm [150], and the *Herschel* Photoconductor Array Camera and Spectrometer (PACS) 110 μm and 170 μm [306] bands; mid-IR observations were completed by the *Spitzer* multi-band Imaging Photometer (MIPS) at 24 μm [**?**]. Fluxes for all five *Herschel* bands used in the HerMES survey are recorded on positions defined by MIPS 24 μm priors with a respective 5σ detection limit at $\sim$ 0.3 mJy. The HerMES SPIRE campaign consisted of a combination of both deep and shallow observations: the center $\sim$ 3 deg^2 region is deeper and reaches 5σ detection limits at 13.8, 11.3, and 16.4 mJy at 250 μm, 350 μm, and 500 μm, respectively; the outer $\sim$ 8.5 deg^2 region surrounding the center reaches 5σ detection limits at 25.8, 21.2 and 30.8 mJy for the 250 μm, 350 μm and 500 μm bands, respectively. The PACS observations occurred over the center $\sim$ 3 deg^2 of the Boötes region reaching 5σ depths of 49.9 and 95.1 mJy for the 110 and 170 μm bands, respectively. Uncertainties in this analysis include both instrumental and confusion noise; we refer the reader to Roseboom et al. 2010 [320] for a more detailed description of flux uncertainty determinations in the HerMES catalogs.

Near/Mid-IR catalogs were compiled from the *Spitzer* Deep, Wide-field Survey (SDWFS) [10] which used all four channels of the *Spitzer* Infrared Array Camera (IRAC) [124] to image the entire $\sim$ 10 deg^2 Boötes field. SDWFS is a combined four epoch survey that contains $\sim 10^5$ sources per band detected at 5σ depths of 19.77, 18.83, 16.50, and 15.82 Vega mag at 3.6 μm, 4.5 μm, 5.8 μm, and 8.0 μm, respectively. We also use J and H-band data from the NEWFIRM Infrared Boötes Imaging Survey [144] which reaches 5σ limits of 22.05 and 21.30 Vega mag, respectively; and optical B_w, R, I and K-band data from the NDWFS survey [192] reaching 5σ depths[2] at 26.6, 26.0, 26.0, and 21.4 AB mag, respectively. For all IR bands, we consider source detections at $> 3\sigma$.

[1] http://hedam.oamp.fr/

[2] https://www.noao.edu/noao/noaodeep/

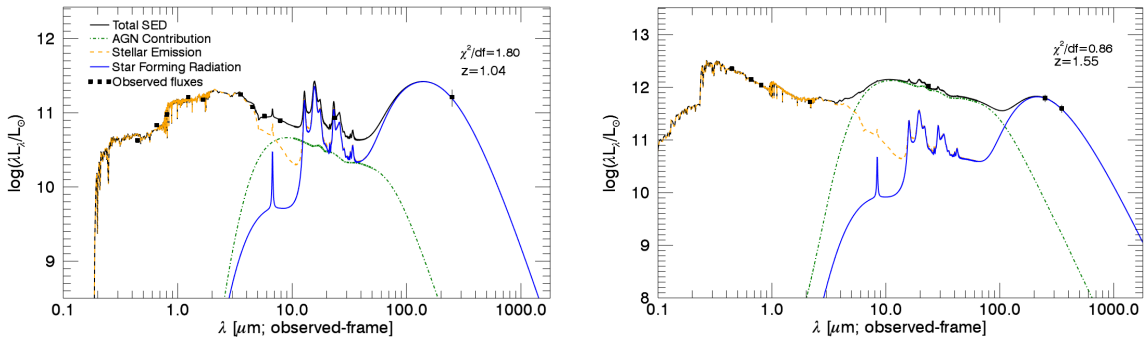

Figure 3.4: Example spectral energy distributions generated by SED3FIT [23]. The dashed gold line is the stellar emission contribution, the blue line is the radiation contributed by star formation processes, the green dashed line is the contaminating radiation from the AGN including the heated dusty torus surrounding the black hole, and the black line is the total SED or the summation of the three components.*Left*: SED for a galaxy with star formation processes dominating the mid to far-infrared spectrum. *Right*: In this SED, the AGN component provides the most contribution in the mid-infrared (and some of the far-IR) spectrum that would typically be attributed to star formation processes.

3.2.3 Redshifts

Spectroscopic redshifts are extracted from the AGN and Galaxy Evolution Survey (AGES) [201], an optical spectroscopic and photometric redshift survey for optically selected sources in 7.7 deg^2 of the Boötes field. We limited our sample to spectroscopic redshifts in the range $z > 0.1$ (Figure 3.2) to avoid the uncertainties associated with photometric redshifts and avoid contamination by local AGN and ULIRGs.

To investigate the evolution of AGN and galaxy properties with redshift, we complete our analysis over five redshift intervals and consider the X-ray - infrared relationship in each respective interval. The following redshift intervals are designed so that each interval has a sufficient number of sources ($\sim 90-200$) to create several statistically significant bins within that range: $z = 0.1-0.4$, $0.4-0.8$, $0.8-1.2$, $1.2-2$, and $2-5$. These redshift bins (z-bins) are consistent in comparison with several other similar studies, and contain 95, 178, 140, 195, and 95 sources, respectively.

3.3 AGN Sample Selection

The final sample used in this study consists of powerful AGN with spectroscopically confirmed redshifts, and a detection in one *Herschel* SPIRE or PACS band. Since all objects in the HerMES campaign are based on *Spitzer* MIPS priors, it follows that every object in our sample has at least one 24 μm detection as well as one *Herschel* detection. We achieve this sample, dubbed the XIR sample, through the following methods.

We matched X-ray AGN to infrared counterparts and spectroscopic redshifts using a nearest neighbor matching technique. First, X-ray sources were matched to the AGES redshift catalog using a 1″ search radius on their optical coordinates from [36], with a spurious match rate estimated at <1%. We were able to use such a small search radius confidently due to prior work by [36] who used a Bayesian matching scheme to determine optical counterparts for 98% of the X-ray sources in the XBoötes survey under a 1″ search radius. We note that AGES redshifts were determined using optical spectroscopy, and as such this study explores the properties of brighter, less dust obscured active galaxies. We also note that the AGES survey misses $\sim 2\,\mathrm{deg}^2$ of the XBo*ö*tes and HerMES survey (Figure 3.1), removing 10% of X-ray sources as possible candidates for this study. Near-IR and optical data were matched to the MIPS 24 μm coordinates from the HerMES catalog [291] using a 3″ search radius, which corresponds to the *Spitzer* MIPS 24 μm half width at half maximum. Finally, we matched the MIPS 24 μm coordinates to the AGES coordinates. Again, we estimate a spurious match rate of <1% when matching infrared data together, and once more when matching infrared data to X-ray sources with spectroscopic redshifts.

Prior to fitting a spectral energy distribution, we require an object to have a 24 μm detection and a detection in one of the *Herschel* bands. The far-IR survey was defined on the coordinates for sources detected at 24 μm, thus any Boötes source detected by *Herschel* will also have a measurement at 24 μm. Even though *Herschel* observational depths varied across the inner and outer region of the survey area, we still find a uniform density of $\sim$ 100 AGN per square degree that satisfy our

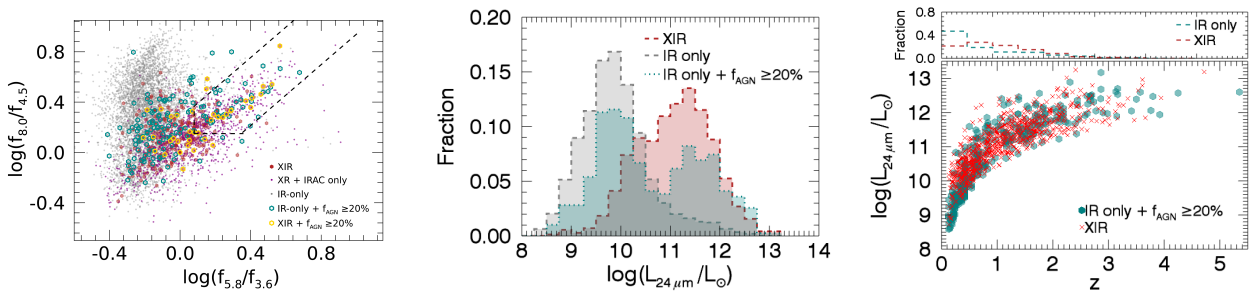

Figure 3.5: *Left*: IRAC color-color space used to identify luminous AGN in Donley et al. 2012 [101]. Grey points represent the IR-only sources with spec-zs, large red dots mark sources from our main sample of XIR sources, and purple points are additional X-ray sources with IRAC counterparts, but no mid or far-IR counterparts. The dashed black lines carve out the region belonging to luminous AGN, with minimal contamination from high redshift star-forming galaxies. We note that 15% of the luminous AGN in the IR only sample also have estimated AGN IR contributions $\geq$ 20% (teal circles), while the same is true for 25% of our XIR sample (gold circles). Generally, sources with AGN IR contributions $\geq$ 20% are dispersed throughout this IRAC color space, indicating that SED decomposition does not lend itself to luminous AGN identification. *Middle*: $L_{24\,\mu m}$ distribution for the 703 X-ray detected sample (red), the 5k IR-only detected sample (grey), and the 389 IR-only sources with $\geq$ 20% of IR SED emissions coming from AGN processes (teal). *Right*: $L_{24\,\mu m}$ vs. redshift distribution for both the 389 IR-only sample with significant IR AGN contribution (teal) and the X-ray detected sample (red). Top histogram represents the fraction of sources from each sample in redshift bins of size 0.5.

selection criteria. Additionally, due to the work by Brand et al. 2006 [36], the majority ($\sim$ 93%) of the sample also has an optical detection.

The mid and far-IR photometry requirement is unique to this work. Comparable studies required only one mid or far-IR detection or relied on stacking techniques and photometric upper limits to supplement, creating large uncertainties when generating AGN SEDs, particularly on the Wien side of the far-IR SED corresponding to dust emission [e.g. 270, 361, 212]. With the mid and far-IR requirement, we can better constrain dusty torus emission for powerful AGN and host star-forming galaxies.

This study is based on the 703 X-ray sources in the Boötes field that have intensive multiband data to fit their individual spectral energy distributions (see Table **??** for exact counts per band). Generating individual SEDs allows us to avoid the restrictions and uncertainties related to stacking and gives us the freedom to disentangle AGN and host galaxy radiation components for each respective source.

Using SED3FIT [23], a multi-component SED fitting tool, we decompose each galaxy's emissions in the infrared spectrum and use the appropriate rest-frame, infrared luminosity integrated from 8 μm to 1000 μm as an indicator of host galaxy star formation rate. SED3FIT is based off of the da Cunha et al. 2015 [**?**] MAGPHYS code and employs a combination of three galaxy radiation processes: stellar emission, warm and cold dust emission from star formation regions, and AGN emission. SED templates are fitted to measured fluxes first using the stellar and star forming components only, then AGN templates are varied to fill in photometric gaps and further reduce the χ^2. We use the ten AGN templates provided with SED3FIT, which were selected to cover the wide range of AGN found in the full Fritz et al. 2006 [129] library. These ten templates span Type 1, intermediate, and Type 2 AGN, with a variety of optical depths ranging from 0.1-6, as viewed face on or edge on. All ten of the templates have a fixed torus opening angle of $\Theta = 100°$, corresponding to an intrinsic covering factor of 75% (see Section 3.4.3 for details on covering factors). Each AGN template can be broken down into three components: dust scattering emission, dust thermal emission and nuclear accretion disk emission. The former two AGN components combined are attributed to the warm, dusty clumpy structure that surrounds the SMBH and accretion disk. See Figure 3.4 for two example spectral energy distributions generated from our sample (left: star formation dominant, right: AGN emission dominant).

To correct for contaminating AGN radiation, we subtract the dusty torus and accretion disk emission from the total SED of a source. The resulting infrared luminosity is attributed to star formation and is hereby represented as L_{IR}^{SF}, while the subtracted infrared AGN luminosity is referred to as L_{IR}^{AGN}; Figure 3.3 (top) shows our resulting population distribution of infrared luminosities attributed to star-formation processes. This procedure applies to 98% of our sample as 13 sources are not fitted with an IR AGN component by SED3FIT. The physical characteristics derived from this procedure will be available for all 703 sources on Vizier.[3]

Out of the remaining 2.6k XBoötes sources not used in our XIR sample, we also find 425 X-ray

[3]http://vizier.cfa.harvard.edu/

AGN with spectroscopic redshifts but no *Spitzer* MIPS and *Herschel* counterparts (marked as purple circles in Figure 3.2) with a similar X-ray and redshift distribution as our main sample – dubbed the non-IR sample (although some of these sources have IRAC detections; see next paragraph). We compare these non-IR AGN plus a sample of 6,583 IR-only galaxies with spectroscopic redshifts to our main sample in section 3.4. The IR-only galaxies have both a MIPS 24 μm and at least one *Herschel* far-IR detection, but no X-ray detection. For the non-IR AGN, we use the *Herschel* SPIRE 250 μm 5σ limiting flux in the deeper region of the HerMES survey as a generous upper limit on star formation luminosity. Out of the IR-only galaxy sample, 99% of sources have an optical counterpart and 91% have an IRAC detection. We ran IR-only photometric data through SED3FIT and found only 72%(~5k) of the ~6.6k galaxies are fitted with an AGN component.

For additional context, we briefly explore the additional two sample populations (6.6k IR-only galaxies and 425 non-IR AGN) in IRAC color-color space in Figure 3.5 (left). Nearly 40% of the non-IR AGN (small purple dots) and 92% of the IR-only galaxies (grey points) have sufficient (3σ) detections in all four IRAC bands; the same is true for 46% of our main XIR AGN sample (large red dots). In the Donley et al. 2012 [101] IRAC color criteria for identifying luminous AGN ($L_{2-10keV} \geq 10^{44}$ergs s^{-1}; wedge outlined by dashed black lines), 60 of 327 XIR sources with detections in all four IRAC bands are categorized as luminous AGN with a median $L_{2-10keV} \sim 5.6 \times 10^{43}$ergs s^{-1}; only 23 of the 58 XIR sources with $L_{2-10keV} \geq 10^{44}$ ergs s^{-1} and IRAC detections are categorized as luminous AGN through the IRAC criteria, which is nearly equivalent to the X-ray luminous AGN recovery rate found in Donley et al. (38%). This shows that, by using X-ray selection criteria, we're probing a larger population of the most powerful AGN. However, we must note that some powerful AGN are heavily obscured and therefore less X-ray bright (30 – 60%, see Section 3.4.3); we caution readers to consider this selection effect throughout this work.

In the same space, 7% of the non-IR AGN are categorized as luminous AGN with a median $L_{2-10keV} \sim 2.3 \times 10^{44}$ ergs s^{-1} and a recovery rate of 32% for all X-ray luminous AGN in the non-

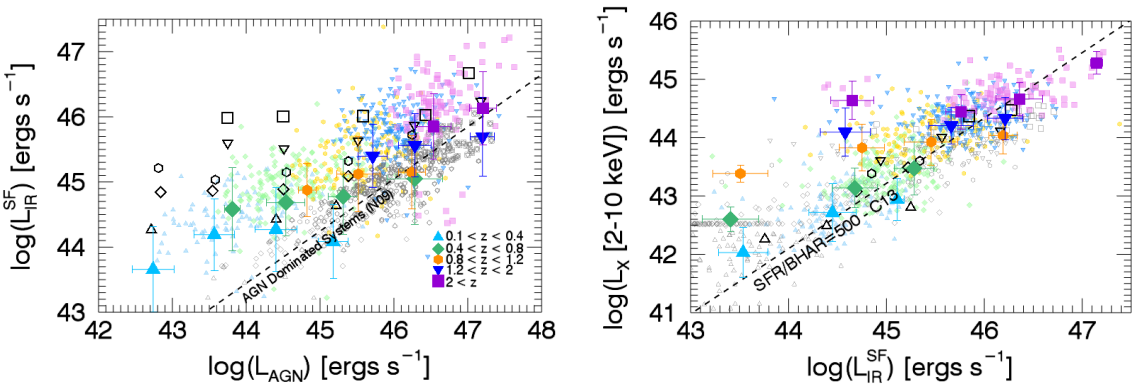

Figure 3.6: *Left*: Distribution of AGN bolometric luminosity ($\propto L_X$) versus L_{IR}^{SF}. The lighter, smaller points are individual AGN. The small, empty gray symbols are X-ray AGN with L_{IR}^{SF} upper limits determined by the HerMES *Herschel* SPIRE 250 μm flux limit. The larger, bolder, filled in points are average $\log(L_{IR}^{SF})$ in bins of $\log(L_{AGN})$ showing both the IR detected (colorful) and IR non-detected (empty grey) X-ray sources. Error bars represent the 1σ dispersion of each bin. Note the star forming luminosity for the most powerful AGN in the $0.4 < z < 0.8$ z-bin lies directly under the corresponding average star forming luminosity for the most powerful AGN in the $0.8 < z < 1.2$ z-bin. The black dashed line represents the relationship found in N09 where objects below the line have infrared luminosities dominated by AGN activity. Black empty symbols are results from Lanzuisi et al. 2017 [212]. *Right*: Average $\log(L_X)$ in bins of $\log(L_{IR}^{SF})$ compared to results from C13 [59]. The C13 sample is represented by the black empty shapes. The dashed line is the constant proportional relationship between star formation rate (SFR) and black hole accretion rate (BHAR) found in C13. Colors, symbols and error bars are calculated in the same fashion as in the left figure, where the empty gray points denote the IR only detected sources with an estimated IR AGN fraction $\geq 20\%$ with X-ray upper limits defined by the XBo$\ddot{o}$tes survey flux limit.

IR sample; and out of the 5.6k IR only sources with spec-zs and sufficient IRAC detections, only 2% (N = 128) of sources are deemed luminous AGN (but members of this sample do not have any bona fied X-ray detections, so we cannot determine the recovery rate).

3.4 Results and Discussion

3.4.1 Average L_{IR}^{SF} vs. Average L_{AGN}

We translate X-ray flux to bolometric AGN luminosity, L_{AGN}, using the equation in Rosario et al. 2012 [318] (R12 hereafter) derived from Maiolino et al. 2007 [240] and Netzer and Trakhtenbrot

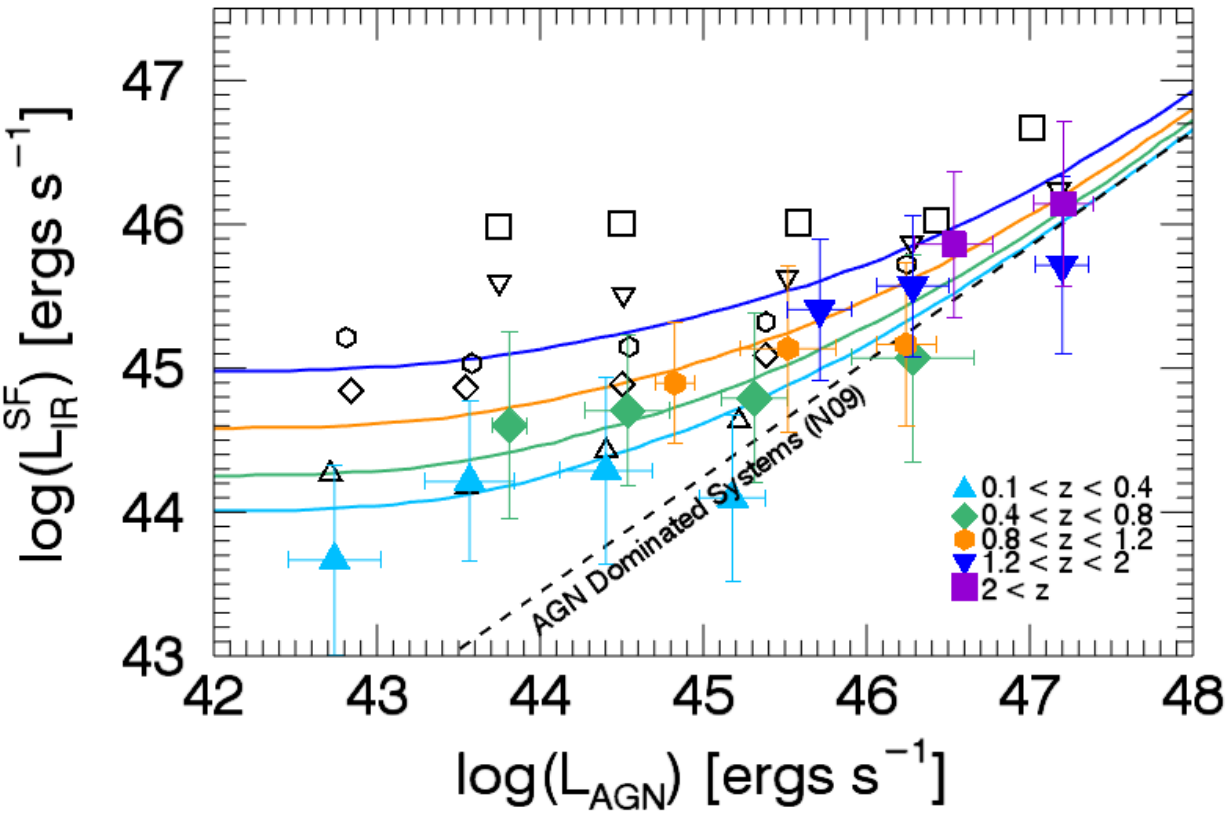

Figure 3.7: Distribution of AGN bolometric luminosity versus L_{IR}^{SF} with the black dashed line as defined in Figure 3.6 (left). The solid lines have colors corresponding to redshift ranges and are the extrapolated trends from the Hickox et al. 2014 [171] simple model incorporating short-term AGN variability, long-term evolving star formation rates and a universal constant of proportion between SFRs and black hole accretion rates.

2007 [285] for spectroscopically confirmed Type 1 (unobscured) AGN:

$$\log L_{AGN} = \frac{\log L_X - 11.78}{0.721} + 0.845 \tag{3.2}$$

where L_X is the 2-10 keV band X-ray luminosity. We average infrared contribution from star forming processes in bins of L_{AGN}, with respect to each redshift interval, and do the same separately for the additional 425 X-ray sources with spectroscopic redshifts but no IR counterparts. We show these results in Figure 3.6(left); the dashed line represents the relationship found in Netzer et al. 2009 [283] (N09, hereafter) for local, low luminosity AGN-dominated systems where L_{AGN} is much larger than L_{IR}. Nearly 50% of X-ray only detected sources fall into the AGN-dominated section, compared to only $\sim$ 5% of individual X-ray and IR detected sources, substantiating the selection of AGN embedded within star-forming galaxies in this analysis and demonstrating the dominance of star-formation driven modes in IR luminosities of *Herschel* detected dusty galaxies. This trend is corroborated in several recent works using IR-bright X-ray selected AGN (e.g. R12, L17), indicating that the power law correlation from N09 is valid when extended to higher luminosities and high-z AGN.

Our low-z ($z \lesssim 1$) sample successfully reflects those of other published results with low luminosity AGN ($L_{AGN} < 10^{45}$ erg s^{-1}) showing a flat or uncorrelated relationship between AGN activity and star formation. The higher luminosity AGN in the low-z bins appear to trend in a more positive linear fashion that approaches the N09 relationship. The stronger, positive relationship is most noticeable in the $0.4 < z < 0.8$ bin where the most powerful AGN, while few in number (N=6), are embedded in star-forming galaxies nearly just as bursty as the brightest AGN in the $0.8 < z < 1.2$ bin. These results also appear in L17 and R12, but conflict with the flat, nonexistent relationships found in Stanley et al. 2015 [361] and Dai et al. 2015 [81].

Hickox et al. 2014 [171] and Volonteri et al. 2015 [400] developed models that match similar observational results as seen in L17, R12, Chen et al. 2013 [59] and Azadi et al. 2015 [13]. In Figure 3.7, we overlay the Hickox et al. model curves and see general agreement with the results for our $z \sim 1$ less powerful active galaxies ($L_{AGN} < 10^{45}$ ergs s^{-1}), but the model over estimates star forming luminosity for the more powerful AGN ($L_{AGN} > 10^{45}$ ergs s^{-1}) in each redshift range. To create the model, Hickox et al. generated a sample of galaxies (up to $z = 2$) in which all star-forming galaxies host an AGN during their lifetime, and then incorporated a constant of proportion between SFR and black hole accretion rate over long time scales (log(SFR/BHAR) = 3.6 [59, 81]) and assigned short time scale variabilities in AGN accretion processes (and therefore, luminosity). Generally, the model successfully produces the observed findings when averaging star formation activity in bins of AGN activity, along with the trends observed in literature when averaging AGN activity in bins of star-formation activity, as analyzed in the following section.

3.4.2 Average L_X vs. Average L_{IR}^{SF}

Recent simulations and observations reveal that AGN accretion (and therefore luminosity) can be highly variable on short timescales – e.g. on the order of 1-2 magnitudes within 0.1-1 Myr [e.g. 95, 171] – whereas star formation processes change at a slower rate over longer timescales. To uncover the relationship between AGN processes and host galaxy star formation rates, it might be more appropriate to average AGN activity (the more rapidly changing variable) based on L_{IR}^{SF} (the more stable variable).

Following the analysis in L17 and Chen et al. 2013 [59] (C13, hereafter), we reversed data dependency by averaging $\log(L_X)$ in bins of $\log(L_{IR}^{SF})$. We include 389 IR only sources with an AGN IR contribution that is $\geq 20\%$ of the total IR SED. These IR-only sources have both a MIPS 24 μm and at least one *Herschel* far-IR detection, but no X-ray detection (see Figure 3.5 for 24 μm population distribution). We take the ratio of IR AGN luminosity to total IR luminosity from the

resulting SED and place a cut at $\geq 20\%$ to capture the sources with the highest likelihood of hosting an AGN [64]. For these objects, we use the XBo$\ddot{o}$tes survey flux limit as an upper limit for X-ray luminosity. Results are shown in Figure 3.6 (right) with L17 results overlaid. Error bars represent the 1σ dispersion of the mean X-ray luminosity in each respective bin. The dashed line represents the constant ratio between black hole accretion rate (BHAR, proportional to X-ray luminosity) and star formation rate found in C13 for 34 X-ray detected AGN at $z = 0.25 - 0.8$.

We find our results to be in good agreement with the C13 SFR/BHAR ratio. The low z-bins ($z \lesssim 1$) have the strongest positive slope between the same L_{IR}^{SF} intervals studied in C13, which is expected as C13 analyzed data from the same Boötes *Chandra*, *Herschel* and *Spitzer* observations used in this paper. While AGN still hover near the SFR/BHAR ratio in the earlier $z > 0.8$ Universe, there is no significantly strong upward trend as L_{IR}^{SF} increases for any z-bin, and the nearly ~0.5 dex increase exhibited within the $z > 2$ sample for the highest range of star formation activity has a very small sample size and is therefore unreliable.

Note that these observations are limited to the depths of the $24\,\mu$m survey; an object at $z \sim 1$ with a $24\,\mu$m luminosity of $L_{24\,\mu m} = 10^{44}\,\mathrm{ergs\,s^{-1}}$ is pushing the survey observational limits and might be undetected. This means that the weakest star formation bins in this analysis may be lacking contributions from some fainter, intermediate redshift galaxies and AGN. Conversely, some powerful AGN are heavily obscured by high column densities of dust and gas. In fact, studies have shown that 90% galaxies with high $24\,\mu$m to optical flux ratios have IR and X-ray signatures indicating the presence of heavily obscured AGN [126, 381]. These AGN are expected to have intrinsic X-ray luminosities in excess of $10^{44}\,\mathrm{ergs\,s^{-1}}$, at $z \sim 1 - 2$, which could drive the more star-forming L_{IR}^{SF} bins further upward and into stronger agreement with the C13 trend.

The observed differences in correlation between the two averaging methods are likely due to the inherent rate of variation between the two physical processes, with star formation being the more stable measurement and AGN accretion being the more variable measurement. These differences in correlation methods were also confirmed by Dai et al. 2015 [81] for similar samples of X-ray

selected AGN. Lapi et al. 2014 [215] found similar results when exploring the observational phenomena of the co-evolutionary relationship between AGN and host galaxies at high redshifts ($z \gtrsim 1.5$) using a semi analytical model. Combining observational data on AGN in star-forming galaxies with high-z AGN luminosity functions and host-galaxy stellar luminosity functions, the model shows galaxy SFRs that remain relatively constant over a long period of time then suddenly undergo a rapid decrease in star formation when the SMBH is triggered into an active phase. The model also predicts that as the supermassive black hole grows, a fraction of the cold interstellar gas and dust within the spiral arms of a galaxy is drawn towards the nucleus to help form and grow the dusty torus. The AGN will feed off this reservoir and the most powerful AGN will have feedback processes that strip away some of the remaining cold gas and dust, further suppressing star formation processes and eventually slowing its own growth as well. Observations at various epochs within the model easily reproduce both of the trends shown in Figure 3.6 and, when combined with the publications and findings discussed in section 3.4.1, indicate that a more detailed study on the relationship between short term AGN variability and host galaxy cold gas and dust properties is necessary to arrive at any definitive conclusions.

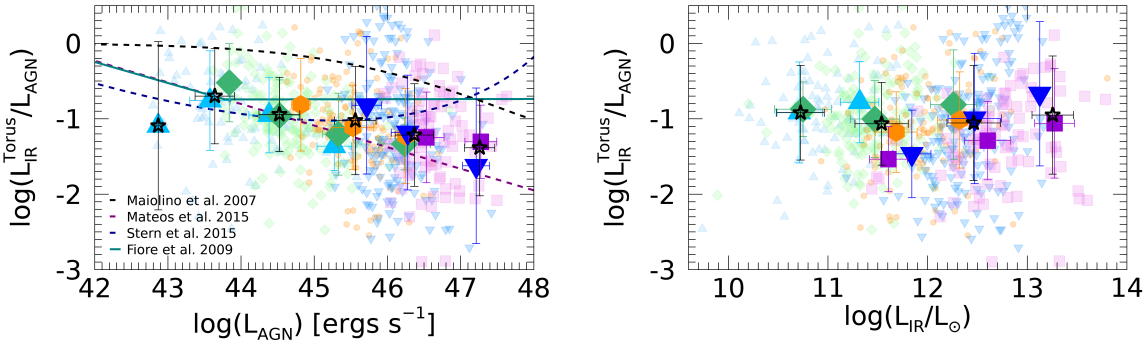

Figure 3.8: *Left*: Covering factor versus bolometric AGN luminosity. Averages for the X-ray detected sample are computed in bins of L_{AGN} and in respective redshift ranges. We also computed averages for the entire sample, irrespective of redshift range, as indicated by the empty black stars. The black dashed line represents the fraction of obscured AGN as a function of bolometric AGN luminosity found by Maiolino et al. 2007 [240]. The purple dashed line, navy dashed line, and turquoise solid line correspond to mid-IR/L_{AGN} fractions found by translating the X-ray-to-6 μm relationships derived in Mateos et al. 2015 [248], Stern et al. 2015 [364], and Fiore et al. 2009 [127], respectively. *Right*: Covering factor versus total infrared luminosity. Averages, colors and symbols are derived in the same fashion as the figure to the left.

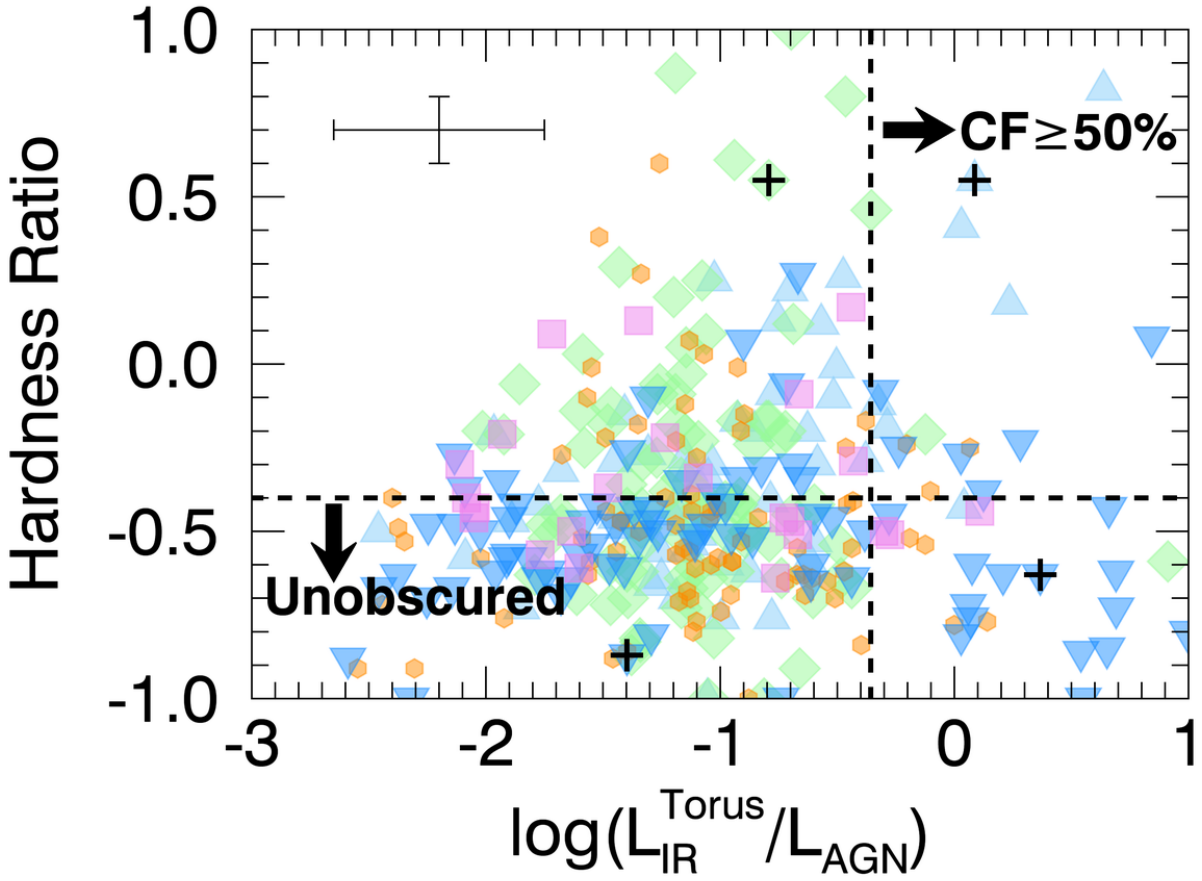

Figure 3.9: Covering factor versus hardness ratio for the 330 XIR AGN with sufficient x-ray counts to determine hardness ratios. Colors and shapes are the same as those in Figure 3.6. Average error bars are presented in the top left corner. To the right of the black dashed vertical line lies AGN with covering factors greater than 50%. Below the black dashed horizontal line lies AGN with hardness ratios indicative of unobscured cores. SEDs for sources marked with crosses are in the appendix, providing examples of some of the more extreme and contradictory AGN in this sample.

3.4.3 Dust Covering Factors

We can determine how dust obscured an accreting SMBH is by assessing the relationship between how much high energy radiation from accretion disk processes is observed (which therefore escapes the dusty torus), versus how much radiation is detected from the dusty torus itself. A commonly used dust covering factor (CF) proxy is the ratio of dusty torus emission, L_{Tor} (which dominates in the mid to far-IR), to bolometric AGN luminosity, L_{AGN} [e.g. 240, 382, 321]. To compute the dust covering factor for our sample, we use the bolometric AGN luminosities derived from Equation (2), and derive L_{Tor} from the dusty torus components in each source's respective AGN SED (i.e. we remove the infrared emission originating solely from the accretion disk from each AGN SED template for each source and keep only the dusty torus emission components). We caution that systematics from the fixed covering factor (75%) in the AGN SEDs may produce biased estimates of dusty torus emission in this analysis (see Section 3.3).

We note that this proxy ($CF = L_{Tor}/L_{AGN}$) is used under the assumption that accretion disk emission and the resulting dusty torus emission are generally isotropic. However, the work of Stalevski et al. 2016 [359] shows that, when considering the anisotropy of these emission processes for Type 1 AGN with $L_{AGN} \sim 10^{45}$ ergs s^{-1}, this proxy can underestimate intrinsically low covering factors and overestimate high covering factors, while for Type 2 AGN of similar luminosities, this proxy always underestimates the true covering factor. We assess the impact of this assumption on our results at the end of this section.

The average dust covering factor decreases with an increase in AGN activity for our X-ray detected AGN sample (Figure 3.8, left). This trend correlates nicely with the luminosity-dependent AGN unified model where dust covering factor is anti-correlated with bolometric luminosity, also known as the *receding torus model* [216]. Taking the model implications a step further, it follows that the average covering factor within a sample of AGN corresponds directly to the fraction of Type 2 (obscured) AGN. In this work, we find an average CF of 33% for the X-ray detected AGN. This

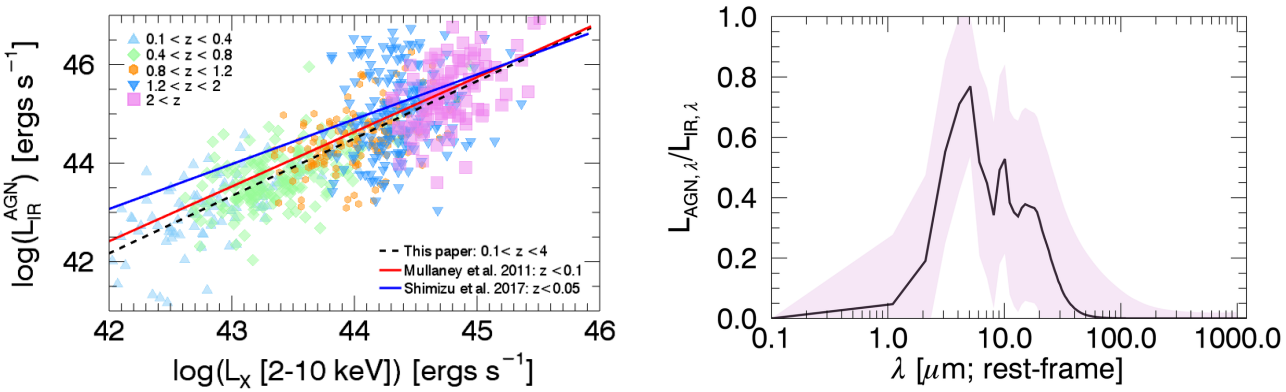

Figure 3.10: *Left*: Infrared AGN luminosity as a function of L_X for the X-ray AGN. The black dashed line represents the linear relationship found in log space between the two AGN luminosities. The red and blue lines represent the relationship determined from generated average SEDs for local AGN by Mullaney et al. 2011 [269] and Shimizu et al. 2017 [345], respectively. *Right*: Composite $f_{\rm AGN}$ as a function of rest-frame wavelength using all 703 X-ray selected AGN. The black line is the median value at all wavelengths in bins of $\Delta\lambda = 1\ \mu$m and the 1σ scatter for each $\Delta\lambda$ is indicated by the shaded pink region.

average CF is similar but slightly lower than those found in literature: Rowan-Robinson et al. 2009 [321] used *Chandra* and/or *Spitzer* data to determine CFs for 658 AGN and found an average dust covering factor of 40%; Mateos et al. 2015 [248] determines a spectroscopically confirmed Type 2 fraction of 43% on a sample of 250 X-ray selected AGN with dust covering factors ranging from 20-50% when averaged in bins of X-ray luminosity; Lanzuisi et al. 2009 [213] found a higher Type 2 fraction at 55% of mid-IR bright X-ray selected AGN, and Hickox et al. 2007 [169] selected IR-AGN in the same field as this study and used spectroscopic and optical to mid-IR color distributions to determine a Type 2 fraction of 43%. The observed luminosity-dependence agrees most with the trend found in Mateos et al. (shown as the purple dashed line in Figure 3.8, left), who also used multi-component SEDs to determine the AGN contribution to mid-IR luminosity. A newer study by Mateos et al. 2017 [249] investigated the lack of one to one correlation between Type 2 fraction and average covering factor for their complete sample of optically classified X-ray AGN. They identify a missing population of X-ray obscured AGN and, when the high covering factors of these obscured AGN are accounted for, the population CF average grows to nearly 60% with a less significant luminosity dependence relationship. It is possible that the CFs of heavily obscured

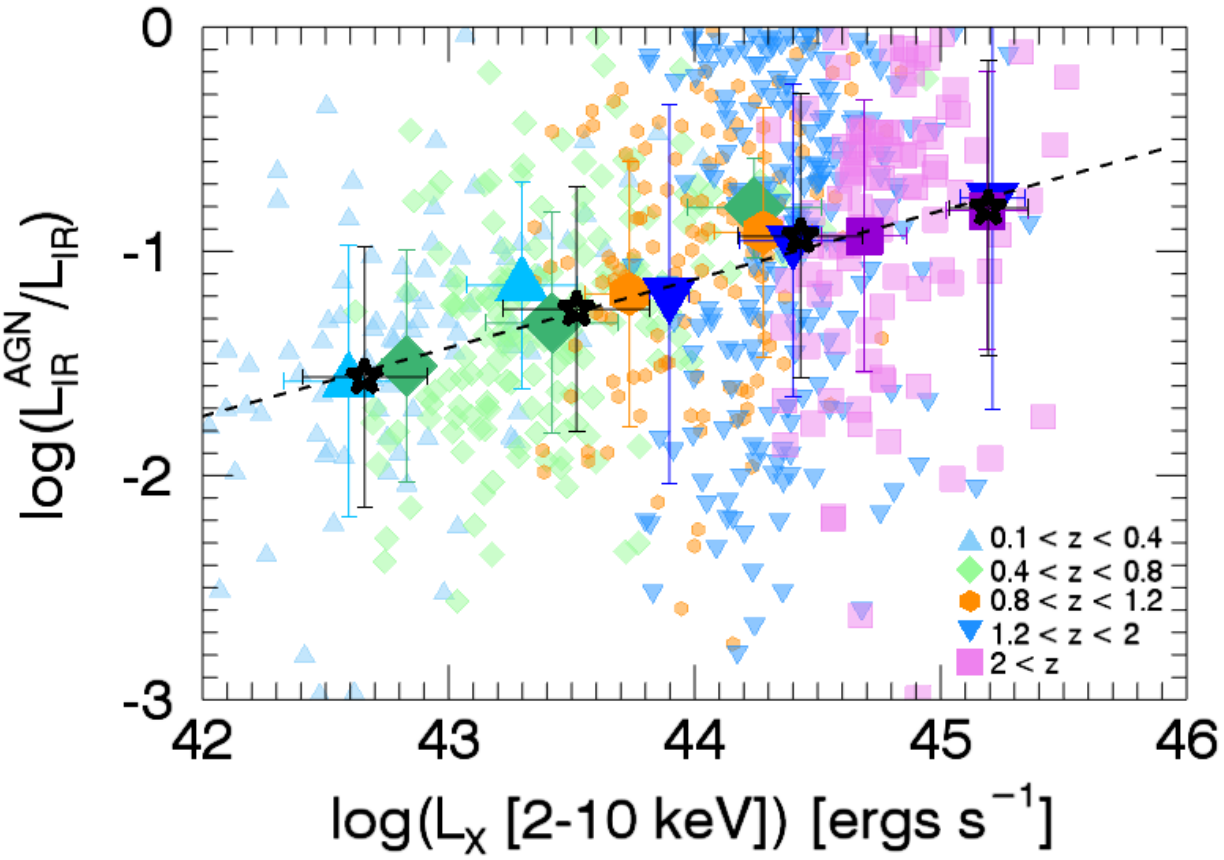

Figure 3.11: AGN fractions for the X-ray detected sample as a function of X-ray luminosity. Averages are computed in bins of L_X, respective of redshift range, with error bars representing the 1σ dispersion of the mean. Black empty stars represent the averages across X-ray luminosity, regardless of age in the universe.

AGN in the Boötes region would effectively raise the average CF across all redshift ranges and AGN luminosities to a similar value, but that analysis it out of scope for this work.

In Figure 3.8, right, we find an overall flat relationship between total infrared luminosity and covering factors for the X-ray selected sample, hovering at an average of $\sim$ 10% across all luminosities. While there appears to be some positive relationship for all redshift bins $z > 0.4$ starting at $\log(L_{IR}/L_{\odot}) \approx 11.5$, the sample dispersion is large, spanning $\pm \sim 50\%$ (or more) for each average data point within each redshift bin. Therefore, any observed positive correlation is weak and would require further investigation for verification.

We also recover trends that challenge the inclination-based unified model: there is no clear bimodal

distribution for covering factors in the XIR AGN population; instead we see a distribution of covering factors that cover the entire possible range at significant percentages. To investigate, we further restrict our sample to the 330 XIR AGN with sufficient X-ray counts to determine hardness ratios (HRs; i.e. H−S / H+S, an indicator of AGN obscuration; e.g. Green et al. 2004 [**?**]) and find the majority ($\sim$ 57%) are unobscured with corresponding HRs $\lesssim -0.5$ and an overall wide spread in covering factors averaging at 35% ± 1.03% (see Figure 3.9). Concentrating only on the 187 XIR AGN with unobscured HRs, we find 11% have CFs $\gtrsim$ 50%, indicating that a defining CF cut off limit between Type 1 and Type 2 AGN based on X-ray absorption is nonexistent. Mateos et al. 2016 [247] found similar results using 227 spectroscopically confirmed and categorized X-ray AGN; while the different types of AGN had clearly different CF distributions (with type 2(1) peaking at high(low) covering factors) there was still a very strong overlap in CF distributions; roughly 20% of Type 1 AGN had CFs > 0.5 and 40% of Type 2 AGN had CFs < 0.5. Merloni ett al. 2014 [257] used optical photometry and/or spectra paired with hard X-ray data for ∼1300 AGN and found 31% of the entire sample sits in a similar contradictory region where optical signatures point towards an unobscured nucleus while X-ray data indicates considerable gas and dust absorption, or vice versa with optical evidence for an obscured nuclear region and no absorption of soft X-rays. This work and the aforementioned suggest that Type 1 and Type 2 AGN may not be observationally distinct due to the line-of-sight inclination of the dusty torus but instead due to other physical accretion related mechanisms.

Recently, Ricci et al. 2017 [314] showed that the relationship between AGN luminosity and covering factor flattens out when dividing X-ray AGN into separate bins of Eddington ratios (λ_E; mass-normalized black hole accretion rate), indicating that the AGN line-of-sight obscuration is not the universal driver of covering factor distributions. Instead, λ_E and CF maintain a steady positive correlation up until the sublimating Eddington limit for dusty gas particles, in which the CF sharply declines. These results point towards strength in radiation pressure from accretion activities being the main regulator of observed obscuration fractions, and that Type 1 and Type 2 AGN are actually physically different objects (as categorized by λ_E) that could be better unified within the context of

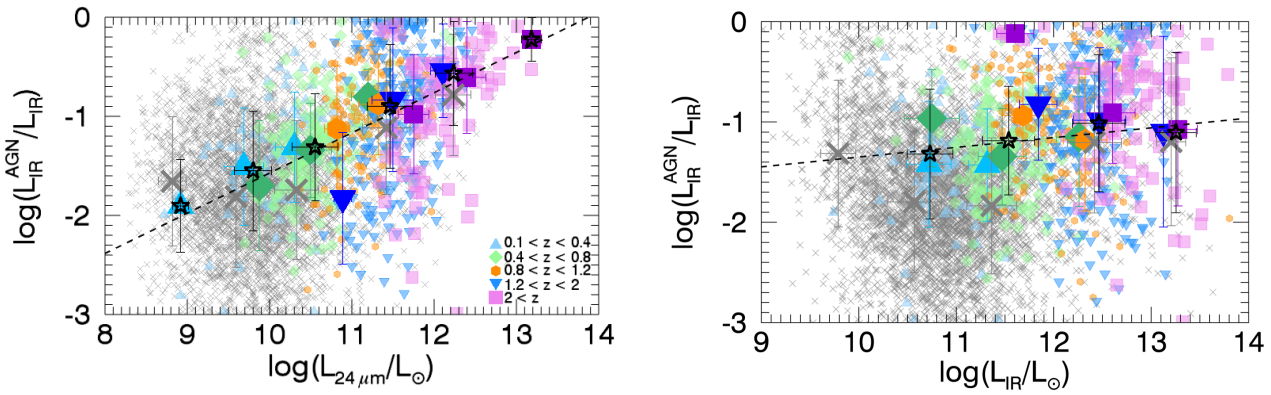

Figure 3.12: These two figures represent the ratio of infrared AGN luminosity to host galaxy total infrared luminosity (i.e. AGN fraction) as a function of host galaxy luminosities. Colors and symbols are the same as in Figure 3.8. *Left*: The logarithm of the AGN fraction as a function of 24 μm luminosity. *Right*: The logarithm of the AGN fraction as a function of total infrared luminosity, following the same legend as in the figure on the left.

black hole growth over time. Exploration of this relationship is out of scope for this analysis; we refer readers to [19, 416, 120, 233, 217, 249] for further discussions that precede the Ricci et al. results.

We explored how the Stalevski et al. 2016 [359] equation and coefficients (Equation 8 and Table 1, inside) for correcting isotropically-assumed dust covering factors affect our results by first identifying Type 1 and Type 2 AGN using the inclination angles used in the SED fitting procedure. The AGN SED fitting model used in this paper include two possible nuclear line of sight angles: 0 degrees (face-on aka Type 1 unobscured nucleus) or 90 degrees (edge-on aka Type 2 nucleus viewed through the disk). Based on this criteria, 61% of our XIR sources are categorized as Type 1 AGN and the remainder are categorized as Type 2 AGN. Interestingly, the majority of Type 2 AGN in this sample (77%) have covering factors below $\leq$ 10%, while Type 1 AGN exhibit no general CF preference. Both AGN types have median AGN luminosities of $L_{AGN} \sim 3 \times 10^{45}$ ergs s^{-1}.

We applied each set of coefficients corresponding to the three reported example optical depths ($\tau_{9.7\mu m} = 3, 5, 10$ in Stalevski et al.) to the respective AGN types. The overall effect is strongest for AGN (of both types) with originally estimated CFs less than 20%, which is nearly three quarters

of the 703 AGN; for each set of coefficients, dust covering factors were increased to $\geq 20\%$, due to the lower limits assumed in Stalevski et al., with the average individual differences being +33% to the respective CFs. This effectively flattens out any trends seen in Figure 3.8, where the original average CF of 32% is now a corrected average CF of 49%. It is worth noting that these equations were originally derived for a luminous AGN with $L_{AGN} \sim 10^{45}$ ergs s^{-1}; the third of our sample at lower AGN luminosities sees an average CF correction of $\sim$ +25%, while the remaining more powerful population has a ten percent higher average CF correction than that of the low luminosity AGN. Thus, due to the the underlying assumptions in covering factors and the wide range in AGN luminosities probed in this work, we are unfortunately limited from interpreting any further.

3.4.4 AGN Contribution in the Infrared

The wide infrared coverage in the Boötes region when paired with the multicomponent SED fitting model SED3FIT is advantageous in effectively constraining intrinsic infrared AGN luminosities across a broad redshift range. This is useful to avoid situations of overestimating host galaxy properties (e.g. star formation rates) in cases with little IR photometry and/or possible indications of AGN activity. In the following, we explore the extracted infrared AGN luminosities in the $8 - 1000\,\mu$m range (L^{IR}_{AGN}, hereafter) as a function of L_X, as well as the fraction of total infrared luminosity attributed to AGN emissions (L^{IR}_{AGN}/L_{IR} or f_{AGN}, hereafter) as a function of L_X, L_{IR}, and $L_{24\,\mu m}$.

There is a strong correlation between X-ray activity and total infrared AGN luminosity within our X-ray detected sample. This relationship is similar to the driving trend determined in Mullaney et al. 2011 [269], even though a large portion of our sample contains galaxies with low AGN fractions ($f_{AGN} < 10\%$) out to high redshifts. Mullaney et al. modeled intrinsic infrared AGN SEDs for only 11 local ($z < 0.1$) AGN with polycyclic aromatic hydrocarbon emission lines indicative of IR luminosities dominated by AGN ($f_{AGN} > 90\%$). As seen in Figure 3.10 (left), we derive a

nearly equivalent relationship for AGN spanning a much larger redshift and AGN fraction range, suggesting that this relationship is universal. The black dashed line denotes our sample relationship, where

$$\log\left(\frac{L_{IR}^{AGN}}{10^{43}\mathrm{erg\,s^{-1}}}\right) = (0.33 \pm 0.06) + (1.16 \pm 0.05)\log\left(\frac{L_X}{10^{43}\mathrm{erg\,s^{-1}}}\right) \quad (3.3)$$

with a strong, positive correlation coefficient of 0.78. The red line denotes the slope found in Mullaney et al. (1.11 ± 0.07) and the blue line denotes the slightly weaker relationship found by Shimizu et al. [345] (0.91 ± 0.06) who analyzed a sample of 313 local X-ray selected AGN with *Herschel* and *WISE* detections; additionally, Kirkpatrick et al. 2017 [**?**] found a more extreme relationship (3.76 ± 0.08, not plotted) for 53 $z \sim 1-2$ composite galaxies in the GOODS-S field with *Spitzer* and *Herschel* detections. Our work provides the first $0.1 < z < 4$ pure AGN infrared SED relationship estimated using a statistically significant population size, providing future studies the ability to estimate the total infrared emission of a high-z AGN using only X-ray data. A deeper X-ray study with a similar amount multiwavelength IR data and de-absorbed X-ray luminosities would be needed to confirm this relationship is complete to lower luminosity X-ray AGN at $z > 0.1$.

The median infrared AGN contribution across all sources is 8 - 30%, indicating that roughly 70 - 90% of infrared light from this set of galaxies is coming from star formation processes. When restricting our sample to the 337 ULIRGs ($L_{IR} > 10^{12}\,L_\odot$), we find a median $f_{AGN} = 13\%$, similar to the fraction found in Nardini et al. 2008 [280] for local ULIRGs. Looking at the median composite, rest-frame f_{AGN} as a function of wavelength in Figure 3.10 (right), we find that AGN contribution heavily affects the mid-IR, with a maximum of nearly 80% at 5-6 μm. While the

impact of AGN contribution trails off at wavelengths greater than ~30 μm in Figure 3.10 (similar to other results, e.g. [199, 269]), the $f_{\rm AGN}$ sample distribution is broad at each wavelength with an average scatter of $\pm 20-30\%$, implying that multi-component SED analysis is crucial in accurately determining the true AGN contribution for individual sources, particularly for cases without X-ray observations to constrain $L_{\rm AGN}^{\rm IR}$.

On average, $f_{\rm AGN}$ increases with increasing X-ray and 24 μm luminosity, but not with total infrared luminosity (see Figure 3.11 and Figure 3.12). The latter tells us that any trends found with $L_{\rm AGN}^{\rm IR}$ are not driven simply by the host galaxy's luminosity; or, in other words, a broad range of infrared AGN fractions can be found embedded in variously luminous galaxies. We also considered the relationship between $f_{\rm AGN}$ and host galaxy stellar mass; again, we find a flat, non-existent correlation. We note that this sample occupies a host galaxy stellar mass distribution similar to those found in literature for AGN host galaxies, with a mean stellar mass of $\log(M_*) = 10.83 \pm 0.58$ [e.g. 170, 419].

We determine a clear but weak relationship in $\log(f_{\rm AGN}) - \log(L_{24\,\mu m})$ and in $\log(f_{\rm AGN}) - \log(L_{\rm X})$, both with slopes $\approx$0.11. Both correlations have large intrinsic scatters and weak correlation coefficients at $\sim \pm 60\%$ and ~ 0.36, respectively. Ciesla et al. 2015 [64] shows that $f_{\rm AGN}$ predictions below 20% are accompanied with large uncertainties and therefore should be disregarded; these uncertainties vary across AGN types and it is unclear how they might vary across AGN luminosities. To investigate whether there is a stronger relationship present in our more certain $f_{\rm AGN}$ calculations, we restrict our sample to $f_{\rm AGN} \geq 20\%$, which is about 28% of the entire sample with an average $\log(L_{24\,\mu m}) = 11.56 \pm 0.66$ and $\log(L_{\rm X}) = 44.30 \pm 0.54$. Instead, we find an even weaker slope at ~0.06 with a correlation coefficient of ~0.12 for both sample populations, and again a large range of values. These results directly indicate a need for individual SED decomposition to infer the fraction of infrared output attributed by an AGN.

3.5 Summary and Conclusions

We explored the relationship between AGN activity and host galaxy dust properties across the tail end of peak AGN and galaxy growth in the Universe (redshifts $0.2 < z < 5$) using *Chandra*, *Herschel*, *Spitzer* and NOAO Telescope observations in the Boötes field. We successfully disentangled AGN and star formation radiative processes in the infrared spectrum for 703 IR bright X-ray AGN using multi-component SED fitting code, SED3FIT [23], and determined the AGN-corrected integrated rest-frame infrared luminosity attributed to star formation, total infrared AGN luminosity, AGN dust covering factors and AGN fractions. Our main results can be summarized as follows:

- We find flat trends consistent with other literature when averaging L_{IR}^{SF} in bins of bolometric AGN luminosity for less powerful AGN ($L_{AGN} < 10^{45}\,erg\,s^{-1}$), as well as the stronger correlations found when averaging L_X in bins of star formation activity for AGN at low redshifts ($0.1 < z < 0.8$).

- We further decompose AGN SEDs to isolate the dusty torus component in the IR and compare to the bolometric AGN luminosity to estimate nuclear obscuration. We determine an average dust covering factor slightly lower than other literature at CF= 33%, which indicates a Type 2 (obscured) population of roughly a third. Further investigation of X-ray hardness reveals several X-ray AGN with covering factors that contradict the expected nuclear obscuration determined by hardness ratios (e.g. high covering factor with a low hardness ratio that is indicative of an unobscured central engine), providing further evidence that observational differences between AGN types are not primarily driven by line-of-sight dusty torus inclination.

- We uncover a wide range in the fraction of infrared luminosity attributed to AGN activity across all redshifts, and determine no statistically significant trend exists when evaluating f_{AGN} as a function of total infrared, X-ray or 24 μm luminosity. The mean f_{AGN} as a function of rest-frame IR wavelength shows peak AGN contamination lives in the mid-IR range and

becomes insignificant at wavelengths larger than $\sim 30\,\mu$m, but the sample dispersion is large ($\pm 20 - 30\%$) at all wavelengths. These results demonstrate the importance of SED decomposition for individual AGN and host galaxies in order to accurately quantify AGN contamination in the IR, particularly prior to using IR photometry to estimate host galaxy properties.

While considering all of the implications discussed in this paper, we should remember that current FIR detections of intermediate and high redshift X-ray AGN in star-forming galaxies are limited by the sensitivity of far-infrared and submillimeter observatories like the *Herschel* Space Observatory. The currently available resolutions limit us to the most powerful star-forming systems and we need deeper, more sensitive observations to capture the dust properties of AGN that reside in smaller and/or quiescent galaxies in order to complete the evolutionary picture.

Chapter 4

Missing Massive Galaxies - Long et al. 2022

4.1 Introduction

Most of what we understand about galaxy evolution in the first six billion years of the Universe is largely based on rest-frame ultraviolet-to-optical (UV2OP) studies. This includes, but is not limited to: the evolution of the galaxy stellar mass function [e.g. 302, 276, 86] used to describe the growth of galaxies over time; the large scale structure of galaxies [e.g. 113, 426] that demonstrates how galaxies are distributed throughout space as they form and grow; and the star-forming main sequence [Table 3 in 356] establishing that the majority of galaxies form their stars steadily, over long periods of time ($\sim$ 1 Gyr), at a rate proportional to their stellar mass. These hereinafter referred to as 'UV-based' relationships are often perceived as fundamental truths that are either fed into or used as benchmarks for success in testing our best cosmological models [e.g. 137, 21]. In other words, our primary understanding of galaxy evolution – from observations to simulations – is deeply and intricately rooted in UV2OP astronomy, including all of its strengths and limitations.

It is now well known that the rest-frame UV2OP spectrum of the Universe contains only a piece of the larger picture on star formation in the cosmos. Nearly *half* of all cosmic starlight in the Universe

is obscured by dust [106], which re-radiates at longer infrared wavelengths. This phenomenon is most evident in the cosmic star formation rate density (cSFRD) where, out to $z \sim 3$, the majority of stellar mass is built in regions obscured by dust and thus primarily detected via infrared (IR) observations [see 236, for a review]. This means that studies using only UV2OP to chart stellar mass assembly throughout cosmic time are incomplete and biased against significantly dusty systems.

Over the last two decades, wide-field far-IR and submillimeter surveys ($\lambda > 40\,\mu$m) have discovered significant populations of dusty, star-forming galaxies (DSFGs, see Casey, Narayanan, and Cooray 2014 [51] for a review). Their extreme rates of star formation ($\sim 10^{2-3}\,M_\odot\,yr^{-1}$) generate massive reservoirs of dust that obscures the starlight, making some DSFGs nearly invisible to even the deepest UV2OP observations, but bright like beacons at far-IR and (sub)millimeter wavelengths [e.g. 76, 414, 242]. Though rare in the local Universe, DSFGs are a thousand times more populous at $z \sim 1-3$ [e.g. 349, 424], dominating cosmic star formation during these times.

While some DSFGs are detected in the deepest of UV2OP surveys, they are generally left out of large surveys broadly describing galaxy evolution. This usually happens through e.g. stringent requirements for photometric coverage over the rest-frame UV2OP spectrum [e.g. requiring *r,* *i,* and z -band detections, 342], and/or "redder" selection bands with observations that are still insufficiently deep to capture the heavily obscured (and redshifted) starlight [e.g. K_s-band < 24 mag, 220]. While often the best available tool for such studies, these requirements are biased against sources with significant attenuation in their UV2OP spectral energy distributions (SEDs); and, if DSFGs are captured, they are often treated as contaminants to the broader goals of the study, to be either removed or ignored as an insignificantly small portion of the broader galaxy population [e.g. $< 10\%$ at its peak fraction 327, 187]. Thus, it is likely that several of the UV-based fundamental relationships used to describe galaxy evolution, used to shape and test our finest models and simulations, are lacking a proper accounting of the DSFG population – a population that drives and dominates stellar mass assembly in the first ~ 6 billion years of the cosmos.

Indeed, the astrophysical community has been struggling to properly model and reproduce DSFG

populations – and their measured physical characteristics – since their discovery [e.g. 148, 18, 183, 166, 7, 251]. This may have to do with a need for more sophisticated dust radiative transfer treatments, degeneracies in constraining DSFG stellar initial mass functions, and/or a general lack of constraints on the physical origins / triggering mechanisms of DSFGs (see e.g. Hayward et al. 2021 [167] for an in depth discussion). Many of the same simulations struggling to properly reproduce DSFG population observations also struggle to produce sufficient populations of massive ($M \sim 10^{11}\,M_\odot$) quiescent galaxies at early times [e.g. 38, 256]. It is possible that these mysteries and shortcomings are related because it is also likely that these galaxy sub-populations are related.

Several lines of evidence suggest that the brightest DSFGs constitute the primary ancestral population of the most massive quiescent galaxies in the Universe. This includes comparable comoving number densities [$n \sim 10^{-5} - 10^{-6}\,\mathrm{Mpc}^{-3}$, e.g. 379, 349], dark matter halo masses and clustering properties [$M \sim 10^{12-13}\,M_\odot$, e.g. 172, 230], physical shapes and effective radii [$r_{\mathrm{eff}} \sim 2\,\mathrm{kpc}$, e.g. 178], star formation histories [strong and bursty with SFRs $\gtrsim 10^{2-3}\,M_\odot\,\mathrm{yr}^{-1}$over 50-100 Myr, e.g. 390], and stellar masses [$\sim 10^{11}\,M_\odot$, e.g. 76, 262]. Prior studies have also demonstrated a clear relationship between stellar mass and dustiness, where the most massive galaxies are more dust-obscured across cosmic time [395, 296, 417, 412, 411, 93]. Recent discoveries of massive, $z > 3$ quiescent galaxies demand short, bursty star-formation histories in line with those exhibited by DSFGs [e.g. 142, 332]. And, finally, the SHARK semi-analytical model (which is largely successful in modeling on-sky DSFG populations) suggests that the majority of the most massive galaxies ($M > 10^{11}\,M_\odot$) at $z \approx 1$ undergo a (sub)millimeter-bright phase at $z > 1$ [e.g. 210]. Thus, in order for us to understand how the most massive galaxies form and quench during the first half of the cosmic time, it is of the utmost importance that we are dogged in our pursuit towards understanding massive, dust-obscured galaxies and placing them into the wider context of massive galaxy evolution at $z > 1$.

The objectives of this work are twofold. The first is to quantify, to first-order, the significance of missing DSFG populations at the massive end of the star-forming galaxy stellar mass function

(SMF). Star-forming SMFs are biased against dusty galaxies as they are determined using UV2OP tracers. Infrared luminosity functions, however, trace the warm dust emission from nebular regions throughout star-forming galaxies. Combined, the UV and IR luminosity functions make up the cosmic star formation rate density known today [236]. Still missing from the picture, however, is a evolutionary depiction of the stellar mass contributions from dust-obscured star-forming galaxies. Using the IR luminosity function as a nearly-complete consensus of DSFGs out to $z \sim 3-4$, we seek to quantify what the dust-obscured stellar mass function might look like, and posit that it would create a more shallow extension beyond the limits of the UV-based SMF.

The second objective is to test the hypothesis that, despite the heterogeneity of the DSFG population, it is sufficient and complete enough to describe and model the assembly of massive quiescent galaxies in the early Universe. Using a suite of simple assumptions to forward evolve mock populations of DSFGs, we are able to reproduce the observed evolution of massive, passive galaxies – without needing to invoke any complex assumptions on merger histories, feedback / quenching mechanisms, or even contributions from outside populations [e.g. blue nuggets, 262].

This paper is organized as follows: in Section 4.2 we describe the basis assumptions and empirical data used to build the model used in our analysis; in Section 4.3 we describe the resulting dust-obscured stellar mass function from our model; in Section 4.4 we discuss the implications of this model, including how we forward evolve mock galaxies to create their quiescent descendants (Sec. 4.4.1), and a comparison of the resulting number densities to comparable observational studies (Sec. 4.4.2). Throughout this work, we adopt a Chabrier IMF [56] and a *Planck* cosmology, where $H_0 = 67.7\,\mathrm{km\,s^{-1}\,Mpc^{-1}}$ and $\Omega_\Lambda = 0.692$ [305].

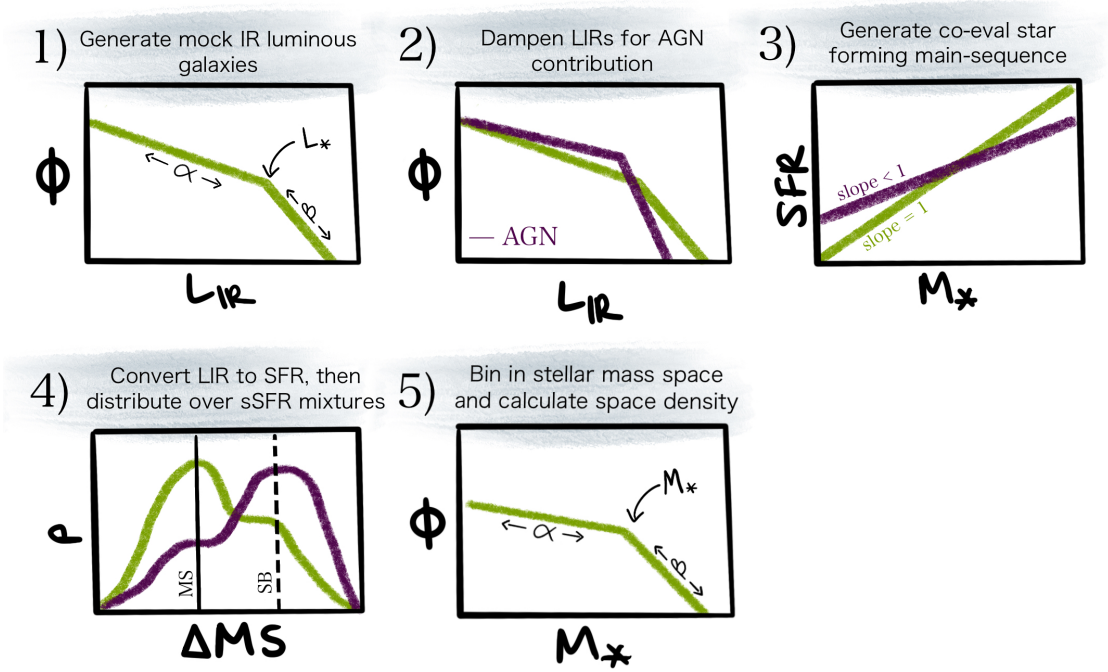

Figure 4.1: A cartoon of the model presented in this work. Several of the parameters highlighted in this cartoon are randomly sampled to account for uncertainties, variation, and unknowns across the literature. **1)** The model begins by generating mock populations of IR luminous galaxies according the the IR luminosity function defined in Casey et al. 2018 [50] and Zavala et al. 2021 [424] (Section 4.2.1). **2)** Then, the mock galaxies undergo a dampening prescription to account for AGN contributions to the IR (Section 4.2.2). **3)** Then, we generate a star forming main-sequence at the co-eval redshift of interest (Section 4.2.3), **4)** convert the (dampened) IR luminosities to star formation rates and use these SFRs to randomly distribute the galaxies in stellar mass space according to various Gaussian mixtures of main-sequence and starburst galaxies (Section 4.2.3). **5)** Finally, we re-bin the galaxies in stellar mass space to derive space densities, which we then describe as the stellar mass function of IR luminous galaxies (Section 4.2.4). This process is repeated a thousand times per 1 deg^2 redshift slice for a given main-sequence vs. starburst ratio, taking care to randomly sample the relevant parameter space (see Table 4.1), then combined to derive an overall stellar mass function for dust-obscured galaxies (see Section 4.3).

4.2 Model Ingredients

Recent theoretical and observational evidence supports the idea that some (or even the majority) of the most massive star-forming galaxies in the $z > 1$ Universe are heavily obscured by dust. This would mean that a significant portion of cosmic stellar mass is enshrouded in dust, and therefore difficult to detect with traditional photometric methods in the UV2OP spectrum. Our goal in this work is to use existing empirical data on dusty, star-forming galaxies to test this hypothesis and quantify the impact of DSFGs on the massive end of galaxy evolution. In this section, we describe the empirical data and assumptions used to build our numerical model, as well as the model itself. There are four main steps to populate the model, each described and motivated in greater detail in the proceeding subsections:

1. Use the infrared luminosity function to derive a mock population of DSFGs (Section 4.2.1).
2. Correct IR luminosities for AGN contamination so that L_{IR} to accounts for only star formation emission (Section 4.2.2).
3. Convert L_{IR} to SFR and distribute SFRs over the star-forming main sequence (i.e. the M_*-SFR relation) to derive stellar masses for the mock DSFGs (Section 4.2.3).
4. Bin in stellar mass space and compute the three dimensional stellar mass density (Section 4.2.4).

In Figure 4.1, we share a cartoon depiction of our model. The model is realized in a light cone of solid angle $1\,\mathrm{deg}^2$ over a given redshift interval; the redshift windows cover $0.5 < z < 6$ and are set to match existing stellar mass functions derived from deep and wide surveys [e.g. 276, 86]. All four steps occur within each of the 10^3 realizations, with each realization drawing from probability density functions that mimic uncertainties based on empirical measurements. In Table 4.1, we summarize the parameters and their probability distributions that we sample in this

Physical Relationship	References	Parameter Space & Modeled Distribution
Infrared Luminosity Function	[55, 424]	Same as in [55, Table 3 therein], except for $\psi(z > z_{\rm turn})$ and $\alpha_{\rm LF}$, reported in [424] as $-6.5^{+0.8}_{-1.8}$ and $-0.42^{+0.02}_{-0.04}$, respectively. We employ skewed Gaussians for both parameters.
AGN Host Selection	[196]	$f_{\rm AGN\ Hosts} = 4-100\%$ over an S-shaped curve increasing as a function of $L_{\rm IR}$ (defined in Fig. 30, therein). We interpolate over the S-shaped curve in each $L_{\rm IR}$ bin.
$L_{\rm IR}$ Dampening of AGN Hosts	[200]	We sample the CDF of composite and AGN hosts in Fig. 3 therein to randomly assign $f_{\rm AGN\ MIR}$. Then, we use the quadratic equation (Eqn. 5 therein) to assign $f_{\rm AGN\ TIR}$. We employ Gaussians for the quadratic equation variables.
Star-Forming Main Sequence	[356]	For the slope, we sample a Gaussian with $\mu = 0.9$ and $\sigma = 0.1$. We keep the time evolution components (Eqn. 28, therein), employing Gaussians for the parameters related to time. The starburst region is fixed to 0.6 dex above the main-sequence at a given stellar mass. We fix $\sigma_{\rm MS} = \sigma_{\rm SB} = 0.3$ dex.
Main Sequence vs. Starburst Decomposition	[327, 76, 334, 260, 308, 28, 107]	We step through six double Gaussian distributions, each with one mean centered on the main sequence and the other centered on the starburst regime (+0.6 dex). The distributions match the following starburst fractions: 50, 40, 30, 20, 10, and 0%.

Table 4.1: Physical relationships and respective parameter spaces used in this model. See Section 4.2 for details on these values and their motivation.

model. See the specific subsections that follow for details and motivation on the chosen parameters and distributions.

Finally, Section 4.3 describes how we combine these realizations to create our resulting stellar mass function, and provides the parameters describing the shape of this dust-obscured SMF.

4.2.1 The Infrared Luminosity Function

We seed our model by generating mock populations of IR luminous galaxies according to the IR luminosity function (IRLF), with the structure described in Casey et al. 2018a,b [55, 50] and updated parameters measured in Zavala et al. 2021 [424]. This IRLF is empirically-constrained at $z < 3$ by well-known DSFG spectral energy distributions and physical properties derived using *Spitzer* and *Herschel* data [55], and at $z > 3$ using ALMA observations[424]. Below, we briefly describe the IRLF parameterization and constraints used in this work, and refer the reader to [55, 50] for more details. We explore the impact of these parameters on our results in Section 4.4.

The IRLF in this model takes the form of a double power-law such that:

$$\Phi(L,z) = \begin{cases} \Phi_\star(z)\left(\frac{L}{L_\star(z)}\right)^{\alpha_{\rm LF}(z)} & \text{if } L < L_\star \\ \Phi_\star(z)\left(\frac{L}{L_\star(z)}\right)^{\beta_{\rm LF}(z)} & \text{if } L \geq L_\star \end{cases} \tag{4.1}$$

where $L_\star$ represents the evolving characteristic 'knee' of the luminosity function, $\alpha_{\rm LF}$ represents the *faint-end* slope of the IRLF (below $L_\star$), $\beta_{\rm LF}$ represents the *bright-end* slope of the IRLF (above $L_\star$), and $\Phi_\star$ represents the evolving characteristic number density of the luminosity function.

Both $\rm L_\star$ and $\Phi_\star$ evolve with redshift, reaching a "turning point" at $z_{\rm turn} \sim 2$ (corresponding to the peak of the CSFRD) such that, at $z > z_{\rm turn}$, $\rm L_\star$ and $\Phi_\star$ evolve with a different slope than at $z < z_{\rm turn}$. In other words, $\rm L_\star$ and $\Phi_\star$ evolve as $(1+z)^\gamma$ and $(1+z)^\psi$, respectively, with γ and ψ changing values at $z \approx z_{\rm turn}$.

In general, the parameters describing the IRLF at $z \lesssim z_{\rm turn}$ are observationally well-constrained. We use the values listed in Table 3 in [55], with the exception of ψ at $z > 2$ for which we use the value derived in [424], and refer the reader to these works for more details on how these values were

determined. Specifically, we fix the bright-end slope to $\beta_{\rm LF} = -3.0$, the redshift evolution of $L_\star$ to $\gamma = 2.8$, and the redshift evolution of $\Phi_\star$ to $\psi = 0.0$. Together, these values successfully reproduce the measured IRLF, $L_\star$, $\Phi_\star$, and the IR luminous galaxy contributions to the CSFRD at $0 < z \lesssim 2$ [see Appendix A.1 in 55]. We note that this combination of variables is not a unique solution; there are other possible combinations that could produce similar results in wide-and-shallow surveys revealing local and/or extremely bright galaxies in the Universe – but these values were chosen to produce observations across wide ranges in both IR luminosity and in epoch.

At $z > z_{\rm turn}$, there is much less information on the evolution of $L_\star$ and $\Phi_\star$. For $L_\star$, studies report γ values as steep as ~ 1.6 [152] and as flat as 0.2 [202]; this IRLF assumes a redshift evolution of $\gamma = 1$, which is in line with the assumption that $L_\star$ evolves towards brighter luminosities at higher redshifts – as seen in several observational studies [e.g. 152, 202, 230]. Higher values (e.g. $\gamma > 1.5$) would create unphysically bright IR luminous galaxies at $z > 4$ that are not known to exist.

For the evolution of $\Phi_\star$ beyond $z_{\rm turn}$, studies report ψ values from $\lesssim -10$ [202] to -0.5 [230], where more positive values correspond to a dust-*rich* early Universe, and more negative values correspond to a dust-*poor* early Universe. In other words, a dust-poor early Universe would manifest as a CSFRD that is *not* dominated by obscured star formation at $z > z_{\rm turn}$, and there would be significantly fewer $z > 3$ DSFGs in blank-field sub-mm surveys than there are at $z \sim 2$. In this work, we adopt the value presented in [424] where $\psi = -6.5^{+0.8}_{-1.8}$, corresponding to a more dust-poor early Universe.

The average faint-end slope collated in [55] is $\alpha_{\rm LF} = -0.6$. However, recent works suggest a potentially shallower slope of $\alpha_{\rm LF} = [-0.2, -0.5]$ [423, 202, 151, 230, 424]. For this work, we adopt the value reported in [424] where $\alpha_{\rm LF} = -0.42^{+0.02}_{-0.04}$; this value is aligned with the best fit faint-end slopes in [202], [423], and [230]. We explore how a steeper slope may affect our results in Section 4.4.

For this analysis, we randomly sample the parameter space for ψ and $\alpha_{\rm LF}$ as listed above and defined in [424]. The parameters are modeled as skewed Gaussians, with values drawn for every realization.

In review, for each of the 10^3 model realizations, we randomly sample IRLF parameter values from their aforementioned distributions, then use the IRLF to generate a mock IR luminous galaxy population. To determine the number of IR luminous galaxies in a light cone slice ($n_{L_{IR}}$), we integrate the IRLF over bins of width $\delta {\rm L_{IR}} = 0.25\,{\rm dex}$. To assign IR luminosities in a way that accurately reflects the shape of the IRLF, we then use the IRLF to generate a cumulative distribution function (CDF) for the respective $\rm L_{IR}$ bin. Then, we draw $n_{\delta L_{IR}}$ galaxies from a random uniform distribution applied to the CDF ordinate. We use the randomly generated IR luminosities to calculate corresponding star formation rates according to Equation 12 in [198, originally derived in [273]] using the variables listed in Table 1 therein for a total IR (TIR) to SFR conversion. We note that not *all* IR luminosity in a DSFG can be attributed to star-forming processes; some likely hails from AGN accretion activity. In the following section, we detail how we model potential AGN hosts and adjust their IR luminosities accordingly.

4.2.2 AGN Contributions to Total Infrared Luminosity

The integrated IR luminosity of galaxies encapsulates dust emission heated by both star formation activity *and* active black hole growth (i.e. active galactic nuclei, or AGN). Young stars embedded in dusty nebulae emit primarily UV and optical light that's absorbed by the enshrouding dust. This warmed dust re-emits in the infrared spectrum. Similarly, actively growing coeval black holes are often surrounded by obscuring clumps of dust and gas that's heated by high energy X-ray, UV, and optical photons, and also re-emits in the infrared. Theoretical and observational studies show that the bright end of the IRLF ($\rm L_{IR} > 0.1 - 1 \times 10^{13}\,L_\odot$, depending on the epoch) is likely dominated by AGN-powered IR emission [183, 130, 152, 371, 372]. Similarly, studies on samples of IR luminous

galaxies demonstrate that the higher the L_{IR}, the more likely an AGN is present [196, 195, 223] – with an incidence rate of $> 50\%$ at $L_{IR} \gtrsim 10^{12}\,L_{\odot}$ at $0 < z < 4$. Together, these lines of evidence indicate that we cannot assume that all IR emission from our mock galaxies hails only from star formation processes. Since we wish to use IR luminosity as an indicator for star-formation activity, we must correct for AGN contamination in the total infrared spectrum ($8 - 1000\,\mu$m).

To create a realistic correction effect, we must first define what fraction of IR luminous galaxies likely host an active supermassive black hole (regardless of how IR luminous the AGN is). For this step, we use the AGN population fraction in 70μm bright sources as a function of IR luminosity reported in [196, Fig. 30 therein]. This analysis included AGN selected through a myriad of techniques – X-ray detections, radio loudness, IRAC colors, and mid-IR power laws. At IR luminosities $< 10^{12}\,L_{\odot}$, less than 20% of the IR luminous galaxies host AGN; but between $10^{12-14}\,L_{\odot}$, the occurrence rate jumps from 60% to nearly 100%. We note that other, more recent studies on AGN-SF host galaxy fractions report *smaller* AGN occurrence rates as a function of IR luminosity [e.g. 223, 372]. Since we're using total IR luminosity as an indicator for star-formation, which in turn will be used to later derive stellar masses (see Section 4.2.3), smaller AGN occurrence rates will result in larger stellar masses in this model. Thus, by using the larger AGN population fractions in Kartaltepe et al. 2010 [196], we are choosing a more conservative approach that is less likely to predict an unphysical overabundance of massive star-forming galaxies.

After selecting a subset of mock IR luminous galaxies to host AGN, we must then decide exactly how much of the IR radiation comes from the AGN. For this step, we use the detailed analysis reporting mid and total IR contributions by AGN in ULIRGs at $z = 0.3 - 2.8$ by Kirkpatrick et al. 2015 [200]. We use the distribution of mid-IR fractions (determined by *Spitzer* IRS mid-IR spectral decomposition, Fig. 3 therein) for designated composite and AGN-dominated galaxies as a probability distribution, and draw from this probability distribution to assign mid-IR AGN fractions to AGN hosts. Then, we use the quadratic relationship between mid-IR AGN fractions and total-IR AGN fractions to determine what percent of the total IR emission can be assigned

to star formation (Equation 5 and Fig 14, therein). The majority ($\sim$ 70%) of AGN hosts in [200] exhibit mid-IR spectral features indicative of AGN mid-IR dominance (where $f_{AGN,mid-IR} \geq 60\%$); it is only at this mid-IR fraction that AGN contamination to the *total* IR luminosity ($8 - 1000\,\mu$m) becomes significant ($\geq 20\%$).

In general, this procedure has the most significant impact our most luminous galaxies of $L_{IR} \geq 10^{13}\,L_{\odot}$ – which often correspond to the most massive galaxies – with an average AGN total IR fraction of $\sim 50\%$. Note that the Kirkpatrick et al. relationship between mid-IR and total IR AGN dominance maxes out at $f_{AGN,mid-IR} = 100\%$, corresponding to $f_{AGN,totalIR} \approx 60\%$. Some studies argue that AGN can be powerful enough to dominate the *entire* IR spectrum [e.g. **?** 370, 371] while other studies argue find AGN contributions are predominantly limited to the mid-IR [e.g. 39]. Additionally, recent results demonstrate the existence of a population of moderate to powerful AGN which were previously missing from these major AGN-galaxy co-evolution studies as they were assumed to be weak AGN but are instead likely heavily obscured [211]. Together, these studies indicate that the true underlying relationship between galaxy IR luminosities and AGN processes is still unknown.

In summation, we use a suite of simple assumptions from the combined works of [196] and [200] to correct a modest fraction of IR luminosities under the assumption that the IR emission is significantly powered by an AGN. These corrected IR luminosities are then used to calculate star formation rates (as detailed at the end of Section 4.2.1). In future work, we will explore more detailed treatments and characterization of AGN in massive dusty galaxies – and the consequences of these treatments and assumptions – in the context of this model.

4.2.3 The Star-Forming Main Sequence

One of the most ubiquitous and well-studied relationships describing galaxy evolution is the correlation between a galaxy's star formation rate and stellar mass. This tight relationship, known

as the star-forming main sequence (SFMS), suggests that most star-forming galaxies sustain steady (i.e. non-bursty) SFRs over several billion years [289, 288, 79], at the end of which a galaxy exhausts its gas supply and moves off the main sequence towards quiescence. The correlation exists unambiguously across several orders of magnitude in stellar mass throughout cosmic time - from $z \sim 0$ [e.g. 225, 307] to as high as $z \sim 4$ [e.g. 335, 325, 301], theoretically making the SFMS useful in predicting stellar masses for a population galaxies with known SFRs, or vice versa.

The exact shape of the SF main sequence and its evolution through time is still the subject of intense debate. There is general agreement that the MS takes the form of a power-law (i.e. $\mathrm{SFR} \propto \mathrm{M}_*^{\alpha}\, 10^{\beta}$) with a tight intrinsic scatter of $0.2 - 0.35$ dex at $\mathrm{M}_* \lesssim 10^{10}\,\mathrm{M}_\odot$ [e.g. 356, 334, 250]. In this same stellar mass regime, recent studies report that the SFMS slope, α, lies between $0.8 - 1$ [e.g. 356, 220, 334, 380]. However, there is less consensus for galaxies with stellar masses $> 10^{10}\,\mathrm{M}_\odot$ – which is the range of stellar mass we are primarily interested in for this work.

Several studies describe a flattening of the main sequence above a certain "turnover" mass, typically reported at $\sim 3 \times 10^{10}\,\mathrm{M}_\odot$ with possible evolution towards higher values during earlier times [e.g. 409, 377, 334, 220, 380]. Above this mass, the main sequence is typically parameterized as a power law with a slope that is more shallow than the slope in the low-mass regime, effectively saturating in SFRs at high stellar mass. This bending could be driven by physical phenomena such as star formation suppression at high-masses or increased bulge contributions [e.g. 408, 295, 226], and/or by observational effects such as contamination by passive galaxies [e.g. 193], biased/incomplete SFR indicators [e.g. 109], or biased/incomplete SF galaxy sample selection techniques [e.g. 316].

For this work, we assume that the turnover at high masses is driven by observational effects, and that the true SFMS is a singular power law. The majority of studies reporting a high mass turnover selected their star-forming galaxy samples using optical / near-IR color cuts [409, 334, 220, 380], such as the *UVJ* technique [418, 410]. However, color diagnostics centered in the ultraviolet to near-IR regime, while often the best available tool for such studies, are imperfect identifiers of dust obscured star-forming galaxies. Depending on colors and sample characteristics, anywhere

from 5-50% of $M_\star > 10^{10}$ dust obscured galaxies could be misclassified as quiescent due to their dust-reddened spectra [334, 100, 299, 326, 308, 187]. This misclassification effectively removes some of the most dust obscured, and therefore star-forming, massive galaxies from the analysis, whose SFRs would likely increase the high-mass SFMS slope. Furthermore, the high mass slope can also be analytically flattened by the misclassification of passive galaxies as star-forming [193].

Studies that sought specifically to constrain the stellar properties of DSFGs find these galaxies sitting on or above a proportionately more massive and more star-forming extension of a singular power law SFMS [e.g. 76, 246, 260, 301]. Recently, a growing body of literature is starting to establish the existence of massive, optically-dark dust obscured galaxy populations that were previously undetected in deep UV2NIR surveys [e.g. 358, 405, 53, 414, 378, 351, 242, (in prep)] – the same surveys used to establish a global SFMS. It is therefore likely that the true underlying SFMS – one that includes massive dust obscured galaxies – takes the form of a power law all the way through the high stellar mass regime.

For this analysis, we randomly sample the power law slope of the SFMS from a Gaussian distribution centered at $\mu_\alpha = 0.9$ with a dispersion of $\sigma_\alpha = 0.1$. Using these slopes as opposed to more shallow ones is a more conservative approach; since we pivot SFRs over the main-sequence power law to derive stellar masses, employing shallower slopes (e.g. $\alpha = 0.4 - 0.6$) generates large, unphysical excesses of massive dust-obscured galaxies. Furthermore, this approach allows us to marginalize our results over the different competing MS slopes established in more recent literature [e.g. 334, 220, 380, 28]. We use the evolving normalization (β) from the SFMS in [356] (Equation 28, therein); this form is generally consistent across several studies using different populations of galaxies to determine SFMS properties [e.g. 193, 334, 380, 207, 301, 308].

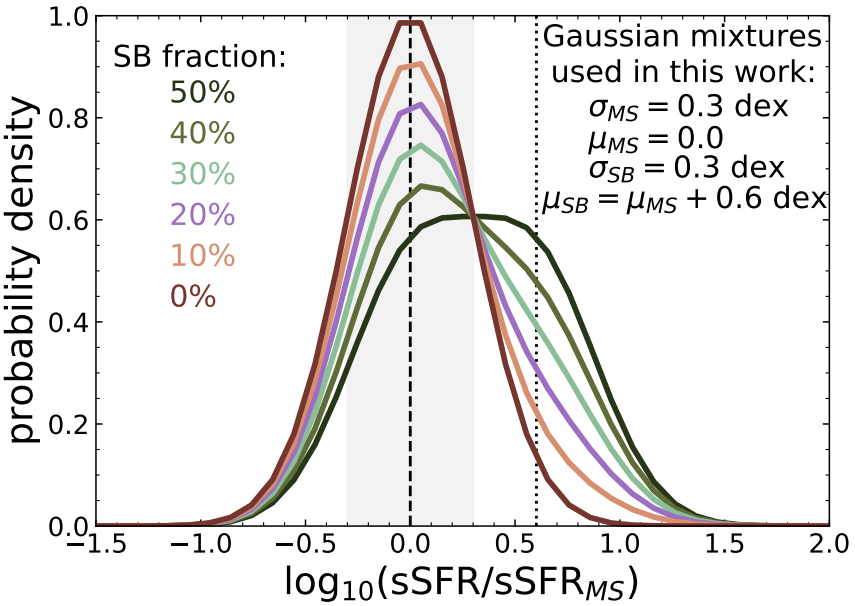

Figure 4.2: The main-sequence and starburst population distributions used to scatter IR luminous galaxies over stellar mass space. Recent studies using more resolved observations with e.g. ALMA [e.g. 76, 260, 107] find that 50-100% of DSFGs are proportionately more massive and more star-forming extensions of main-sequence galaxies. Since this exact distribution is not well known, we instead step through different Gaussian mixtures that span these observed distributions. For example, the purple line shows a distribution where half of DSFGs are starbursts and half are main-sequence galaxies, and the green line shows a distribution where all DSFGs are main-sequence galaxies and none are starbursts.

Main Sequence vs. Starburst Decomposition

In order to derive stellar masses for our mock IR luminous galaxies, we distribute them over the star-forming main-sequence space. However, there is currently no consensus on exactly where DSFGs as a population lie in main-sequence space. Some studies suggest these objects are primarily starburst galaxies, sitting $\sim 4\times$ above the main-sequence at a given stellar mass, with such extreme SFRs driven potentially by mergers [e.g. 80, 157, 219, 238]. In this work, we adopt the same starburst galaxy definition.[1] As a whole, the starburst population is a relatively small portion of the overall star-forming galaxy population [e.g. $\sim 3-15\%$ at $z = 0-3$, 327, 334, 28, 308], but DSFGs are sometimes believed to be a 'starburst-dominated' sub-population of galaxies. Such a designation is likely driven by catastrophic projection / blending effects stemming from the large angular resolutions in most canonical wide-field sub-mm surveys built by both space-based [e.g. *Herschel*, 26] and ground-based telescopes [e.g. SCUBA, 74]. Starburst-dominated populations could also stem from sensitivity limits by the same surveys, where only the most extreme sources at $z > 1$ will be detected.

Recent studies with better angular resolutions (using e.g. ALMA) reveal that significant percentages (50-100%) of DSFGs are just proportionately more massive and star-forming extensions of coeval main-sequence galaxies [76, 260, 405, 107]. This fraction may evolve with redshift, as shown in [76] and [260], but to generalize these fractions as evolutionary trends is problematic as they are dependent on the juxtaposed main-sequence parameterization and the far-IR / sub-mm selection limits; there is also a dearth of sufficiently large samples at epochs beyond $z = 2$ to derive a statistically-relevant evolutionary picture. Thus, the true starburst vs. main-sequence population distribution of DSFGs (at least the particularly massive and IR luminous ones) is still unknown, with the truth value likely lying somewhere in between a ratio of 1:1 and 0:1.

[1] Though we note that there exists other definitions of starburst galaxies based not on their distance from the SFMS, but on their rates of gas consumption (i.e. M_{H_2}/SFR, also known as the integrated Kennicutt-Schmidt relationship or star formation efficiency [e.g. 328]).

Instead of forcing a singular underlying distribution as truth, we sample the model over several steps within the observed 50-100% range. Specifically, our model steps through DSFGs-as-main-sequence fractions of 0, 10, 20, 30, 40, and 50%, with the remainder belonging to the starburst regime. The distribution is modeled as a double Gaussian over main-sequence space, with one Gaussian centered over the main-sequence and the other centered +0.6 dex away [4× above the main-sequence, 315]. Both distributions have fixed width of $\sigma_{\rm MS} = \sigma_{\rm SB} = 0.3$ dex, similar to those found in many main-sequence studies [e.g. 356]. We tested the impact of these chosen widths by running the model with both smaller and larger dispersions ($\sigma = 0.2$ and 0.4, respectively) and found no significant difference (< 3%) in our results. These distributions are shown in Figure 4.2.

Similar to Section 4.2.1, we wish to randomly assign stellar masses in a way that accounts for Eddington bias: if we were to simply draw from the starburst vs. main-sequence Gaussian mixtures as a way to assign stellar mass, more numerous low star-forming galaxies would up-scatter into higher mass bins than high SFR galaxies into lower mass bins. Instead, we model the main-sequence vs. starburst mixtures as cumulative distribution functions, from which we sample a uniform distribution of stellar masses for our mock galaxy populations. This method ensures that galaxies with higher SFRs are more likely to have larger stellar masses, in alignment with observations.

4.2.4 Stellar Mass Number Density

After using the star-forming main-sequence to generate stellar masses for the mock IR luminous galaxies, we can then bin in stellar mass space to determine the three dimensional stellar mass number density. Galaxies are binned based on their stellar mass in bins of size $\delta_{\rm m} = 0.3$ dex – corresponding to the average spread in stellar mass in the SFMS [356]. The stellar mass histograms are then divided by the same respective light cone volumes used to generate mock galaxies from the IRLF.

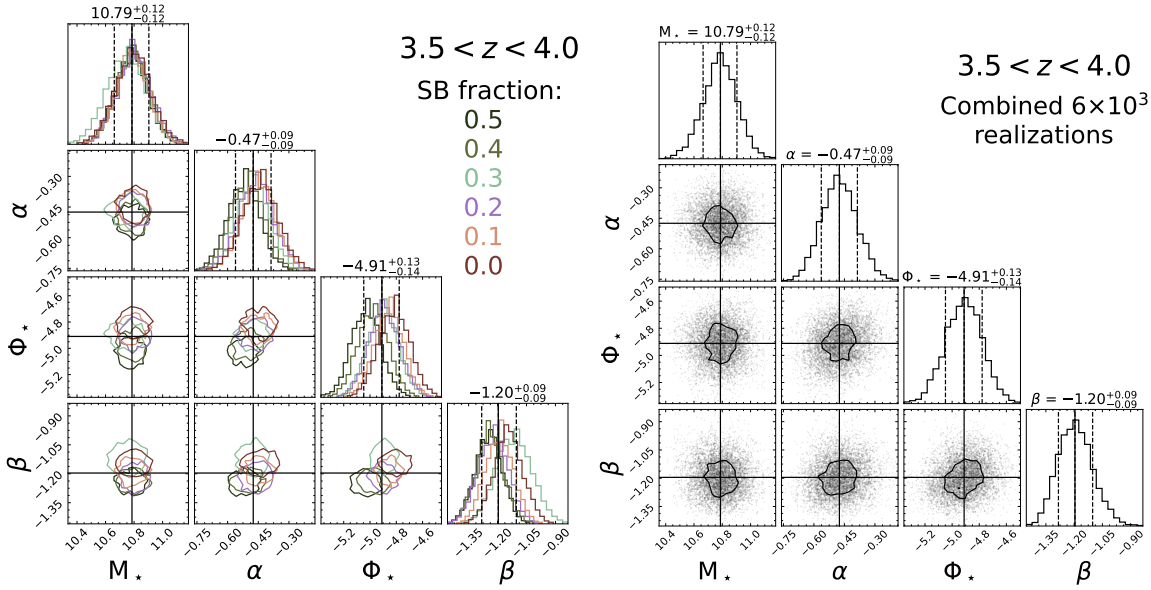

Figure 4.3: Corner plots for the stellar mass function parameters derived in the $3 < z < 3.5$ redshift bin. On the left, we show the distributions of the best-fit parameters for each separate main-sequence vs. starburst mixture. We sample each of these parameters 10^3 times (for a total of 6×10^3 samples, a thousand per mixture) then combine them to create an average stellar mass function for each redshift bin, as shown on the right. There is an overall $< 5\%$ difference between the parameters derived using different mixtures, which is captured within the 1σ uncertainties listed at the top of each parameter column. However, it is important to note that the 68% confidence intervals listed at the tops of the columns *do not* include the extra 10% uncertainty we add to account for additional uncertainties in the IRLF (discussed in Section 4.3). The ultimate values used in this work are reported in Table 4.2.

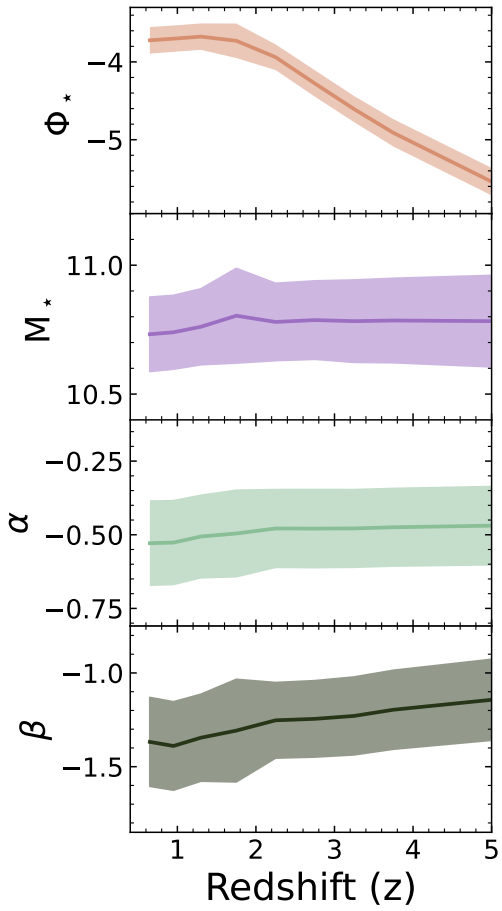

Figure 4.4: The redshift evolution of the SMF broken power-law parameters used in this work, also listed in Table 4.2. The solid line is the median value found when combining the best 1000 BPL fits across all starburst vs. main-sequence mixtures, and the shaded area corresponds to the 68% confidence interval. In the top panel, we show the evolution of $\Phi_\star$, the normalization of the space density, decreases at higher-z, which is expected within the context of galaxy growth and assembly. In the second panel, we find that the 'knee' of the dust-obscured SMF, $M_\star$ does not evolve significantly with time, steadily hovering around $6 \times 10^{10}\,M_\odot$. In the third and fourth panel, we show the evolution of the low and high mass slopes (before and after the 'knee'), α and β, respectively. Neither of these parameters evolve significantly with redshift, which is likely a consequence of the fixed bright-end slope and narrow priors of the faint end slope in the IRLF for this model (Sec. 4.2.1). See Section **??** and Table 4.2 for more discussion on these resulting parameters, and how they may or may not change under different assumptions.

4.3 Model Results | The Dust-Obscured Stellar Mass Function

A brief review of the model thus far (Sections 4.2.1-4.2.4): we use the IR luminosity function to generate a mock catalog of dust-obscured star-forming galaxies. We correct the IR luminosities for AGN contributions, then convert the corrected luminosities to star formation rates. Then, we use the SFRs to pivot the mock galaxies over the star-forming main sequence to generate mock stellar masses. Finally, we bin the mock galaxies in stellar mass space and divide by the light cone volume to calculate stellar mass number densities across cosmic time (as a function of stellar mass).

This entire procedure is repeated $6{\times}10^3$ times: a thousand realizations for each of the six different main-sequence vs. starburst distributions (described in Section 4.2.3 and shown in Figure 4.2). Median values of the number densities within each of the six runs are calculated (across the abscissa, i.e. stellar mass bins), and uncertainties determined from the inner 68% confidence interval. This allows us to directly gauge the impact of varying main-sequence vs. starburst Gaussian mixtures on the resulting stellar mass function.

Then, within each of the six starburst vs. main-sequence mixtures and for each respective redshift window, we fit a broken power law to the stellar mass number densities. Historically, stellar mass functions are modeled as Schechter functions [331], but the underlying distribution that our model draws from is a broken power law [the IRLF, 55]. Thus, we computed the Bayesian information criterion [336] to determine whether the Schechter function or a broken power law better models our data. The Bayesian information criterion (BIC) is a tool used to choose between two or more models, where models are penalized for the number of parameters included in the fit. A smaller BIC corresponds to the better fit, with a difference of $\delta\,\mathrm{BIC} \geq 10$ indicating a very strong case for the best model. Across all mixtures/redshifts, we found that the broken power law resulted in a weakly stronger model (with $\delta\,\mathrm{BIC} \geq 2-6$ in nearly all cases). Thus, while both functional forms would likely be sufficient within uncertainty, we adopt the following broken power law form to define the number density of dust-obscured galaxies, $\Phi(\mathrm{M})$, as:

$$\Phi(M,z) = \begin{cases} \Phi_\star(z)\left(\frac{M}{M_\star(z)}\right)^{\alpha(z)} & \text{if } M < M_\star(z) \\ \Phi_\star(z)\left(\frac{M}{M_\star(z)}\right)^{\beta(z)} & \text{if } M \geq M_\star(z) \end{cases} \tag{4.2}$$

where $\Phi_\star$ is the number density normalization, $\mathrm{M} = \mathrm{M_{star}}/\mathrm{M_\odot}$, α is the low mass slope, $\mathrm{M}_\star$ is the characteristic mass or 'knee' of the SMF, and β is the high mass slope (beyond the knee). We use the SciPy `curve_fit` function [398] to find the best fit for each mixture-redshift combination. We only include stellar mass number densities with 68% confidence intervals that are less than an order of magnitude away from the median value (i.e. $\log_{10}(\sigma) < 1$); this primarily affects the highest mass bins ($\mathrm{M} > 10^{12}\,\mathrm{M_\odot}$) where mock IR luminous galaxies appear rarely and therefore aren't produced consistently in the 10^3 realizations. When running `curve_fit`, we also include the spread in diversity within each stellar mass density bin (i.e. the 68% confidence intervals) as uncertainty in the fitting procedure.

To derive a singular stellar mass function from the six different main-sequence vs. starburst mixtures, we randomly generate 10^3 combinations of ($\Phi_\star$, α, $\mathrm{M}_\star$, β) sampled from the covariance matrices (i.e. parameter / posterior distributions) of each broken power law fit in each mixture. We collate the $6{\times}10^3$ samples of the parameters and determine the median and standard deviation to arrive at the final stellar mass function used in this analysis. This is process completed separately for each redshift window. In Figure 4.3, we show an example of the SMF parameter values extracted from the $6{\times}10^3$ realizations for the $3.5 < z < 4$ redshift bin.

The knee of the SMF ($\mathrm{M}_\star$) is invariant to the various main-sequence vs. starburst mixtures (< 1% difference between the six mixtures). By eye, it appears that the number density evolution ($\Phi_\star$) is anti-correlated with higher populations of starbursts; despite this potential trend, the difference between $\Phi_\star$ derived across the different mixture is also < 1%, and therefore insignificant for the purposes for this work. The low mass slope of the SMF (α) becomes slightly more

shallow with decreasing starburst fraction. This shallowing effect likely emerges because, with low starburst fractions, more galaxies are deemed main-sequence-like and thus scatter to higher stellar masses; this effect creates more numerous massive galaxies than model realizations with "high" starburst fractions, and causes the population density near $M_\star$ to increase. This is likely the same phenomenon driving the aforementioned changes in $\Phi_\star$, and similar changes in the slope for the massive end of the SMF, β. Both of the resulting SMF slopes are consistent (within $\lesssim 5\%$) across the six main-sequence starburst mixtures. For all four SMF parameters, the differences across mixtures are well below the derived 68% confidence intervals of the ultimate/averaged SMF values used in this work. We also note that, when considering the combination of all four parameters ($\Phi_\star$, α, $M_\star$, β) across the six mixtures, there is no clear preferred mixture that aligns best with the final values adopted in this work (i.e. the resulting parameters are not best modeled by the 'middle-most' mixture). In Figure 4.2.4 and listed in Table 4.2, we show the final parameters (as a function of redshift) that describe the SMF used in the remainder of this work.

It's important to note that the main basis of this model hinges upon the accuracy of the modeled IR luminosity function. Unfortunately, as reviewed in Section 4.2.1, the evolution of the IRLF beyond $z \sim 2$ is not well constrained. While we marginalize over several parameters to account for these $z > 2$ unknowns, there are still some fixed assumptions in this work, such as the evolution of $L_\star$ at $z > z_{\rm turn}$, or the lack thereof for the faint-end slope, α. As discussed in Section **??**, we find that a steeper $\alpha = -0.7$ results in a less than 3% difference in the final derivations of the parameters describing the dust-obscured SMF ($\Phi_\star$, $M_\star$, α, and β); and a flatter evolution of $L_\star$ with $\psi = 0.5$ results in a less than 1% difference in the resulting SMF parameters. Thus, to be conservative and account for the impacts of our model's main assumptions, we add an additional 10% uncertainty on the ultimate stellar mass function parameters (included in Table 4.2).

Star-Forming Dust-Obscured Galaxies				
Redshift	$\log_{10}(\Phi_\star)$	$\log_{10}(M_\star)$	α	β
$0.5 < z < 0.8$	-3.72 ± 0.17	10.73 ± 0.14	-0.53 ± 0.15	-1.37 ± 0.24
$0.8 < z < 1.1$	-3.7 ± 0.17	10.74 ± 0.14	-0.53 ± 0.15	-1.39 ± 0.24
$1.1 < z < 1.5$	-3.67 ± 0.17	10.76 ± 0.15	-0.5 ± 0.14	-1.34 ± 0.23
$1.5 < z < 2.0$	-3.73 ± 0.22	10.8 ± 0.18	-0.5 ± 0.15	-1.31 ± 0.27
$2.0 < z < 2.5$	-3.94 ± 0.17	10.78 ± 0.15	-0.48 ± 0.13	-1.25 ± 0.2
$2.5 < z < 3.0$	-4.28 ± 0.17	10.79 ± 0.15	-0.48 ± 0.14	-1.24 ± 0.2
$3.0 < z < 3.5$	-4.61 ± 0.17	10.78 ± 0.16	-0.48 ± 0.13	-1.23 ± 0.21
$3.5 < z < 4.0$	-4.91 ± 0.18	10.78 ± 0.16	-0.47 ± 0.13	-1.2 ± 0.21
$4.0 < z < 6.0$	-5.54 ± 0.18	10.78 ± 0.18	-0.47 ± 0.14	-1.14 ± 0.22
Quiescent Descendant Galaxies				
Redshift	$\log_{10}(\Phi_\star)$	$\log_{10}(M_\star)$	α	β
$0.5 < z < 0.8$	-3.72 ± 0.17	10.73 ± 0.14	-0.53 ± 0.15	-1.37 ± 0.24
$0.8 < z < 1.1$	-3.7 ± 0.17	10.74 ± 0.14	-0.53 ± 0.15	-1.39 ± 0.24
$1.1 < z < 1.5$	-3.67 ± 0.17	10.76 ± 0.15	-0.5 ± 0.14	-1.34 ± 0.23
$1.5 < z < 2.0$	-3.73 ± 0.22	10.8 ± 0.18	-0.5 ± 0.15	-1.31 ± 0.27
$2.0 < z < 2.5$	-3.94 ± 0.17	10.78 ± 0.15	-0.48 ± 0.13	-1.25 ± 0.2
$2.5 < z < 3.0$	-4.28 ± 0.17	10.79 ± 0.15	-0.48 ± 0.14	-1.24 ± 0.2
$3.0 < z < 3.5$	-4.61 ± 0.17	10.78 ± 0.16	-0.48 ± 0.13	-1.23 ± 0.21
$3.5 < z < 4.0$	-4.91 ± 0.18	10.78 ± 0.16	-0.47 ± 0.13	-1.2 ± 0.21
$4.0 < z < 6.0$	-5.54 ± 0.18	10.78 ± 0.18	-0.47 ± 0.14	-1.14 ± 0.22

Table 4.2: Parameters for the resulting broken power law fits.

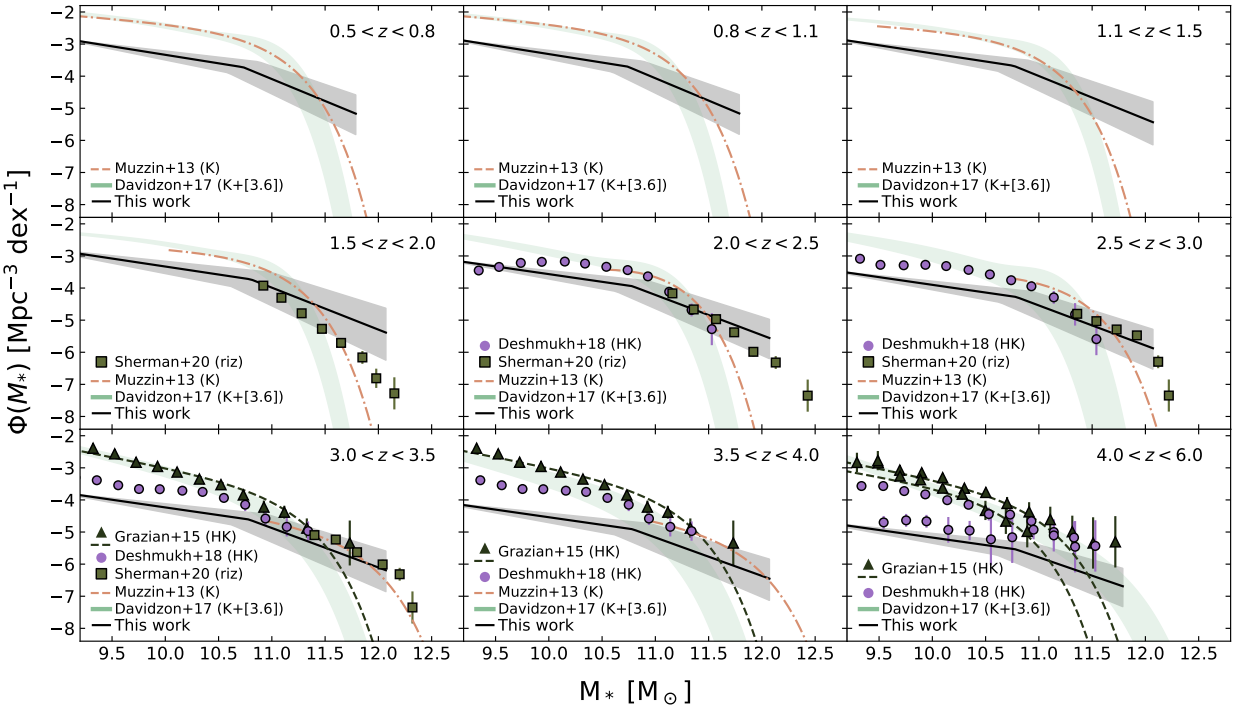

Figure 4.5: The resulting stellar mass function of the IR luminous galaxy population as derived from this model. Our results are shown as the black line, with 1σ uncertainty shaded in grey. We only plot out to stellar mass bins where the 1σ uncertainty is less than one order of magnitude; this results in a truncation for most redshift bins around $M \sim 10^{12}\,M_{\odot}$. Shown for comparison are UV-based SMFs from the literature, with a particular focus on those using the deepest available observational data: [276, pink dash-dotted line], [86, green curve], [342, green squares], [93, purple circles], [149, dark green triangles and dashed line]. In this work, UV-bright galaxies tend to dominate the star-forming population at lower stellar masses ($M \lesssim 10^{10.5-11}\,M_{\odot}$) by $\sim$ an order of magnitude, but become comparatively or even less abundant at high stellar masses, particularly at $1 < z < 4$. See Section 4.4 for more details.

4.4 Discussion

We compare our resulting stellar mass function to others published in the literature in Figure 4.5. At $z < 3$, the majority of UV-derived stellar mass functions are described using a Schechter [331] function, with a declining linear slope at the low -mass end that transitions to an exponential decline beyond the characteristic stellar mass ($M_\star$) typically around $3 \times 10^{10}\,M_\odot$ [e.g. 189, 276, 86]. This is in line with the cosmic downsizing scenario, where the most massive star-forming galaxies built the majority of their stellar mass in the first few Gyr; by $z \sim 2$ they quench, and the majority of star-forming galaxies are less massive than $M_\star$. It follows that at higher redshifts, e.g. $z > 3$, one might expect to find a more shallow tail at $M > 10^{10}\,M_\odot$ as the progenitors of massive quiescent galaxies are still in intense phases of growth. This would be evident in an increasingly massive $M_\star$ at higher redshifts, but the vast majority of studies find no statistically significant evolution in $M_\star$ from $z = 0.2$ to $z \gtrsim 4$ [e.g. 303, 189, 276, 86].

Interestingly, our model demonstrates that the decline in star-forming galaxy populations at masses beyond the 'knee' ($M > 3 \times 10^{10}\,M_\odot$) might be somewhat shallower if all dust-obscured galaxies were truly accounted for in modern day stellar mass functions. Direct comparison between the various SMF parameters (and their evolutionary properties) is not possible in this work as we use a different functional form to describe the dust-obscured SMF. We can, however, explore some of the integrated differences between our results and UV-based SMFs in the literature. In the following subsections, we propose a simple evolutionary model to evolve mock DSFGs to their quiescent descendants, then explore how the resulting number densities and stellar mass densities for both the DSFG and quiescent descendant compare to those observed and modeled in the literature.

	Star-forming DSFGs		Quiescent Descendants	
Redshift	$\log_{10}(n)$	$\log_{10}(\rho)$	$\log_{10}(n)$	$\log_{10}(\rho)$
$0.5 < z < 0.8$	-4.03 ± 0.25	7.02 ± 0.03	-3.87 ± 0.24	7.02 ± 0.03
$0.8 < z < 1.1$	-4.02 ± 0.25	7.04 ± 0.03	-3.82 ± 0.24	7.04 ± 0.03
$1.1 < z < 1.5$	-4.03 ± 0.24	7.03 ± 0.03	-3.78 ± 0.16	7.03 ± 0.03
$1.5 < z < 2.0$	-4.09 ± 0.24	7.00 ± 0.03	-3.85 ± 0.16	7.00 ± 0.03
$2.0 < z < 2.5$	-4.35 ± 0.24	6.73 ± 0.03	-4.1 ± 0.17	6.73 ± 0.03
$2.5 < z < 3.0$	-4.7 ± 0.24	6.38 ± 0.03	-4.45 ± 0.18	6.38 ± 0.03
$3.0 < z < 3.5$	-5.06 ± 0.25	6.03 ± 0.03	-4.81 ± 0.18	6.03 ± 0.03
$3.5 < z < 4.0$	-5.38 ± 0.26	5.70 ± 0.04	-5.33 ± 0.26	5.70 ± 0.04
$4.0 < z < 6.0$	-6.03 ± 0.24	5.11 ± 0.04	-5.78 ± 0.28	5.11 ± 0.04

Table 4.3: Number densities and stellar mass densities as shown in Figures 4.6 and **??** for mock galaxies of stellar mass $M > 10^{10.5}\,M_\odot$ in this numerical model.

4.4.1 The Descendant Quiescent Stellar Mass Function

The discovery and follow up observations of massive galaxies within the first 1-2 Gyr of the Universe suggest that they form via extremely efficient and rapid star formation mechanisms during the early cosmos [e.g. 142, 332, 333, 245, 94, 390]. This is likely in the form of bursts of extreme star formation ($300 - 1000\,M_\odot\,yr^{-1}$) lasting $\sim 100 - 300$ Myr [e.g. 374, 16, 8, 421, 94], after which the cold gas reservoir is depleted, heated, and/or blown out.

In our model, we make the following simplistic assumptions to derive descendant quiescent galaxy masses to compare with observations in the literature. We assume that the current SFR of a mock galaxy is maintained for an additional $50 - 300$ Myr, in alignment with the gas depletion timescales seen in the aforementioned observational studies. These timescales are sampled from a uniform grid with steps of $\delta_{\rm time} = 5$ Myr. Then, we forward evolve the galaxy, adding the additional stellar mass that is built assuming a continuous SFR over the given timescale; to determine the redshift of the 'quenched' galaxy, we add the same timescale to the galaxy's initial star forming redshift (which is assigned from a continuous uniform distribution over the respective redshift window).

We note that these assumptions on a galaxy's journey to becoming passive are simplistic: we do not include any prescriptions for AGN feedback, merging activity, or any other potential phenomenon that could theoretically slow down or speed up the SFRs / gas depletion timescales assigned to our mock galaxies. This method allows us to circumvent the need to invoke complex assumptions on e.g. available gas mass reservoirs and potential heating mechanisms. Furthermore, it is entirely possible that these more second-order corrections can be accounted for in the marginalization / uncertainty propagation process. For example, minor bumps or dips in the IRLF due to major mergers triggering IR-luminous star-formation would be accounted for in the uncertainty in the IRLF parameter space. Thus, while a more sophisticated model may be more "complete" in it's assumptions, our results (discussed in later sections) demonstrate that these complex assumptions do not appear to be necessary to describe massive galaxy evolution to a first-order approximation.

4.4.2 Massive, Dust-Obscured Galaxies and Their Descendants

For the remainder of this work, we focused on the massive, dust-obscured population of galaxies predicted by our model, defined as all objects with $M \geq 10^{10.5}\,M_{\odot}$ and $L_{IR} \geq 10^{11}\,L_{\odot}$. We emphasize that the latter criterion emerged naturally in this model: nearly all ($\geq$ 99%) $M \geq 10^{10.5}\,M_{\odot}$ star-forming galaxies produced by our model, across the redshift space probed here, have LIRG or greater IR luminosities; moreover, $>$ 75% of these massive star-forming galaxies have ultra-LIRG (ULIRG, $L_{IR} \geq 10^{12}\,L_{\odot}$) luminosities or higher. For the remainder of this work, we refer to these IR luminous massive galaxies as Massive Dust Obscured Galaxies, aka MDOGs.

MDOG Number Densities

In Figure 4.6, we show the redshift evolution of the number density of MDOGs (left), and of their quiescent descendants (right). During the ~ 1 Gyr between $z = 3$ and 6, we predict an order of magnitude increase in number density of $M > 10^{10.5}\,M_{\odot}$ dust obscured SF galaxies, similar to

that seen in Marsan et al. 2020 [245]. This growth rate tapers off at later times, taking another $\sim 2\,\mathrm{Gyr}$ (from $z = 3$ to 1.5) to achieve another order of magnitude in population density. This $z > 3$ evolution is steeper than that exhibited by UV-based estimates from e.g. Davidzon et al. 2017 [86], where it takes an additional ∼half a billion years to achieve similar growth. In general, across $0.5 < z < 3$ (i.e. 'Cosmic Noon'), massive UV-bright SF galaxies are similarly populous as massive dust-obscured SF galaxies. There is a visible departure around $z \sim 3$ where UV-bright galaxies become ∼2-4× more populous. This is qualitatively in line with recent constraints on the obscured portion of the $z > 3$ cosmic star formation rate density, where dust-obscured star formation is expected to become less prominent at earlier times [e.g. 424].

One of the primary pieces of evidence that pins $z > 3$ DSFGs as ancestors to giant ellipticals at later times is the similar co-moving number densities between the two populations [e.g. 379]. However, the strength of this evolutionary picture is discrepant depending on the sample size, depths, and sensitivities of far-IR and sub-mm surveys used to characterized the massive, dust-obscured population. For example, *Herschel* discovered DSFGs at $z > 2$ are often comprised of a rare and extreme star-forming population (with SFRs up to and exceeding $1000\,\mathrm{M_\odot\,yr^{-1}}$); their number densities are insufficient to match those estimated for massive quiescent galaxies at $z > 2$ [103, 191, 108, 235, 267]. Instead, the recently discovered H-band dropouts, or alternatively the larger umbrella of galaxies that are optically "invisible" but sufficiently bright in the far-IR/sub-mm regime ($S_{850\mu m} \gtrsim 1$ mJy), may make up the bulk of the massive, star-forming galaxy population at $z > 3$ [414, 405, 210, 242]. Thus, it is perhaps more important to successfully model these more common, less extreme dusty, star-forming galaxies.

At $z = 2 - 3$, when integrated over similar redshift ranges, our model successfully predicts similar space densities of the massive ($M_\star \gtrsim 3 \times 10^{10}\,\mathrm{M_\odot}$) submillimeter galaxy populations presented in [107, $\sim 10^{-4}\,\mathrm{Mpc^3}$ at $z = 1.8 - 3.4$], but predicts up to 10× more MDOGs than those in a SCUBA-2 detected sample in a similar redshift range [260]. This difference is likely due to the employed SFR cutoff in the latter work, which only includes galaxies with SFRs $> 300\,\mathrm{M_\odot\,yr^{-1}}$.

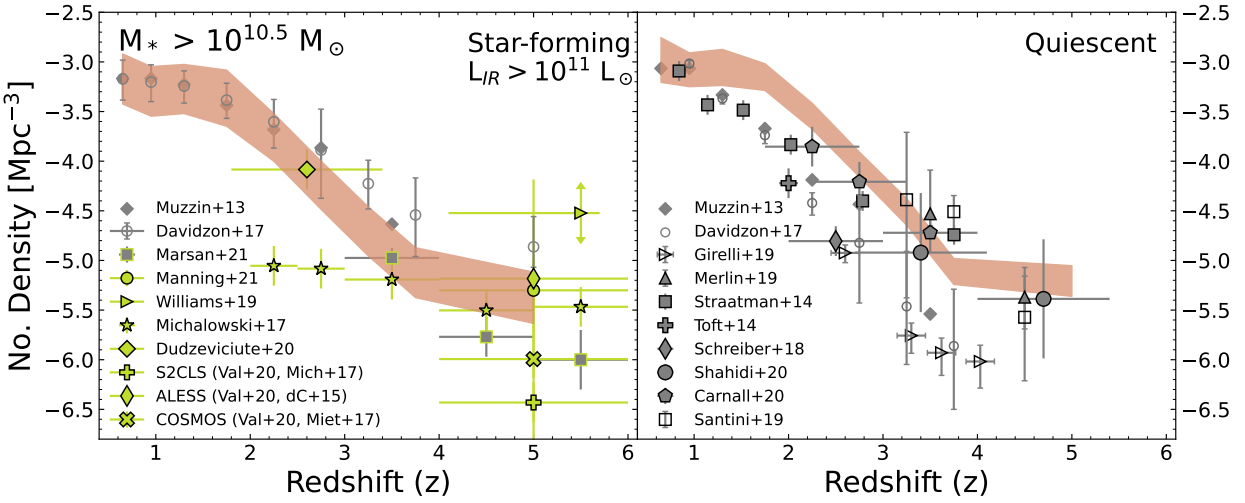

Figure 4.6: Number density of massive M > $10^{10.5}$ M$_\odot$ galaxies. It is important to note that, for the observational data in green, the uncertainties on the abscissa demarcate the redshift bins of each observational sample. For example, when integrating this model over a similar redshift bin as the Dudzeviciute et al. 2020 [107] sample, we achieve a similar number density estimate (demonstrated by the overlap between the $z \sim 2$ portion of our model and the low redshift-end of the Dudzeviciute et al. sample).

In this model, 20 – 40% of M $\geq 3 \times 10^{10}$ M$_\odot$ galaxies at $z \sim 2$ have SFRs < 300 M$_\odot$ yr^{-1} (with the percent decreasing with increasing redshift) – this difference in population distribution nearly – but not quite – sufficient to match the gap (including uncertainties) between our $z \sim 2$ results and those seen in [260].

At $z > 3$, the model's success is difficult to quantify due to lack of strong observational constraints, including insufficient sample sizes and highly uncertain redshifts. Still, we find general agreement between the model and observations out to $z \sim 5$. At $z = 3 - 6$, the model predicts MDOG number densities in agreement (within uncertainty) with [260]. We also compare to the massive galaxy (M > 10^{11} M$_\odot$) sample from Marsan et al. 2020 [245]. According to multiwavelength SED analysis (from the rest-frame optical to far-IR), this $3 < z < 6$ sample includes a mixture of post-starbursts, UV-bright star-forming galaxies, and DSFGs, where at $z = 3 - 4$ ($4 - 6$) roughly a third (a fifth) of the sample is deemed a DSFG based on faint and/or missing UV flux and evidence of dust heating in IRAC bands. Applying these fractions to the number densities derived therein

brings these estimates down to within ∼0.3 dex of our results for MDOGs at $M > 10^{11}\,M_\odot$ (where $n \sim 1 - 2 \times 10^{-6}\,\mathrm{Mpc}^{-3}$ and $n \sim 2 \times 10^{-7}\,\mathrm{Mpc}^{-3}$ at $z = 3 - 4$ and $z = 4 - 6$, respectively).

At $4 < z < 6$, we compare to the ALESS [76], COSMOS [262], and S2CLS [260] samples as calculated in Valentino et al. 2020[390, pre-duty cycle correction]. To derive number densities for these surveys, Valentino et al. took strict photometric redshift constraints, requiring that both upper and lower limits on the photo-zs sit at or above $z = 4$. As seen with the S2CLS derivations between Michalowski et al. and Valentino et al., this requirement can reduce the number densities *by an entire order of magnitude*, thereby demonstrating to first order one of the main difficulties in constraining DSFG number densities at $z > 3$. Across these three surveys with conservative photo-z restrictions, our model most agrees with those derived from the COSMOS sample [262], where $n \sim 10^{-6}\,\mathrm{Mpc}^3$ at $4 < z < 6$.

Comparing to the observed number densities of the (potentially more populous) optically dark dust-obscured galaxies at $4 < z < 6$ is particularly difficult as observational constraints suffer either from extremely small sample sizes ($n = 1 - 4$, e.g. [414, 242]), or are averaged over extremely large redshift ranges (e.g. $z = 3 - 6$ in [405]). When comparing to estimates derived from a single exceptional object in Williams et al. 2019 [414], our model predicts nearly 30× smaller populations of MDOGs. Such a large discrepancy could be driven by the small survey area ($8\,\mathrm{arcmin}^2$) of the Williams et al. object; a larger probed area would result in a larger probed volume and thus drive the number density down. While the Wang et al. 2019 [405] sample of H-band dropouts includes a larger sample size ($n = 39$) over a larger survey area ($\sim 600\,\mathrm{arcmin}^2$), these objects span a (photometric redshift) range of $3 < z < 8$, with over half of the sample exhibiting redshift errors $\delta z \geq 1$. Still, when integrating our model across $3 < z < 5$, we find a similar space density as the authors (reported as $n \sim 2 \times 10^{-5}\,\mathrm{Mpc}^3$) as well as the entire sample of 2 mm detected galaxies in Manning et al. 2022 [242].

MDOG Descendant Densities

On the right panel of Figure 4.6, we show the expected evolution in the number density of MDOG quiescent descendants (see Section 4.4.1 for details on how this was derived). In general, this model does an fair job at modeling observed number counts in heterogeneous samples of massive, passive galaxies across $z = 2-6$ [276, 379, 367, 86, 333, 256, 326, 340, 45]. This is particularly promising because of the heterogeneity across these samples: each of the aforementioned bodies of work has their own methods/thresholds of selection and characterization of passive galaxies, yet we are able to successfully reproduce similar estimates across such diversity. Some have slightly lower stellar mass thresholds [e.g. $M > 10^{10}\,M_{\odot}$, 340, 45], or are only complete at higher stellar masses than those explored in this work [e.g. $M > 10^{11}\,M_{\odot}$ at $z = 3-4$, 276]. Some employ specific SFR ($sSFR = SFR/M_{\star}$) cuts that capture post-starbursts [e.g. $\log(sSFR) < -10$, 367], which are likely more in line with our model's assumptions / definition of MDOG descendants, while others focus strictly on fully quiescent galaxies [e.g. $\log(sSFR) < -11$, 86]. Our model most disagrees with the work of Girelli et al. 2019 [139], where we predict roughly an order of magnitude more passive galaxies at $3 < z < 4$.

Like the ancestral MDOG population, this model predicts an order of magnitude increase in the number density of passive galaxies from $z = 6$ to 3 (i.e. over ~ 1 Gyr), a growth rate similar to that seen in [326] and [256], and another order of magnitude over nearly twice the amount of time from $z = 3$ to 1.5. This is unsurprising given the relatively short gas-to-stars duty cycles used in this work and exhibited by DSFGs at high redshifts [e.g. 374, 8].

The rapid build up of massive quiescent and dusty galaxies at $z = 3-6$ points to an extreme time in the Universe, perhaps a precursor to the well-described 'Cosmic Noon' at $z \sim 1-2$. While most galaxies were forming the majority of their stars during this later epoch, it is likely that the Universe's most massive galaxies had already underwent violent and rapid growth in prior starburst episodes lasting a few hundred million years at most. Turning the implications of this story (and this

model) towards observations: this would result in a significant population of post-starburst galaxies at $z \approx 3-4$, with evolved stellar populations *and* residual gas and dust emission. Indeed, these exact properties have been found in some post-starburst galaxies at $z > 3$ [e.g. 348], but statistical studies in this regime are lacking (on both galaxy properties, and in the literal since in population sample sizes). Future panchromatic studies combining e.g. the *James Webb Space Telescope* and the Atacama Large Millimeter Array (ALMA) will be critical to constraining the stellar population properties as well as the gas and dust properties in massive galaxies in the $z = 3-6$ Universe. Such studies will lead to a deeper understanding of star formation in extreme environments, dust destruction timescales, and potentially even discern between the variety of possible quenching pathways for the first massive galaxies [e.g. 241].

Chapter 5

Summary and Conclusion

This dissertation represents ~7 years of learning, growing, and doing. I am beyond proud of how far I come, and I could not have done it without an incredible community of support, both within academia and without. Below I share the main takeaways from these works and, following that, I share future directions for me and my science.

5.1 A Case Study at $z = 4$ - Long et al. 2020

In this paper, we present a multiwavelength analysis on a $z = 4.002$ SMG-rich, ultra-massive protocluster: the Distant Red Core. We combine new *HST* and *Spitzer* data with existing Gemini, *Herschel*, and ALMA data to model spectral energy distributions for each respective ALMA object (Figure 2.3, except DRC-4), taking care to deblend low resolution *Spitzer* IRAC data where needed (Section 2.3.4). Stellar masses and SFRs are derived from SED-fitting with CIGALE (Section 2.4). Molecular gas mass estimates are derived using the observed-frame 2 mm ALMA data (probing the Rayleigh-Jeans region of the dust continuum) with the [339] methodology.

We confirm a population of massive ($M_* > 10^{10}\,M_\odot$) galaxies in place when the Universe was only

1.5 Gyr old. When comparing to field galaxies on SFR-M_* plane (Figure 2.4), our results confirm that – even at $z = 4$ – protocluster galaxies can be viewed as a high-mass (and possibly more bursty) extension of the star-forming main-sequence for coeval isolated field galaxies. Similarly, though several objects contain large gas reservoirs ($M_{H_2} \gtrsim 10^{11}\,M_\odot$), all lie within the SFR-M_{H_2} main-sequence plane. When compared to $z = 2 - 3$ protocluster and $z \sim 4$ field counterparts, the DRC objects have similar gas mass fractions that follow the expected inverse $f_{gas} - M_*$ relationship. These systems also have short gas depletion timescales ($\sim 260 \pm 180$ Myr) on par with field SMGs which, in a closed box scenario, means that these objects will exhaust their gas supplies in time to become massive quiescent galaxies that dominate at cluster cores by $z \sim 3$.

Using multiple methods, we derive a total $z = 4$ protocluster halo mass of $\sim 10^{14}\,M_\odot$, and show that this value teeters on the edge of the most massive halo allowable/observable in the 600 deg^2 *H*-ATLAS survey volume (Figure 2.6). We estimate that the DRC will evolve to become an ultra-massive cluster with a total halo mass $> 10^{15}\,M_\odot$ (possibly even $> 10^{16}\,M_\odot$) at $z = 0$ (Figure 2.7). For both the $z = 4$ and $z = 0$ calculations, we argue that a more massive estimate may be appropriate based on the assumption that other significant galaxy populations within the protocluster's large scale structure are not included in this analysis. Still, even if additional protocluster members are confirmed, more multi-wavelength studies of $z > 3$ DSFG-rich protoclusters combined with studies on the evolution of mass distributions and the gas duty cycle in cluster formation simulations are necessary to fully appreciate and characterize complex systems such as the Distant Red Core.

5.2 Growing Black Holes Do Not Quench DSFGs - Brown et al. 2019

We explored the relationship between AGN activity and host galaxy dust properties across the tail end of peak AGN and galaxy growth in the Universe (redshifts $0.2 < z < 5$) using *Chandra*, *Her-*

schel, *Spitzer* and NOAO Telescope observations in the Boötes field. We successfully disentangled AGN and star formation radiative processes in the infrared spectrum for 703 IR bright X-ray AGN using multi-component SED fitting code, SED3FIT [23], and determined the AGN-corrected integrated rest-frame infrared luminosity attributed to star formation, total infrared AGN luminosity, AGN dust covering factors and AGN fractions. Our main results can be summarized as follows:

- We find flat trends consistent with other literature when averaging L_{IR}^{SF} in bins of bolometric AGN luminosity for less powerful AGN ($L_{AGN} < 10^{45}\,erg\,s^{-1}$), as well as the stronger correlations found when averaging L_X in bins of star formation activity for AGN at low redshifts ($0.1 < z < 0.8$).

- We further decompose AGN SEDs to isolate the dusty torus component in the IR and compare to the bolometric AGN luminosity to estimate nuclear obscuration. We determine an average dust covering factor slightly lower than other literature at CF= 33%, which indicates a Type 2 (obscured) population of roughly a third. Further investigation of X-ray hardness reveals several X-ray AGN with covering factors that contradict the expected nuclear obscuration determined by hardness ratios (e.g. high covering factor with a low hardness ratio that is indicative of an unobscured central engine), providing further evidence that observational differences between AGN types are not primarily driven by line-of-sight dusty torus inclination.

- We uncover a wide range in the fraction of IR luminosity attributed to AGN activity across all redshifts, and determine no statistically significant trend exists when evaluating f_{AGN} as a function of total IR, X-ray or 24 μm luminosity. The mean f_{AGN} as a function of rest-frame IR wavelength shows peak AGN contamination lives in the mid-IR range and becomes insignificant at wavelengths larger than $\sim 30\,\mu$m, but the sample dispersion is large ($\pm 20 - 30\%$) at all wavelengths. These results demonstrate the importance of SED decomposition for individual AGN host galaxies in order to accurately quantify AGN contamination in the IR, particularly prior to using IR photometry to estimate host galaxy properties.

While considering all of the implications discussed in this paper, we should remember that current FIR detections of intermediate and high redshift X-ray AGN in star-forming galaxies are limited by the sensitivity of far-infrared and submillimeter observatories like the *Herschel* Space Observatory. The currently available resolutions limit us to the most powerful star-forming systems and we need deeper, more sensitive observations to capture the dust properties of AGN that reside in smaller and/or quiescent galaxies in order to complete the evolutionary picture.

5.3 Missing Massive Galaxies - Long et al. 2022

In this work, I combine empirical data on massive dusty, star-forming galaxies to model the evolution of their number density throughout cosmic time. The objectives of this work are twofold. The first was to quantify, to first-order, the significance of missing DSFG populations at the massive end of the star-forming galaxy stellar mass function (SMF). Star-forming SMFs are biased against dusty galaxies as they are determined using UV2OP tracers. Using the IR luminosity function as a nearly-complete consensus of DSFGs, we demonstrated that the dust-obscured stellar mass function creates a more shallow extension beyond the limits of the UV-based SMF, therefore prediction *more* massive star-forming galaxies than previously thought. Furthermore, this model does a fair job describing the number densities of massive dust-obscured galaxies observed in the literature.

The second objective was to test the hypothesis that, despite the heterogeneity of the DSFG population, it is sufficient and complete enough to describe and model the assembly of massive quiescent galaxies in the early Universe. Using a suite of simple assumptions to forward evolve mock populations of DSFGs, we are able to reproduce the observed evolution of massive, passive galaxies – without needing to invoke any complex assumptions on merger histories, feedback / quenching mechanisms, or even contributions from outside populations. In particular, our model is most aligned with studies that include post-starburst galaxy populations (not strictly passive galaxies). This finding highlights the importance of understanding this specific phase of galaxy

evolution that has been historically difficult to observed due to its likely short-lived nature. The post-starburst population likely holds the keys to understanding both extreme star formation in the early Universe, *and* the secrets as to why these galaxies quench so early on. Future studies on this population will likely span multiple galaxy sub-types (e.g. optically dark galaxies, galaxies with strong Balmer breaks *and* cold gas/dust emission), and will thus require the bridging of multiple fields (and their respective tools) in galaxy evolution.

5.4 Future

This combined body of work has inspired multitudes within me. Over the next few years, I will perform several multi-wavelength studies on massive galaxies at $z > 3$ to learn how they form, grow, and die. One of the greatest challenges in modeling galaxy evolution is to understand how significant populations of massive galaxies build their stars and then rapidly quench within the first 2 Gyr of the cosmos. The major drivers in massive galaxy formation could be dark matter halo growth and/or specific underlying physical conditions of the star-forming medium (i.e. the cold gas). The dominant quenching mechanisms at these epochs could also be dark matter halo related, or driven by energetic internal phenomenon like extreme stellar feedback. In my postdoctoral work as a NASA Hubble Fellow at UT Austin, I will study the gas, stellar, and dark matter content of $\sim$3000 newly discovered massive galaxies at $z > 3$ in order to reach a better understanding of the dominant processes regulating the evolution of the first massive galaxies. I will leverage archival and incoming Atacama Large Millimeter Array (ALMA) data as well as guaranteed James Webb Space Telescope (JWST) observations to derive galaxy gas and stellar properties such as gas mass fractions, star formation histories, and stellar effective radii. I will connect these properties to dark matter halos to pinpoint co-evolutionary trends between the halos and their massive galaxies within.

Bibliography

[1] O. Agertz, R. Teyssier, and B. Moore. Disc formation and the origin of clumpy galaxies at high redshift. *Monthly Notices of the Royal Astronomical Society*, 397(1):L64–L68, Jul 2009.

[2] J. Aird, A. L. Coil, J. Moustakas, M. R. Blanton, S. M. Burles, R. J. Cool, D. J. Eisenstein, M. S. M. Smith, K. C. Wong, and G. Zhu. PRIMUS: The Dependence of AGN Accretion on Host Stellar Mass and Color. *The Astrophysical Journal*, 746:90, Feb. 2012.

[3] J. Aird, K. Nandra, E. S. Laird, A. Georgakakis, M. L. N. Ashby, P. Barmby, A. L. Coil, J.-S. Huang, A. M. Koekemoer, C. C. Steidel, and C. N. A. Willmer. The evolution of the hard X-ray luminosity function of AGN. *Monthly Notices of the Royal Astronomical Society*, 401:2531–2551, Feb. 2010.

[4] D. M. Alexander, F. E. Bauer, W. N. Brandt, A. E. Hornschemeier, C. Vignali, G. P. Garmire, D. P. Schneider, G. Chartas, and S. C. Gallagher. The Chandra Deep Field North Survey. XIV. X-Ray-Detected Obscured AGNs and Starburst Galaxies in the Bright Submillimeter Source Population. *Astronomical Journal*, 125:383–397, Feb. 2003.

[5] D. M. Alexander and R. C. Hickox. What drives the growth of black holes? *New Astronomy Review*, 56:93–121, June 2012.

[6] R. Antonucci. Unified models for active galactic nuclei and quasars. *Annual Review of Astronomy & Astrophysics*, 31:473–521, 1993.

[7] S. Aoyama, H. Hirashita, C.-F. Lim, Y.-Y. Chang, W.-H. Wang, K. Nagamine, K.-C. Hou, I. Shimizu, H.-H. Chung, C.-H. Lee, and X.-Z. Zheng. Comparison of cosmological simulations and deep submillimetre galaxy surveys. *Monthly Notices of the Royal Astronomical Society*, 484(2):1852–1864, Apr. 2019.

[8] M. Aravena, J. S. Spilker, M. Bethermin, M. Bothwell, S. C. Chapman, C. de Breuck, R. M. Furstenau, J. Gónzalez-López, T. R. Greve, K. Litke, J. Ma, M. Malkan, D. P. Marrone, E. J. Murphy, A. Stark, M. Strandet, J. D. Vieira, A. Weiss, N. Welikala, G. F. Wong, and J. D. Collier. A survey of the cold molecular gas in gravitationally lensed star-forming galaxies at z > 2. *Monthly Notices of the Royal Astronomical Society*, 457(4):4406–4420, Apr 2016.

[9] V. Asboth, A. Conley, J. Sayers, M. Béthermin, S. C. Chapman, D. L. Clements, A. Cooray, H. Dannerbauer, D. Farrah, J. Glenn, S. R. Golwala, M. Halpern, E. Ibar, R. J. Ivison, P. R.

Maloney, R. Marques-Chaves, P. I. Martinez-Navajas, S. J. Oliver, I. Pérez-Fournon, D. A. Riechers, M. Rowan-Robinson, D. Scott, S. R. Siegel, J. D. Vieira, M. Viero, L. Wang, J. Wardlow, and J. Wheeler. HerMES: a search for high-redshift dusty galaxies in the HerMES Large Mode Survey - catalogue, number counts and early results. *Monthly Notices of the Royal Astronomical Society*, 462(2):1989–2000, Oct 2016.

[10] M. L. N. Ashby, D. Stern, M. Brodwin, R. Griffith, P. Eisenhardt, S. Kozłowski, C. S. Kochanek, J. J. Bock, C. Borys, K. Brand, M. J. I. Brown, R. Cool, A. Cooray, S. Croft, A. Dey, D. Eisenstein, A. H. Gonzalez, V. Gorjian, N. A. Grogin, R. J. Ivison, J. Jacob, B. T. Jannuzi, A. Mainzer, L. A. Moustakas, H. J. A. Röttgering, N. Seymour, H. A. Smith, S. A. Stanford, J. R. Stauffer, I. Sullivan, W. van Breugel, S. P. Willner, and E. L. Wright. The Spitzer Deep, Wide-field Survey. *ApJ*, 701:428–453, Aug. 2009.

[11] Astropy Collaboration, A. M. Price-Whelan, B. M. Sipőcz, H. M. Günther, P. L. Lim, S. M. Crawford, S. Conseil, D. L. Shupe, M. W. Craig, N. Dencheva, A. Ginsburg, J. T. VanderPlas, L. D. Bradley, D. Pérez-Suárez, M. de Val-Borro, T. L. Aldcroft, K. L. Cruz, T. P. Robitaille, E. J. Tollerud, C. Ardelean, T. Babej, Y. P. Bach, M. Bachetti, A. V. Bakanov, S. P. Bamford, G. Barentsen, P. Barmby, A. Baumbach, K. L. Berry, F. Biscani, M. Boquien, K. A. Bostroem, L. G. Bouma, G. B. Brammer, E. M. Bray, H. Breytenbach, H. Buddelmeijer, D. J. Burke, G. Calderone, J. L. Cano Rodríguez, M. Cara, J. V. M. Cardoso, S. Cheedella, Y. Copin, L. Corrales, D. Crichton, D. D'Avella, C. Deil, É. Depagne, J. P. Dietrich, A. Donath, M. Droettboom, N. Earl, T. Erben, S. Fabbro, L. A. Ferreira, T. Finethy, R. T. Fox, L. H. Garrison, S. L. J. Gibbons, D. A. Goldstein, R. Gommers, J. P. Greco, P. Greenfield, A. M. Groener, F. Grollier, A. Hagen, P. Hirst, D. Homeier, A. J. Horton, G. Hosseinzadeh, L. Hu, J. S. Hunkeler, Ž. Ivezić, A. Jain, T. Jenness, G. Kanarek, S. Kendrew, N. S. Kern, W. E. Kerzendorf, A. Khvalko, J. King, D. Kirkby, A. M. Kulkarni, A. Kumar, A. Lee, D. Lenz, S. P. Littlefair, Z. Ma, D. M. Macleod, M. Mastropietro, C. McCully, S. Montagnac, B. M. Morris, M. Mueller, S. J. Mumford, D. Muna, N. A. Murphy, S. Nelson, G. H. Nguyen, J. P. Ninan, M. Nöthe, S. Ogaz, S. Oh, J. K. Parejko, N. Parley, S. Pascual, R. Patil, A. A. Patil, A. L. Plunkett, J. X. Prochaska, T. Rastogi, V. Reddy Janga, J. Sabater, P. Sakurikar, M. Seifert, L. E. Sherbert, H. Sherwood-Taylor, A. Y. Shih, J. Sick, M. T. Silbiger, S. Singanamalla, L. P. Singer, P. H. Sladen, K. A. Sooley, S. Sornarajah, O. Streicher, P. Teuben, S. W. Thomas, G. R. Tremblay, J. E. H. Turner, V. Terrón, M. H. van Kerkwijk, A. de la Vega, L. L. Watkins, B. A. Weaver, J. B. Whitmore, J. Woillez, V. Zabalza, and Astropy Contributors. The Astropy Project: Building an Open-science Project and Status of the v2.0 Core Package. *Astronomical Journal*, 156:123, Sept. 2018.

[12] Astropy Collaboration, T. P. Robitaille, E. J. Tollerud, P. Greenfield, M. Droettboom, E. Bray, T. Aldcroft, M. Davis, A. Ginsburg, A. M. Price-Whelan, W. E. Kerzendorf, A. Conley, N. Crighton, K. Barbary, D. Muna, H. Ferguson, F. Grollier, M. M. Parikh, P. H. Nair, H. M. Unther, C. Deil, J. Woillez, S. Conseil, R. Kramer, J. E. H. Turner, L. Singer, R. Fox, B. A. Weaver, V. Zabalza, Z. I. Edwards, K. Azalee Bostroem, D. J. Burke, A. R. Casey, S. M. Crawford, N. Dencheva, J. Ely, T. Jenness, K. Labrie, P. L. Lim, F. Pierfederici, A. Pontzen, A. Ptak, B. Refsdal, M. Servillat, and O. Streicher. Astropy: A community Python package for astronomy. *Astronomy & Astrophysics*, 558:A33, Oct. 2013.

[13] M. Azadi, J. Aird, A. L. Coil, J. Moustakas, A. J. Mendez, M. R. Blanton, R. J. Cool, D. J. Eisenstein, K. C. Wong, and G. Zhu. PRIMUS: The Relationship between Star Formation and AGN Accretion. *The Astrophysical Journal*, 806:187, June 2015.

[14] M. Azadi, A. L. Coil, J. Aird, N. Reddy, A. Shapley, W. R. Freeman, M. Kriek, G. C. K. Leung, B. Mobasher, S. H. Price, R. L. Sanders, I. Shivaei, and B. Siana. The MOSDEF Survey: AGN Multi-wavelength Identification, Selection Biases, and Host Galaxy Properties. *The Astrophysical Journal*, 835:27, Jan. 2017.

[15] P. Barmby, A. Alonso-Herrero, J. L. Donley, E. Egami, G. G. Fazio, A. Georgakakis, J.-S. Huang, E. S. Laird, S. Miyazaki, K. Nandra, S. Q. Park, P. G. Pérez-González, G. H. Rieke, J. R. Rigby, and S. P. Willner. Mid-Infrared Properties of X-Ray Sources in the Extended Groth Strip. *The Astrophysical Journal*, 642:126–139, May 2006.

[16] G. Barro, J. R. Trump, D. C. Koo, A. Dekel, S. A. Kassin, D. D. Kocevski, S. M. Faber, A. van der Wel, Y. Guo, P. G. Pérez-González, E. Toloba, J. J. Fang, C. Pacifici, R. Simons, R. D. Campbell, D. Ceverino, S. L. Finkelstein, B. Goodrich, M. Kassis, A. M. Koekemoer, N. P. Konidaris, R. C. Livermore, J. E. Lyke, B. Mobasher, H. Nayyeri, M. Peth, J. R. Primack, L. Rizzi, R. S. Somerville, G. D. Wirth, and A. Zolotov. Keck-I MOSFIRE Spectroscopy of Compact Star-forming Galaxies at z $\gtrsim$ 2: High Velocity Dispersions in Progenitors of Compact Quiescent Galaxies. *The Astrophysical Journal*, 795(2):145, Nov. 2014.

[17] C. M. Baugh, C. G. Lacey, C. S. Frenk, G. L. Granato, L. Silva, A. Bressan, A. J. Benson, and S. Cole. Can the faint submillimetre galaxies be explained in the Λ cold dark matter model? , 356(3):1191–1200, Jan 2005.

[18] C. M. Baugh, C. G. Lacey, C. S. Frenk, G. L. Granato, L. Silva, A. Bressan, A. J. Benson, and S. Cole. Can the faint submillimetre galaxies be explained in the Λ cold dark matter model? *Monthly Notices of the Royal Astronomical Society*, 356(3):1191–1200, Jan. 2005.

[19] V. Beckmann, S. Soldi, C. Ricci, J. Alfonso-Garzón, T. J.-L. Courvoisier, A. Domingo, N. Gehrels, P. Lubiński, J. M. Mas-Hesse, and A. A. Zdziarski. The second INTEGRAL AGN catalogue. *Astronomy & Astrophysics*, 505:417–439, Oct. 2009.

[20] P. Behroozi and J. Silk. The most massive galaxies and black holes allowed by ΛCDM. *Monthly Notices of the Royal Astronomical Society*, 477(4):5382–5387, Jul 2018.

[21] P. Behroozi, R. H. Wechsler, A. P. Hearin, and C. Conroy. UNIVERSEMACHINE: The correlation between galaxy growth and dark matter halo assembly from z = 0-10. *Monthly Notices of the Royal Astronomical Society*, 488(3):3143–3194, Sep 2019.

[22] P. S. Behroozi, R. H. Wechsler, and C. Conroy. The Average Star Formation Histories of Galaxies in Dark Matter Halos from z = 0-8. *The Astrophysical Journal*, 770:57, Jun 2013.

[23] S. Berta, D. Lutz, P. Santini, S. Wuyts, D. Rosario, D. Brisbin, A. Cooray, A. Franceschini, C. Gruppioni, E. Hatziminaoglou, H. S. Hwang, E. Le Floc'h, B. Magnelli, R. Nordon, S. Oliver, M. J. Page, P. Popesso, L. Pozzetti, F. Pozzi, L. Riguccini, G. Rodighiero, I. Roseboom, D. Scott, M. Symeonidis, I. Valtchanov, M. Viero, and L. Wang. Panchromatic spectral energy distributions of Herschel sources. *AAP*, 551:A100, Mar. 2013.

[24] E. Bertin and S. Arnouts. SExtractor: Software for source extraction. , 117:393–404, June 1996.

[25] E. Bertin, Y. Mellier, M. Radovich, G. Missonnier, P. Didelon, and B. Morin. The TERAPIX Pipeline. In D. A. Bohlender, D. Durand, and T. H. Handley, editors, *Astronomical Data Analysis Software and Systems XI*, volume 281 of *Astronomical Society of the Pacific Conference Series*, page 228, 2002.

[26] M. Béthermin, H.-Y. Wu, G. Lagache, I. Davidzon, N. Ponthieu, M. Cousin, L. Wang, O. Doré, E. Daddi, and A. Lapi. The impact of clustering and angular resolution on far-infrared and millimeter continuum observations. *Astronomy & Astrophysics*, 607:A89, Nov. 2017.

[27] S. Bianchi, R. Maiolino, and G. Risaliti. AGN Obscuration and the Unified Model. *Advances in Astronomy*, 2012:782030, 2012.

[28] L. Bisigello, K. I. Caputi, N. Grogin, and A. Koekemoer. Analysis of the SFR-M* plane at z < 3: single fitting versus multi-Gaussian decomposition. *Astronomy & Astrophysics*, 609:A82, Jan. 2018.

[29] A. W. Blain, S. C. Chapman, I. Smail, and R. Ivison. Clustering of Submillimeter-selected Galaxies. *The Astrophysical Journal*, 611:725–731, Aug. 2004.

[30] R. D. Blandford and D. G. Payne. Hydromagnetic flows from accretion discs and the production of radio jets. *Monthly Notices of the Royal Astronomical Society*, 199:883–903, June 1982.

[31] L. E. Bleem, B. Stalder, T. de Haan, K. A. Aird, S. W. Allen, D. E. Applegate, M. L. N. Ashby, M. Bautz, M. Bayliss, B. A. Benson, S. Bocquet, M. Brodwin, J. E. Carlstrom, C. L. Chang, I. Chiu, H. M. Cho, A. Clocchiatti, T. M. Crawford, A. T. Crites, S. Desai, J. P. Dietrich, M. A. Dobbs, R. J. Foley, W. R. Forman, E. M. George, M. D. Gladders, A. H. Gonzalez, N. W. Halverson, C. Hennig, H. Hoekstra, G. P. Holder, W. L. Holzapfel, J. D. Hrubes, C. Jones, R. Keisler, L. Knox, A. T. Lee, E. M. Leitch, J. Liu, M. Lueker, D. Luong-Van, A. Mantz, D. P. Marrone, M. McDonald, J. J. McMahon, S. S. Meyer, L. Mocanu, J. J. Mohr, S. S. Murray, S. Padin, C. Pryke, C. L. Reichardt, A. Rest, J. Ruel, J. E. Ruhl, B. R. Saliwanchik, A. Saro, J. T. Sayre, K. K. Schaffer, T. Schrabback, E. Shirokoff, J. Song, H. G. Spieler, S. A. Stanford, Z. Staniszewski, A. A. Stark, K. T. Story, C. W. Stubbs, K. Vand erlinde, J. D. Vieira, A. Vikhlinin, R. Williamson, O. Zahn, and A. Zenteno. Galaxy Clusters Discovered via the Sunyaev-Zel'dovich Effect in the 2500-Square-Degree SPT-SZ Survey. *The Astrophysical Journals*, 216(2):27, Feb 2015.

[32] D. G. Bonfield, M. J. Jarvis, M. J. Hardcastle, A. Cooray, E. Hatziminaoglou, R. J. Ivison, M. J. Page, J. A. Stevens, G. de Zotti, R. Auld, M. Baes, S. Buttiglione, A. Cava, A. Dariush, J. S. Dunlop, L. Dunne, S. Dye, S. Eales, J. Fritz, R. Hopwood, E. Ibar, S. J. Maddox, M. J. Michałowski, E. Pascale, M. Pohlen, E. E. Rigby, G. Rodighiero, S. Serjeant, D. J. B. Smith, P. Temi, and P. van der Werf. Herschel-ATLAS: the link between accretion luminosity and star formation in quasar host galaxies. *Monthly Notices of the Royal Astronomical Society*, 416:13–21, Sept. 2011.

[33] M. Boquien, D. Burgarella, Y. Roehlly, V. Buat, L. Ciesla, D. Corre, A. K. Inoue, and H. Salas. CIGALE: a python Code Investigating GALaxy Emission. *Astronomy & Astrophysics*, 622:A103, Feb 2019.

[34] M. S. Bothwell, I. Smail, S. C. Chapman, R. Genzel, R. J. Ivison, L. J. Tacconi, S. Alaghband -Zadeh, F. Bertoldi, A. W. Blain, C. M. Casey, P. Cox, T. R. Greve, D. Lutz, R. Neri, A. Omont, and A. M. Swinbank. A survey of molecular gas in luminous sub-millimetre galaxies. *Monthly Notices of the Royal Astronomical Society*, 429(4):3047–3067, Mar 2013.

[35] F. Bournaud, V. Perret, F. Renaud, A. Dekel, B. G. Elmegreen, D. M. Elmegreen, R. Teyssier, P. Amram, E. Daddi, P.-A. Duc, D. Elbaz, B. Epinat, J. M. Gabor, S. Juneau, K. Kraljic, and E. Le Floch'. The Long Lives of Giant Clumps and the Birth of Outflows in Gas-rich Galaxies at High Redshift. *The Astrophysical Journal*, 780(1):57, Jan 2014.

[36] K. Brand, M. J. Brown, A. Dey, B. T. Jannuzi, C. S. Kochanek, A. T. Kenter, D. Fabricant, G. G. Fazio, W. R. Forman, P. J. Green, et al. The chandra xboötes survey. iii. optical and near-infrared counterparts. *ApJ*, 641(1):140, 2006.

[37] W. N. Brandt and D. M. Alexander. Cosmic X-ray surveys of distant active galaxies. The demographics, physics, and ecology of growing supermassive black holes. *Astronomy & Astrophysics Reviews*, 23:1, Jan. 2015.

[38] R. Brennan, V. Pandya, R. S. Somerville, G. Barro, E. N. Taylor, S. Wuyts, E. F. Bell, A. Dekel, H. C. Ferguson, D. H. McIntosh, C. Papovich, and J. Primack. Quenching and morphological transformation in semi-analytic models and CANDELS. *Monthly Notices of the Royal Astronomical Society*, 451(3):2933–2956, Aug. 2015.

[39] A. Brown, H. Nayyeri, A. Cooray, J. Ma, R. C. Hickox, and M. Azadi. Infrared Contributions of X-Ray Selected Active Galactic Nuclei in Dusty Star-forming Galaxies. *The Astrophysical Journal*, 871(1):87, Jan. 2019.

[40] G. Bruzual and S. Charlot. Stellar population synthesis at the resolution of 2003. *Monthly Notices of the Royal Astronomical Society*, 344:1000–1028, Oct. 2003.

[41] D. Burgarella, V. Buat, and J. Iglesias-Páramo. Star formation and dust attenuation properties in galaxies from a statistical ultraviolet-to-far-infrared analysis. *Monthly Notices of the Royal Astronomical Society*, 360:1413–1425, July 2005.

[42] Z.-Y. Cai, G. De Zotti, and M. Bonato. High-z dusty star-forming galaxies: a top-heavy initial mass function? *arXiv e-prints*, page arXiv:1910.06970, Oct 2019.

[43] D. Calzetti, L. Armus, R. C. Bohlin, A. L. Kinney, J. Koornneef, and T. Storchi-Bergmann. The Dust Content and Opacity of Actively Star-forming Galaxies. *The Astrophysical Journal*, 533(2):682–695, Apr 2000.

[44] P. L. Capak, D. Riechers, N. Z. Scoville, C. Carilli, P. Cox, R. Neri, B. Robertson, M. Salvato, E. Schinnerer, L. Yan, G. W. Wilson, M. Yun, F. Civano, M. Elvis, A. Karim, B. Mobasher, and J. G. Staguhn. A massive protocluster of galaxies at a redshift of z$\sim$5.3. *Nature*, 470(7333):233–235, Feb 2011.

[45] A. C. Carnall, S. Walker, R. J. McLure, J. S. Dunlop, D. J. McLeod, F. Cullen, V. Wild, R. Amorin, M. Bolzonella, M. Castellano, A. Cimatti, O. Cucciati, A. Fontana, A. Gargiulo, B. Garilli, M. J. Jarvis, L. Pentericci, L. Pozzetti, G. Zamorani, A. Calabro, N. P. Hathi, and A. M. Koekemoer. Timing the earliest quenching events with a robust sample of massive quiescent galaxies at 2 < z < 5. *Monthly Notices of the Royal Astronomical Society*, 496(1):695–707, July 2020.

[46] C. M. Casey. Far-infrared spectral energy distribution fitting for galaxies near and far. *Monthly Notices of the Royal Astronomical Society*, 425(4):3094–3103, Oct 2012.

[47] C. M. Casey. The Ubiquity of Coeval Starbursts in Massive Galaxy Cluster Progenitors. *The Astrophysical Journal*, 824(1):36, Jun 2016.

[48] C. M. Casey, A. Cooray, P. Capak, H. Fu, K. Kovac, S. Lilly, D. B. Sanders, N. Z. Scoville, and E. Treister. A Massive, Distant Proto-cluster at z = 2.47 Caught in a Phase of Rapid Formation? *The Astrophysical Journall*, 808(2):L33, Aug 2015.

[49] C. M. Casey, A. Cooray, M. Killi, P. Capak, C.-C. Chen, C.-L. Hung, J. Kartaltepe, D. B. Sanders, and N. Z. Scoville. Near-infrared MOSFIRE Spectra of Dusty Star-forming Galaxies at 0.2 < z < 4. , 840(2):101, May 2017.

[50] C. M. Casey, J. Hodge, J. A. Zavala, J. Spilker, E. da Cunha, J. Staguhn, S. L. Finkelstein, and P. Drew. An Analysis of ALMA Deep Fields and the Perceived Dearth of High-z Galaxies. *The Astrophysical Journal*, 862(1):78, July 2018.

[51] C. M. Casey, D. Narayanan, and A. Cooray. Dusty star-forming galaxies at high redshift. *Physics Reports*, 541(2):45–161, 2014.

[52] C. M. Casey, N. Z. Scoville, D. B. Sanders, N. Lee, A. Cooray, S. L. Finkelstein, P. Capak, A. Conley, G. De Zotti, and D. Farrah. Are Dusty Galaxies Blue? Insights on UV Attenuation from Dust-selected Galaxies. *The Astrophysical Journal*, 796(2):95, Dec 2014.

[53] C. M. Casey, J. A. Zavala, M. Aravena, M. Béthermin, K. I. Caputi, J. B. Champagne, D. L. Clements, E. da Cunha, P. Drew, S. L. Finkelstein, C. C. Hayward, J. S. Kartaltepe, K. Knudsen, A. M. Koekemoer, G. E. Magdis, A. Man, S. M. Manning, N. Z. Scoville, K. Sheth, J. Spilker, J. Staguhn, M. Talia, Y. Taniguchi, S. Toft, E. Treister, and M. Yun. Physical Characterization of an Unlensed, Dusty Star-forming Galaxy at z = 5.85. *The Astrophysical Journal*, 887(1):55, Dec. 2019.

[54] C. M. Casey, J. A. Zavala, M. Aravena, M. Béthermin, K. I. Caputi, J. B. Champagne, D. L. Clements, E. da Cunha, P. Drew, S. L. Finkelstein, C. C. Hayward, J. S. Kartaltepe, K. Knudsen, A. M. Koekemoer, G. E. Magdis, A. Man, S. M. Manning, N. Z. Scoville, K. Sheth, J. Spilker, J. Staguhn, M. Talia, Y. Taniguchi, S. Toft, E. Treister, and M. Yun. Physical Characterization of an Unlensed, Dusty Star-forming Galaxy at z = 5.85. *The Astrophysical Journal*, 887(1):55, Dec 2019.

[55] C. M. Casey, J. A. Zavala, J. Spilker, E. da Cunha, J. Hodge, C.-L. Hung, J. Staguhn, S. L. Finkelstein, and P. Drew. The Brightest Galaxies in the Dark Ages: Galaxies' Dust

Continuum Emission during the Reionization Era. *The Astrophysical Journal*, 862(1):77, Jul 2018.

[56] G. Chabrier. Galactic Stellar and Substellar Initial Mass Function. *Publications of the Astronomical Society of the Pacific*, 115(809):763–795, Jul 2003.

[57] J. B. Champagne, R. Decarli, C. M. Casey, B. Venemans, E. Bañados, F. Walter, F. Bertoldi, X. Fan, E. P. Farina, C. Mazzucchelli, D. A. Riechers, M. A. Strauss, R. Wang, and Y. Yang. No Evidence for Millimeter Continuum Source Overdensities in the Environments of $z \gtrsim 6$ Quasars. *The Astrophysical Journal*, 867(2):153, Nov 2018.

[58] S. C. Chapman, A. Blain, R. Ibata, R. J. Ivison, I. Smail, and G. Morrison. Do Submillimeter Galaxies Really Trace the Most Massive Dark-Matter Halos? Discovery of a High-z Cluster in a Highly Active Phase of Evolution. *The Astrophysical Journal*, 691(1):560–568, Jan 2009.

[59] C.-T. J. Chen, R. C. Hickox, S. Alberts, M. Brodwin, C. Jones, S. S. Murray, D. M. Alexander, R. J. Assef, M. J. I. Brown, A. Dey, W. R. Forman, V. Gorjian, A. D. Goulding, E. Le Floc'h, B. T. Jannuzi, J. R. Mullaney, and A. Pope. A Correlation between Star Formation Rate and Average Black Hole Accretion in Star-forming Galaxies. *ApJ*, 773:3, Aug. 2013.

[60] C.-T. J. Chen, R. C. Hickox, S. Alberts, C. M. Harrison, D. M. Alexander, R. Assef, M. Brodwin, M. J. I. Brown, A. Del Moro, W. R. Forman, V. Gorjian, A. D. Goulding, K. N. Hainline, C. Jones, C. S. Kochanek, S. S. Murray, A. Pope, E. Rovilos, and D. Stern. A Connection between Obscuration and Star Formation in Luminous Quasars. *The Astrophysical Journal*, 802:50, Mar. 2015.

[61] Y.-K. Chiang, R. Overzier, and K. Gebhardt. Ancient Light from Young Cosmic Cities: Physical and Observational Signatures of Galaxy Proto-clusters. *The Astrophysical Journal*, 779(2):127, Dec 2013.

[62] Y.-K. Chiang, R. A. Overzier, K. Gebhardt, S. L. Finkelstein, C.-T. Chiang, G. J. Hill, G. A. Blanc, N. Drory, T. S. Chonis, G. R. Zeimann, A. Hagen, D. P. Schneider, S. Jogee, R. Ciardullo, and C. Gronwall. SURVEYING GALAXY PROTO-CLUSTERS IN EMISSION: A LARGE-SCALE STRUCTURE ATz= 2.44 AND THE OUTLOOK FOR HETDEX. *The Astrophysical Journal*, 808(1):37, jul 2015.

[63] Y.-K. Chiang, R. A. Overzier, K. Gebhardt, and B. Henriques. Galaxy Protoclusters as Drivers of Cosmic Star Formation History in the First 2 Gyr. *The Astrophysical Journal*, 844(2):L23, Aug 2017.

[64] L. Ciesla, V. Charmandaris, A. Georgakakis, E. Bernhard, P. D. Mitchell, V. Buat, D. Elbaz, E. LeFloc'h, C. G. Lacey, G. E. Magdis, and M. Xilouris. Constraining the properties of AGN host galaxies with spectral energy distribution modelling. *Astronomy & Astrophysics*, 576:A10, Apr. 2015.

[65] D. L. Clements, F. G. Braglia, A. K. Hyde, I. Pérez-Fournon, J. Bock, A. Cava, S. Chapman, A. Conley, A. Cooray, D. Farrah, E. A. González Solares, L. Marchetti, G. Marsden, S. J.

Oliver, I. G. Roseboom, B. Schulz, A. J. Smith, M. Vaccari, J. Vieira, M. Viero, L. Wang, J. Wardlow, M. Zemcov, and G. de Zotti. Herschel Multitiered Extragalactic Survey: clusters of dusty galaxies uncovered by Herschel and Planck. *Monthly Notices of the Royal Astronomical Society*, 439(2):1193–1211, Apr 2014.

[66] J. J. Condon, E. Anderson, and J. J. Broderick. Radio Identifications of Extragalactic IRAS Sources. *Astronomical Journal*, 109:2318, June 1995.

[67] E. Contini, G. De Lucia, N. Hatch, S. Borgani, and X. Kang. Semi-analytic model predictions of the galaxy population in protoclusters. *Monthly Notices of the Royal Astronomical Society*, 456(2):1924–1935, Feb 2016.

[68] E. A. Cooke, N. A. Hatch, D. Stern, A. Rettura, M. Brodwin, A. Galametz, D. Wylezalek, C. Bridge, C. J. Conselice, C. De Breuck, A. H. Gonzalez, and M. Jarvis. A Mature Galaxy Cluster at z=1.58 around the Radio Galaxy 7C1753+6311. *The Astrophysical Journal*, 816(2):83, Jan 2016.

[69] K. C. Cooke, J. S. Kartaltepe, K. D. Tyler, B. Darvish, C. M. Casey, O. Le Fèvre, M. Salvato, and N. Scoville. Stellar Mass Growth of Brightest Cluster Galaxy Progenitors in COSMOS Since z $\sim$ 3. *The Astrophysical Journal*, 881(2):150, Aug 2019.

[70] M. C. Cooper, A. L. Coil, B. F. Gerke, J. A. Newman, K. Bundy, C. J. Conselice, D. J. Croton, M. Davis, S. M. Faber, P. Guhathakurta, D. C. Koo, L. Lin, B. J. Weiner, C. N. A. Willmer, and R. Yan. Absence of evidence is not evidence of absence: the colour-density relation at fixed stellar mass persists to z $\sim$1. *Monthly Notices of the Royal Astronomical Society*, 409(1):337–345, Nov 2010.

[71] L. L. Cowie, J. González-López, A. J. Barger, F. E. Bauer, L. Y. Hsu, and W. H. Wang. A Submillimeter Perspective on the GOODS Fields (SUPER GOODS). III. A Large Sample of ALMA Sources in the GOODS-S. *The Astrophysical Journal*, 865(2):106, Oct 2018.

[72] L. L. Cowie, E. M. Hu, and A. Songaila. Faintest Galaxy Morphologies From HST WFPC2 Imaging of the Hawaii Survey Fields. *Astronomical Journal*, 110:1576, Oct 1995.

[73] M. J. Cowley, L. R. Spitler, K.-V. H. Tran, G. A. Rees, I. Labbé, R. J. Allen, G. B. Brammer, K. Glazebrook, A. M. Hopkins, S. Juneau, G. G. Kacprzak, J. R. Mullaney, T. Nanayakkara, C. Papovich, R. F. Quadri, C. M. S. Straatman, A. R. Tomczak, and P. G. van Dokkum. ZFOURGE catalogue of AGN candidates: an enhancement of 160-μm-derived star formation rates in active galaxies to z = 3.2. *Monthly Notices of the Royal Astronomical Society*, 457:629–641, Mar. 2016.

[74] W. I. Cowley, C. G. Lacey, C. M. Baugh, and S. Cole. Simulated observations of sub-millimetre galaxies: the impact of single-dish resolution and field variance. *Monthly Notices of the Royal Astronomical Society*, 446(2):1784–1798, Jan 2015.

[75] D. J. Croton, V. Springel, S. D. M. White, G. De Lucia, C. S. Frenk, L. Gao, A. Jenkins, G. Kauffmann, J. F. Navarro, and N. Yoshida. The many lives of active galactic nuclei: cooling flows, black holes and the luminosities and colours of galaxies. *Monthly Notices of the Royal Astronomical Society*, 365:11–28, Jan. 2006.

[76] E. da Cunha, F. Walter, I. R. Smail, A. M. Swinbank, J. M. Simpson, R. Decarli, J. A. Hodge, A. Weiss, P. P. van der Werf, F. Bertoldi, S. C. Chapman, P. Cox, A. L. R. Danielson, H. Dannerbauer, T. R. Greve, R. J. Ivison, A. Karim, and A. Thomson. An ALMA Survey of Sub-millimeter Galaxies in the Extended Chandra Deep Field South: Physical Properties Derived from Ultraviolet-to-radio Modeling. *The Astrophysical Journal*, 806(1):110, June 2015.

[77] E. Daddi, D. M. Alexander, M. Dickinson, R. Gilli, A. Renzini, D. Elbaz, A. Cimatti, R. Chary, D. Frayer, F. E. Bauer, W. N. Brandt, M. Giavalisco, N. A. Grogin, M. Huynh, J. Kurk, M. Mignoli, G. Morrison, A. Pope, and S. Ravindranath. Multiwavelength Study of Massive Galaxies at z˜2. II. Widespread Compton-thick Active Galactic Nuclei and the Concurrent Growth of Black Holes and Bulges. *The Astrophysical Journal*, 670:173–189, Nov. 2007.

[78] E. Daddi, H. Dannerbauer, D. Stern, M. Dickinson, G. Morrison, D. Elbaz, M. Giavalisco, C. Mancini, A. Pope, and H. Spinrad. Two Bright Submillimeter Galaxies in a z = 4.05 Protocluster in Goods-North, and Accurate Radio-Infrared Photometric Redshifts. *The Astrophysical Journal*, 694(2):1517–1538, Apr 2009.

[79] E. Daddi, M. Dickinson, G. Morrison, R. Chary, A. Cimatti, D. Elbaz, D. Frayer, A. Renzini, A. Pope, D. M. Alexander, F. E. Bauer, M. Giavalisco, M. Huynh, J. Kurk, and M. Mignoli. Multiwavelength Study of Massive Galaxies at z˜2. I. Star Formation and Galaxy Growth. *The Astrophysical Journal*, 670:156–172, Nov. 2007.

[80] E. Daddi, D. Elbaz, F. Walter, F. Bournaud, F. Salmi, C. Carilli, H. Dannerbauer, M. Dickinson, P. Monaco, and D. Riechers. Different Star Formation Laws for Disks Versus Starbursts at Low and High Redshifts. *The Astrophysical Journall*, 714(1):L118–L122, May 2010.

[81] Y. S. Dai, B. J. Wilkes, J. Bergeron, J. Kuraszkiewicz, A. Omont, A. Atanas, and H. I. Teplitz. Is there a relationship between AGN and star formation in IR-bright AGNs? *ArXiv e-prints*, May 2017.

[82] H. Dannerbauer, J. D. Kurk, C. De Breuck, D. Wylezalek, J. S. Santos, Y. Koyama, N. Seymour, M. Tanaka, N. Hatch, B. Altieri, D. Coia, A. Galametz, T. Kodama, G. Miley, H. Röttgering, M. Sanchez-Portal, I. Valtchanov, B. Venemans, and B. Ziegler. An excess of dusty starbursts related to the Spiderweb galaxy. *Astronomy & Astrophysics*, 570:A55, Oct 2014.

[83] H. Dannerbauer, M. D. Lehnert, B. Emonts, B. Ziegler, B. Altieri, C. De Breuck, N. Hatch, T. Kodama, Y. Koyama, J. D. Kurk, T. Matiz, G. Miley, D. Narayanan, R. P. Norris, R. Overzier, H. J. A. Röttgering, M. Sargent, N. Seymour, M. Tanaka, I. Valtchanov, and D. Wylezalek. The implications of the surprising existence of a large, massive CO disk in a distant protocluster. *Astronomy & Astrophysics*, 608:A48, Dec 2017.

[84] B. Darvish, N. Z. Scoville, C. Martin, B. Mobasher, T. Diaz-Santos, and L. Shen. Similar Scaling Relations for the Gas Content of Galaxies Across Environments to z 3.5. *The Astrophysical Journal*, 860(2):111, Jun 2018.

[85] R. Davé, K. Finlator, B. D. Oppenheimer, M. Fardal, N. Katz, D. Kereš, and D. H. Weinberg. The nature of submillimetre galaxies in cosmological hydrodynamic simulations. *Monthly Notices of the Royal Astronomical Society*, 404(3):1355–1368, May 2010.

[86] I. Davidzon, O. Ilbert, C. Laigle, J. Coupon, H. J. McCracken, I. Delvecchio, D. Masters, P. Capak, B. C. Hsieh, O. Le Fèvre, L. Tresse, M. Bethermin, Y. Y. Chang, A. L. Faisst, E. Le Floc'h, C. Steinhardt, S. Toft, H. Aussel, C. Dubois, G. Hasinger, M. Salvato, D. B. Sanders, N. Scoville, and J. D. Silverman. The COSMOS2015 galaxy stellar mass function. Thirteen billion years of stellar mass assembly in ten snapshots. *Astronomy & Astrophysics*, 605:A70, Sept. 2017.

[87] R. I. Davies, L. Burtscher, D. Rosario, T. Storchi-Bergmann, A. Contursi, R. Genzel, J. Graciá-Carpio, E. Hicks, A. Janssen, M. Koss, M.-Y. Lin, D. Lutz, W. Maciejewski, F. Müller-Sánchez, G. Orban de Xivry, C. Ricci, R. Riffel, R. A. Riffel, M. Schartmann, A. Schnorr-Müller, A. Sternberg, E. Sturm, L. Tacconi, and S. Veilleux. Insights on the Dusty Torus and Neutral Torus from Optical and X-Ray Obscuration in a Complete Volume Limited Hard X-Ray AGN Sample. *The Astrophysical Journal*, 806:127, June 2015.

[88] G. De Lucia and J. Blaizot. The hierarchical formation of the brightest cluster galaxies. *Monthly Notices of the Royal Astronomical Society*, 375(1):2–14, Feb 2007.

[89] A. Dekel and Y. Birnboim. Galaxy bimodality due to cold flows and shock heating. *Monthly Notices of the Royal Astronomical Society*, 368(1):2–20, May 2006.

[90] A. Dekel, Y. Birnboim, G. Engel, J. Freundlich, T. Goerdt, M. Mumcuoglu, E. Neistein, C. Pichon, R. Teyssier, and E. Zinger. Cold streams in early massive hot haloes as the main mode of galaxy formation. *Nature*, 457:451–454, Jan. 2009.

[91] A. Del Moro, D. M. Alexander, J. R. Mullaney, E. Daddi, M. Pannella, F. E. Bauer, A. Pope, M. Dickinson, D. Elbaz, P. D. Barthel, M. A. Garrett, W. N. Brandt, V. Charmandaris, R. R. Chary, K. Dasyra, R. Gilli, R. C. Hickox, H. S. Hwang, R. J. Ivison, S. Juneau, E. Le Floc'h, B. Luo, G. E. Morrison, E. Rovilos, M. T. Sargent, and Y. Q. Xue. GOODS-Herschel: radio-excess signature of hidden AGN activity in distant star-forming galaxies. *Astronomy & Astrophysics*, 549:A59, Jan. 2013.

[92] I. Delvecchio, D. Lutz, S. Berta, D. J. Rosario, G. Zamorani, F. Pozzi, C. Gruppioni, C. Vignali, M. Brusa, A. Cimatti, D. L. Clements, A. Cooray, D. Farrah, G. Lanzuisi, S. Oliver, G. Rodighiero, P. Santini, and M. Symeonidis. Mapping the average AGN accretion rate in the SFR-M_* plane for Herschel-selected galaxies at $0 < z \leq 2.5$. *Monthly Notices of the Royal Astronomical Society*, 449:373–389, May 2015.

[93] S. Deshmukh, K. I. Caputi, M. L. N. Ashby, W. I. Cowley, H. J. McCracken, J. P. U. Fynbo, O. Le Fèvre, B. Milvang-Jensen, and O. Ilbert. The Spitzer Matching Survey of the UltraVISTA Ultra-deep Stripes (SMUVS): The Evolution of Dusty and Nondusty Galaxies with Stellar Mass at z = 2-6. *The Astrophysical Journal*, 864(2):166, Sept. 2018.

[94] C. D'Eugenio, E. Daddi, R. Gobat, V. Strazzullo, P. Lustig, I. Delvecchio, S. Jin, A. Puglisi, A. Calabró, C. Mancini, M. Dickinson, A. Cimatti, and M. Onodera. The Typical Massive

Quiescent Galaxy at z ∼ 3 is a Post-starburst. *The Astrophysical Journall*, 892(1):L2, Mar. 2020.

[95] T. Di Matteo, V. Springel, and L. Hernquist. Energy input from quasars regulates the growth and activity of black holes and their host galaxies. *Nature*, 433:604–607, Feb. 2005.

[96] A. M. Diamond-Stanic, J. Moustakas, C. A. Tremonti, A. L. Coil, R. C. Hickox, A. R. Robaina, G. H. Rudnick, and P. H. Sell. High-velocity Outflows without AGN Feedback: Eddington-limited Star Formation in Compact Massive Galaxies. *The Astrophysical Journall*, 755:L26, Aug. 2012.

[97] C. Diener, S. J. Lilly, C. Ledoux, G. Zamorani, M. Bolzonella, D. N. A. Murphy, P. Capak, O. Ilbert, and H. McCracken. A Protocluster at z = 2.45. , 802(1):31, Mar 2015.

[98] M. Dijkstra and A. Loeb. Lyα blobs as an observational signature of cold accretion streams into galaxies. *Monthly Notices of the Royal Astronomical Society*, 400:1109–1120, Dec. 2009.

[99] M. Doherty, M. Tanaka, C. De Breuck, C. Ly, T. Kodama, J. Kurk, N. Seymour, J. Vernet, D. Stern, B. Venemans, M. Kajisawa, and I. Tanaka. Optical and near-IR spectroscopy of candidate red galaxies in two z ∼2.5 proto-clusters. *Astronomy & Astrophysics*, 509:A83, Jan 2010.

[100] H. Domínguez Sánchez, P. G. Pérez-González, P. Esquej, M. C. Eliche-Moral, G. Barro, A. Cava, A. M. Koekemoer, B. Alcalde Pampliega, A. Alonso Herrero, G. Bruzual, N. Cardiel, J. Cenarro, D. Ceverino, S. Charlot, and A. Hernán Caballero. Pathways to quiescence: SHARDS view on the star formation histories of massive quiescent galaxies at 1.0 < z < 1.5. *Monthly Notices of the Royal Astronomical Society*, 457(4):3743–3768, Apr. 2016.

[101] J. L. Donley, A. M. Koekemoer, M. Brusa, P. Capak, C. N. Cardamone, F. Civano, O. Ilbert, C. D. Impey, J. S. Kartaltepe, T. Miyaji, M. Salvato, D. B. Sanders, J. R. Trump, and G. Zamorani. Identifying Luminous Active Galactic Nuclei in Deep Surveys: Revised IRAC Selection Criteria. *The Astrophysical Journal*, 748:142, Apr. 2012.

[102] J. L. Donley, G. H. Rieke, J. R. Rigby, and P. G. Pérez-González. Unveiling a Population of AGNs Not Detected in X-Rays. *The Astrophysical Journal*, 634:169–182, Nov. 2005.

[103] C. D. Dowell, A. Conley, J. Glenn, V. Arumugam, V. Asboth, H. Aussel, F. Bertoldi, M. Béthermin, J. Bock, A. Boselli, C. Bridge, V. Buat, D. Burgarella, A. Cabrera-Lavers, C. M. Casey, S. C. Chapman, D. L. Clements, L. Conversi, A. Cooray, H. Dannerbauer, F. De Bernardis, T. P. Ellsworth-Bowers, D. Farrah, A. Franceschini, M. Griffin, M. A. Gurwell, M. Halpern, E. Hatziminaoglou, S. Heinis, E. Ibar, R. J. Ivison, N. Laporte, L. Marchetti, P. Martínez-Navajas, G. Marsden, G. E. Morrison, H. T. Nguyen, B. O'Halloran, S. J. Oliver, A. Omont, M. J. Page, A. Papageorgiou, C. P. Pearson, G. Petitpas, I. Pérez-Fournon, M. Pohlen, D. Riechers, D. Rigopoulou, I. G. Roseboom, M. Rowan-Robinson, J. Sayers, B. Schulz, D. Scott, N. Seymour, D. L. Shupe, A. J. Smith, A. Streblyanska, M. Symeonidis, M. Vaccari, I. Valtchanov, J. D. Vieira, M. Viero, L. Wang, J. Wardlow, C. K. Xu, and

M. Zemcov. HerMES: Candidate High-redshift Galaxies Discovered with Herschel/SPIRE. *The Astrophysical Journal*, 780(1):75, Jan. 2014.

[104] B. T. Draine, G. Aniano, O. Krause, B. Groves, K. Sandstrom, R. Braun, A. Leroy, U. Klaas, H. Linz, H.-W. Rix, E. Schinnerer, A. Schmiedeke, and F. Walter. Andromeda's Dust. *The Astrophysical Journal*, 780(2):172, Jan 2014.

[105] B. T. Draine, D. A. Dale, G. Bendo, K. D. Gordon, J. D. T. Smith, L. Armus, C. W. Engelbracht, G. Helou, J. Kennicutt, R. C., A. Li, H. Roussel, F. Walter, D. Calzetti, J. Moustakas, E. J. Murphy, G. H. Rieke, C. Bot, D. J. Hollenbach, K. Sheth, and H. I. Teplitz. Dust Masses, PAH Abundances, and Starlight Intensities in the SINGS Galaxy Sample. *The Astrophysical Journal*, 663(2):866–894, Jul 2007.

[106] S. P. Driver, C. C. Popescu, R. J. Tuffs, A. W. Graham, J. Liske, and I. Baldry. The Energy Output of the Universe from 0.1 to 1000 μm. *The Astrophysical Journall*, 678(2):L101, May 2008.

[107] U. Dudzevičiūtė, I. Smail, A. M. Swinbank, S. M. Stach, O. Almaini, E. da Cunha, F. X. An, V. Arumugam, J. Birkin, A. W. Blain, S. C. Chapman, C. C. Chen, C. J. Conselice, K. E. K. Coppin, J. S. Dunlop, D. Farrah, J. E. Geach, B. Gullberg, W. G. Hartley, J. A. Hodge, R. J. Ivison, D. T. Maltby, D. Scott, C. J. Simpson, J. M. Simpson, A. P. Thomson, F. Walter, J. L. Wardlow, A. Weiss, and P. van der Werf. An ALMA survey of the SCUBA-2 CLS UDS field: Physical properties of 707 Sub-millimetre Galaxies. *Monthly Notices of the Royal Astronomical Society*, Apr. 2020.

[108] S. Duivenvoorden, S. Oliver, J. M. Scudder, J. Greenslade, D. A. Riechers, S. M. Wilkins, V. Buat, S. C. Chapman, D. L. Clements, A. Cooray, K. E. K. Coppin, H. Dannerbauer, G. De Zotti, J. S. Dunlop, S. A. Eales, A. Efstathiou, D. Farrah, J. E. Geach, W. S. Holland, P. D. Hurley, R. J. Ivison, L. Marchetti, G. Petitpas, M. T. Sargent, D. Scott, M. Symeonidis, M. Vaccari, J. D. Vieira, L. Wang, J. Wardlow, and M. Zemcov. Red, redder, reddest: SCUBA-2 imaging of colour-selected Herschel sources. *Monthly Notices of the Royal Astronomical Society*, 477(1):1099–1119, June 2018.

[109] J. S. Dunlop, R. J. McLure, A. D. Biggs, J. E. Geach, M. J. Michałowski, R. J. Ivison, W. Rujopakarn, E. van Kampen, A. Kirkpatrick, A. Pope, D. Scott, A. M. Swinbank, T. A. Targett, I. Aretxaga, J. E. Austermann, P. N. Best, V. A. Bruce, E. L. Chapin, S. Charlot, M. Cirasuolo, K. Coppin, R. S. Ellis, S. L. Finkelstein, C. C. Hayward, D. H. Hughes, E. Ibar, P. Jagannathan, S. Khochfar, M. P. Koprowski, D. Narayanan, K. Nyland, C. Papovich, J. A. Peacock, G. H. Rieke, B. Robertson, T. Vernstrom, P. P. v. d. Werf, G. W. Wilson, and M. Yun. A deep ALMA image of the Hubble Ultra Deep Field. *Monthly Notices of the Royal Astronomical Society*, 466(1):861–883, Apr. 2017.

[110] S. Eales, L. Dunne, D. Clements, A. Cooray, G. De Zotti, S. Dye, R. Ivison, M. Jarvis, G. Lagache, S. Maddox, M. Negrello, S. Serjeant, M. A. Thompson, E. Van Kampen, A. Amblard, P. Andreani, M. Baes, A. Beelen, G. J. Bendo, D. Benford, F. Bertoldi, J. Bock, D. Bonfield, A. Boselli, C. Bridge, V. Buat, D. Burgarella, R. Carlberg, A. Cava, P. Chanial, S. Charlot, N. Christopher, P. Coles, L. Cortese, A. Dariush, E. da Cunha, G. Dalton,

L. Danese, H. Dannerbauer, S. Driver, J. Dunlop, L. Fan, D. Farrah, D. Frayer, C. Frenk, J. Geach, J. Gardner, H. Gomez, J. González- Nuevo, E. González-Solares, M. Griffin, M. Hardcastle, E. Hatziminaoglou, D. Herranz, D. Hughes, E. Ibar, W.-S. Jeong, C. Lacey, A. Lapi, A. Lawrence, M. Lee, L. Leeuw, J. Liske, M. López-Caniego, T. Müller, K. Nandra, P. Panuzzo, A. Papageorgiou, G. Patanchon, J. Peacock, C. Pearson, S. Phillipps, M. Pohlen, C. Popescu, S. Rawlings, E. Rigby, M. Rigopoulou, A. Robotham, G. Rodighiero, A. Sansom, B. Schulz, D. Scott, D. J. B. Smith, B. Sibthorpe, I. Smail, J. Stevens, W. Sutherland, T. Takeuchi, J. Tedds, P. Temi, R. Tuffs, M. Trichas, M. Vaccari, I. Valtchanov, P. van der Werf, A. Verma, J. Vieria, C. Vlahakis, and G. J. White. The Herschel ATLAS. *Publications of the Astronomical Society of the Pacific*, 122:499, May 2010.

[111] R. A. Edelson and M. A. Malkan. Spectral Energy Distributions of Active Galactic Nuclei between 0.1 and 100 Microns. *The Astrophysical Journal*, 308:59, Sep 1986.

[112] P. R. M. Eisenhardt, M. Brodwin, A. H. Gonzalez, S. A. Stanford, D. Stern, P. Barmby, M. J. I. Brown, K. Dawson, A. Dey, M. Doi, A. Galametz, B. T. Jannuzi, C. S. Kochanek, J. Meyers, T. Morokuma, and L. A. Moustakas. Clusters of Galaxies in the First Half of the Universe from the IRAC Shallow Survey. *The Astrophysical Journal*, 684(2):905–932, Sep 2008.

[113] D. J. Eisenstein, D. H. Weinberg, E. Agol, H. Aihara, C. Allende Prieto, S. F. Anderson, J. A. Arns, É. Aubourg, S. Bailey, E. Balbinot, and et al. SDSS-III: Massive Spectroscopic Surveys of the Distant Universe, the Milky Way, and Extra-Solar Planetary Systems. *Astronomical Journal*, 142(3):72, Sept. 2011.

[114] D. Elbaz, M. Dickinson, H. S. Hwang, T. Díaz-Santos, G. Magdis, B. Magnelli, D. Le Borgne, F. Galliano, M. Pannella, P. Chanial, L. Armus, V. Charmandaris, E. Daddi, H. Aussel, P. Popesso, J. Kartaltepe, B. Altieri, I. Valtchanov, D. Coia, H. Dannerbauer, K. Dasyra, R. Leiton, J. Mazzarella, D. M. Alexander, V. Buat, D. Burgarella, R. R. Chary, R. Gilli, R. J. Ivison, S. Juneau, E. Le Floc'h, D. Lutz, G. E. Morrison, J. R. Mullaney, E. Murphy, A. Pope, D. Scott, M. Brodwin, D. Calzetti, C. Cesarsky, S. Charlot, H. Dole, P. Eisenhardt, H. C. Ferguson, N. Förster Schreiber, D. Frayer, M. Giavalisco, M. Huynh, A. M. Koekemoer, C. Papovich, N. Reddy, C. Surace, H. Teplitz, M. S. Yun, and G. Wilson. GOODS-Herschel: an infrared main sequence for star-forming galaxies. *Astronomy & Astrophysics*, 533:A119, Sep 2011.

[115] S. L. Ellison, J. T. Mendel, D. R. Patton, and J. M. Scudder. Galaxy pairs in the Sloan Digital Sky Survey - VIII. The observational properties of post-merger galaxies. *Monthly Notices of the Royal Astronomical Society*, 435:3627–3638, Nov. 2013.

[116] S. L. Ellison, H. Teimoorinia, D. J. Rosario, and J. T. Mendel. The star formation rates of active galactic nuclei host galaxies. *Monthly Notices of the Royal Astronomical Society*, 458:L34–L38, May 2016.

[117] D. M. Elmegreen, B. G. Elmegreen, and A. C. Hirst. Discovery of Face-on Counterparts of Chain Galaxies in the Tadpole Advanced Camera for Surveys Field. *The Astrophysical Journall*, 604(1):L21–L23, Mar 2004.

[118] D. M. Elmegreen, B. G. Elmegreen, S. Ravindranath, and D. A. Coe. Resolved Galaxies in the Hubble Ultra Deep Field: Star Formation in Disks at High Redshift. *The Astrophysical Journal*, 658(2):763–777, Apr 2007.

[119] A. E. Evrard, J. Bialek, M. Busha, M. White, S. Habib, K. Heitmann, M. Warren, E. Rasia, G. Tormen, L. Moscardini, C. Power, A. R. Jenkins, L. Gao, C. S. Frenk, V. Springel, S. D. M. White, and J. Diemand. Virial Scaling of Massive Dark Matter Halos: Why Clusters Prefer a High Normalization Cosmology. *The Astrophysical Journal*, 672(1):122–137, Jan 2008.

[120] S. H. Ezhikode, P. Gandhi, C. Done, M. Ward, G. C. Dewangan, R. Misra, and N. Sajeeth Philip. Determining the torus covering factors for a sample of type 1 AGN in the local Universe. *ArXiv e-prints*, Oct. 2016.

[121] A. C. Fabian. Observational Evidence of Active Galactic Nuclei Feedback. *Annual Review of Astronomy & Astrophysics*, 50:455–489, Sept. 2012.

[122] O. Fakhouri and C.-P. Ma. Environmental dependence of dark matter halo growth - I. Halo merger rates. *Monthly Notices of the Royal Astronomical Society*, 394(4):1825–1840, Apr 2009.

[123] O. Fakhouri and C.-P. Ma. Dark matter halo growth - II. Diffuse accretion and its environmental dependence. , 401(4):2245–2256, Feb 2010.

[124] G. G. Fazio, J. L. Hora, L. E. Allen, M. L. N. Ashby, P. Barmby, L. K. Deutsch, J.-S. Huang, S. Kleiner, M. Marengo, S. T. Megeath, G. J. Melnick, M. A. Pahre, B. M. Patten, J. Polizotti, H. A. Smith, R. S. Taylor, Z. Wang, S. P. Willner, W. F. Hoffmann, J. L. Pipher, W. J. Forrest, C. W. McMurty, C. R. McCreight, M. E. McKelvey, R. E. McMurray, D. G. Koch, S. H. Moseley, R. G. Arendt, J. E. Mentzell, C. T. Marx, P. Losch, P. Mayman, W. Eichhorn, D. Krebs, M. Jhabvala, D. Y. Gezari, D. J. Fixsen, J. Flores, K. Shakoorzadeh, R. Jungo, C. Hakun, L. Workman, G. Karpati, R. Kichak, R. Whitley, S. Mann, E. V. Tollestrup, P. Eisenhardt, D. Stern, V. Gorjian, B. Bhattacharya, S. Carey, B. O. Nelson, W. J. Glaccum, M. Lacy, P. J. Lowrance, S. Laine, W. T. Reach, J. A. Stauffer, J. A. Surace, G. Wilson, E. L. Wright, A. Hoffman, G. Domingo, and M. Cohen. The Infrared Array Camera (IRAC) for the Spitzer Space Telescope. *ApJ Supplement Series*, 154:10–17, Sept. 2004.

[125] L. Ferrarese and D. Merritt. A Fundamental Relation between Supermassive Black Holes and Their Host Galaxies. *The Astrophysical Journall*, 539:L9–L12, Aug. 2000.

[126] F. Fiore, A. Grazian, P. Santini, S. Puccetti, M. Brusa, C. Feruglio, A. Fontana, E. Giallongo, A. Comastri, C. Gruppioni, F. Pozzi, G. Zamorani, and C. Vignali. Unveiling Obscured Accretion in the Chandra Deep Field-South. *The Astrophysical Journal*, 672:94–101, Jan. 2008.

[127] F. Fiore, S. Puccetti, M. Brusa, M. Salvato, G. Zamorani, T. Aldcroft, H. Aussel, H. Brunner, P. Capak, N. Cappelluti, F. Civano, A. Comastri, M. Elvis, C. Feruglio, A. Finoguenov, A. Fruscione, R. Gilli, G. Hasinger, A. Koekemoer, J. Kartaltepe, O. Ilbert, C. Impey, E. Le Floc'h, S. Lilly, V. Mainieri, A. Martinez-Sansigre, H. J. McCracken, N. Menci, A. Merloni, T. Miyaji, D. B. Sanders, M. Sargent, E. Schinnerer, N. Scoville, J. Silverman, V. Smolcic,

A. Steffen, P. Santini, Y. Taniguchi, D. Thompson, J. R. Trump, C. Vignali, M. Urry, and L. Yan. Chasing Highly Obscured QSOs in the COSMOS Field. *The Astrophysical Journal*, 693:447–462, Mar. 2009.

[128] B. Forrest, M. Annunziatella, G. Wilson, D. Marchesini, A. Muzzin, M. C. Cooper, Z. C. Marsan, I. McConachie, J. C. C. Chan, P. Gomez, E. Kado-Fong, F. La Barbera, I. Labbé, D. Lange-Vagle, J. Nantais, M. Nonino, T. Peña, P. Saracco, M. Stefanon, and R. F. J. van der Burg. An Extremely Massive Quiescent Galaxy at z = 3.493: Evidence of Insufficiently Rapid Quenching Mechanisms in Theoretical Models. *arXiv e-prints*, page arXiv:1910.10158, Oct 2019.

[129] J. Fritz, A. Franceschini, and E. Hatziminaoglou. Revisiting the infrared spectra of active galactic nuclei with a new torus emission model. *Monthly Notices of the Royal Astronomical Society*, 366:767–786, Mar. 2006.

[130] H. Fu, L. Yan, N. Z. Scoville, P. Capak, H. Aussel, E. Le Floc'h, O. Ilbert, M. Salvato, J. S. Kartaltepe, D. T. Frayer, D. B. Sanders, K. Sheth, and Y. Taniguchi. Decomposing Star Formation and Active Galactic Nucleus with Spitzer Mid-infrared Spectra: Luminosity Functions and Co-evolution. *The Astrophysical Journal*, 722(1):653–667, Oct. 2010.

[131] Y. Fudamoto, R. J. Ivison, I. Oteo, M. Krips, Z. Y. Zhang, A. Weiss, H. Dannerbauer, A. Omont, S. C. Chapman, L. Christensen, V. Arumugam, F. Bertoldi, M. Bremer, D. L. Clements, L. Dunne, S. A. Eales, J. Greenslade, S. Maddox, P. Martinez-Navajas, M. Michalowski, I. Pérez-Fournon, D. Riechers, J. M. Simpson, B. Stalder, E. Valiante, and P. van der Werf. The most distant, luminous, dusty star-forming galaxies: redshifts from NOEMA and ALMA spectral scans. *Monthly Notices of the Royal Astronomical Society*, 472(2):2028–2041, Dec 2017.

[132] S. Fujimoto, M. Ouchi, T. Shibuya, and H. Nagai. Demonstrating a New Census of Infrared Galaxies with ALMA (DANCING-ALMA). I. FIR Size and Luminosity Relation at z = 0-6 Revealed with 1034 ALMA Sources. *The Astrophysical Journal*, 850:83, Nov. 2017.

[133] J. M. Gabor and F. Bournaud. Active galactic nuclei-driven outflows without immediate quenching in simulations of high-redshift disc galaxies. *Monthly Notices of the Royal Astronomical Society*, 441:1615–1627, June 2014.

[134] R. Gavazzi, C. Adami, F. Durret, J. C. Cuillandre, O. Ilbert, A. Mazure, R. Pelló, and M. P. Ulmer. A weak lensing study of the Coma cluster. , 498(2):L33–L36, May 2009.

[135] J. E. Geach, R. C. Hickox, A. M. Diamond-Stanic, M. Krips, G. H. Rudnick, C. A. Tremonti, P. H. Sell, A. L. Coil, and J. Moustakas. Stellar feedback as the origin of an extended molecular outflow in a starburst galaxy. *Nature*, 516:68–70, Dec. 2014.

[136] J. E. Geach, I. Smail, R. S. Ellis, S. M. Moran, G. P. Smith, T. Treu, J. P. Kneib, A. C. Edge, and T. Kodama. A Panoramic Mid-Infrared Survey of Two Distant Clusters. *The Astrophysical Journal*, 649(2):661–672, Oct 2006.

[137] S. Genel, M. Vogelsberger, V. Springel, D. Sijacki, D. Nelson, G. Snyder, V. Rodriguez-Gomez, P. Torrey, and L. Hernquist. Introducing the Illustris project: the evolution of galaxy populations across cosmic time. *Monthly Notices of the Royal Astronomical Society*, 445(1):175–200, Nov. 2014.

[138] R. Genzel, L. J. Tacconi, D. Lutz, A. Saintonge, S. Berta, B. Magnelli, F. Combes, S. García-Burillo, R. Neri, A. Bolatto, T. Contini, S. Lilly, J. Boissier, F. Boone, N. Bouché, F. Bournaud, A. Burkert, M. Carollo, L. Colina, M. C. Cooper, P. Cox, C. Feruglio, N. M. Förster Schreiber, J. Freundlich, J. Gracia-Carpio, S. Juneau, K. Kovac, M. Lippa, T. Naab, P. Salome, A. Renzini, A. Sternberg, F. Walter, B. Weiner, A. Weiss, and S. Wuyts. Combined CO and Dust Scaling Relations of Depletion Time and Molecular Gas Fractions with Cosmic Time, Specific Star-formation Rate, and Stellar Mass. *The Astrophysical Journal*, 800(1):20, Feb 2015.

[139] G. Girelli, M. Bolzonella, and A. Cimatti. Massive and old quiescent galaxies at high redshift. *Astronomy & Astrophysics*, 632:A80, Dec. 2019.

[140] M. Gitti and S. Schindler. XMM-Newton observation of the most X-ray-luminous galaxy cluster RX J1347.5-1145. , 427:L9–L12, Nov 2004.

[141] M. D. Gladders and H. K. C. Yee. A New Method For Galaxy Cluster Detection. I. The Algorithm. *Astronomical Journal*, 120(4):2148–2162, Oct 2000.

[142] K. Glazebrook, C. Schreiber, I. Labbé, T. Nanayakkara, G. G. Kacprzak, P. A. Oesch, C. Papovich, L. R. Spitler, C. M. S. Straatman, K.-V. H. Tran, and T. Yuan. A massive, quiescent galaxy at a redshift of 3.717. *Nature*, 544(7648):71–74, Apr. 2017.

[143] C. Gómez-Guijarro, D. A. Riechers, R. Pavesi, G. E. Magdis, T. K. D. Leung, F. Valentino, S. Toft, M. Aravena, S. C. Chapman, D. L. Clements, H. Dannerbauer, S. J. Oliver, I. Pérez-Fournon, and I. Valtchanov. Confirming Herschel Candidate Protoclusters from ALMA/VLA CO Observations. *The Astrophysical Journal*, 872(2):117, Feb 2019.

[144] A. H. Gonzalez, M. Brodwin, M. J. I. Brown, A. Dey, M. Dickinson, D. Gettings, S. A. Stanford, D. Stern, J. Bock, S. Bussman, A. Cooray, P. R. M. Eisenhardt, B. Jannuzi, Y. T. Lin, A. Mainzer, and I. Sullivan. A NEWFIRM Survey of the Spitzer Deep Wide Field. In *American Astronomical Society Meeting Abstracts #216*, volume 216 of *American Astronomical Society Meeting Abstracts*, page 415.13, May 2010.

[145] J. E. González, C. G. Lacey, C. M. Baugh, and C. S. Frenk. The role of submillimetre galaxies in hierarchical galaxy formation. *Monthly Notices of the Royal Astronomical Society*, 413(2):749–762, May 2011.

[146] S. Gottlöber, A. Klypin, and A. V. Kravtsov. Merging History as a Function of Halo Environment. *The Astrophysical Journal*, 546(1):223–233, Jan 2001.

[147] A. D. Goulding, D. M. Alexander, F. E. Bauer, W. R. Forman, R. C. Hickox, C. Jones, J. R. Mullaney, and M. Trichas. Deep Silicate Absorption Features in Compton-thick Active Galactic Nuclei Predominantly Arise due to Dust in the Host Galaxy. *The Astrophysical Journal*, 755:5, Aug. 2012.

[148] G. L. Granato, C. G. Lacey, L. Silva, A. Bressan, C. M. Baugh, S. Cole, and C. S. Frenk. The Infrared Side of Galaxy Formation. I. The Local Universe in the Semianalytical Framework. *The Astrophysical Journal*, 542(2):710–730, Oct. 2000.

[149] A. Grazian, A. Fontana, P. Santini, J. S. Dunlop, H. C. Ferguson, M. Castellano, R. Amorin, M. L. N. Ashby, G. Barro, P. Behroozi, K. Boutsia, K. I. Caputi, R. R. Chary, A. Dekel, M. E. Dickinson, S. M. Faber, G. G. Fazio, S. L. Finkelstein, A. Galametz, E. Giallongo, M. Giavalisco, N. A. Grogin, Y. Guo, D. Kocevski, A. M. Koekemoer, D. C. Koo, K. S. Lee, Y. Lu, E. Merlin, B. Mobasher, M. Nonino, C. Papovich, D. Paris, L. Pentericci, N. Reddy, A. Renzini, B. Salmon, M. Salvato, V. Sommariva, M. Song, and E. Vanzella. The galaxy stellar mass function at $3.5 \leq z \leq 7.5$ in the CANDELS/UDS, GOODS-South, and HUDF fields. *Astronomy & Astrophysics*, 575:A96, Mar. 2015.

[150] M. J. Griffin, A. Abergel, A. Abreu, P. A. R. Ade, P. André, J.-L. Augueres, T. Babbedge, Y. Bae, T. Baillie, J.-P. Baluteau, M. J. Barlow, G. Bendo, D. Benielli, J. J. Bock, P. Bonhomme, D. Brisbin, C. Brockley-Blatt, M. Caldwell, C. Cara, N. Castro-Rodriguez, R. Cerulli, P. Chanial, S. Chen, E. Clark, D. L. Clements, L. Clerc, J. Coker, D. Communal, L. Conversi, P. Cox, D. Crumb, C. Cunningham, F. Daly, G. R. Davis, P. de Antoni, J. Delderfield, N. Devin, A. di Giorgio, I. Didschuns, K. Dohlen, M. Donati, A. Dowell, C. D. Dowell, L. Duband, L. Dumaye, R. J. Emery, M. Ferlet, D. Ferrand, J. Fontignie, M. Fox, A. Franceschini, M. Frerking, T. Fulton, J. Garcia, R. Gastaud, W. K. Gear, J. Glenn, A. Goizel, D. K. Griffin, T. Grundy, S. Guest, L. Guillemet, P. C. Hargrave, M. Harwit, P. Hastings, E. Hatziminaoglou, M. Herman, B. Hinde, V. Hristov, M. Huang, P. Imhof, K. J. Isaak, U. Israelsson, R. J. Ivison, D. Jennings, B. Kiernan, K. J. King, A. E. Lange, W. Latter, G. Laurent, P. Laurent, S. J. Leeks, E. Lellouch, L. Levenson, B. Li, J. Li, J. Lilienthal, T. Lim, S. J. Liu, N. Lu, S. Madden, G. Mainetti, P. Marliani, D. McKay, K. Mercier, S. Molinari, H. Morris, H. Moseley, J. Mulder, M. Mur, D. A. Naylor, H. Nguyen, B. O'Halloran, S. Oliver, G. Olofsson, H.-G. Olofsson, R. Orfei, M. J. Page, I. Pain, P. Panuzzo, A. Papageorgiou, G. Parks, P. Parr-Burman, A. Pearce, C. Pearson, I. Pérez-Fournon, F. Pinsard, G. Pisano, J. Podosek, M. Pohlen, E. T. Polehampton, D. Pouliquen, D. Rigopoulou, D. Rizzo, I. G. Roseboom, H. Roussel, M. Rowan-Robinson, B. Rownd, P. Saraceno, M. Sauvage, R. Savage, G. Savini, E. Sawyer, C. Scharmberg, D. Schmitt, N. Schneider, B. Schulz, A. Schwartz, R. Shafer, D. L. Shupe, B. Sibthorpe, S. Sidher, A. Smith, A. J. Smith, D. Smith, L. Spencer, B. Stobie, R. Sudiwala, K. Sukhatme, C. Surace, J. A. Stevens, B. M. Swinyard, M. Trichas, T. Tourette, H. Triou, S. Tseng, C. Tucker, A. Turner, M. Vaccari, I. Valtchanov, L. Vigroux, E. Virique, G. Voellmer, H. Walker, R. Ward, T. Waskett, M. Weilert, R. Wesson, G. J. White, N. Whitehouse, C. D. Wilson, B. Winter, A. L. Woodcraft, G. S. Wright, C. K. Xu, A. Zavagno, M. Zemcov, L. Zhang, and E. Zonca. The Herschel-SPIRE instrument and its in-flight performance. *A&A*, 518:L3, July 2010.

[151] C. Gruppioni, M. Béthermin, F. Loiacono, O. Le Fèvre, P. Capak, P. Cassata, A. L. Faisst, D. Schaerer, J. Silverman, L. Yan, S. Bardelli, M. Boquien, R. Carraro, A. Cimatti, M. Dessauges-Zavadsky, M. Ginolfi, S. Fujimoto, N. P. Hathi, G. C. Jones, Y. Khusanova, A. M. Koekemoer, G. Lagache, B. C. Lemaux, P. A. Oesch, F. Pozzi, D. A. Riechers, G. Rodighiero, M. Romano, M. Talia, L. Vallini, D. Vergani, G. Zamorani, and E. Zucca.

The ALPINE-ALMA [CII] survey. The nature, luminosity function, and star formation history of dusty galaxies up to z 6. *Astronomy & Astrophysics*, 643:A8, Nov. 2020.

[152] C. Gruppioni, F. Pozzi, G. Rodighiero, I. Delvecchio, S. Berta, L. Pozzetti, G. Zamorani, P. Andreani, A. Cimatti, O. Ilbert, E. Le Floc'h, D. Lutz, B. Magnelli, L. Marchetti, P. Monaco, R. Nordon, S. Oliver, P. Popesso, L. Riguccini, I. Roseboom, D. J. Rosario, M. Sargent, M. Vaccari, B. Altieri, H. Aussel, A. Bongiovanni, J. Cepa, E. Daddi, H. Domínguez-Sánchez, D. Elbaz, N. Förster Schreiber, R. Genzel, A. Iribarrem, M. Magliocchetti, R. Maiolino, A. Poglitsch, A. Pérez García, M. Sanchez-Portal, E. Sturm, L. Tacconi, I. Valtchanov, A. Amblard, V. Arumugam, M. Bethermin, J. Bock, A. Boselli, V. Buat, D. Burgarella, N. Castro-Rodríguez, A. Cava, P. Chanial, D. L. Clements, A. Conley, A. Cooray, C. D. Dowell, E. Dwek, S. Eales, A. Franceschini, J. Glenn, M. Griffin, E. Hatziminaoglou, E. Ibar, K. Isaak, R. J. Ivison, G. Lagache, L. Levenson, N. Lu, S. Madden, B. Maffei, G. Mainetti, H. T. Nguyen, B. O'Halloran, M. J. Page, P. Panuzzo, A. Papageorgiou, C. P. Pearson, I. Pérez-Fournon, M. Pohlen, D. Rigopoulou, M. Rowan-Robinson, B. Schulz, D. Scott, N. Seymour, D. L. Shupe, A. J. Smith, J. A. Stevens, M. Symeonidis, M. Trichas, K. E. Tugwell, L. Vigroux, L. Wang, G. Wright, C. K. Xu, M. Zemcov, S. Bardelli, M. Carollo, T. Contini, O. Le Févre, S. Lilly, V. Mainieri, A. Renzini, M. Scodeggio, and E. Zucca. The Herschel PEP/HerMES luminosity function - I. Probing the evolution of PACS selected Galaxies to z 4. *Monthly Notices of the Royal Astronomical Society*, 432(1):23–52, June 2013.

[153] K. Gültekin, D. O. Richstone, K. Gebhardt, T. R. Lauer, S. Tremaine, M. C. Aller, R. Bender, A. Dressler, S. M. Faber, A. V. Filippenko, R. Green, L. C. Ho, J. Kormendy, J. Magorrian, J. Pinkney, and C. Siopis. The M-σ and M-L Relations in Galactic Bulges, and Determinations of Their Intrinsic Scatter. *The Astrophysical Journal*, 698:198–221, June 2009.

[154] Q. Guo and S. D. M. White. Galaxy growth in the concordance ΛCDM cosmology. *Monthly Notices of the Royal Astronomical Society*, 384(1):2–10, Feb 2008.

[155] F. Haardt and L. Maraschi. A two-phase model for the X-ray emission from Seyfert galaxies. *The Astrophysical Journall*, 380:L51–L54, Oct. 1991.

[156] M. Haas, U. Klaas, S. A. H. Müller, F. Bertoldi, M. Camenzind, R. Chini, O. Krause, D. Lemke, K. Meisenheimer, P. J. Richards, and B. J. Wilkes. The ISO view of Palomar-Green quasars. *Astronomy & Astrophysics*, 402:87–111, Apr. 2003.

[157] L. J. Hainline, A. W. Blain, I. Smail, D. M. Alexand er, L. Armus, S. C. Chapman, and R. J. Ivison. The Stellar Mass Content of Submillimeter-selected Galaxies. *The Astrophysical Journal*, 740(2):96, Oct 2011.

[158] L. J. Hainline, A. W. Blain, I. Smail, D. T. Frayer, S. C. Chapman, R. J. Ivison, and D. M. Alexand er. A Mid-Infrared Imaging Survey of Submillimeter-Selected Galaxies with the Spitzer Space Telescope. *The Astrophysical Journal*, 699(2):1610–1632, Jul 2009.

[159] K. R. Hall, D. Crichton, T. Marriage, N. L. Zakamska, and R. Mandelbaum. Downsizing of star formation measured from the clustered infrared background correlated with quasars. *Monthly Notices of the Royal Astronomical Society*, 480(1):149–181, Oct. 2018.

[160] Y. Harikane, M. Ouchi, Y. Ono, S. Fujimoto, D. Donevski, T. Shibuya, A. L. Faisst, T. Goto, B. Hatsukade, N. Kashikawa, K. Kohno, T. Hashimoto, R. Higuchi, A. K. Inoue, Y.-T. Lin, C. L. Martin, R. Overzier, I. Smail, J. Toshikawa, H. Umehata, Y. Ao, S. Chapman, D. L. Clements, M. Im, Y. Jing, T. Kawaguchi, C.-H. Lee, M. M. Lee, L. Lin, Y. Matsuoka, M. Marinello, T. Nagao, M. Onodera, S. Toft, and W.-H. Wang. SILVERRUSH. VIII. Spectroscopic Identifications of Early Large-scale Structures with Protoclusters over 200 Mpc at z $\sim$ 67: Strong Associations of Dusty Star-forming Galaxies. *The Astrophysical Journal*, 883(2):142, Oct 2019.

[161] C. M. Harrison, D. M. Alexander, J. R. Mullaney, and A. M. Swinbank. Kiloparsec-scale outflows are prevalent among luminous AGN: outflows and feedback in the context of the overall AGN population. *Monthly Notices of the Royal Astronomical Society*, 441:3306–3347, July 2014.

[162] I. Harrison and P. Coles. Testing cosmology with extreme galaxy clusters. *Monthly Notices of the Royal Astronomical Society*, 421(1):L19–L23, Mar 2012.

[163] I. Harrison and S. Hotchkiss. A consistent approach to falsifying ΛCDM with rare galaxy clusters. , 2013(7):022, Jul 2013.

[164] C. C. Hayward, P. Jonsson, D. Kereš, B. Magnelli, L. Hernquist, and T. J. Cox. How to distinguish starbursts and quiescently star-forming galaxies: the 'bimodal' submillimetre galaxy population as a case study. *Monthly Notices of the Royal Astronomical Society*, 424(2):951–970, Aug 2012.

[165] C. C. Hayward, D. Kereš, P. Jonsson, D. Narayanan, T. J. Cox, and L. Hernquist. What Does a Submillimeter Galaxy Selection Actually Select? The Dependence of Submillimeter Flux Density on Star Formation Rate and Dust Mass. *The Astrophysical Journal*, 743(2):159, Dec 2011.

[166] C. C. Hayward, D. Narayanan, D. Kereš, P. Jonsson, P. F. Hopkins, T. J. Cox, and L. Hernquist. Submillimetre galaxies in a hierarchical universe: number counts, redshift distribution and implications for the IMF. *Monthly Notices of the Royal Astronomical Society*, 428(3):2529–2547, Jan 2013.

[167] C. C. Hayward, M. Sparre, S. C. Chapman, L. Hernquist, D. Nelson, R. Pakmor, A. Pillepich, V. Springel, P. Torrey, M. Vogelsberger, and R. Weinberger. Submillimetre galaxies in cosmological hydrodynamical simulations - an opportunity for constraining feedback models. *Monthly Notices of the Royal Astronomical Society*, 502(2):2922–2933, Apr. 2021.

[168] B. Henriques, C. Maraston, P. Monaco, F. Fontanot, N. Menci, G. De Lucia, and C. Tonini. The effect of thermally pulsating asymptotic giant branch stars on the evolution of the rest-frame near-infrared galaxy luminosity function. *Monthly Notices of the Royal Astronomical Society*, 415(4):3571–3579, Aug 2011.

[169] R. C. Hickox, C. Jones, W. R. Forman, S. S. Murray, M. Brodwin, M. J. I. Brown, P. R. Eisenhardt, D. Stern, C. S. Kochanek, D. Eisenstein, R. J. Cool, B. T. Jannuzi, A. Dey, K. Brand, V. Gorjian, and N. Caldwell. A Large Population of Mid-Infrared-selected, Obscured Active Galaxies in the Boötes Field. *The Astrophysical Journal*, 671:1365–1387, Dec. 2007.

[170] R. C. Hickox, C. Jones, W. R. Forman, S. S. Murray, C. S. Kochanek, D. Eisenstein, B. T. Jannuzi, A. Dey, M. J. I. Brown, D. Stern, P. R. Eisenhardt, V. Gorjian, M. Brodwin, R. Narayan, R. J. Cool, A. Kenter, N. Caldwell, and M. E. Anderson. Host Galaxies, Clustering, Eddington Ratios, and Evolution of Radio, X-Ray, and Infrared-Selected AGNs. *The Astrophysical Journal*, 696:891–919, May 2009.

[171] R. C. Hickox, J. R. Mullaney, D. M. Alexander, C.-T. J. Chen, F. M. Civano, A. D. Goulding, and K. N. Hainline. Black Hole Variability and the Star Formation-Active Galactic Nucleus Connection: Do All Star-forming Galaxies Host an Active Galactic Nucleus? *ApJ*, 782:9, Feb. 2014.

[172] R. C. Hickox, J. L. Wardlow, I. Smail, A. D. Myers, D. M. Alexander, A. M. Swinbank, A. L. R. Danielson, J. P. Stott, S. C. Chapman, K. E. K. Coppin, J. S. Dunlop, E. Gawiser, D. Lutz, P. van der Werf, and A. Weiß. The LABOCA survey of the Extended Chandra Deep Field-South: clustering of submillimetre galaxies. *Monthly Notices of the Royal Astronomical Society*, 421(1):284–295, Mar 2012.

[173] R. Higuchi, M. Ouchi, Y. Ono, T. Shibuya, J. Toshikawa, Y. Harikane, T. Kojima, Y.-K. Chiang, E. Egami, N. Kashikawa, R. Overzier, A. Konno, A. K. Inoue, K. Hasegawa, S. Fujimoto, T. Goto, S. Ishikawa, K. Ito, Y. Komiyama, and M. Tanaka. SILVERRUSH. VII. Subaru/HSC Identifications of Protocluster Candidates at z $\sim$ 67: Implications for Cosmic Reionization. *The Astrophysical Journal*, 879(1):28, Jul 2019.

[174] R. Hill, S. Chapman, D. Scott, Y. Apostolovski, M. Aravena, M. Bethermin, C. M. Bradford, C. de Breuck, R. E. A. Canning, C. Dong, A. Gonzalez, T. R. Greve, C. C. Hayward, Y. Hezaveh, K. Litke, M. Malkan, D. P. Marrone, K. Phadke, C. Reuter, J. Spilker, J. D. Vieira, and A. Weiss. An extended proto-cluster of galaxies surrounding SPT2349−56 at $z = 4.3$. *arXiv e-prints*, page arXiv:2002.11600, Feb. 2020.

[175] N. K. Hine, J. E. Geach, D. M. Alexander, B. D. Lehmer, S. C. Chapman, and Y. Matsuda. An enhanced merger fraction within the galaxy population of the SSA22 protocluster at z = 3.1. *Monthly Notices of the Royal Astronomical Society*, 455(3):2363–2370, Jan 2016.

[176] L. C. Ho. Nuclear Activity in Nearby Galaxies. *Annual Review of Astronomy & Astrophysics*, 46:475–539, Sept. 2008.

[177] J. A. Hodge, C. L. Carilli, F. Walter, E. Daddi, and D. Riechers. High-resolution Spectroscopic Imaging of CO in a z = 4.05 Proto-cluster. *The Astrophysical Journal*, 776(1):22, Oct 2013.

[178] J. A. Hodge, A. M. Swinbank, J. M. Simpson, I. Smail, F. Walter, D. M. Alexander, F. Bertoldi, A. D. Biggs, W. N. Brandt, S. C. Chapman, C. C. Chen, K. E. K. Coppin, P. Cox,

H. Dannerbauer, A. C. Edge, T. R. Greve, R. J. Ivison, A. Karim, K. K. Knudsen, K. M. Menten, H. W. Rix, E. Schinnerer, J. L. Wardlow, A. Weiss, and P. van der Werf. Kiloparsec-scale Dust Disks in High-redshift Luminous Submillimeter Galaxies. *The Astrophysical Journal*, 833(1):103, Dec 2016.

[179] P. F. Hopkins, C. C. Hayward, D. Narayanan, and L. Hernquist. The origins of active galactic nuclei obscuration: the 'torus' as a dynamical, unstable driver of accretion. *Monthly Notices of the Royal Astronomical Society*, 420:320–339, Feb. 2012.

[180] P. F. Hopkins and L. Hernquist. A Characteristic Division Between the Fueling of Quasars and Seyferts: Five Simple Tests. *The Astrophysical Journal*, 694:599–609, Mar. 2009.

[181] P. F. Hopkins, L. Hernquist, T. J. Cox, T. Di Matteo, B. Robertson, and V. Springel. A Unified, Merger-driven Model of the Origin of Starbursts, Quasars, the Cosmic X-Ray Background, Supermassive Black Holes, and Galaxy Spheroids. *The Astrophysical Journals*, 163:1–49, Mar. 2006.

[182] P. F. Hopkins, J. D. Younger, C. C. Hayward, D. Narayanan, and L. Hernquist. Mergers, active galactic nuclei and 'normal' galaxies: contributions to the distribution of star formation rates and infrared luminosity functions. *Monthly Notices of the Royal Astronomical Society*, 402(3):1693–1713, Mar. 2010.

[183] P. F. Hopkins, J. D. Younger, C. C. Hayward, D. Narayanan, and L. Hernquist. Mergers, active galactic nuclei and 'normal' galaxies: contributions to the distribution of star formation rates and infrared luminosity functions. *Monthly Notices of the Royal Astronomical Society*, 402(3):1693–1713, Mar 2010.

[184] C.-L. Hung, C. M. Casey, Y.-K. Chiang, P. L. Capak, M. J. Cowley, B. Darvish, G. G. Kacprzak, K. Kovač, S. J. Lilly, T. Nanayakkara, L. R. Spitler, K.-V. H. Tran, and T. Yuan. Large-scale Structure around a z=2.1 Cluster. *The Astrophysical Journal*, 826(2):130, Aug 2016.

[185] P. D. Hurley, S. Oliver, M. Betancourt, C. Clarke, W. I. Cowley, S. Duivenvoorden, D. Farrah, M. Griffin, C. Lacey, E. Le Floc'h, A. Papadopoulos, M. Sargent, J. M. Scudder, M. Vaccari, I. Valtchanov, and L. Wang. HELP: XID+, the probabilistic de-blender for Herschel SPIRE maps. *Monthly Notices of the Royal Astronomical Society*, 464(1):885–896, Jan 2017.

[186] H. S. Hwang, D. Elbaz, G. Magdis, E. Daddi, M. Symeonidis, B. Altieri, A. Amblard, P. Andreani, V. Arumugam, R. Auld, H. Aussel, T. Babbedge, S. Berta, A. Blain, J. Bock, A. Bongiovanni, A. Boselli, V. Buat, D. Burgarella, N. Castro-Rodríguez, A. Cava, J. Cepa, P. Chanial, E. Chapin, R. R. Chary, A. Cimatti, D. L. Clements, A. Conley, L. Conversi, A. Cooray, H. Dannerbauer, M. Dickinson, H. Dominguez, C. D. Dowell, J. S. Dunlop, E. Dwek, S. Eales, D. Farrah, N. F. Schreiber, M. Fox, A. Franceschini, W. Gear, R. Genzel, J. Glenn, M. Griffin, C. Gruppioni, M. Halpern, E. Hatziminaoglou, E. Ibar, K. Isaak, R. J. Ivison, W. S. Jeong, G. Lagache, D. Le Borgne, E. Le Floc'h, H. M. Lee, J. C. Lee, M. G. Lee, L. Levenson, N. Lu, D. Lutz, S. Madden, B. Maffei, B. Magnelli, G. Mainetti, R. Maiolino, L. Marchetti, A. M. J. Mortier, H. T. Nguyen, R. Nordon, B. O'Halloran, K. Okumura, S. J.

Oliver, A. Omont, M. J. Page, P. Panuzzo, A. Papageorgiou, C. P. Pearson, I. Pérez-Fournon, A. M. P. García, A. Poglitsch, M. Pohlen, P. Popesso, F. Pozzi, J. I. Rawlings, D. Rigopoulou, L. Riguccini, D. Rizzo, G. Rodighiero, I. G. Roseboom, M. Rowan-Robinson, A. Saintonge, M. S. Portal, P. Santini, M. Sauvage, B. Schulz, D. Scott, N. Seymour, L. Shao, D. L. Shupe, A. J. Smith, J. A. Stevens, E. Sturm, L. Tacconi, M. Trichas, K. E. Tugwell, M. Vaccari, I. Valtchanov, J. D. Vieira, L. Vigroux, L. Wang, R. Ward, G. Wright, C. K. Xu, and M. Zemcov. Evolution of dust temperature of galaxies through cosmic time as seen by Herschel. *Monthly Notices of the Royal Astronomical Society*, 409(1):75–82, Nov 2010.

[187] Y.-H. Hwang, W.-H. Wang, Y.-Y. Chang, C.-F. Lim, C.-C. Chen, Z.-K. Gao, J. S. Dunlop, Y. Gao, L. C. Ho, H. S. Hwang, M. Koprowski, M. J. Michałowski, Y.-j. Peng, H. Shim, J. M. Simpson, and Y. Toba. Revisiting the Color-Color Selection: Submillimeter and AGN Properties of NUV-r-J Selected Quiescent Galaxies. *The Astrophysical Journal*, 913(1):6, May 2021.

[188] E. Ibar, R. J. Ivison, P. N. Best, K. Coppin, A. Pope, I. Smail, and J. S. Dunlop. Deep multi-frequency radio imaging in the Lockman Hole - II. The spectral index of submillimetre galaxies. *Monthly Notices of the Royal Astronomical Society*, 401(1):L53–L57, Jan 2010.

[189] O. Ilbert, H. J. McCracken, O. Le Fèvre, P. Capak, J. Dunlop, A. Karim, M. A. Renzini, K. Caputi, S. Boissier, S. Arnouts, H. Aussel, J. Comparat, Q. Guo, P. Hudelot, J. Kartaltepe, J. P. Kneib, J. K. Krogager, E. Le Floc'h, S. Lilly, Y. Mellier, B. Milvang-Jensen, T. Moutard, M. Onodera, J. Richard, M. Salvato, D. B. Sanders, N. Scoville, J. D. Silverman, Y. Taniguchi, L. Tasca, R. Thomas, S. Toft, L. Tresse, D. Vergani, M. Wolk, and A. Zirm. Mass assembly in quiescent and star-forming galaxies since z 4 from UltraVISTA. *Astronomy and Astrophysics*, 556:A55, Aug 2013.

[190] K. Ito, N. Kashikawa, J. Toshikawa, R. Overzier, M. Tanaka, M. Kubo, T. Shibuya, S. Ishikawa, M. Onoue, H. Uchiyama, Y. Liang, R. Higuchi, C. L. Martin, C.-H. Lee, Y. Komiyama, and S. Huang. The Brightest UV-selected Galaxies in Protoclusters at z 4: Ancestors of Brightest Cluster Galaxies? *The Astrophysical Journal*, 878(1):68, Jun 2019.

[191] R. J. Ivison, A. J. R. Lewis, A. Weiss, V. Arumugam, J. M. Simpson, W. S. Holland, S. Maddox, L. Dunne, E. Valiante, P. van der Werf, A. Omont, H. Dannerbauer, I. Smail, F. Bertoldi, M. Bremer, R. S. Bussmann, Z. Y. Cai, D. L. Clements, A. Cooray, G. De Zotti, S. A. Eales, C. Fuller, J. Gonzalez-Nuevo, E. Ibar, M. Negrello, I. Oteo, I. Pérez-Fournon, D. Riechers, J. A. Stevens, A. M. Swinbank, and J. Wardlow. The Space Density of Luminous Dusty Star-forming Galaxies at z > 4: SCUBA-2 and LABOCA Imaging of Ultrared Galaxies from Herschel-ATLAS. *The Astrophysical Journal*, 832:78, Nov. 2016.

[192] B. T. Jannuzi and A. Dey. The NOAO Deep Wide-Field Survey. In R. Weymann, L. Storrie-Lombardi, M. Sawicki, and R. Brunner, editors, *Photometric Redshifts and the Detection of High Redshift Galaxies*, volume 191 of *Astronomical Society of the Pacific Conference Series*, page 111, 1999.

[193] R. Johnston, M. Vaccari, M. Jarvis, M. Smith, E. Giovannoli, B. Häußler, and M. Prescott. The evolving relation between star formation rate and stellar mass in the VIDEO survey

since z = 3. *Monthly Notices of the Royal Astronomical Society*, 453(3):2540–2557, Nov. 2015.

[194] S. G. Jorstad, A. P. Marscher, M. L. Lister, A. M. Stirling, T. V. Cawthorne, W. K. Gear, J. L. Gómez, J. A. Stevens, P. S. Smith, J. R. Forster, and E. I. Robson. Polarimetric Observations of 15 Active Galactic Nuclei at High Frequencies: Jet Kinematics from Bimonthly Monitoring with the Very Long Baseline Array. *Astronomical Journal*, 130:1418–1465, Oct. 2005.

[195] S. Juneau, M. Dickinson, F. Bournaud, D. M. Alexander, E. Daddi, J. R. Mullaney, B. Magnelli, J. S. Kartaltepe, H. S. Hwang, S. P. Willner, A. L. Coil, D. J. Rosario, J. R. Trump, B. J. Weiner, C. N. A. Willmer, M. C. Cooper, D. Elbaz, S. M. Faber, D. T. Frayer, D. D. Kocevski, E. S. Laird, J. A. Monkiewicz, K. Nandra, J. A. Newman, S. Salim, and M. Symeonidis. Widespread and Hidden Active Galactic Nuclei in Star-forming Galaxies at Redshift >0.3. *The Astrophysical Journal*, 764(2):176, Feb. 2013.

[196] J. S. Kartaltepe, D. B. Sanders, E. Le Floc'h, D. T. Frayer, H. Aussel, S. Arnouts, O. Ilbert, M. Salvato, N. Z. Scoville, J. Surace, L. Yan, M. Brusa, P. Capak, K. Caputi, C. M. Carollo, F. Civano, M. Elvis, C. Faure, G. Hasinger, A. M. Koekemoer, N. Lee, S. Lilly, C. T. Liu, H. J. McCracken, E. Schinnerer, V. Smolčić, Y. Taniguchi, D. J. Thompson, and J. Trump. A Multiwavelength Study of a Sample of 70 μm Selected Galaxies in the COSMOS Field. I. Spectral Energy Distributions and Luminosities. *The Astrophysical Journal*, 709(2):572–596, Feb. 2010.

[197] G. Kauffmann and M. Haehnelt. A unified model for the evolution of galaxies and quasars. *Monthly Notices of the Royal Astronomical Society*, 311:576–588, Jan. 2000.

[198] R. C. Kennicutt and N. J. Evans. Star Formation in the Milky Way and Nearby Galaxies. *Annual Review of Astronomy & Astrophysics*, 50:531–608, Sept. 2012.

[199] A. Kirkpatrick, A. Pope, D. M. Alexander, V. Charmandaris, E. Daddi, M. Dickinson, D. Elbaz, J. Gabor, H. S. Hwang, R. Ivison, J. Mullaney, M. Pannella, D. Scott, B. Altieri, H. Aussel, F. Bournaud, V. Buat, D. Coia, H. Dannerbauer, K. Dasyra, J. Kartaltepe, R. Leiton, L. Lin, G. Magdis, B. Magnelli, G. Morrison, P. Popesso, and I. Valtchanov.

[200] A. Kirkpatrick, A. Pope, A. Sajina, E. Roebuck, L. Yan, L. Armus, T. Díaz-Santos, and S. Stierwalt. The Role of Star Formation and an AGN in Dust Heating of z = 0.3-2.8 Galaxies. I. Evolution with Redshift and Luminosity. *The Astrophysical Journal*, 814(1):9, Nov. 2015.

[201] C. S. Kochanek, D. J. Eisenstein, R. J. Cool, N. Caldwell, R. J. Assef, B. T. Jannuzi, C. Jones, S. S. Murray, W. R. Forman, A. Dey, M. J. I. Brown, P. Eisenhardt, A. H. Gonzalez, P. Green, and D. Stern. AGES: The AGN and Galaxy Evolution Survey. *ApJS*, 200:8, May 2012.

[202] M. P. Koprowski, J. S. Dunlop, M. J. Michałowski, K. E. K. Coppin, J. E. Geach, R. J. McLure, D. Scott, and P. P. van der Werf. The evolving far-IR galaxy luminosity function and dust-obscured star formation rate density out to z5. *Monthly Notices of the Royal Astronomical Society*, 471(4):4155–4169, Nov. 2017.

[203] J. Kormendy and L. C. Ho. Coevolution (Or Not) of Supermassive Black Holes and Host Galaxies. *Annual Review of A&A*, 51:511–653, Aug. 2013.

[204] J. Kormendy and D. Richstone. Inward Bound—The Search For Supermassive Black Holes In Galactic Nuclei. *Annual Review of Astronomy & Astrophysics*, 33:581, 1995.

[205] Y. Koyama, I. Smail, J. Kurk, J. E. Geach, D. Sobral, T. Kodama, F. Nakata, A. M. Swinbank, P. N. Best, M. Hayashi, and K.-i. Tadaki. On the evolution and environmental dependence of the star formation rate versus stellar mass relation since z 2. *Monthly Notices of the Royal Astronomical Society*, 434(1):423–436, Sep 2013.

[206] E. Kuiper, N. A. Hatch, G. K. Miley, N. P. H. Nesvadba, H. J. A. Röttgering, J. D. Kurk, M. D. Lehnert, R. A. Overzier, L. Pentericci, J. Schaye, and B. P. Venemans. A SINFONI view of flies in the Spiderweb: a galaxy cluster in the making. , 415(3):2245–2256, Aug 2011.

[207] P. Kurczynski, E. Gawiser, V. Acquaviva, E. F. Bell, A. Dekel, D. F. de Mello, H. C. Ferguson, J. P. Gardner, N. A. Grogin, Y. Guo, P. F. Hopkins, A. M. Koekemoer, D. C. Koo, S.-K. Lee, B. Mobasher, J. R. Primack, M. Rafelski, E. Soto, and H. I. Teplitz. Evolution of Intrinsic Scatter in the SFR-Stellar Mass Correlation at 0.5 < z < 3. *The Astrophysical Journall*, 820(1):L1, Mar. 2016.

[208] J. D. Kurk, H. J. A. Röttgering, L. Pentericci, G. K. Miley, W. van Breugel, C. L. Carilli, H. Ford, T. Heckman, P. McCarthy, and A. Moorwood. A Search for clusters at high redshift. I. Candidate Lyalpha emitters near 1138-262 at z=2.2. , 358:L1–L4, Jun 2000.

[209] K. M. Lacaille, S. C. Chapman, I. Smail, C. C. Steidel, A. W. Blain, J. Geach, A. Golob, M. Gurwell, R. J. Ivison, N. Reddy, and M. Sawicki. Two sub-millimetre bright proto-clusters bounding the epoch of peak star-formation activity. *Monthly Notices of the Royal Astronomical Society*, 488(2):1790–1812, Sep 2019.

[210] C. d. P. Lagos, E. da Cunha, A. S. G. Robotham, D. Obreschkow, F. Valentino, S. Fujimoto, G. E. Magdis, and R. Tobar. Physical properties and evolution of (sub-)millimetre-selected galaxies in the galaxy formation simulation SHARK. *Monthly Notices of the Royal Astronomical Society*, 499(2):1948–1971, Dec. 2020.

[211] E. L. Lambrides, M. Chiaberge, T. Heckman, R. Gilli, F. Vito, and C. Norman. A Large Population of Obscured AGN in Disguise as Low-luminosity AGN in Chandra Deep Field South. *The Astrophysical Journal*, 897(2):160, July 2020.

[212] G. Lanzuisi, I. Delvecchio, S. Berta, M. Brusa, A. Comastri, R. Gilli, C. Gruppioni, S. Marchesi, M. Perna, F. Pozzi, M. Salvato, M. Symeonidis, C. Vignali, F. Vito, M. Volonteri, and G. Zamorani. AGN vs. host galaxy properties in the COSMOS field. *ArXiv e-prints*, Feb. 2017.

[213] G. Lanzuisi, E. Piconcelli, F. Fiore, C. Feruglio, C. Vignali, M. Salvato, and C. Gruppioni. Revealing X-ray obscured quasars in SWIRE sources with extreme mid-IR/optical flux ratios. *Astronomy & Astrophysics*, 498:67–81, Apr. 2009.

[214] G. Lanzuisi, P. Ranalli, I. Georgantopoulos, A. Georgakakis, I. Delvecchio, T. Akylas, S. Berta, A. Bongiorno, M. Brusa, N. Cappelluti, F. Civano, A. Comastri, R. Gilli, C. Gruppioni, G. Hasinger, K. Iwasawa, A. Koekemoer, E. Lusso, S. Marchesi, V. Mainieri, A. Merloni, M. Mignoli, E. Piconcelli, F. Pozzi, D. J. Rosario, M. Salvato, J. Silverman, B. Trakhtenbrot, C. Vignali, and G. Zamorani. Compton thick AGN in the XMM-COSMOS survey. *Astronomy & Astrophysics*, 573:A137, Jan. 2015.

[215] A. Lapi, S. Raimundo, R. Aversa, Z.-Y. Cai, M. Negrello, A. Celotti, G. De Zotti, and L. Danese. The Coevolution of Supermassive Black Holes and Massive Galaxies at High Redshift. *ApJ*, 782:69, Feb. 2014.

[216] A. Lawrence. The relative frequency of broad-lined and narrow-lined active galactic nuclei - Implications for unified schemes. *Monthly Notices of the Royal Astronomical Society*, 252:586–592, Oct. 1991.

[217] A. Lawrence and M. Elvis. Misaligned Discs as Obscurers in Active Galaxies. *ArXiv e-prints*, Feb. 2010.

[218] M. M. Lee, I. Tanaka, R. Kawabe, K. Kohno, T. Kodama, M. Kajisawa, M. S. Yun, K. Nakanishi, D. Iono, Y. Tamura, B. Hatsukade, H. Umehata, T. Saito, T. Izumi, I. Aretxaga, K.-i. Tadaki, M. Zeballos, S. Ikarashi, G. W. Wilson, D. H. Hughes, and R. J. Ivison. A Radio-to-mm Census of Star-forming Galaxies in Protocluster 4C23.56 at Z = 2.5: Gas Mass and Its Fraction Revealed with ALMA. *The Astrophysical Journal*, 842(1):55, Jun 2017.

[219] N. Lee, D. B. Sanders, C. M. Casey, N. Z. Scoville, C.-L. Hung, E. Le Floc'h, O. Ilbert, H. Aussel, P. Capak, J. S. Kartaltepe, I. Roseboom, M. Salvato, M. Aravena, S. Berta, J. Bock, S. J. Oliver, L. Riguccini, and M. Symeonidis. Multi-wavelength SEDs of Herschel-selected Galaxies in the COSMOS Field. *The Astrophysical Journal*, 778(2):131, Dec. 2013.

[220] N. Lee, D. B. Sanders, C. M. Casey, S. Toft, N. Z. Scoville, C.-L. Hung, E. Le Floc'h, O. Ilbert, H. J. Zahid, H. Aussel, P. Capak, J. S. Kartaltepe, L. J. Kewley, Y. Li, K. Schawinski, K. Sheth, and Q. Xiao. A Turnover in the Galaxy Main Sequence of Star Formation at M $_*$ $\sim 10^{10}$ M for Redshifts z < 1.3. *The Astrophysical Journal*, 801(2):80, Mar. 2015.

[221] B. D. Lehmer, D. M. Alexander, S. C. Chapman, I. Smail, F. E. Bauer, W. N. Brandt, J. E. Geach, Y. Matsuda, J. R. Mullaney, and A. M. Swinbank. The Chandra Deep Protocluster Survey: point-source catalogues for a 400-ks observation of the z = 3.09 protocluster in SSA22. , 400(1):299–316, Nov 2009.

[222] B. C. Lemaux, O. Le Fèvre, O. Cucciati, B. Ribeiro, L. A. M. Tasca, G. Zamorani, O. Ilbert, R. Thomas, S. Bardelli, P. Cassata, N. P. Hathi, J. Pforr, V. Smolčić, I. Delvecchio, M. Novak, S. Berta, H. J. McCracken, A. Koekemoer, R. Amorín, B. Garilli, D. Maccagni, D. Schaerer, and E. Zucca. The VIMOS Ultra-Deep Survey: Emerging from the dark, a massive protocluster at z 4.57. *Astronomy & Astrophysics*, 615:A77, Jul 2018.

[223] B. C. Lemaux, E. Le Floc'h, O. Le Fèvre, O. Ilbert, L. Tresse, L. M. Lubin, G. Zamorani, R. R. Gal, P. Ciliegi, P. Cassata, D. D. Kocevski, E. J. McGrath, S. Bardelli, E. Zucca, and G. K. Squires. Hidden starbursts and active galactic nuclei at 0 < z < 4 from the

Herschel-VVDS-CFHTLS-D1 field: Inferences on coevolution and feedback. *Astronomy & Astrophysics*, 572:A90, Dec. 2014.

[224] B. C. Lemaux, A. R. Tomczak, L. M. Lubin, R. R. Gal, L. Shen, D. Pelliccia, P. F. Wu, D. Hung, S. Mei, O. Le Fèvre, N. Rumbaugh, D. D. Kocevski, and G. K. Squires. Persistence of the colour-density relation and efficient environmental quenching to z 1.4. *Monthly Notices of the Royal Astronomical Society*, 490(1):1231–1254, Nov 2019.

[225] A. K. Leroy, K. M. Sandstrom, D. Lang, A. Lewis, S. Salim, E. A. Behrens, J. Chastenet, I.-D. Chiang, M. J. Gallagher, S. Kessler, and D. Utomo. A z = 0 Multiwavelength Galaxy Synthesis. I. A WISE and GALEX Atlas of Local Galaxies. *The Astrophysical Journals*, 244(2):24, Oct. 2019.

[226] S. K. Leslie, E. Schinnerer, D. Liu, B. Magnelli, H. Algera, A. Karim, I. Davidzon, G. Gozaliasl, E. F. Jiménez-Andrade, P. Lang, M. T. Sargent, M. Novak, B. Groves, V. Smolčić, G. Zamorani, M. Vaccari, A. Battisti, E. Vardoulaki, Y. Peng, and J. Kartaltepe. The VLA-COSMOS 3 GHz Large Project: Evolution of Specific Star Formation Rates out to z ~ 5. *The Astrophysical Journal*, 899(1):58, Aug. 2020.

[227] G. C. K. Leung, A. L. Coil, M. Azadi, J. Aird, A. Shapley, M. Kriek, B. Mobasher, N. Reddy, B. Siana, W. R. Freeman, S. H. Price, R. L. Sanders, and I. Shivaei. The MOSDEF Survey: The Prevalence and Properties of Galaxy-wide AGN-driven Outflows at z∼2. *The Astrophysical Journal*, 849:48, Nov. 2017.

[228] A. J. R. Lewis, R. J. Ivison, P. N. Best, J. M. Simpson, A. Weiss, I. Oteo, Z. Y. Zhang, V. Arumugam, M. N. Bremer, S. C. Chapman, D. L. Clements, H. Dannerbauer, L. Dunne, S. Eales, S. Maddox, S. J. Oliver, A. Omont, D. A. Riechers, S. Serjeant, E. Valiante, J. Wardlow, P. van der Werf, and G. De Zotti. Ultra-red Galaxies Signpost Candidate Protoclusters at High Redshift. *The Astrophysical Journal*, 862:96, Aug. 2018.

[229] I. Lewis, M. Balogh, R. De Propris, W. Couch, R. Bower, A. Offer, J. Bland -Hawthorn, I. K. Baldry, C. Baugh, T. Bridges, R. Cannon, S. Cole, M. Colless, C. Collins, N. Cross, G. Dalton, S. P. Driver, G. Efstathiou, R. S. Ellis, C. S. Frenk, K. Glazebrook, E. Hawkins, C. Jackson, O. Lahav, S. Lumsden, S. Maddox, D. Madgwick, P. Norberg, J. A. Peacock, W. Percival, B. A. Peterson, W. Sutherland, and K. Taylor. The 2dF Galaxy Redshift Survey: the environmental dependence of galaxy star formation rates near clusters. *Monthly Notices of the Royal Astronomical Society*, 334(3):673–683, Aug 2002.

[230] C.-F. Lim, W.-H. Wang, I. Smail, D. Scott, C.-C. Chen, Y.-Y. Chang, J. M. Simpson, Y. Toba, X. Shu, D. Clements, J. Greenslade, Y. Ao, A. Babul, J. Birkin, S. C. Chapman, T.-A. Cheng, B. S. Cho, H. Dannerbauer, U. Dudzevičiūtė, J. Dunlop, Y. Gao, T. Goto, L. C. Ho, L.-T. Hsu, H. S. Hwang, W.-S. Jeong, M. Koprowski, C.-H. Lee, M.-Y. Lin, W.-C. Lin, M. J. Michałowski, H. Parsons, M. Sawicki, R. Shirley, H. Shim, S. Urquhart, J. Wang, and T. Wang. SCUBA-2 Ultra Deep Imaging EAO Survey (Studies). III. Multiwavelength Properties, Luminosity Functions, and Preliminary Source Catalog of 450 μm Selected Galaxies. *The Astrophysical Journal*, 889(2):80, Feb. 2020.

[231] J. M. Lotz, C. Papovich, S. M. Faber, H. C. Ferguson, N. Grogin, Y. Guo, D. Kocevski, A. M. Koekemoer, K.-S. Lee, D. McIntosh, I. Momcheva, G. Rudnick, A. Saintonge, K.-V. Tran, A. van der Wel, and C. Willmer. Caught in the Act: The Assembly of Massive Cluster Galaxies at z = 1.62. *The Astrophysical Journal*, 773(2):154, Aug 2013.

[232] C. C. Lovell, P. A. Thomas, and S. M. Wilkins. Characterising and identifying galaxy protoclusters. *Monthly Notices of the Royal Astronomical Society*, 474(4):4612–4628, Mar 2018.

[233] E. Lusso, A. Comastri, B. D. Simmons, M. Mignoli, G. Zamorani, C. Vignali, M. Brusa, F. Shankar, D. Lutz, J. R. Trump, R. Maiolino, R. Gilli, M. Bolzonella, S. Puccetti, M. Salvato, C. D. Impey, F. Civano, M. Elvis, V. Mainieri, J. D. Silverman, A. M. Koekemoer, A. Bongiorno, A. Merloni, S. Berta, E. Le Floc'h, B. Magnelli, F. Pozzi, and L. Riguccini. Bolometric luminosities and Eddington ratios of X-ray selected active galactic nuclei in the XMM-COSMOS survey. *Monthly Notices of the Royal Astronomical Society*, 425:623–640, Sept. 2012.

[234] D. Lutz, E. Sturm, L. J. Tacconi, E. Valiante, M. Schweitzer, H. Netzer, R. Maiolino, P. Andreani, O. Shemmer, and S. Veilleux. Star Formation in the Hosts of High-z QSOs: Evidence from Spitzer PAH Detections. *The Astrophysical Journal*, 684:853–861, Sept. 2008.

[235] J. Ma, A. Cooray, H. Nayyeri, A. Brown, N. Ghotbi, R. Ivison, I. Oteo, S. Duivenvoorden, J. Greenslade, D. Clements, J. Wardlow, A. Battisti, E. da Cunha, M. L. N. Ashby, I. Perez-Fournon, D. Riechers, S. Oliver, S. Eales, M. Negrello, S. Dye, L. Dunne, A. Omont, D. Scott, P. Cox, S. Serjeant, S. Maddox, and E. Valiante. Spitzer Catalog of Herschel-selected Ultrared Dusty Star-forming Galaxies. *The Astrophysical Journals*, 244(2):30, Oct 2019.

[236] P. Madau and M. Dickinson. Cosmic Star-Formation History. *Annual Review of Astronomy & Astrophysics*, 52:415–486, Aug 2014.

[237] S. J. Maddox, E. Valiante, P. Cigan, L. Dunne, S. Eales, M. W. L. Smith, S. Dye, C. Furlanetto, E. Ibar, G. de Zotti, J. S. Millard, N. Bourne, H. L. Gomez, R. J. Ivison, D. Scott, and I. Valtchanov. The Herschel-ATLAS Data Release 2. Paper II. Catalogs of Far-infrared and Submillimeter Sources in the Fields at the South and North Galactic Poles. *The Astrophysical Journals*, 236(2):30, Jun 2018.

[238] B. Magnelli, D. Lutz, A. Saintonge, S. Berta, P. Santini, M. Symeonidis, B. Altieri, P. Andreani, H. Aussel, M. Béthermin, J. Bock, A. Bongiovanni, J. Cepa, A. Cimatti, A. Conley, E. Daddi, D. Elbaz, N. M. Förster Schreiber, R. Genzel, R. J. Ivison, E. Le Floc'h, G. Magdis, R. Maiolino, R. Nordon, S. J. Oliver, M. Page, A. Pérez García, A. Poglitsch, P. Popesso, F. Pozzi, L. Riguccini, G. Rodighiero, D. Rosario, I. Roseboom, M. Sanchez-Portal, D. Scott, E. Sturm, L. J. Tacconi, I. Valtchanov, L. Wang, and S. Wuyts. The evolution of the dust temperatures of galaxies in the SFR-M_* plane up to z ~ 2. *Astronomy & Astrophysics*, 561:A86, Jan. 2014.

[239] J. Magorrian, S. Tremaine, D. Richstone, R. Bender, G. Bower, A. Dressler, S. M. Faber, K. Gebhardt, R. Green, C. Grillmair, J. Kormendy, and T. Lauer. The Demography of Massive Dark Objects in Galaxy Centers. *Astronomical Journal*, 115:2285–2305, June 1998.

[240] R. Maiolino, O. Shemmer, M. Imanishi, H. Netzer, E. Oliva, D. Lutz, and E. Sturm. Dust covering factor, silicate emission, and star formation in luminous QSOs. *Astronomy & Astrophysics*, 468:979–992, June 2007.

[241] A. Man and S. Belli. Star formation quenching in massive galaxies. *Nature Astronomy*, 2:695–697, Sept. 2018.

[242] S. M. Manning, C. M. Casey, J. A. Zavala, G. E. Magdis, P. M. Drew, J. B. Champagne, M. Aravena, M. Béthermin, D. L. Clements, S. L. Finkelstein, S. Fujimoto, C. C. Hayward, J. A. Hodge, O. Ilbert, J. S. Kartaltepe, K. K. Knudsen, A. M. Koekemoer, A. W. S. Man, D. B. Sanders, K. Sheth, J. S. Spilker, J. Staguhn, M. Talia, E. Treister, and M. S. Yun. Characterization of Two 2 mm detected Optically Obscured Dusty Star-forming Galaxies. , 925(1):23, Jan. 2022.

[243] A. B. Mantz, Z. Abdulla, J. E. Carlstrom, C. H. Greer, E. M. Leitch, D. P. Marrone, S. Muchovej, C. Adami, M. Birkinshaw, M. Bremer, N. Clerc, P. Giles, C. Horellou, B. Maughan, F. Pacaud, M. Pierre, and J. Willis. The XXL Survey. V. Detection of the Sunyaev-Zel'dovich Effect of the Redshift 1.9 Galaxy Cluster XLSSU J021744.1-034536 with CARMA. *The Astrophysical Journal*, 794(2):157, Oct 2014.

[244] A. Marconi and L. K. Hunt. The Relation between Black Hole Mass, Bulge Mass, and Near-Infrared Luminosity. *The Astrophysical Journall*, 589:L21–L24, May 2003.

[245] Z. C. Marsan, A. Muzzin, D. Marchesini, M. Stefanon, N. Martis, M. Annunziatella, J. C. C. Chan, M. C. Cooper, B. Forrest, P. Gomez, I. McConachie, and G. Wilson. The Number Densities and Stellar Populations of Massive Galaxies at $3 < z < 6$: A Diverse, Rapidly Forming Population in the Early Universe. *arXiv e-prints*, page arXiv:2010.04725, Oct. 2020.

[246] N. S. Martis, D. Marchesini, G. B. Brammer, A. Muzzin, I. Labbé, I. G. Momcheva, R. E. Skelton, M. Stefanon, P. G. van Dokkum, and K. E. Whitaker. The Evolution of the Fractions of Quiescent and Star-forming Galaxies as a Function of Stellar Mass Since $z = 3$: Increasing Importance of Massive, Dusty Star-forming Galaxies in the Early Universe. *The Astrophysical Journall*, 827(2):L25, Aug. 2016.

[247] S. Mateos, F. J. Carrera, A. Alonso-Herrero, A. Hernán-Caballero, X. Barcons, A. Asensio Ramos, M. G. Watson, A. Blain, A. Caccianiga, L. Ballo, V. Braito, and C. Ramos Almeida. X-Ray Absorption, Nuclear Infrared Emission, and Dust Covering Factors of AGNs: Testing Unification Schemes. *The Astrophysical Journal*, 819:166, Mar. 2016.

[248] S. Mateos, F. J. Carrera, A. Alonso-Herrero, E. Rovilos, A. Hernán-Caballero, X. Barcons, A. Blain, A. Caccianiga, R. Della Ceca, and P. Severgnini. Revisiting the relationship

between 6 μm and 2-10 keV continuum luminosities of AGN. *Monthly Notices of the Royal Astronomical Society*, 449:1422–1440, May 2015.

[249] S. Mateos, F. J. Carrera, X. Barcons, A. Alonso-Herrero, A. Hernán-Caballero, M. Page, C. Ramos Almeida, A. Caccianiga, T. Miyaji, and A. Blain. Survival of the Obscuring Torus in the Most Powerful Active Galactic Nuclei. *The Astrophysical Journall*, 841:L18, June 2017.

[250] J. Matthee and J. Schaye. The origin of scatter in the star formation rate-stellar mass relation. *Monthly Notices of the Royal Astronomical Society*, 484(1):915–932, Mar. 2019.

[251] S. McAlpine, I. Smail, R. G. Bower, A. M. Swinbank, J. W. Trayford, T. Theuns, M. Baes, P. Camps, R. A. Crain, and J. Schaye. The nature of submillimetre and highly star-forming galaxies in the EAGLE simulation. *Monthly Notices of the Royal Astronomical Society*, 488(2):2440–2454, Sept. 2019.

[252] J. McBride, O. Fakhouri, and C.-P. Ma. Mass accretion rates and histories of dark matter haloes. , 398(4):1858–1868, Oct 2009.

[253] A. J. Mendez, A. L. Coil, J. Aird, A. M. Diamond-Stanic, J. Moustakas, M. R. Blanton, R. J. Cool, D. J. Eisenstein, K. C. Wong, and G. Zhu. PRIMUS: Infrared and X-Ray AGN Selection Techniques at $0.2 < z < 1.2$. *The Astrophysical Journal*, 770:40, June 2013.

[254] E. Merlin, N. Bourne, M. Castellano, H. C. Ferguson, T. Wang, S. Derriere, J. S. Dunlop, D. Elbaz, and A. Fontana. T-PHOT version 2.0: Improved algorithms for background subtraction, local convolution, kernel registration, and new options. *Astronomy & Astrophysics*, 595:A97, Nov. 2016.

[255] E. Merlin, A. Fontana, H. C. Ferguson, J. S. Dunlop, D. Elbaz, N. Bourne, V. A. Bruce, F. Buitrago, M. Castellano, C. Schreiber, A. Grazian, R. J. McLure, K. Okumura, X. Shu, T. Wang, R. Amorín, K. Boutsia, N. Cappelluti, A. Comastri, S. Derriere, S. M. Faber, and P. Santini. T-PHOT: A new code for PSF-matched, prior-based, multiwavelength extragalactic deconfusion photometry. *Astronomy & Astrophysics*, 582:A15, Oct. 2015.

[256] E. Merlin, F. Fortuni, M. Torelli, P. Santini, M. Castellano, A. Fontana, A. Grazian, L. Pentericci, S. Pilo, and K. B. Schmidt. Red and dead CANDELS: massive passive galaxies at the dawn of the Universe. *Monthly Notices of the Royal Astronomical Society*, 490(3):3309–3328, Dec. 2019.

[257] A. Merloni, A. Bongiorno, M. Brusa, K. Iwasawa, V. Mainieri, B. Magnelli, M. Salvato, S. Berta, N. Cappelluti, A. Comastri, F. Fiore, R. Gilli, A. Koekemoer, E. Le Floc'h, E. Lusso, D. Lutz, T. Miyaji, F. Pozzi, L. Riguccini, D. J. Rosario, J. Silverman, M. Symeonidis, E. Treister, C. Vignali, and G. Zamorani. The incidence of obscuration in active galactic nuclei. *Monthly Notices of the Royal Astronomical Society*, 437:3550–3567, Feb. 2014.

[258] M. Michałowski, J. Hjorth, and D. Watson. Cosmic evolution of submillimeter galaxies and their contribution to stellar mass assembly. *Astronomy & Astrophysics*, 514:A67, May 2010.

[259] M. J. Michałowski, J. S. Dunlop, M. Cirasuolo, J. Hjorth, C. C. Hayward, and D. Watson. The stellar masses and specific star-formation rates of submillimetre galaxies. *Astronomy & Astrophysics*, 541:A85, May 2012.

[260] M. J. Michałowski, J. S. Dunlop, M. P. Koprowski, M. Cirasuolo, J. E. Geach, R. A. A. Bowler, A. Mortlock, K. I. Caputi, I. Aretxaga, V. Arumugam, C.-C. Chen, R. J. McLure, M. Birkinshaw, N. Bourne, D. Farrah, E. Ibar, P. van der Werf, and M. Zemcov. The SCUBA-2 Cosmology Legacy Survey: the nature of bright submm galaxies from 2 $\deg^2$ of 850-μm imaging. *Monthly Notices of the Royal Astronomical Society*, 469(1):492–515, July 2017.

[261] M. J. Michałowski, C. C. Hayward, J. S. Dunlop, V. A. Bruce, M. Cirasuolo, F. Cullen, and L. Hernquist. Determining the stellar masses of submillimetre galaxies: the critical importance of star formation histories. *Astronomy & Astrophysics*, 571:A75, Nov 2014.

[262] O. Miettinen, I. Delvecchio, V. Smolčić, M. Aravena, D. Brisbin, A. Karim, B. Magnelli, M. Novak, E. Schinnerer, M. Albrecht, H. Aussel, F. Bertoldi, P. L. Capak, C. M. Casey, C. C. Hayward, O. Ilbert, H. T. Intema, C. Jiang, O. Le Fèvre, H. J. McCracken, A. M. Muñoz Arancibia, F. Navarrete, N. D. Padilla, D. A. Riechers, M. Salvato, K. S. Scott, K. Sheth, and L. A. M. Tasca. An ALMA survey of submillimetre galaxies in the COSMOS field: Physical properties derived from energy balance spectral energy distribution modelling. *Astronomy & Astrophysics*, 606:A17, Sept. 2017.

[263] G. Miley. The structure of extended extragalactic radio sources. *Annual Review of Astronomy & Astrophysics*, 18:165–218, 1980.

[264] T. B. Miller, S. C. Chapman, M. Aravena, M. L. N. Ashby, C. C. Hayward, J. D. Vieira, A. Weiß, A. Babul, M. Béthermin, C. M. Bradford, M. Brodwin, J. E. Carlstrom, C.-C. Chen, D. J. M. Cunningham, C. De Breuck, A. H. Gonzalez, T. R. Greve, J. Harnett, Y. Hezaveh, K. Lacaille, K. C. Litke, J. Ma, M. Malkan, D. P. Marrone, W. Morningstar, E. J. Murphy, D. Narayanan, E. Pass, R. Perry, K. A. Phadke, D. Rennehan, K. M. Rotermund, J. Simpson, J. S. Spilker, J. Sreevani, A. A. Stark, M. L. Strandet, and A. L. Strom. A massive core for a cluster of galaxies at a redshift of 4.3. *Nature*, 556:469–472, Apr. 2018.

[265] S. Mineo, M. Gilfanov, and R. Sunyaev. X-ray emission from star-forming galaxies - I. High-mass X-ray binaries. *Monthly Notices of the Royal Astronomical Society*, 419:2095–2115, Jan. 2012.

[266] S. Mineo, M. Gilfanov, and R. Sunyaev. X-ray emission from star-forming galaxies - II. Hot interstellarmedium. *Monthly Notices of the Royal Astronomical Society*, 426:1870–1883, Nov. 2012.

[267] A. Montaña, J. A. Zavala, I. Aretxaga, D. H. Hughes, R. J. Ivison, A. Pope, D. Sánchez-Argüelles, G. W. Wilson, M. Yun, O. A. Cantua, M. McCrackan, M. J. Michałowski, E. Valiante, V. Arumugam, C. M. Casey, R. Chávez, E. Colín-Beltrán, H. Dannerbauer, J. S. Dunlop, L. Dunne, S. Eales, D. Ferrusca, V. Gómez-Rivera, A. I. Gómez-Ruiz, V. H. de la Luz, S. J. Maddox, G. Narayanan, A. Omont, I. Rodríguez-Montoya, S. Serjeant,

F. P. Schloerb, M. Velázquez, S. Ventura-González, P. van der Werf, and M. Zeballos. Early science with the Large Millimeter Telescope: a 1.1 mm AzTEC survey of red-Herschel dusty star-forming galaxies. *Monthly Notices of the Royal Astronomical Society*, 505(4):5260–5282, Aug. 2021.

[268] J. R. Mullaney, D. M. Alexander, J. Aird, E. Bernhard, E. Daddi, A. Del Moro, M. Dickinson, D. Elbaz, C. M. Harrison, S. Juneau, D. Liu, M. Pannella, D. Rosario, P. Santini, M. Sargent, C. Schreiber, J. Simpson, and F. Stanley. ALMA and Herschel reveal that X-ray-selected AGN and main-sequence galaxies have different star formation rate distributions. *Monthly Notices of the Royal Astronomical Society*, 453:L83–L87, Oct. 2015.

[269] J. R. Mullaney, D. M. Alexander, A. D. Goulding, and R. C. Hickox. Defining the intrinsic AGN infrared spectral energy distribution and measuring its contribution to the infrared output of composite galaxies. *Monthly Notices of the Royal Astronomical Society*, 414:1082–1110, June 2011.

[270] J. R. Mullaney, M. Pannella, E. Daddi, D. M. Alexander, D. Elbaz, R. C. Hickox, F. Bournaud, B. Altieri, H. Aussel, D. Coia, H. Dannerbauer, K. Dasyra, M. Dickinson, H. S. Hwang, J. Kartaltepe, R. Leiton, G. Magdis, B. Magnelli, P. Popesso, I. Valtchanov, F. E. Bauer, W. N. Brandt, A. Del Moro, D. J. Hanish, R. J. Ivison, S. Juneau, B. Luo, D. Lutz, M. T. Sargent, D. Scott, and Y. Q. Xue. GOODS-Herschel: the far-infrared view of star formation in active galactic nucleus host galaxies since z < 3. *Monthly Notices of the Royal Astronomical Society*, 419:95–115, Jan. 2012.

[271] C. R. Mullis, P. Rosati, G. Lamer, H. Böhringer, A. Schwope, P. Schuecker, and R. Fassbender. Discovery of an X-Ray-luminous Galaxy Cluster at z=1.4. *The Astrophysical Journall*, 623(2):L85–L88, Apr 2005.

[272] E. J. Murphy, R. R. Chary, D. M. Alexander, M. Dickinson, B. Magnelli, G. Morrison, A. Pope, and H. I. Teplitz. Balancing the Energy Budget Between Star Formation and Active Galactic Nuclei in High-Redshift Infrared Luminous Galaxies. *The Astrophysical Journal*, 698(2):1380–1397, Jun 2009.

[273] E. J. Murphy, J. J. Condon, E. Schinnerer, R. C. Kennicutt, D. Calzetti, L. Armus, G. Helou, J. L. Turner, G. Aniano, P. Beirão, A. D. Bolatto, B. R. Brandl, K. V. Croxall, D. A. Dale, J. L. Donovan Meyer, B. T. Draine, C. Engelbracht, L. K. Hunt, C. N. Hao, J. Koda, H. Roussel, R. Skibba, and J. D. T. Smith. Calibrating Extinction-free Star Formation Rate Diagnostics with 33 GHz Free-free Emission in NGC 6946. *The Astrophysical Journal*, 737(2):67, Aug. 2011.

[274] S. S. Murray, A. Kenter, W. R. Forman, C. Jones, P. J. Green, C. S. Kochanek, A. Vikhlinin, D. Fabricant, G. Fazio, K. Brand, M. J. I. Brown, A. Dey, B. T. Jannuzi, J. Najita, B. McNamara, J. Shields, and M. Rieke. XBootes: An X-Ray Survey of the NDWFS Bootes Field. I. Overview and Initial Results. *ApJS*, 161:1–8, Nov. 2005.

[275] R. Mushotzky. How are AGN Found? In A. J. Barger, editor, *Supermassive Black Holes in the Distant Universe*, volume 308 of *Astrophysics and Space Science Library*, page 53, Aug. 2004.

[276] A. Muzzin, D. Marchesini, M. Stefanon, M. Franx, H. J. McCracken, B. Milvang-Jensen, J. S. Dunlop, J. P. U. Fynbo, G. Brammer, I. Labbé, and P. G. van Dokkum. The Evolution of the Stellar Mass Functions of Star-forming and Quiescent Galaxies to z = 4 from the COSMOS/UltraVISTA Survey. *The Astrophysical Journal*, 777(1):18, Nov 2013.

[277] K. Nandra and K. A. Pounds. GINGA Observations of the X-Ray Spectra of Seyfert Galaxies. *MNRAS*, 268:405, May 1994.

[278] D. Narayanan, C. C. Hayward, T. J. Cox, L. Hernquist, P. Jonsson, J. D. Younger, and B. Groves. The formation of high-redshift submillimetre galaxies. *Monthly Notices of the Royal Astronomical Society*, 401(3):1613–1619, Jan 2010.

[279] D. Narayanan, M. Turk, R. Feldmann, T. Robitaille, P. Hopkins, R. Thompson, C. Hayward, D. Ball, C.-A. Faucher-Giguère, and D. Kereš. The formation of submillimetre-bright galaxies from gas infall over a billion years. *Nature*, 525(7570):496–499, Sep 2015.

[280] E. Nardini, G. Risaliti, M. Salvati, E. Sani, M. Imanishi, A. Marconi, and R. Maiolino. Spectral decomposition of starbursts and active galactic nuclei in 5-8 μm Spitzer-IRS spectra of local ultraluminous infrared galaxies. *Monthly Notices of the Royal Astronomical Society*, 385:L130–L134, Mar. 2008.

[281] M. Nenkova, M. M. Sirocky, Ž. Ivezić, and M. Elitzur. AGN Dusty Tori. I. Handling of Clumpy Media. *The Astrophysical Journal*, 685:147–159, Sept. 2008.

[282] M. Nenkova, M. M. Sirocky, R. Nikutta, Ž. Ivezić, and M. Elitzur. AGN Dusty Tori. II. Observational Implications of Clumpiness. *The Astrophysical Journal*, 685:160–180, Sept. 2008.

[283] H. Netzer. Accretion and star formation rates in low-redshift type II active galactic nuclei. *MNRAS*, 399:1907–1920, Nov. 2009.

[284] H. Netzer. Revisiting the Unified Model of Active Galactic Nuclei. *Annual Review of Astronomy & Astrophysics*, 53:365–408, Aug. 2015.

[285] H. Netzer and B. Trakhtenbrot. Cosmic Evolution of Mass Accretion Rate and Metallicity in Active Galactic Nuclei. *The Astrophysical Journal*, 654:754–763, Jan. 2007.

[286] A. B. Newman, R. S. Ellis, S. Andreon, T. Treu, A. Raichoor, and G. Trinchieri. Spectroscopic Confirmation of the Rich z = 1.80 Galaxy Cluster JKCS 041 using the WFC3 Grism: Environmental Trends in the Ages and Structure of Quiescent Galaxies. *The Astrophysical Journal*, 788(1):51, Jun 2014.

[287] A. G. Noble, M. McDonald, A. Muzzin, J. Nantais, G. Rudnick, E. van Kampen, T. M. A. Webb, G. Wilson, H. K. C. Yee, K. Boone, M. C. Cooper, A. DeGroot, A. Delahaye, R. Demarco, R. Foltz, B. Hayden, C. Lidman, A. Manilla-Robles, and S. Perlmutter. ALMA Observations of Gas-rich Galaxies in z 1.6 Galaxy Clusters: Evidence for Higher Gas Fractions in High-density Environments. *The Astrophysical Journall*, 842(2):L21, Jun 2017.

[288] K. G. Noeske, S. M. Faber, B. J. Weiner, D. C. Koo, J. R. Primack, A. Dekel, C. Papovich, C. J. Conselice, E. Le Floc'h, G. H. Rieke, A. L. Coil, J. M. Lotz, R. S. Somerville, and K. Bundy. Star Formation in AEGIS Field Galaxies since z=1.1: Staged Galaxy Formation and a Model of Mass-dependent Gas Exhaustion. *The Astrophysical Journall*, 660(1):L47–L50, May 2007.

[289] K. G. Noeske, B. J. Weiner, S. M. Faber, C. Papovich, D. C. Koo, R. S. Somerville, K. Bundy, C. J. Conselice, J. A. Newman, D. Schiminovich, E. Le Floc'h, A. L. Coil, G. H. Rieke, J. M. Lotz, J. R. Primack, P. Barmby, M. C. Cooper, M. Davis, R. S. Ellis, G. G. Fazio, P. Guhathakurta, J. Huang, S. A. Kassin, D. C. Martin, A. C. Phillips, R. M. Rich, T. A. Small, C. N. A. Willmer, and G. Wilson. Star Formation in AEGIS Field Galaxies since z=1.1: The Dominance of Gradually Declining Star Formation, and the Main Sequence of Star-forming Galaxies. *The Astrophysical Journall*, 660(1):L43–L46, May 2007.

[290] S. Noll, D. Burgarella, E. Giovannoli, V. Buat, D. Marcillac, and J. C. Muñoz-Mateos. Analysis of galaxy spectral energy distributions from far-UV to far-IR with CIGALE: studying a SINGS test sample. *Astronomy & Astrophysics*, 507(3):1793–1813, Dec 2009.

[291] S. J. Oliver, J. Bock, B. Altieri, A. Amblard, V. Arumugam, H. Aussel, T. Babbedge, A. Beelen, M. Béthermin, A. Blain, A. Boselli, C. Bridge, D. Brisbin, V. Buat, D. Burgarella, N. Castro-Rodríguez, A. Cava, P. Chanial, M. Cirasuolo, D. L. Clements, A. Conley, L. Conversi, A. Cooray, C. D. Dowell, E. N. Dubois, E. Dwek, S. Dye, S. Eales, D. Elbaz, D. Farrah, A. Feltre, P. Ferrero, N. Fiolet, M. Fox, A. Franceschini, W. Gear, E. Giovannoli, J. Glenn, Y. Gong, E. A. González Solares, M. Griffin, M. Halpern, M. Harwit, E. Hatziminaoglou, S. Heinis, P. Hurley, H. S. Hwang, A. Hyde, E. Ibar, O. Ilbert, K. Isaak, R. J. Ivison, G. Lagache, E. Le Floc'h, L. Levenson, B. L. Faro, N. Lu, S. Madden, B. Maffei, G. Magdis, G. Mainetti, L. Marchetti, G. Marsden, J. Marshall, A. M. J. Mortier, H. T. Nguyen, B. O'Halloran, A. Omont, M. J. Page, P. Panuzzo, A. Papageorgiou, H. Patel, C. P. Pearson, I. Pérez-Fournon, M. Pohlen, J. I. Rawlings, G. Raymond, D. Rigopoulou, L. Riguccini, D. Rizzo, G. Rodighiero, I. G. Roseboom, M. Rowan-Robinson, M. Sánchez Portal, B. Schulz, D. Scott, N. Seymour, D. L. Shupe, A. J. Smith, J. A. Stevens, M. Symeonidis, M. Trichas, K. E. Tugwell, M. Vaccari, I. Valtchanov, J. D. Vieira, M. Viero, L. Vigroux, L. Wang, R. Ward, J. Wardlow, G. Wright, C. K. Xu, and M. Zemcov. The Herschel Multi-tiered Extragalactic Survey: HerMES. *MNRAS*, 424:1614–1635, Aug. 2012.

[292] A. Omont, P. Cox, F. Bertoldi, R. G. McMahon, C. Carilli, and K. G. Isaak. A 1.2 mm MAMBO/IRAM-30 m survey of dust emission from the highest redshift PSS quasars. *Astronomy & Astrophysics*, 374:371–381, Aug. 2001.

[293] I. Oteo, R. J. Ivison, L. Dunne, A. Manilla-Robles, S. Maddox, A. J. R. Lewis, G. de Zotti, M. Bremer, D. L. Clements, A. Cooray, H. Dannerbauer, S. Eales, J. Greenslade, A. Omont, I. PerezFournón, D. Riechers, D. Scott, P. van der Werf, A. Weiss, and Z. Y. Zhang. An Extreme Protocluster of Luminous Dusty Starbursts in the Early Universe. *The Astrophysical Journal*, 856:72, Mar. 2018.

[294] R. A. Overzier. The realm of the galaxy protoclusters. A review. *Astronomy & Astrophysics Reviews*, 24(1):14, Nov 2016.

[295] Z. Pan, X. Zheng, and X. Kong. The Quenched Mass Portion of Star-forming Galaxies and the Origin of the Star Formation Sequence Slope. *The Astrophysical Journal*, 834(1):39, Jan. 2017.

[296] M. Pannella, C. L. Carilli, E. Daddi, H. J. McCracken, F. N. Owen, A. Renzini, V. Strazzullo, F. Civano, A. M. Koekemoer, E. Schinnerer, N. Scoville, V. Smolčić, Y. Taniguchi, H. Aussel, J. P. Kneib, O. Ilbert, Y. Mellier, M. Salvato, D. Thompson, and C. J. Willott. Star Formation and Dust Obscuration at z $\approx$ 2: Galaxies at the Dawn of Downsizing. *The Astrophysical Journall*, 698(2):L116–L120, June 2009.

[297] C. Papovich, I. Momcheva, C. N. A. Willmer, K. D. Finkelstein, S. L. Finkelstein, K. V. Tran, M. Brodwin, J. S. Dunlop, D. Farrah, S. A. Khan, J. Lotz, P. McCarthy, R. J. McLure, M. Rieke, G. Rudnick, S. Sivanandam, F. Pacaud, and M. Pierre. A Spitzer-selected Galaxy Cluster at z = 1.62. *The Astrophysical Journal*, 716(2):1503–1513, Jun 2010.

[298] S. G. Patel, B. P. Holden, D. D. Kelson, G. D. Illingworth, and M. Franx. The Dependence of Star Formation Rates on Stellar Mass and Environment at z $\sim$0.8. *The Astrophysical Journall*, 705(1):L67–L70, Nov 2009.

[299] P. Patil, K. Nyland, M. Lacy, D. Farrah, J. Afonso, W. Barkhouse, and J. Surace. Multiband Optical and Near-Infrared Properties of Faint Submillimeter Galaxies with Serendipitous ALMA Detections. *The Astrophysical Journal*, 871(1):109, Jan. 2019.

[300] R. Pavesi, D. A. Riechers, C. E. Sharon, V. Smolčić, A. L. Faisst, E. Schinnerer, C. L. Carilli, P. L. Capak, N. Scoville, and G. J. Stacey. Hidden in Plain Sight: A Massive, Dusty Starburst in a Galaxy Protocluster at z = 5.7 in the COSMOS Field. *The Astrophysical Journal*, 861(1):43, Jul 2018.

[301] W. J. Pearson, L. Wang, P. D. Hurley, K. Małek, V. Buat, D. Burgarella, D. Farrah, S. J. Oliver, D. J. B. Smith, and F. F. S. van der Tak. Main sequence of star forming galaxies beyond the Herschel confusion limit. *Astronomy & Astrophysics*, 615:A146, July 2018.

[302] Y.-j. Peng, S. J. Lilly, K. Kovač, M. Bolzonella, L. Pozzetti, A. Renzini, G. Zamorani, O. Ilbert, C. Knobel, A. Iovino, C. Maier, O. Cucciati, L. Tasca, C. M. Carollo, J. Silverman, P. Kampczyk, L. de Ravel, D. Sanders, N. Scoville, T. Contini, V. Mainieri, M. Scodeggio, J.-P. Kneib, O. Le Fèvre, S. Bardelli, A. Bongiorno, K. Caputi, G. Coppa, S. de la Torre, P. Franzetti, B. Garilli, F. Lamareille, J.-F. Le Borgne, V. Le Brun, M. Mignoli, E. Perez Montero, R. Pello, E. Ricciardelli, M. Tanaka, L. Tresse, D. Vergani, N. Welikala, E. Zucca, P. Oesch, U. Abbas, L. Barnes, R. Bordoloi, D. Bottini, A. Cappi, P. Cassata, A. Cimatti, M. Fumana, G. Hasinger, A. Koekemoer, A. Leauthaud, D. Maccagni, C. Marinoni, H. McCracken, P. Memeo, B. Meneux, P. Nair, C. Porciani, V. Presotto, and R. Scaramella. Mass and Environment as Drivers of Galaxy Evolution in SDSS and zCOSMOS and the Origin of the Schechter Function. *The Astrophysical Journal*, 721(1):193–221, Sept. 2010.

[303] P. G. Pérez-González, G. H. Rieke, V. Villar, G. Barro, M. Blaylock, E. Egami, J. Gallego, A. Gil de Paz, S. Pascual, J. Zamorano, and J. L. Donley. The Stellar Mass Assembly of Galaxies from z = 0 to z = 4: Analysis of a Sample Selected in the Rest-Frame Near-Infrared with Spitzer. *The Astrophysical Journal*, 675(1):234–261, Mar. 2008.

[304] G. L. Pilbratt, J. R. Riedinger, T. Passvogel, G. Crone, D. Doyle, U. Gageur, A. M. Heras, C. Jewell, L. Metcalfe, S. Ott, and M. Schmidt. Herschel Space Observatory. An ESA facility for far-infrared and submillimetre astronomy. *Astronomy & Astrophysics*, 518:L1, July 2010.

[305] Planck Collaboration, P. A. R. Ade, N. Aghanim, M. Arnaud, M. Ashdown, J. Aumont, C. Baccigalupi, A. J. Banday, R. B. Barreiro, J. G. Bartlett, and et al. Planck 2015 results. XIII. Cosmological parameters. *Astronomy & Astrophysics*, 594:A13, Sept. 2016.

[306] A. Poglitsch, C. Waelkens, N. Geis, H. Feuchtgruber, B. Vandenbussche, L. Rodriguez, O. Krause, E. Renotte, C. van Hoof, P. Saraceno, J. Cepa, F. Kerschbaum, P. Agnèse, B. Ali, B. Altieri, P. Andreani, J.-L. Augueres, Z. Balog, L. Barl, O. H. Bauer, N. Belbachir, M. Benedettini, N. Billot, O. Boulade, H. Bischof, J. Blommaert, E. Callut, C. Cara, R. Cerulli, D. Cesarsky, A. Contursi, Y. Creten, W. De Meester, V. Doublier, E. Doumayrou, L. Duband, K. Exter, R. Genzel, J.-M. Gillis, U. Grözinger, T. Henning, J. Herreros, R. Huygen, M. Inguscio, G. Jakob, C. Jamar, C. Jean, J. de Jong, R. Katterloher, C. Kiss, U. Klaas, D. Lemke, D. Lutz, S. Madden, B. Marquet, J. Martignac, A. Mazy, P. Merken, F. Montfort, L. Morbidelli, T. Müller, M. Nielbock, K. Okumura, R. Orfei, R. Ottensamer, S. Pezzuto, P. Popesso, J. Putzeys, S. Regibo, V. Reveret, P. Royer, M. Sauvage, J. Schreiber, J. Stegmaier, D. Schmitt, J. Schubert, E. Sturm, M. Thiel, G. Tofani, R. Vavrek, M. Wetzstein, E. Wieprecht, and E. Wiezorrek. The Photodetector Array Camera and Spectrometer (PACS) on the Herschel Space Observatory. *A&A*, 518:L2, July 2010.

[307] P. Popesso, A. Concas, L. Morselli, C. Schreiber, G. Rodighiero, G. Cresci, S. Belli, G. Erfanianfar, C. Mancini, H. Inami, M. Dickinson, O. Ilbert, M. Pannella, and D. Elbaz. The main sequence of star-forming galaxies - I. The local relation and its bending. *Monthly Notices of the Royal Astronomical Society*, 483(3):3213–3226, Mar. 2019.

[308] P. Popesso, L. Morselli, A. Concas, C. Schreiber, G. Rodighiero, G. Cresci, S. Belli, O. Ilbert, G. Erfanianfar, C. Mancini, H. Inami, M. Dickinson, M. Pannella, and D. Elbaz. The main sequence of star-forming galaxies - II. A non-evolving slope at the high-mass end. *Monthly Notices of the Royal Astronomical Society*, 490(4):5285–5299, Dec. 2019.

[309] G. Popping, K. I. Caputi, R. S. Somerville, and S. C. Trager. An indirect measurement of gas evolution in galaxies at 0.5 < z < 2.0. *Monthly Notices of the Royal Astronomical Society*, 425(3):2386–2400, Sep 2012.

[310] C. Ragone-Figueroa, G. L. Granato, M. E. Ferraro, G. Murante, V. Biffi, S. Borgani, S. Planelles, and E. Rasia. BCG mass evolution in cosmological hydro-simulations. *Monthly Notices of the Royal Astronomical Society*, 479(1):1125–1136, Sep 2018.

[311] P. Ranalli, A. Comastri, and G. Setti. The 2-10 keV luminosity as a Star Formation Rate indicator. *Astronomy & Astrophysics*, 399:39–50, Feb. 2003.

[312] J. N. Reeves, P. T. O'Brien, V. Braito, E. Behar, L. Miller, T. J. Turner, A. C. Fabian, S. Kaspi, R. Mushotzky, and M. Ward. A Compton-thick Wind in the High-luminosity Quasar, PDS 456. *The Astrophysical Journal*, 701:493–507, Aug. 2009.

[313] A. Rettura, S. Mei, S. A. Stanford, A. Raichoor, S. Moran, B. Holden, P. Rosati, R. Ellis, F. Nakata, M. Nonino, T. Treu, J. P. Blakeslee, R. Demarco, P. Eisenhardt, H. C. Ford, R. A. E. Fosbury, G. Illingworth, M. Huertas-Company, M. J. Jee, T. Kodama, M. Postman, M. Tanaka, and R. L. White. Early-type Galaxies at z ∼1.3. III. On the Dependence of Formation Epochs and Star Formation Histories on Stellar Mass and Environment. *The Astrophysical Journal*, 732(2):94, May 2011.

[314] C. Ricci, B. Trakhtenbrot, M. J. Koss, Y. Ueda, K. Schawinski, K. Oh, I. Lamperti, R. Mushotzky, E. Treister, L. C. Ho, A. Weigel, F. E. Bauer, S. Paltani, A. C. Fabian, Y. Xie, and N. Gehrels. The close environments of accreting massive black holes are shaped by radiative feedback. *Nature*, 549:488–491, Sept. 2017.

[315] G. Rodighiero, E. Daddi, I. Baronchelli, A. Cimatti, A. Renzini, H. Aussel, P. Popesso, D. Lutz, P. Andreani, S. Berta, A. Cava, D. Elbaz, A. Feltre, A. Fontana, N. M. Förster Schreiber, A. Franceschini, R. Genzel, A. Grazian, C. Gruppioni, O. Ilbert, E. Le Floch, G. Magdis, M. Magliocchetti, B. Magnelli, R. Maiolino, H. McCracken, R. Nordon, A. Poglitsch, P. Santini, F. Pozzi, L. Riguccini, L. J. Tacconi, S. Wuyts, and G. Zamorani. The Lesser Role of Starbursts in Star Formation at z = 2. *The Astrophysical Journall*, 739:L40, Oct. 2011.

[316] G. Rodighiero, A. Renzini, E. Daddi, I. Baronchelli, S. Berta, G. Cresci, A. Franceschini, C. Gruppioni, D. Lutz, C. Mancini, P. Santini, G. Zamorani, J. Silverman, D. Kashino, P. Andreani, A. Cimatti, H. D. Sánchez, E. Le Floch, B. Magnelli, P. Popesso, and F. Pozzi. A multiwavelength consensus on the main sequence of star-forming galaxies at z ~ 2. *Monthly Notices of the Royal Astronomical Society*, 443(1):19–30, Sept. 2014.

[317] D. J. Rosario, D. H. McIntosh, A. van der Wel, J. Kartaltepe, P. Lang, P. Santini, S. Wuyts, D. Lutz, M. Rafelski, C. Villforth, D. M. Alexander, F. E. Bauer, E. F. Bell, S. Berta, W. N. Brandt, C. J. Conselice, A. Dekel, S. M. Faber, H. C. Ferguson, R. Genzel, N. A. Grogin, D. D. Kocevski, A. M. Koekemoer, D. C. Koo, J. M. Lotz, B. Magnelli, R. Maiolino, M. Mozena, J. R. Mullaney, C. J. Papovich, P. Popesso, L. J. Tacconi, J. R. Trump, S. Avadhuta, R. Bassett, A. Bell, M. Bernyk, F. Bournaud, P. Cassata, E. Cheung, D. Croton, J. Donley, L. DeGroot, J. Guedes, N. Hathi, J. Herrington, M. Hilton, K. Lai, C. Lani, M. Martig, E. McGrath, S. Mutch, A. Mortlock, C. McPartland, E. O'Leary, M. Peth, A. Pillepich, G. Poole, D. Snyder, A. Straughn, O. Telford, C. Tonini, and P. Wandro. The host galaxies of X-ray selected active galactic nuclei to z = 2.5: Structure, star formation, and their relationships from CANDELS and Herschel/PACS. *Astronomy & Astrophysics*, 573:A85, Jan. 2015.

[318] D. J. Rosario, P. Santini, D. Lutz, L. Shao, R. Maiolino, D. M. Alexander, B. Altieri, P. Andreani, H. Aussel, F. E. Bauer, S. Berta, A. Bongiovanni, W. N. Brandt, M. Brusa, J. Cepa, A. Cimatti, T. J. Cox, E. Daddi, D. Elbaz, A. Fontana, N. M. Förster Schreiber, R. Genzel, A. Grazian, E. Le Floch, B. Magnelli, V. Mainieri, H. Netzer, R. Nordon, I. Pérez Garcia, A. Poglitsch, P. Popesso, F. Pozzi, L. Riguccini, G. Rodighiero, M. Salvato, M. Sanchez-Portal, E. Sturm, L. J. Tacconi, I. Valtchanov, and S. Wuyts. The mean star formation rate of X-ray selected active galaxies and its evolution from z ˜ 2.5: results from PEP-Herschel. *AAP*, 545:A45, Sept. 2012.

[319] P. Rosati, S. Borgani, and C. Norman. The Evolution of X-ray Clusters of Galaxies. *Annual Review of Astronomy & Astrophysics*, 40:539–577, Jan 2002.

[320] I. G. Roseboom, S. J. Oliver, M. Kunz, B. Altieri, A. Amblard, V. Arumugam, R. Auld, H. Aussel, T. Babbedge, M. Béthermin, A. Blain, J. Bock, A. Boselli, D. Brisbin, V. Buat, D. Burgarella, N. Castro-Rodríguez, A. Cava, P. Chanial, E. Chapin, D. L. Clements, A. Conley, L. Conversi, A. Cooray, C. D. Dowell, E. Dwek, S. Dye, S. Eales, D. Elbaz, D. Farrah, M. Fox, A. Franceschini, W. Gear, J. Glenn, E. A. G. Solares, M. Griffin, M. Halpern, M. Harwit, E. Hatziminaoglou, J. Huang, E. Ibar, K. Isaak, R. J. Ivison, G. Lagache, L. Levenson, N. Lu, S. Madden, B. Maffei, G. Mainetti, L. Marchetti, G. Marsden, A. M. J. Mortier, H. T. Nguyen, B. O'Halloran, A. Omont, M. J. Page, P. Panuzzo, A. Papageorgiou, H. Patel, C. P. Pearson, I. Pérez-Fournon, M. Pohlen, J. I. Rawlings, G. Raymond, D. Rigopoulou, D. Rizzo, M. Rowan-Robinson, M. S. Portal, B. Schulz, D. Scott, N. Seymour, D. L. Shupe, A. J. Smith, J. A. Stevens, M. Symeonidis, M. Trichas, K. E. Tugwell, M. Vaccari, I. Valtchanov, J. D. Vieira, L. Vigroux, L. Wang, R. Ward, G. Wright, C. K. Xu, and M. Zemcov. The Herschel Multi-Tiered Extragalactic Survey: source extraction and cross-identifications in confusion-dominated SPIRE images. , 409:48–65, Nov. 2010.

[321] M. Rowan-Robinson, I. Valtchanov, and K. Nandra. AGN dust tori: the X-ray-infrared connection. *Monthly Notices of the Royal Astronomical Society*, 397:1326–1337, Aug. 2009.

[322] D. S. N. Rupke and S. Veilleux. Integral Field Spectroscopy of Massive, Kiloparsec-scale Outflows in the Infrared-luminous QSO Mrk 231. *The Astrophysical Journall*, 729:L27, Mar. 2011.

[323] D. B. Sanders, N. Z. Scoville, J. S. Young, B. T. Soifer, F. P. Schloerb, W. L. Rice, and G. E. Danielson. Molecular Gas in High-Luminosity IRAS Galaxies. *The Astrophysical Journall*, 305:L45, Jun 1986.

[324] D. B. Sanders, B. T. Soifer, J. H. Elias, B. F. Madore, K. Matthews, G. Neugebauer, and N. Z. Scoville. Ultraluminous Infrared Galaxies and the Origin of Quasars. *The Astrophysical Journal*, 325:74, Feb 1988.

[325] P. Santini, A. Fontana, M. Castellano, M. Di Criscienzo, E. Merlin, R. Amorin, F. Cullen, E. Daddi, M. Dickinson, J. S. Dunlop, A. Grazian, A. Lamastra, R. J. McLure, M. J. Michałowski, L. Pentericci, and X. Shu. The Star Formation Main Sequence in the Hubble Space Telescope Frontier Fields. *The Astrophysical Journal*, 847(1):76, Sept. 2017.

[326] P. Santini, E. Merlin, A. Fontana, B. Magnelli, D. Paris, M. Castellano, A. Grazian, L. Pentericci, S. Pilo, and M. Torelli. Passive galaxies in the early Universe: ALMA confirmation of z ~ 3-5 candidates in the CANDELS GOODS-South field. *Monthly Notices of the Royal Astronomical Society*, 486(1):560–569, June 2019.

[327] M. T. Sargent, M. Béthermin, E. Daddi, and D. Elbaz. The Contribution of Starbursts and Normal Galaxies to Infrared Luminosity Functions at $z < 2$. *The Astrophysical Journal*, 747(2):L31, Mar. 2012.

[328] M. T. Sargent, E. Daddi, M. Béthermin, H. Aussel, G. Magdis, H. S. Hwang, S. Juneau, D. Elbaz, and E. da Cunha. Regularity Underlying Complexity: A Redshift-independent Description of the Continuous Variation of Galaxy-scale Molecular Gas Properties in the Mass-star Formation Rate Plane. *The Astrophysical Journal*, 793(1):19, Sep 2014.

[329] A. Saro, S. Borgani, L. Tornatore, G. De Lucia, K. Dolag, and G. Murante. Simulating the formation of a protocluster at z $\sim$2. *Monthly Notices of the Royal Astronomical Society*, 392(2):795–800, Jan 2009.

[330] M. Sawicki. SEDfit: Software for Spectral Energy Distribution Fitting of Photometric Data. *Publications of the Astronomical Society of the Pacific*, 124(921):1208, Nov 2012.

[331] P. Schechter. An analytic expression for the luminosity function for galaxies. *The Astrophysical Journal*, 203:297–306, Jan. 1976.

[332] C. Schreiber, K. Glazebrook, T. Nanayakkara, G. G. Kacprzak, I. Labbé, P. Oesch, T. Yuan, K. V. Tran, C. Papovich, L. Spitler, and C. Straatman. Near infrared spectroscopy and star-formation histories of $3 \leq z \leq 4$ quiescent galaxies. *Astronomy & Astrophysics*, 618:A85, Oct. 2018.

[333] C. Schreiber, I. Labbé, K. Glazebrook, G. Bekiaris, C. Papovich, T. Costa, D. Elbaz, G. G. Kacprzak, T. Nanayakkara, P. Oesch, M. Pannella, L. Spitler, C. Straatman, K. V. Tran, and T. Wang. Jekyll & Hyde: quiescence and extreme obscuration in a pair of massive galaxies 1.5 Gyr after the Big Bang. *Astronomy & Astrophysics*, 611:A22, Mar. 2018.

[334] C. Schreiber, M. Pannella, D. Elbaz, M. Béthermin, H. Inami, M. Dickinson, B. Magnelli, T. Wang, H. Aussel, E. Daddi, S. Juneau, X. Shu, M. T. Sargent, V. Buat, S. M. Faber, H. C. Ferguson, M. Giavalisco, A. M. Koekemoer, G. Magdis, G. E. Morrison, C. Papovich, P. Santini, and D. Scott. The Herschel view of the dominant mode of galaxy growth from z = 4 to the present day. *Astronomy and Astrophysics*, 575:A74, Mar 2015.

[335] C. Schreiber, M. Pannella, R. Leiton, D. Elbaz, T. Wang, K. Okumura, and I. Labbé. The ALMA Redshift 4 Survey (AR4S). I. The massive end of the z = 4 main sequence of galaxies. *Astronomy and Astrophysics*, 599:A134, Mar 2017.

[336] G. Schwarz. Estimating the Dimension of a Model. *Annals of Statistics*, 6(2):461–464, July 1978.

[337] N. Scoville, S. Arnouts, H. Aussel, A. Benson, A. Bongiorno, K. Bundy, M. A. A. Calvo, P. Capak, M. Carollo, F. Civano, J. Dunlop, M. Elvis, A. Faisst, A. Finoguenov, H. Fu, M. Giavalisco, Q. Guo, O. Ilbert, A. Iovino, M. Kajisawa, J. Kartaltepe, A. Leauthaud, O. Le Fèvre, E. LeFloch, S. J. Lilly, C. T. C. Liu, S. Manohar, R. Massey, D. Masters, H. J. McCracken, B. Mobasher, Y. J. Peng, A. Renzini, J. Rhodes, M. Salvato, D. B. Sanders, B. D. Sarvestani, C. Scarlata, E. Schinnerer, K. Sheth, P. L. Shopbell, V. Smolčić, Y. Taniguchi, J. E. Taylor, S. D. M. White, and L. Yan. Evolution of Galaxies and Their Environments at z = 0.1-3 in COSMOS. *The Astrophysical Journals*, 206(1):3, May 2013.

[338] N. Scoville, H. Aussel, M. Brusa, P. Capak, C. M. Carollo, M. Elvis, M. Giavalisco, L. Guzzo, G. Hasinger, C. Impey, J.-P. Kneib, O. LeFevre, S. J. Lilly, B. Mobasher, A. Renzini, R. M. Rich, D. B. Sanders, E. Schinnerer, D. Schminovich, P. Shopbell, Y. Taniguchi, and N. D. Tyson. The Cosmic Evolution Survey (COSMOS): Overview. *The Astrophysical Journals*, 172:1–8, Sept. 2007.

[339] N. Scoville, K. Sheth, H. Aussel, P. Vanden Bout, P. Capak, A. Bongiorno, C. M. Casey, L. Murchikova, J. Koda, J. Alvarez-Marquez, N. Lee, C. Laigle, H. J. McCracken, O. Ilbert, A. Pope, D. Sanders, J. Chu, S. Toft, R. J. Ivison, and S. Manohar. ISM Masses and the Star formation Law at Z = 1 to 6: ALMA Observations of Dust Continuum in 145 Galaxies in the COSMOS Survey Field. *The Astrophysical Journal*, 820(2):83, Apr. 2016.

[340] A. Shahidi, B. Mobasher, H. Nayyeri, S. Hemmati, T. Wiklind, N. Chartab, M. Dickinson, S. L. Finkelstein, C. Pacifici, C. Papovich, H. C. Ferguson, A. Fontana, M. Giavalisco, A. Koekemoer, J. Newman, Z. Sattari, and R. Somerville. Selection of Massive Evolved Galaxies at $3 \leq z \leq 4.5$ in the CANDELS Fields. *The Astrophysical Journal*, 897(1):44, July 2020.

[341] F. Shankar. The demography of supermassive black holes: Growing monsters at the heart of galaxies. *New Astronomy Review*, 53:57–77, Apr. 2009.

[342] S. Sherman, S. Jogee, J. Florez, M. L. Stevans, L. Kawinwanichakij, I. Wold, S. L. Finkelstein, C. Papovich, V. Acquaviva, R. Ciardullo, C. Gronwall, and Z. Escalante. Exploring the high-mass end of the stellar mass function of star-forming galaxies at cosmic noon. *Monthly Notices of the Royal Astronomical Society*, 491(3):3318–3335, Jan. 2020.

[343] T. Shibuya, M. Ouchi, M. Kubo, and Y. Harikane. Morphologies of ~190,000 Galaxies at z = 0-10 Revealed with HST Legacy Data. II. Evolution of Clumpy Galaxies. *The Astrophysical Journal*, 821(2):72, Apr 2016.

[344] G. A. Shields and S. Salviander. The Black Hole-Bulge Relationship for AGN at High Redshift. In S. Jogee, I. Marinova, L. Hao, and G. A. Blanc, editors, *Galaxy Evolution: Emerging Insights and Future Challenges*, volume 419 of *Astronomical Society of the Pacific Conference Series*, page 392, Dec. 2009.

[345] T. T. Shimizu, R. F. Mushotzky, M. Meléndez, M. J. Koss, A. J. Barger, and L. L. Cowie. Herschel far-infrared photometry of the Swift Burst Alert Telescope active galactic nuclei sample of the local universe - III. Global star-forming properties and the lack of a connection to nuclear activity. *Monthly Notices of the Royal Astronomical Society*, 466:3161–3183, Apr. 2017.

[346] R. Siebenmorgen, F. Heymann, and A. Efstathiou. Self-consistent two-phase AGN torus models. SED library for observers. *Astronomy & Astrophysics*, 583:A120, Nov. 2015.

[347] J. Silk and A. Nusser. The Massive-black-hole-Velocity-dispersion Relation and the Halo Baryon Fraction: A Case for Positive Active Galactic Nucleus Feedback. *The Astrophysical Journal*, 725:556–560, Dec. 2010.

[348] J. M. Simpson, I. Smail, W.-H. Wang, D. Riechers, J. S. Dunlop, Y. Ao, N. Bourne, A. Bunker, S. C. Chapman, C.-C. Chen, H. Dannerbauer, J. E. Geach, T. Goto, C. M. Harrison, H. S. Hwang, R. J. Ivison, T. Kodama, C. H. Lee, H. M. Lee, M. Lee, C. F. Lim, M. J. Michałowski, D. J. Rosario, H. Shim, X. W. Shu, A. M. Swinbank, W. L. Tee, Y. Toba, E. Valiante, J. Wang, and X. Z. Zheng. An Imperfectly Passive Nature: Bright Submillimeter Emission from Dust-obscured Star Formation in the z = 3.717 "Passive" System, ZF 20115. , 844(1):L10, July 2017.

[349] J. M. Simpson, A. M. Swinbank, I. Smail, D. M. Alexand er, W. N. Brandt, F. Bertoldi, C. de Breuck, S. C. Chapman, K. E. K. Coppin, E. da Cunha, A. L. R. Danielson, H. Dannerbauer, T. R. Greve, J. A. Hodge, R. J. Ivison, A. Karim, K. K. Knudsen, B. M. Poggianti, E. Schinnerer, A. P. Thomson, F. Walter, J. L. Wardlow, A. Weiß, and P. P. van der Werf. An ALMA Survey of Submillimeter Galaxies in the Extended Chandra Deep Field South: The Redshift Distribution and Evolution of Submillimeter Galaxies. *The Astrophysical Journal*, 788(2):125, Jun 2014.

[350] M. F. Skrutskie, R. M. Cutri, R. Stiening, M. D. Weinberg, S. Schneider, J. M. Carpenter, C. Beichman, R. Capps, T. Chester, J. Elias, J. Huchra, J. Liebert, C. Lonsdale, D. G. Monet, S. Price, P. Seitzer, T. Jarrett, J. D. Kirkpatrick, J. E. Gizis, E. Howard, T. Evans, J. Fowler, L. Fullmer, R. Hurt, R. Light, E. L. Kopan, K. A. Marsh, H. L. McCallon, R. Tam, S. Van Dyk, and S. Wheelock. The Two Micron All Sky Survey (2MASS). , 131(2):1163–1183, Feb. 2006.

[351] I. Smail, U. Dudzevičiūtė, S. M. Stach, O. Almaini, J. E. Birkin, S. C. Chapman, C.-C. Chen, J. E. Geach, B. Gullberg, J. A. Hodge, S. Ikarashi, R. J. Ivison, D. Scott, C. Simpson, A. M. Swinbank, A. P. Thomson, F. Walter, J. L. Wardlow, and P. van der Werf. An ALMA survey of the S2CLS UDS field: optically invisible submillimetre galaxies. *Monthly Notices of the Royal Astronomical Society*, 502(3):3426–3435, Apr. 2021.

[352] R. Smit, R. J. Bouwens, I. Labbé, M. Franx, S. M. Wilkins, and P. A. Oesch. Inferred H Flux as a Star Formation Rate Indicator at z $\sim$4-5: Implications for Dust Properties, Burstiness, and the z = 4-8 Star Formation Rate Functions. *The Astrophysical Journal*, 833(2):254, Dec 2016.

[353] D. J. B. Smith, M. J. Jarvis, M. Lacy, and A. Martínez-Sansigre. Infrared and millimetre-wavelength evidence for cold accretion within a z = 2.83 Lyman α blob. *Monthly Notices of the Royal Astronomical Society*, 389:799–805, Sept. 2008.

[354] R. S. Somerville, R. C. Gilmore, J. R. Primack, and A. Domínguez. Galaxy properties from the ultraviolet to the far-infrared: Λ cold dark matter models confront observations. *Monthly Notices of the Royal Astronomical Society*, 423(3):1992–2015, Jul 2012.

[355] R. S. Somerville, P. F. Hopkins, T. J. Cox, B. E. Robertson, and L. Hernquist. A semi-analytic model for the co-evolution of galaxies, black holes and active galactic nuclei. *Monthly Notices of the Royal Astronomical Society*, 391:481–506, Dec. 2008.

[356] J. S. Speagle, C. L. Steinhardt, P. L. Capak, and J. D. Silverman. A Highly Consistent Framework for the Evolution of the Star-Forming "Main Sequence" from z ~0-6. *The Astrophysical Journal Supplement Series*, 214(2):15, Oct 2014.

[357] L. R. Spitler, I. Labbé, K. Glazebrook, S. E. Persson, A. Monson, C. Papovich, K.-V. H. Tran, G. B. Poole, R. Quadri, P. van Dokkum, D. D. Kelson, G. G. Kacprzak, P. J. McCarthy, D. Murphy, C. M. S. Straatman, and V. Tilvi. First Results from Z -FOURGE: Discovery of a Candidate Cluster at z = 2.2 in COSMOS. *The Astrophysical Journall*, 748(2):L21, Apr 2012.

[358] L. R. Spitler, C. M. S. Straatman, I. Labbé, K. Glazebrook, K.-V. H. Tran, G. G. Kacprzak, R. F. Quadri, C. Papovich, S. E. Persson, P. van Dokkum, R. Allen, L. Kawinwanichakij, D. D. Kelson, P. J. McCarthy, N. Mehrtens, A. J. Monson, T. Nanayakkara, G. Rees, V. Tilvi, and A. R. Tomczak. Exploring the z = 3-4 Massive Galaxy Population with ZFOURGE: The Prevalence of Dusty and Quiescent Galaxies. *The Astrophysical Journall*, 787(2):L36, June 2014.

[359] M. Stalevski, C. Ricci, Y. Ueda, P. Lira, J. Fritz, and M. Baes. The dust covering factor in active galactic nuclei. *Monthly Notices of the Royal Astronomical Society*, 458:2288–2302, May 2016.

[360] S. A. Stanford, M. Brodwin, A. H. Gonzalez, G. Zeimann, D. Stern, A. Dey, P. R. Eisenhardt, G. F. Snyder, and C. Mancone. IDCS J1426.5+3508: Discovery of a Massive, Infrared-selected Galaxy Cluster at z = 1.75. *The Astrophysical Journal*, 753:164, July 2012.

[361] F. Stanley, C. M. Harrison, D. M. Alexander, A. M. Swinbank, J. A. Aird, A. Del Moro, R. C. Hickox, and J. R. Mullaney. A remarkably flat relationship between the average star formation rate and AGN luminosity for distant X-ray AGN. *MNRAS*, 453:591–604, Oct. 2015.

[362] C. C. Steidel, K. L. Adelberger, M. Dickinson, M. Giavalisco, M. Pettini, and M. Kellogg. A Large Structure of Galaxies at Redshift Z approximately 3 and Its Cosmological Implications. , 492(2):428–438, Jan 1998.

[363] C. C. Steidel, K. L. Adelberger, A. E. Shapley, D. K. Erb, N. A. Reddy, and M. Pettini. Spectroscopic Identification of a Protocluster at z=2.300: Environmental Dependence of Galaxy Properties at High Redshift. *The Astrophysical Journal*, 626(1):44–50, Jun 2005.

[364] D. Stern. The X-Ray to Mid-infrared Relation of AGNs at High Luminosity. *The Astrophysical Journal*, 807:129, July 2015.

[365] D. Stern, P. Eisenhardt, V. Gorjian, C. S. Kochanek, N. Caldwell, D. Eisenstein, M. Brodwin, M. J. I. Brown, R. Cool, A. Dey, P. Green, B. T. Jannuzi, S. S. Murray, M. A. Pahre, and S. P. Willner. Mid-Infrared Selection of Active Galaxies. *The Astrophysical Journal*, 631:163–168, Sept. 2005.

[366] J. A. Stevens, M. J. Jarvis, K. E. K. Coppin, M. J. Page, T. R. Greve, F. J. Carrera, and R. J. Ivison. An excess of star-forming galaxies in the fields of high-redshift QSOs. *Monthly Notices of the Royal Astronomical Society*, 405:2623–2638, July 2010.

[367] C. M. S. Straatman, I. Labbé, L. R. Spitler, R. Allen, B. Altieri, G. B. Brammer, M. Dickinson, P. van Dokkum, H. Inami, K. Glazebrook, G. G. Kacprzak, L. Kawinwanichakij, D. D. Kelson, P. J. McCarthy, N. Mehrtens, A. Monson, D. Murphy, C. Papovich, S. E. Persson, R. Quadri, G. Rees, A. Tomczak, K.-V. H. Tran, and V. Tilvi. A Substantial Population of Massive Quiescent Galaxies at z ∼4 from ZFOURGE. *The Astrophysical Journall*, 783(1):L14, Mar. 2014.

[368] E. Sturm, E. González-Alfonso, S. Veilleux, J. Fischer, J. Graciá-Carpio, S. Hailey-Dunsheath, A. Contursi, A. Poglitsch, A. Sternberg, R. Davies, R. Genzel, D. Lutz, L. Tacconi, A. Verma, R. Maiolino, and J. A. de Jong. Massive Molecular Outflows and Negative Feedback in ULIRGs Observed by Herschel-PACS. *The Astrophysical Journall*, 733:L16, May 2011.

[369] T. Suwa, A. Habe, and K. Yoshikawa. Protoclusters in the ΛCDM Universe. *The Astrophysical Journall*, 646(1):L5–L8, Jul 2006.

[370] M. Symeonidis, B. M. Giblin, M. J. Page, C. Pearson, G. Bendo, N. Seymour, and S. J. Oliver. AGN are cooler than you think: the intrinsic far-IR emission from QSOs. *MNRAS*, 459:257–276, June 2016.

[371] M. Symeonidis and M. J. Page. What powers hyperluminous infrared galaxies at z ∼ 1-2? *Monthly Notices of the Royal Astronomical Society*, 479(1):L91–L95, Sept. 2018.

[372] M. Symeonidis and M. J. Page. AGN and star formation across cosmic time. *Monthly Notices of the Royal Astronomical Society*, Mar. 2021.

[373] L. J. Tacconi, R. Genzel, I. Smail, R. Neri, S. C. Chapman, R. J. Ivison, A. Blain, P. Cox, A. Omont, F. Bertoldi, T. Greve, N. M. Förster Schreiber, S. Genel, D. Lutz, A. M. Swinbank, A. E. Shapley, D. K. Erb, A. Cimatti, E. Daddi, and A. J. Baker. Submillimeter Galaxies at z ∼2: Evidence for Major Mergers and Constraints on Lifetimes, IMF, and CO-H_2 Conversion Factor. *The Astrophysical Journal*, 680(1):246–262, Jun 2008.

[374] L. J. Tacconi, R. Neri, S. C. Chapman, R. Genzel, I. Smail, R. J. Ivison, F. Bertoldi, A. Blain, P. Cox, T. Greve, and A. Omont. High-Resolution Millimeter Imaging of Submillimeter Galaxies. *The Astrophysical Journal*, 640(1):228–240, Mar. 2006.

[375] K.-i. Tadaki, T. Kodama, M. Hayashi, R. Shimakawa, Y. Koyama, M. Lee, I. Tanaka, B. Hatsukade, D. Iono, K. Kohno, Y. Matsuda, T. L. Suzuki, Y. Tamura, J. Toshikawa, and H. Umehata. Environmental impacts on molecular gas in protocluster galaxies at z 2. , 71(2):40, Apr 2019.

[376] Y. Tamura, K. Kohno, K. Nakanishi, B. Hatsukade, D. Iono, G. W. Wilson, M. S. Yun, T. Takata, Y. Matsuda, T. Tosaki, H. Ezawa, T. A. Perera, K. S. Scott, J. E. Austermann, D. H. Hughes, I. Aretxaga, A. Chung, T. Oshima, N. Yamaguchi, K. Tanaka, and R. Kawabe. Spatial correlation between submillimetre and Lyman-α galaxies in the SSA22 protocluster. , 459(7243):61–63, May 2009.

[377] L. A. M. Tasca, O. Le Fèvre, N. P. Hathi, D. Schaerer, O. Ilbert, G. Zamorani, B. C. Lemaux, P. Cassata, B. Garilli, V. Le Brun, D. Maccagni, L. Pentericci, R. Thomas, E. Vanzella, E. Zucca, R. Amorin, S. Bardelli, L. P. Cassarà, M. Castellano, A. Cimatti, O. Cucciati, A. Durkalec, A. Fontana, M. Giavalisco, A. Grazian, S. Paltani, B. Ribeiro, M. Scodeggio, V. Sommariva, M. Talia, L. Tresse, D. Vergani, P. Capak, S. Charlot, T. Contini, S. de la Torre, J. Dunlop, S. Fotopoulou, A. Koekemoer, C. López-Sanjuan, Y. Mellier, J. Pforr, M. Salvato, N. Scoville, Y. Taniguchi, and P. W. Wang. The evolving star formation rate: $M_\star$ relation and sSFR since z 5 from the VUDS spectroscopic survey. *Astronomy & Astrophysics*, 581:A54, Sept. 2015.

[378] Y. Toba, T. Goto, N. Oi, T.-W. Wang, S. J. Kim, S. C. C. Ho, D. Burgarella, T. Hashimoto, B.-C. Hsieh, T.-C. Huang, H. S. Hwang, H. Ikeda, H. K. Kim, S. Kim, D. Lee, M. A. Malkan, H. Matsuhara, T. Miyaji, R. Momose, Y. Ohyama, S. Oyabu, C. Pearson, D. J. D. Santos, H. Shim, T. Takagi, Y. Ueda, Y. Utsumi, and T. Wada. Search for Optically Dark Infrared Galaxies without Counterparts of Subaru Hyper Suprime-Cam in the AKARI North Ecliptic Pole Wide Survey Field. *The Astrophysical Journal*, 899(1):35, Aug. 2020.

[379] S. Toft, V. Smolčić, B. Magnelli, A. Karim, A. Zirm, M. Michalowski, P. Capak, K. Sheth, K. Schawinski, J. K. Krogager, S. Wuyts, D. Sanders, A. W. S. Man, D. Lutz, J. Staguhn, S. Berta, H. Mccracken, J. Krpan, and D. Riechers. Submillimeter Galaxies as Progenitors of Compact Quiescent Galaxies. *The Astrophysical Journal*, 782(2):68, Feb 2014.

[380] A. R. Tomczak, R. F. Quadri, K.-V. H. Tran, I. Labbé, C. M. S. Straatman, C. Papovich, K. Glazebrook, R. Allen, G. B. Brammer, M. Cowley, M. Dickinson, D. Elbaz, H. Inami, G. G. Kacprzak, G. E. Morrison, T. Nanayakkara, S. E. Persson, G. A. Rees, B. Salmon, C. Schreiber, L. R. Spitler, and K. E. Whitaker. The SFR-M* Relation and Empirical Star-Formation Histories from ZFOURGE* at 0.5 < z < 4. *The Astrophysical Journal*, 817(2):118, Feb 2016.

[381] E. Treister, C. N. Cardamone, K. Schawinski, C. M. Urry, E. Gawiser, S. Virani, P. Lira, J. Kartaltepe, M. Damen, E. N. Taylor, E. Le Floc'h, S. Justham, and A. M. Koekemoer. Heavily Obscured AGN in Star-Forming Galaxies at z sime 2. *The Astrophysical Journal*, 706:535–552, Nov. 2009.

[382] E. Treister, J. H. Krolik, and C. Dullemond. Measuring the Fraction of Obscured Quasars by the Infrared Luminosity of Unobscured Quasars. *The Astrophysical Journal*, 679:140–148, May 2008.

[383] E. Treister, K. Schawinski, C. M. Urry, and B. D. Simmons. Major Galaxy Mergers Only Trigger the Most Luminous Active Galactic Nuclei. *The Astrophysical Journall*, 758:L39, Oct. 2012.

[384] E. Treister, C. M. Urry, E. Chatzichristou, F. Bauer, D. M. Alexander, A. Koekemoer, J. Van Duyne, W. N. Brandt, J. Bergeron, D. Stern, L. A. Moustakas, R.-R. Chary, C. Conselice, S. Cristiani, and N. Grogin. Obscured Active Galactic Nuclei and the X-Ray, Optical, and Far-Infrared Number Counts of Active Galactic Nuclei in the GOODS Fields. *The Astrophysical Journal*, 616:123–135, Nov. 2004.

[385] K. R. W. Tristram, K. Meisenheimer, W. Jaffe, M. Schartmann, H.-W. Rix, C. Leinert, S. Morel, M. Wittkowski, H. Röttgering, G. Perrin, B. Lopez, D. Raban, W. D. Cotton, U. Graser, F. Paresce, and T. Henning. Resolving the complex structure of the dust torus in the active nucleus of the Circinus galaxy. *Astronomy & Astrophysics*, 474:837–850, Nov. 2007.

[386] K. R. W. Tristram, D. Raban, K. Meisenheimer, W. Jaffe, H. Röttgering, L. Burtscher, W. D. Cotton, U. Graser, T. Henning, C. Leinert, B. Lopez, S. Morel, G. Perrin, and M. Wittkowski. Parsec-scale dust distributions in Seyfert galaxies. Results of the MIDI AGN snapshot survey. *Astronomy & Astrophysics*, 502:67–84, July 2009.

[387] H. Umehata, M. Fumagalli, I. Smail, Y. Matsuda, A. M. Swinbank, S. Cantalupo, C. Sykes, R. J. Ivison, C. C. Steidel, A. E. Shapley, J. Vernet, T. Yamada, Y. Tamura, M. Kubo, K. Nakanishi, M. Kajisawa, B. Hatsukade, and K. Kohno. Gas filaments of the cosmic web located around active galaxies in a protocluster. *Science*, 366(6461):97–100, Oct 2019.

[388] H. Umehata, Y. Tamura, K. Kohno, R. J. Ivison, D. M. Alexander, J. E. Geach, B. Hatsukade, D. H. Hughes, S. Ikarashi, Y. Kato, T. Izumi, R. Kawabe, M. Kubo, M. Lee, B. Lehmer, R. Makiya, Y. Matsuda, K. Nakanishi, T. Saito, I. Smail, T. Yamada, Y. Yamaguchi, and M. Yun. ALMA Deep Field in SSA22: A Concentration of Dusty Starbursts in a z = 3.09 Protocluster Core. *The Astrophysical Journall*, 815(1):L8, Dec 2015.

[389] C. M. Urry and P. Padovani. Unified Schemes for Radio-Loud Active Galactic Nuclei. *Publications of the Astronomical Society of the Pacific*, 107:803, Sept. 1995.

[390] F. Valentino, M. Tanaka, I. Davidzon, S. Toft, C. Gómez-Guijarro, M. Stockmann, M. Onodera, G. Brammer, D. Ceverino, A. L. Faisst, A. Gallazzi, C. C. Hayward, O. Ilbert, M. Kubo, G. E. Magdis, J. Selsing, R. Shimakawa, M. Sparre, C. Steinhardt, K. Yabe, and J. Zabl. Quiescent Galaxies 1.5 Billion Years after the Big Bang and Their Progenitors. *The Astrophysical Journal*, 889(2):93, Feb. 2020.

[391] E. Valiante, M. W. L. Smith, S. Eales, S. J. Maddox, E. Ibar, R. Hopwood, L. Dunne, P. J. Cigan, S. Dye, E. Pascale, E. E. Rigby, N. Bourne, C. Furlanetto, and R. J. Ivison. The Herschel-ATLAS data release 1 - I. Maps, catalogues and number counts. *Monthly Notices of the Royal Astronomical Society*, 462(3):3146–3179, Nov 2016.

[392] S. van den Bergh, R. G. Abraham, R. S. Ellis, N. R. Tanvir, B. X. Santiago, and K. G. Glazebrook. A Morphological Catalog of Galaxies in the Hubble deep Field. *Astronomical Journal*, 112:359, Aug 1996.

[393] R. F. J. van der Burg, A. Muzzin, H. Hoekstra, C. Lidman, A. Rettura, G. Wilson, H. K. C. Yee, H. Hildebrandt, D. Marchesini, M. Stefanon, R. Demarco, and K. Kuijken. The environmental dependence of the stellar mass function at z $\sim$1. Comparing cluster and field between the GCLASS and UltraVISTA surveys. *Astronomy & Astrophysics*, 557:A15, Sep 2013.

[394] R. F. J. van der Burg, A. Muzzin, H. Hoekstra, G. Wilson, C. Lidman, and H. K. C. Yee. A census of stellar mass in ten massive haloes at z ∼1 from the GCLASS Survey. *Astronomy and Astrophysics*, 561:A79, Jan 2014.

[395] P. G. van Dokkum, R. Quadri, D. Marchesini, G. Rudnick, M. Franx, E. Gawiser, D. Herrera, S. Wuyts, P. Lira, I. Labbé, J. Maza, G. D. Illingworth, N. M. Förster Schreiber, M. Kriek, H. W. Rix, E. N. Taylor, S. Toft, T. Webb, and S. K. Yi. The Space Density and Colors of Massive Galaxies at 2 < z < 3: The Predominance of Distant Red Galaxies. *The Astrophysical Journall*, 638(2):L59–L62, Feb. 2006.

[396] B. P. Venemans, H. J. A. Röttgering, G. K. Miley, W. J. M. van Breugel, C. de Breuck, J. D. Kurk, L. Pentericci, S. A. Stanford, R. A. Overzier, S. Croft, and H. Ford. Protoclusters associated with z > 2 radio galaxies . I. Characteristics of high redshift protoclusters. *Astronomy & Astrophysics*, 461(3):823–845, Jan 2007.

[397] C. Vignali, W. N. Brandt, D. P. Schneider, and S. Kaspi. X-Ray Lighthouses of the High-Redshift Universe. II. Further Snapshot Observations of the Most Luminous z≳ 4 Quasars with Chandra. *Astronomical Journal*, 129:2519–2530, June 2005.

[398] P. Virtanen, R. Gommers, T. E. Oliphant, M. Haberland, T. Reddy, D. Cournapeau, E. Burovski, P. Peterson, W. Weckesser, J. Bright, S. J. van der Walt, M. Brett, J. Wilson, K. J. Millman, N. Mayorov, A. R. J. Nelson, E. Jones, R. Kern, E. Larson, C. J. Carey, İ. Polat, Y. Feng, E. W. Moore, J. VanderPlas, D. Laxalde, J. Perktold, R. Cimrman, I. Henriksen, E. A. Quintero, C. R. Harris, A. M. Archibald, A. H. Ribeiro, F. Pedregosa, P. van Mulbregt, and SciPy 1.0 Contributors. SciPy 1.0: Fundamental Algorithms for Scientific Computing in Python. *Nature Methods*, 17:261–272, 2020.

[399] M. Volonteri. Formation of supermassive black holes. *The A&A Review*, 18:279–315, July 2010.

[400] M. Volonteri, P. R. Capelo, H. Netzer, J. Bellovary, M. Dotti, and F. Governato. Black hole accretion versus star formation rate: theory confronts observations. *Monthly Notices of the Royal Astronomical Society*, 452:L6–L10, Sept. 2015.

[401] M. Volonteri, F. Haardt, and P. Madau. The Assembly and Merging History of Supermassive Black Holes in Hierarchical Models of Galaxy Formation. *The Astrophysical Journal*, 582:559–573, Jan. 2003.

[402] D. A. Wake, C. A. Collins, R. C. Nichol, L. R. Jones, and D. J. Burke. The Environmental Dependence of Galaxy Colors in Intermediate-Redshift X-Ray-selected Clusters. *The Astrophysical Journal*, 627(1):186–202, Jul 2005.

[403] F. Walter, R. Decarli, C. Carilli, F. Bertoldi, P. Cox, E. da Cunha, E. Daddi, M. Dickinson, D. Downes, D. Elbaz, R. Ellis, J. Hodge, R. Neri, D. A. Riechers, A. Weiss, E. Bell, H. Dannerbauer, M. Krips, M. Krumholz, L. Lentati, R. Maiolino, K. Menten, H.-W. Rix, B. Robertson, H. Spinrad, D. P. Stark, and D. Stern. The intense starburst HDF 850.1 in a galaxy overdensity at z ≈ 5.2 in the Hubble Deep Field. *Nature*, 486(7402):233–236, Jun 2012.

[404] L. Wang, G. De Lucia, F. Fontanot, and M. Hirschmann. Starburst galaxies in semi-analytic models of galaxy formation and evolution. *Monthly Notices of the Royal Astronomical Society*, 482(4):4454–4465, Feb. 2019.

[405] T. Wang, C. Schreiber, D. Elbaz, Y. Yoshimura, K. Kohno, X. Shu, Y. Yamaguchi, M. Pannella, M. Franco, J. Huang, C. F. Lim, and W. H. Wang. A dominant population of optically invisible massive galaxies in the early Universe. *Nature*, 572(7768):211–214, Aug. 2019.

[406] M. C. Weisskopf, B. Brinkman, C. Canizares, G. Garmire, S. Murray, and L. P. Van Speybroeck. An Overview of the Performance and Scientific Results from the Chandra X-Ray Observatory. *Publications of the Astronomical Society of the Pacific*, 114:1–24, Jan. 2002.

[407] M. W. Werner, T. L. Roellig, F. J. Low, G. H. Rieke, M. Rieke, W. F. Hoffmann, E. Young, J. R. Houck, B. Brandl, G. G. Fazio, J. L. Hora, R. D. Gehrz, G. Helou, B. T. Soifer, J. Stauffer, J. Keene, P. Eisenhardt, D. Gallagher, T. N. Gautier, W. Irace, C. R. Lawrence, L. Simmons, J. E. Van Cleve, M. Jura, E. L. Wright, and D. P. Cruikshank. The Spitzer Space Telescope Mission. *The Astrophysical Journals*, 154:1–9, Sept. 2004.

[408] K. E. Whitaker, M. Franx, R. Bezanson, G. B. Brammer, P. G. van Dokkum, M. T. Kriek, I. Labbé, J. Leja, I. G. Momcheva, E. J. Nelson, J. R. Rigby, H.-W. Rix, R. E. Skelton, A. van der Wel, and S. Wuyts. Galaxy Structure as a Driver of the Star Formation Sequence Slope and Scatter. *The Astrophysical Journall*, 811(1):L12, Sept. 2015.

[409] K. E. Whitaker, M. Franx, J. Leja, P. G. van Dokkum, A. Henry, R. E. Skelton, M. Fumagalli, I. G. Momcheva, G. B. Brammer, I. Labbé, E. J. Nelson, and J. R. Rigby. Constraining the Low-mass Slope of the Star Formation Sequence at $0.5 < z < 2.5$. *The Astrophysical Journal*, 795(2):104, Nov. 2014.

[410] K. E. Whitaker, I. Labbé, P. G. van Dokkum, G. Brammer, M. Kriek, D. Marchesini, R. F. Quadri, M. Franx, A. Muzzin, R. J. Williams, R. Bezanson, G. D. Illingworth, K.-S. Lee, B. Lundgren, E. J. Nelson, G. Rudnick, T. Tal, and D. A. Wake. The NEWFIRM Medium-band Survey: Photometric Catalogs, Redshifts, and the Bimodal Color Distribution of Galaxies out to $z \sim 3$. *The Astrophysical Journal*, 735(2):86, July 2011.

[411] K. E. Whitaker, A. Pope, R. Cybulski, C. M. Casey, G. Popping, and M. S. Yun. The Constant Average Relationship between Dust-obscured Star Formation and Stellar Mass from $z = 0$ to $z = 2.5$. *The Astrophysical Journal*, 850(2):208, Dec. 2017.

[412] K. E. Whitaker, P. G. van Dokkum, G. Brammer, and M. Franx. The Star Formation Mass Sequence Out to $z = 2.5$. *The Astrophysical Journall*, 754(2):L29, Aug. 2012.

[413] T. Wiklind, C. J. Conselice, T. Dahlen, M. E. Dickinson, H. C. Ferguson, N. A. Grogin, Y. Guo, A. M. Koekemoer, B. Mobasher, A. Mortlock, A. Fontana, R. Davé, H. Yan, V. Acquaviva, M. L. N. Ashby, G. Barro, K. I. Caputi, M. Castellano, A. Dekel, J. L. Donley, G. G. Fazio, M. Giavalisco, A. Grazian, N. P. Hathi, P. Kurczynski, Y. Lu, E. J. McGrath, D. F. de Mello, M. Peth, M. Safarzadeh, M. Stefanon, and T. Targett. Properties of

Submillimeter Galaxies in the CANDELS GOODS-South Field. *The Astrophysical Journal*, 785(2):111, Apr 2014.

[414] C. C. Williams, I. Labbe, J. Spilker, M. Stefanon, J. Leja, K. Whitaker, R. Bezanson, D. Narayanan, P. Oesch, and B. Weiner. Discovery of a Dark, Massive, ALMA-only Galaxy at z ~ 5-6 in a Tiny 3 mm Survey. *The Astrophysical Journal*, 884(2):154, Oct. 2019.

[415] J. P. Willis, N. Clerc, M. N. Bremer, M. Pierre, C. Adami, O. Ilbert, B. Maughan, S. Maurogordato, F. Pacaud, I. Valtchanov, L. Chiappetti, K. Thanjavur, S. Gwyn, E. R. Stanway, and C. Winkworth. Distant galaxy clusters in the XMM Large Scale Structure survey. *Monthly Notices of the Royal Astronomical Society*, 430(1):134–156, Mar 2013.

[416] L. M. Winter, R. F. Mushotzky, C. S. Reynolds, and J. Tueller. X-Ray Spectral Properties of the BAT AGN Sample. *The Astrophysical Journal*, 690:1322–1349, Jan. 2009.

[417] S. Wuyts, N. M. Förster Schreiber, A. van der Wel, B. Magnelli, Y. Guo, R. Genzel, D. Lutz, H. Aussel, G. Barro, S. Berta, A. Cava, J. Graciá-Carpio, N. P. Hathi, K.-H. Huang, D. D. Kocevski, A. M. Koekemoer, K.-S. Lee, E. Le Floc'h, E. J. McGrath, R. Nordon, P. Popesso, F. Pozzi, L. Riguccini, G. Rodighiero, A. Saintonge, and L. Tacconi. Galaxy Structure and Mode of Star Formation in the SFR-Mass Plane from z $\sim$2.5 to z $\sim$0.1. *The Astrophysical Journal*, 742(2):96, Dec. 2011.

[418] S. Wuyts, I. Labbé, M. Franx, G. Rudnick, P. G. van Dokkum, G. G. Fazio, N. M. Förster Schreiber, J. Huang, A. F. M. Moorwood, H.-W. Rix, H. Röttgering, and P. van der Werf. What Do We Learn from IRAC Observations of Galaxies at 2 < z < 3.5? *The Astrophysical Journal*, 655(1):51–65, Jan. 2007.

[419] Y. Q. Xue, W. N. Brandt, B. Luo, D. A. Rafferty, D. M. Alexander, F. E. Bauer, B. D. Lehmer, D. P. Schneider, and J. D. Silverman. Color-Magnitude Relations of Active and Non-active Galaxies in the Chandra Deep Fields: High-redshift Constraints and Stellar-mass Selection Effects. *The Astrophysical Journal*, 720:368–391, Sept. 2010.

[420] C. Yang, A. Omont, A. Beelen, Y. Gao, P. van der Werf, R. Gavazzi, Z. Y. Zhang, R. Ivison, M. Lehnert, D. Liu, I. Oteo, E. González-Alfonso, H. Dannerbauer, P. Cox, M. Krips, R. Neri, D. Riechers, A. J. Baker, M. J. Michałowski, A. Cooray, and I. Smail. Molecular gas in the Herschel-selected strongly lensed submillimeter galaxies at $z = 2 - 4$ as probed by multi-J CO lines. *Astronomy & Astrophysics*, 608:A144, Dec 2017.

[421] C. Yang, A. Omont, A. Beelen, Y. Gao, P. van der Werf, R. Gavazzi, Z. Y. Zhang, R. Ivison, M. Lehnert, D. Liu, I. Oteo, E. González-Alfonso, H. Dannerbauer, P. Cox, M. Krips, R. Neri, D. Riechers, A. J. Baker, M. J. Michałowski, A. Cooray, and I. Smail. Molecular gas in the Herschel-selected strongly lensed submillimeter galaxies at z 2-4 as probed by multi-J CO lines. , 608:A144, Dec. 2017.

[422] T. Yuan, T. Nanayakkara, G. G. Kacprzak, K.-V. H. Tran, K. Glazebrook, L. J. Kewley, L. R. Spitler, G. B. Poole, I. Labbé, C. M. S. Straatman, and A. R. Tomczak. Keck/MOSFIRE Spectroscopic Confirmation of a Virgo-like Cluster Ancestor at z = 2.095. , 795(1):L20, Nov 2014.

[423] J. A. Zavala, C. M. Casey, E. da Cunha, J. Spilker, J. Staguhn, J. Hodge, and P. M. Drew. Constraining the Volume Density of Dusty Star-forming Galaxies through the First 3 mm Number Counts from ALMA. *The Astrophysical Journal*, 869(1):71, Dec 2018.

[424] J. A. Zavala, C. M. Casey, S. M. Manning, M. Aravena, M. Bethermin, K. I. Caputi, D. L. Clements, E. d. Cunha, P. Drew, S. L. Finkelstein, S. Fujimoto, C. Hayward, J. Hodge, J. S. Kartaltepe, K. Knudsen, A. M. Koekemoer, A. S. Long, G. E. Magdis, A. W. S. Man, G. Popping, D. Sanders, N. Scoville, K. Sheth, J. Staguhn, S. Toft, E. Treister, J. D. Vieira, and M. S. Yun. The Evolution of the IR Luminosity Function and Dust-obscured Star Formation over the Past 13 Billion Years. *The Astrophysical Journal*, 909(2):165, Mar. 2021.

[425] J. A. Zavala, C. M. Casey, N. Scoville, J. B. Champagne, Y. Chiang, H. Dannerbauer, P. Drew, H. Fu, J. Spilker, L. Spitler, K. V. Tran, E. Treister, and S. Toft. On the Gas Content, Star Formation Efficiency, and Environmental Quenching of Massive Galaxies in Protoclusters at z $\approx$ 2.02.5. *The Astrophysical Journal*, 887(2):183, Dec 2019.

[426] I. Zehavi, Z. Zheng, D. H. Weinberg, M. R. Blanton, N. A. Bahcall, A. A. Berlind, J. Brinkmann, J. A. Frieman, J. E. Gunn, R. H. Lupton, R. C. Nichol, W. J. Percival, D. P. Schneider, R. A. Skibba, M. A. Strauss, M. Tegmark, and D. G. York. Galaxy Clustering in the Completed SDSS Redshift Survey: The Dependence on Color and Luminosity. *The Astrophysical Journal*, 736(1):59, July 2011.

[427] G. R. Zeimann, S. A. Stanford, M. Brodwin, A. H. Gonzalez, G. F. Snyder, D. Stern, P. Eisenhardt, C. Mancone, and A. Dey. IDCS J1433.2+3306: An Infrared-selected Galaxy Cluster at z = 1.89. *The Astrophysical Journal*, 756(2):115, Sep 2012.

[428] Z.-Y. Zhang, D. Romano, R. J. Ivison, P. P. Papadopoulos, and F. Matteucci. Stellar populations dominated by massive stars in dusty starburst galaxies across cosmic time. *Nature*, 558(7709):260–263, Jun 2018.

Appendix A

Appendix Title

Supplementary material goes here. See for instance Figure A.1.

A.1 Lorem Ipsum

dolor sit amet, consectetur adipisicing elit, sed do eiusmod tempor incididunt ut labore et dolore magna aliqua. Ut enim ad minim veniam, quis nostrud exercitation ullamco laboris nisi ut aliquip ex ea commodo consequat. Duis aute irure dolor in reprehenderit in voluptate velit esse cillum dolore eu fugiat nulla pariatur. Excepteur sint occaecat cupidatat non proident, sunt in culpa qui officia deserunt mollit anim id est laborum.

"I am glad I was up so late,
for that's the reason I was up so early."
William Shakespeare (1564-1616), British dramatist, poet.
Cloten, in Cymbeline, act 2, sc. 3, l. 33-4.

Figure A.1: A deep quote.